DEPOSITION OF SUB-MICRON PARTICLES ONTO AGR FUEL ELEMENTS

by

A. A. EL-KADY

Thesis submitted in accordance with the requirements of

the University of Liverpool

for the Degree of Doctor of Philosophy

Department of Mechanical Engineering

University of Liverpool

May 1988

BEST COPY AVAILABLE.

VARIABLE PRINT QUALITY

VOLUME CONTAINS

CLEAR OVERLAYS

OVERLAYS HAVE BEEN

SCANNED SEPERATELY

AND THEN AGAIN OVER

THE RELEVANT PAGE

ABSTRACT

The deposition of sub-micron particles onto AGR fuel elements has been studied. Modelling of the deposition was achieved by using uranin particles in a full scale laboratory flow rig using air at ambient conditions instead of CO_2 at reactor conditions. The particles were produced by a well established atomizer-impactor method. Electron microscope analysis was used to determine the diameter of the particles which were moderately monodispersed, having mass-median diameter of 0.25 μm and 0.05 μm with geometric standard deviation of 1.64 and 1.47 respectively. A fluorimetric analysis was used to measure the mass of the particles deposited and the free stream particle concentration.

The theoretical considerations showed that the particles which collide with the test surface must be captured, to confirm this an experimental test showed no evidence for particle re-entrainment. The mechanism which is mainly responsible for the deposition process is that of eddy-diffusion resisted by the thermophoretic force in the case of heated surfaces. The theoretical approach was based on a rough surface model and used an established formula for the velocity of thermophoresis.

The air flow was characterised for six different Reynolds numbers; the deposition tests were carried out for three of them, viz. 300000, 60000 and 5000. The deposition tests were also carried out using a hydraulically smooth rod to obtain a comparison between the deposition rate onto the ribbed surface and those onto the smooth one. The smooth surface results could then also be used to compare the present study with published data.

The experimental results for the isothermal rods show clearly that the deposition velocity of particles for the ribbed surface is much higher than for the smooth surface, especially at higher Reynolds numbers, this can be up to twenty fold at flow Reynolds number of 300000. For both cases the deposition velocity increases as the flow Reynolds number is increased. The deposition velocity for smaller particles is higher than that of the larger ones. For the ribbed rod at higher flow Reynolds number the particle diameter has nearly lost its effect on the deposition velocity.

For the heated surfaces, for both rods, the effect of thermophoresis on the smaller particles is less than that on the larger ones at the same surface temperature and flow Reynods numbers. For a given particle diameter and flow Reynolds number, the effect of thermophoresis increases as the surface temperature increases. The effect of thermophoresis reduces as the flow Reynolds number is increased and also reduces over the ribbed rod compared with its effect over the smooth one.

Comparison of the experimental results with the available data of other investigators showed that the present results are consistent with these earlier studies.

i

Comparison of the experimental results with the values of the proposed theoretical model showed significantly differences for the smooth isothermal rod. Considering the surface roughness, which was measured using a Talysurf, leads to a good agreement between the theoretical values and the experimental results for the smooth rod. The calculation of the equivalent roughness of the ribbed rod failed to achieve an agreement between theoretical and experimental values. The factor of 0.1 had to use for scaling the equivalent roughness of the ribbed rod to align the theoretical values with the experimental data.

Comparison for the heated rods showed a huge discrepancy between the theoretically predicted values and the experimentally measured results. A correction factor of 0.2 was used to scale the temperature gradient to fit the theoretical values with that experimentally obtained.

Apart from the scaling factors, deposition calculations for typical AGR operating conditions were carried out which, in general terms, agree with the observed trends of the reactor operating conditions.

ACKNOWLEDGEMENTS

CONTENTS

NOMENCLATURE

A   cross-sectional area of the channel or constant

A_1 cross-sectional area of the passage bounded by r_1 and r_m

$\bar{A}$ Hamaker constant

A' universal constant

a   function notation

a_1 constant

B   constant

B' universal constant

b   function notation

C   constant

C_1 constant

C_1 dimensionless constant related to the roughness geometry

C_c Cunningham correction factor

C_m momentum exchange coefficient

C_s thermal slip coefficient

C_t thermal jump coefficient

c   particle concentration in the flow

c_0 particle free stream concentration

c^* dimensionless particle concentration in the flow

$\bar{c}$ mean molecular speed or constant

c_Δ particle concentration at a distance Δ from the surface

c_Δ^* dimensionless particle concentration at Δ^*

D   Brownian particle diffusivity

d   diameter of the pipe flow or the particle in the samples

d_e effective diameter of the channel

d_{e_1} effective diameter of the passage bounded by r_1 and r_m

d_g geometric mean diameter

d_m arithmetic mean diameter

d_{mm} mass-median diameter

d_p particle diameter

d_0 diameter of Preston tube

e   rib height

e_0 displacement in the origin of the rough surface velocity profile

F   function notation

F_T therophoretic force

F_T^* free-molecule thermal force

f   Fanning friction factor

f_1 friction factor for a rough surface

f_d fully developed value of the friction factor through the channel

f_e friction factor through the entry length

f(d)   frequency of the particles observations with diameter d

G   function notation

g   gravity acceleration

h   convection heat transfer coefficient

I   numerical value of an integration

I_B value of the integration in the buffer layer

I_s value of the integration in the laminar sub-layer

Kn   Knudsen number

K_1 constant

k   thermal conductivity

k_B Boltzman's constant

k_g gas thermal conductivity

k_p particle thermal conductivity

k_s	mean height of roughness element
k_s^*	dimensionless height of roughness element
L_e	entry length
m^2	function notation
N	particle mass transfer rate
N_o	particle mass flux onto the isothermal rod
N_{th}	particle mass flux onto the heated rod
Nu	Nusselt number
N_0	particle mass flux in the wall region
P	perimeter of the test surface
P_i	individual reading of the fluorimeter
Pr	Prandtl number
P_1	function notation
P_1	function notation
p	gas pressure or rib pitch
Q	heat transfer per unit area
Q_1	function notation
q^o	heat generation per unit volume of the test surface
$\mathcal{R}$	specific gas constant
R^*	dimensionless hydraulic radius of the channel
Re	flow Reynolds number
r	radius in flow or fuel pin radius
r_e	coefficient of restitution
r_m	radius of maximum velocity
r_p	particle radius
r^*	dimensionless radius in flow
r_p^*	dimensionless particle radius

r_1	inside radius of the channel
r_2	outside radius of the channel
Sc	Schmidt number
Sh	Sherwood number
St	Stanton number for the ribbed rod
St_s	Stanton number for the smooth rod
s	stopping distance
s^*	dimensionless stopping distance
T	absolute gas temperature
T_a	air flow temperature
T_c	fuel clad temperature
T_g	gas temperature
T_s	surface temperature
T_0	mean gas temperature in the vicinity of the particle
T_ℓ	temperature at the laminar sub-layer
t	time required for particle displacement
U	flow mean velocity
U_1	fluid velocity at the axis of the pipe or free stream velocity
u	instantaneous velocity
u_E	equilibrium velocity of particles towards the surface
u^*	dimensionless instantaneous velocity
u_E^*	dimensionless equilibrium velocity of particles
u_*	shear velocity
V	deposition velocity of particles
V_i	incident velocity of particle
$V_{i.c}$	critical incident velocity of particle
V_o	deposition velocity of particles onto the isothermal rod

V_r velocity of particle at the rebound

V_s terminal settling velocity

V_T velocity of thermophoresis

V_{th} deposition velocity of particles onto the heated rod

V_0 normal incident velocity of particle

V^* dimensionless deposition velocity

V_0^* dimensionless deposition velocity without thermophoresis

V_T^* dimensionless velocity of thermophoresis

V_{th}^* dimensionless deposition velocity with thermophoresis

V_0^* dimensionless incident velocity of particle

v_B r.m.s. fluctuating velocity of particle due to Brownian motion

v_t free flight particle velocity

v' r.m.s. radial air velocity

v_B^* dimensionless component due to Brownian motion of the particle

v_f^* dimensionless component due to the normal motion of fluid

v_t^* dimensionless free flight particle velocity

v'^* dimensionless r.m.s. radial air velocity

v_Δ^* dimensionless radial fluctuation of velocity at distance Δ^*

X characteristic length of the flow or function notation

X_1 function notation

X^2 mean square displacement of particles

x distance along the surface

Y function notation

Y_1 function notation

y normal distance from the surface

y_T normal distance measured above the crests of the ribbed rod

y_d diffusion layer thickness

y_0	roughness length
y^*	dimensionless normal distance from the surface
y_d^*	dimensionless diffusion layer thickness
y_1^*	dimensionless distance normal to the surface at which $c \to 0$
y_0^*	dimensionless roughness length
Z	function notation
Z_0	equilibrium separation of sphere
α	accommodation coefficient or coefficient of thermal reflection or scaling factor of surface roughness
β	function notation or scaling factor of the temperature gradient
γ	function notation
Δ	capture distance of particle onto rough surface
Δp	pressure difference between Preston tube and static pressure
$\Delta u / u_*$	roughness function
Δ^*	dimensionless capture distance of particle
δ	boundary layer thickness
ε	fluid eddy diffusivity
ε_p	particle eddy diffusivity
ε_0	distance below the crests of origin of the logarithmic asymptote
θ	temperature difference $(T_s - T_a)$
λ	mean free path of gas molecules
μ	dynamic viscosity of the fluid
ν	kinematic viscosity of the fluid
ρ	fluid density
ρ_p	particle density
σ	standard deviation of the fluorimetric readings
σ	standard deviation of the mean

σ_g geometric standard deviation

σ_k standard deviation of average height of pipe surface roughness

τ particle relaxation time

τ_0 wall shear stress

τ^* dimensionless particle relaxation time

ϕ function notation

ϕ_1 function notation

ϕ^* function notation

∇T temperature gradient in the gas

$\sum n$ total number of particles in the observations

CHAPTER 1

INTRODUCTION

§1.1. Preamble :

Aerosol deposition onto surfaces is encountered in several industrial situations including spray dryers, atomisers, liquid fuel combustion chambers, gas cleaning, atmospheric pollution, and more recently and of particular concern to this project, in nuclear reactors.

The reactor is that part of a nuclear power plant where the energy is produced from the fission process. An atom, on absorbing a neutron, becomes unstable and splits into fragments. Some of the matter in the original atom disappears in the process and is converted into heat and other radiant energy. This heat is used to produce the power of the plant.

The core of the reactor is essentially an assembly of fuel elements, control rods, coolant and moderator. The fuel elements contain the Uranium fuel. Spaces are provided between the individual fuel elements to allow for passage of the coolant. The coolant, which can be a gas, water or organic liquid material, removes the heat produced in the fuel elements. The moderator, commonly water or graphite, is dispersed between the fuel assemblies. It serves to slow down or moderate the fast neutrons produced in fission. The lower velocities provides a better opportunity for the neutrons to cause further fission. The control rods are made of a neutron absorbing material and upon

movement in or out of the core, vary the number of neutrons available to maintain the chain reaction, therefore, the rate of fission can be controlled.

One of the unusual features of the nuclear reactor is that there is no theoretical upper limit to the rate of energy release due to the fission process. In practice, however, the maximum power level of a reactor is normally determined by the rate at which energy can be removed. The heat transfer from the fuel elements to the coolant can be improved by increasing the coolant area and/or the coolant channel volume. The addition of a coolant to the core to increase the heat removed disturbs the nuclear characteristics of the core and since the coolant can absorb neutrons and possibly becomes radioactive, it is highly desirable to keep the volume of the coolant to a minimum. In the interest of minimising pumping costs, a high velocity coolant flow is also undesirable.

§1.2. Advanced Gas-Cooled Nuclear Reactor :

In the advanced Gas-Cooled Nuclear Reactor (AGR) the fuel is contained in small diameter fuel rods which are held, approximately, equispaced in circular channels within the core of the reactor. The surface of these rods are machined to produce transverse ribs closely spaced along the length of the rod. The purpose of the ribs is to increase the heat transfer from the surface of the fuel rods by generating turbulence near the surface which destroys the structure of the boundary layer and prevents the formation of the viscous sub-layer.

The shape, size and spacing of these ribs is important. After extensive experimental work by Wilkie, [1], a pitch to height ratio of 7.2 has been chosen for the AGR fuel element rods. Fig. 1.1 shows a flow channel configuration in which 36 ribbed fuel rods are contained within a graphite sleeve. This configuration is used in commercial nuclear reactors in the U.K. The obvious drawback of this roughening is that it also increase the surface friction factor, and hence the pumping costs.

The coolant used in the experimental Windscale AGR nuclear reactor is carbon dioxide gas and the moderator is graphite. The coolant leaves the reactor at about 600°C and 19.6 bar. Fig. 1.2 shows the typical distribution of clad surface temperature and the coolant temperature along the fuel rods [2].

§1.3. Carbon Deposition in the AGR :

Carbon deposition has been observed in the AGR on the cladding of the fuel elements and on the fuel sleeves, Fig. 1.1. Two distinct types of deposit have been noted, the first at about 630°C clad temperature known as low temperature deposit (LTD) and the second about 700°C clad temperature known as high temperature deposit (HTD).

It was proposed that the low temperature deposit was produced by the following mechanism [3]:

(i) Circuit materials generated iron carbonyl $(Fe(CO)_5)$
    and possibly some nickel carbonyl $(Ni(CO)_4)$.

(ii) The carbonyls are rapidly destroyed in the hot gas and lead to formation of fine metallic particles.

3

(iii) The fine metallic particles act as centres for the condensation of a long lived product of the radiolysis of methane in the space under the core.

(iv) The particles of about 0.2 μm diameter, or small aggregates of them, are deposited onto the fuel elements by eddy-diffusion impaction resisted by thermophoretic forces.

(v) The particulate deposition may be subject to re-entrainment in high flow channels where turbulent bursts take place and possibly overcome the particle-surface adhesive forces.

In the event of the spaces between the roughness elements being filled by the deposit, the beneficial effects of roughening are soon lost. There are two reasons for this: firstly, the material forms an insulating layer and secondly, the level of turbulence in the flow is reduced as the surface becomes more smooth.

§1.4. The present work :

The aim of the work reported in this thesis is to study the deposition of sub-micron particles onto an AGR fuel rod surface. This study has been approached from two directions: firstly, by developing a theoretical model to describe the particle deposition process. This has required a determination of the mechanisms which contribute to the deposition process and a review of some aspects of particle behaviour such as collision with the surface and re-entrainment. Secondly, an experimental study has been carried out in the laboratory to obtain data to complement the theoretical approach.

The experimental work has involved the use of an air pipe flow rig into which sub-micron aerosols were injected. The procedure of the experimental work took the following steps:

a- Calibration of the particle generator to produce particles with diameters, of 0.25 and 0.05 μm. These were considered to be particiulary sensitive to thermophoretic effects.

b- Establishment of the aerodynamic performance of the pipe flow rig by means of a hot wire anemometer to measure the velocity and turbulence intensity of the flow through the channel. The skin friction factor for a smooth surface was determined by using Clauser's technique, [4], and by Preston tube measurement, [5]. The technique of Perry and Joubert, [6], was used to determine the friction factor for the regular ribbed surface.

c- To assess the effect of thermophoresis over the ribbed and the smooth surfaces, both were heated. The technique used was that of electrical resistance heating. The tie rod which was used to assemble the sections of the test rod was heated and three temperature distributions for both smooth and ribbed surfaces were considered at constant flow conditions.

d- Deposition tests were carried out to obtain a complete picture of the effect of the variable parameters, i.e. the surface roughness, the surface temperature, the flow Reynolds number and the particle diameter.

§1.5. Aerosol Particle Generation, Size Control
and Sampling

§1.5.1. Choice of particle material :

The simulation of any deposition phenomena in the laboratory requires that particles be generated at a constant rate and with a controlled size distribution. Then they have to be injected into the air stream, from which they will deposit onto the test surface.

The generator must have the ability to produce particles at a sufficient rate and in steady state conditions during the experiment. Also it must be easy to work with and be economical.

There are also some technical, economical and health considerations for choosing the material of the particles. Firstly, it must be dissolved easily in pure water. Secondly, the particles after the deposition process, must be stable from the physical and chemical point of view. The material must not react with the surface or be absorbed by it. Thirdly, during the preparation it may be dispersed into the air, therefore, it must not be toxic or radio-active or harmful. Finally, it must be available in any required amount.

Wohers et al., [7], and Whilby et al., [8], discussed the advantages and disadvantages of some suitable materials from the technical and economical point of view. It was concluded that a suitable material would be the fluorescent dye sodium derivative of fluorescein which is known technically as uranin.

This material has already been used in the simulation of fog droplet deposition onto a low-pressure steam turbine blade , [9 - 13], and it was therefore decided to use uranin for the simulation of particle deposition in the nuclear reactor.

The sub-micron particles have a very minute mass and even after the deposition process onto the surface, the accumulated mass is still very small. Therefore a very sensitive technique for tracing and detection is required. A sensitive and efficient technique to achieve this purpose is fluorimetric analysis which is already available in the laboratory of the Mechanical Engineering Department at the University of Liverpool.

§1.5.2. Generation of particles by condensation methods :

The particles could be generated by either of two main methods which are condensation or dispersion. In the condensation process clusters of molecules come together to build up particles of colloidal dimensions. In dispersion methods a substance initially in bulk or in a state of relatively course sub-division is further split up into fine particles.

The conditions necessary for the formation of uncoagulated aerosols are more complicated in condensation processes. Evidently, the formation of all aerosol particles should occur under completely identical conditions, in particular, the supersaturation should be the same over the whole volume where condensation takes place. When conventional methods of generation of condensation aerosol are used, for example, by cooling a hot vapour-gas mixture in a heat exchanger, or by mixing it with a cold gas, differences in the degree of supersaturation at

7

different points in the gas stream are inevitable and affect adversely the monodispersity of the aerosols formed. More details about the condensation methods are discussed by Fuchs and Sutugin, [14], and by Green and Lane, [15].

§1.5.3. Generation of monodisperse aerosol by dispersion methods :

The widely differing dispersion methods of generating monodisperse aerosols can be divided into the following three groups:

- a- Atomisation of liquids.
- b- Atomisation of solutions.
- a- Dispersion of powders.

a- Atomisation of liquids:

The principle of atomisation is that under the action of hydraulic pressure or a centrifugal or aerodynamic force, the liquid is drawn into narrow ligaments or films which subsequently disintegrate into droplets under action of surface tension. The mean sizes of these droplets generated by these methods are greater than 1 μm diameter. For the present study it is solid aerosols that are required.

b- Atomisation of solutions.:

If the liquid in the previous method is replaced by a solution of substance, solid particles can be produced by subsequently drying the mist of the atomiser output. The main control of the particle size would be achieved by altering the strength of the solution. Some of these methods and the corresponding apparatus are as follows:

1- Atomiser-impactor:

The principle of this technique has been developed by Whitby et al., [8]. The main idea is that smaller aerosols having narrower size distribution could be obtained by using impacting surfaces with the atomiser. Standard British Collison atomisers were used with a sharp cut-off impactor and moderately homogeneous aerosols were obtained having mass-medium diameters in the range of 0.01 μm to 1.0 μm with geometric standard deviations (σ_g) < 1.5. The diameter of the particles produced can be controlled by changing the solution strength, and/or the gap of the impactor plate, and/or the pressure of the compressed air.

This technique has already been used successfully by a number of investigators, [9 - 13], and it was used in the present work with some changes in the atomiser dimensions to suit experimental conditions.

2- Spinning Disc Atomiser:

To extend the range of the particle diameters produced, another method of atomisation can be used, which is the spinning disc atomiser, in which homogeneous particles can be obtained over the size range from about 0.5 to 30 μm with a geometric standard deviation of σ_g < 1.1. Three models of this technique were developed by Whitby et al., [8].

The atomisation is achieved by a continuous slow feeding of the solution onto the centre of a sharp-edged, rotating disc. The solution is spun off as a mixture of primary homogeneous droplets, $\sigma_g \simeq 1.1$ and moderately homogeneous followers, $\sigma_g = 1.8$. The followers have

a particle size of about one-fourth that of the primary droplets, and are several times more numerous. Consequently, after separation and evaporation, either the primary or the followers may be used as an aerosol.

Particle size could be controlled by altering the solution strength, and/or the feed rate, and/or the disc size and its speed.

3- Vibrating Orifice monodisperse aerosols generator:

This technique was designed by Bergland and Liu, [16], by which monodisperse aerosols of a size from approximately 0.5 to 50 µm diameter could be produced with an average geometric standard deviation about 1.0. The particle diameter is calculable from the generator operating conditions. A brief summary of this generator and its parts, and operating condition was described by El-Shobokshy, [11].

c- Dispersion of powders:

Powders with any required degree of dispersity could be prepared depending on the spending of time and costs. The main disadvantages of this method are the great difficulty for dispersing particles less than 1 µm and the presence of moisture in the powders impairs their dispersion considerably.

§1.5.4. The particle generator :

Making a comparison between the previous aerosol generation methods, it can be concluded that the most simple and suitable one for studying the deposition of sub-micron particles is the atomiser-impactor developed by Whitby et al., [8]. Full details of the atomiser-impactors, their operating conditions and arrangements were given by Parker and Ryley, [9], and by Parker and Lee, [10].

It was found necessary to modify the original atomiser by increasing the distance between the inlet of the solution and the outlet of the spray to investigate the time dependance in the experimental work. Also four atomiser units were used with two impactor plates assemblies to increase the final output produced from the generator. After much trial and error, it was found necessary to adjust the impactor plate gap to be equal to 1.8 mm.

The main side-effect of the atomisation process is that the droplets produced are electrically charged. This electric charge will be conserved while the droplet evaporates until it becomes a small particle having a high charge-mass ratio, which has a considerable effect on the deposition process. To overcome this problem an ion generator, described by Whitby, [17], was used. The ion generator produces a highly concentrated sonic jet of positive and negative ions, which are mixed with the aerosol cloud from the atomiser-impactor and, therefore, the electrical charges resulting from atomisation process are neutralised.

The cloud then, passes through a holding chamber, (see Fig. 4.1) in which the cloud is held for a short time to allow charge equilibrium to be established, and the evaporation process to be completed. From the holding chamber, the particles were injected into the main inlet box of the wind tunnel through a 4.0 cm delivery pipe. A two-way valve was fixed between the holding chamber and the inlet box, so that the particles could either be injected into the inlet box or ejected from the laboratory.

§1.5.5. Particle size Measurement :

There are many methods for particle size measurement. The general classification of these methods depends on the technique used in the measurement. Al-Azzawy, [13], gave a short summary of some of these methods. After reviewing these methods, the technique of Electron Microscopy was found to be the most suitable and useful one for the range of particles which were produced for this simulation study, especially since it is applicable to particle sizes from about 0.001 to 10 µm.

This technique has been successfully used by previous investigators in different ways. Parker and Ryley, [9], obtained the samples by passing the aerosol cloud over 3mm diameter electron microscope grids covered with a thin support membrane of Collodion. Parker and Lee, [10], drew the sample iso-kinetically and passed it through a "Millipore" filter (0.01 µm pore-size), then the filter was shadowed with gold palladium followed by a coating of carbon. The central part of the filter was then sub-divided into 1 mm squares and the cellulose ester dissolved away in acetone leaving the carbon layer carrying the particles floating on the acetone surface. Finally the carbon layer was picked up by the microscope grids and left to dry to be ready for electron microscopy.

El-Shobokshy, [11], prepared the samples by collecting the aerosol particles on a 75 mm × 25 mm glass slide, which had been coated with a thin layer of hard grade carbon, by evaporation, and a small amount (about 1 mg) of paraffin wax to ease the removal of the carbon film. The samples were obtained by placing the glass slide axially in the

aerosol output pipe at a position between the holding chamber and the point of injection into the tunnel. A shadow process was used after that to improve the appearance of the particles under the microscope and to give the third dimension of the particle. The carbon film was taken off by dipping the glass slide at an angle, gradually into a petri-dish containing some de-ionized water. Sections of the film were then caught on 3 mm diameter electron microscope grids using very fine tweezers. The grids were left to dry and then taken to the electron microscope for analysis. The same technique was used by Davies, [12], and Al-Azzawi, [13].

The procedure used in the present work is summarised as follows:

The glass slide, 75 mm × 25 mm, is washed by tap water with a detergent, then washed again by boiling in de-ionized water, finally it is cleaned using ultrasonic apparatus. Before placing the slide axially in the pipe from the holding chamber, it is cleaned again by an air jet to insure that it becomes completely free of dust.

Starting with the operating condition recommended by El-Shobokshy, [11], the atomiser-impactor was calibrated using the scanning microscope. After collecting the aerosol on the slide, the slide was coated by gold and then examined using the scanning electron microscope. After many attempts, the operating conditions which gave the required particle sizes were found so that the pressure of the air to the atomiser was at 40 psi ≃ 2.8 bar, while the air to the ion generator was at 30 psi ≃ 2.0 bar and the gap of the impactor plates were 1.8 mm. These air pressures are the same as those re- commended by Whitby et al., [8].

Due to the limitations of the scanning microscope, a transmission microscope was used to get a better image of the particles. For this microscope, the particles are collected on the glass slide and after that, the shadowing process takes place using a platinum wire before the coating process with carbon. The shadowing and coating processes were described in detail by El-Shobokshy, [11].

The carbon film is cut into small squares (less than 3 mm × 3 mm), then the slide is dipped gradually into a petri-dish containing de-ionised water, the squares of carbon film lift from the slide and float on the water surface. The carbon squares are transferred to another dish containing de-ionized water to ensure that all particles are dissolved from the film which now contain the impression of the particles. This process is called a "replication process". Finally the squares are picked up by a microscope grid using very fine tweezer and left to dry for electron microscope analysis. Two photographs show the particles produced from 5 percent and 0.2 percent of uranin solutions in plates 1 and 2 respectively.

§1.5.6. Statistical analysis :

The particles produced by the atomiser-impactor generator are moderately monodispersed. It is necessary to use a statistical method to calculate the degree of particle dispersion by determining the mean diameter and the geometric standard deviation. Statistical methods give several kinds of the mean diameter, such as arithmetic, geometric, number, surface-volume and mass-median. Among these kinds, the mass-median diameter is of most interest since it is the mass of the particles which influence the deposition process. The mass-median

diameter is the diameter which divides the mass contained in the samples into two equal parts.

Distributions of polydispersed particles are not in a normal (Gausian) form. The curves are usually right skewed, increasing rapidly at the lower-size and decreasing gradually at the larger-size.

Drinker, [18], and Loveland and Trivelli, [19], have shown that the asymmetrical or skewed frequency curves of ploydispersed particles can, in general, be transformed into symmetrical curves following the normal probability curves, when the logarithms of the sizes are substituted for the sizes themselves. In this case, the geometric mean diameter is a measure of the particle size, and larger and smaller particles will be distributed equally about its value.

The equation of the log-normal probability curve may be expressed in the following form:

$$f(d) = \frac{\sum n_i}{\sqrt{2\pi} \ln \sigma_g} \exp\left\{ - \frac{(\ln d - \ln dg)^2}{2 \ln^2 \sigma_g} \right\} \qquad (1.1)$$

where $f(d)$ is the frequency of the particles observations with diameter d, $\sum n$ the total number of the particles, d_g is the geometric mean diameter defined by:

$$\log d_g = \frac{\sum n_i \log d}{\sum n_i} \qquad (1.2)$$

and σ_g is the geometric standard deviation given by:

15

$$\log \sigma_g = \sqrt{\frac{\sum n_i (\log d - \log dg)^2}{\sum n_i}} \qquad (1.3)$$

The size of the particles were obtained from the photograph taken by the microscope, by a simple and convenient method. Using a transparent plastic circular template provided with holes having diameters from 1 mm to 10 mm, each photograph was scanned and the particles counted and assessed by comparison with the holes. The actual size range was determined by dividing the observed range in millimetres by the magnification of the photograph.

If the cumulative percentage of number and mass of the particles up to various stated sizes are plotted against the diameter on a logarithmic-probability paper, straight lines should theoretically be obtained for each case. The scale of ordinates is graduated according to a normal probability distribution, while the abscissae is logarithmic as shown in figures 1.3 and 1.4.

The geometric mean diameter can be obtained by reading the diameter corresponding to the intersection of 50 percent on the probability scale with the number line, while the mass-median diameter can be obtained by reading the diameter corresponding to the intersection of 50 percent on the probability scale with the mass line, as shown in figures 1.3 and 1.4.

Table 1.1 shows the analysis performed for particles produced from 5 percent of uranin solution. The "number line" is plotted using the values in columns 2 and 6 from table 1.1, while the "mass line" is plotted using the values of the columns 2 and 11 from the same table.

The geometric standard deviation can be obtained from the same graph by reading the values of number diameters corresponding to the probability of 84.13 and 50 percent respectively, and substituting in the following formula:

$$\sigma_g = \frac{84.13 \text{ percent size}}{50 \text{ percent size}} \qquad (1.4)$$

Hatch and Choate, [21], considered the frequency of particles between two diameter d_1 and d_2 as differing infinitesimally according to the equation:

$$f(d) = \frac{\Sigma \ n_i}{\sqrt{2\pi} \ \ln \sigma_g} \ \exp\{ - \frac{(\ln d - \ln dg)^2}{2 \ \ln^2 \sigma_g} \} \times \ln \frac{d_2}{d_1} \qquad (1.5)$$

and derived a simple mathematical expressions for the arithmetic mean diameter and the mass-median diameter, as a function of geometric mean diameter and geometric standard deviation, in the following form:

$$\log d_m = \log d_g + 1.51 \log^2 \sigma_g \qquad (1.6)$$

$$\log d_{mm}^{\ 3} = \log d_g^{\ 3} + 10.363 \log^2 \sigma_g \qquad (1.7)$$

where d_m is the arithmetic mean diameter, and d_{mm} is the mass-median diameter. The calculation of particle characteristics are shown in Appendix A according to Hatch-Choate equation.

The Gaussian frequency distribution has been plotted in figures 1.5 and 1.6 using the values of columns 1 and 3 from table 1.2 and 1.4 respectively. values of columns 1 and 5 could also be used to

17

plot cumulative percentage number on a logarithmic-probability paper to get the geometric mean diameter and evaluate the geometric standard deviation.

The previous analysis was carried out for the particles produced from 5 percent and 0.2 percent of uranin solutions.

CHAPTER 2

GENERAL SURVEY

§2.1. Deposition Mechanisms

In turbulent fluid flow contaminated with particles, the particles are transported rapidly through the turbulent core into the buffer region by eddy diffusion. The overall deposition rate, however, is governed by the mechanism by which the particles penetrate the laminar sub-layer, since there the eddy diffusion coefficient becomes negligible.

For small particles the final penetration is by Brownian diffusion. This was confirmed by Wells and Chamberlain, [22], who showed that for sub-micron particles the mass transfer coefficient versus Schmidt number relationship fell on the same straight line as that obtained for molecular sizes.

As the particle size increases, the Brownian diffusion coefficient reduces, and so does the deposition rate. However, the inertia of a particle increases with the size, and hence, provided the particle is projected towards the surface with sufficient velocity, its inertia will allow it to coast through the laminar sub-layer. In this inertial regime, as Friedlander and Johnstone, [23], first showed, the deposition rate increases with the particle size.

In fact, Lui and Agrawal, [24], showed that the transfer coefficient changes fairly abruptly to a slow falling value with respect to particle size. This is because as the particle size increases, the inertia becomes so large that the particles cannot attain the eddy velocity during the time they are caught up by an eddy and, in consequence, the deposition rate falls more and more rapidly. The previous description is shown in Fig. 2.1 after Gardner, [25].

The deposition rate of particles from turbulent flowing fluid to a solid boundary is often presented, for both prediction and experimental results, in a nondimensional form

$$V^* = f\,(\tau^*) \tag{2.1}$$

where $V^* = V/u_*$ is the deposition velocity non-dimensionalised relative to the fluid friction velocity u_* where $u_* = \sqrt{\tau_0/\rho}$ is the fluid shear stress at the solid boundary and ρ is the fluid density.

The deposition velocity is the particle mass transfer rate, N divided by the mean or bulk concentration of particles c_0 in the flow.

$$V = \frac{N}{c_0} \tag{2.2}$$

The independent variable, τ is the relaxation time for particles subject to aerodynamic resistance in the Stokes drag regime, i.e. where the Reynolds number based on the particle diameter is of order unity or less, and is given by:

$$\tau = \frac{\rho_p \, d_p^{\,2}}{18 \, \mu} \qquad (2.3)$$

It is made dimensionless as

$$\tau^* = \tau \, \frac{u_*^2}{\nu} = \frac{1}{18} \, \frac{\rho_p}{\rho} \, \left(\frac{d_p \, u_*}{\nu}\right)^2 \qquad (2.4)$$

where ρ_p and d_p are the particle density and diameter respectively, μ and ν are respectively the fluid dynamic and kinematic viscosity. This implies the assumption of spherical particles, but for other shapes it is usually possible to assign an effective spherical diameter.

If V^* is plotted as a function of τ^* the results fall into three deposition regimes as the classification according to the particle size.

For very small particles ($\tau^* \leq 1$) Brownian diffusion becomes significant and deposition is effected by a combination of Brownian and eddy diffusion. The theory proposed for this regime by Davies, [26], gives

$$V^* = \frac{(D/\nu)^{2/3}}{14.5 \left[\dfrac{1}{6} \ln \dfrac{(1+\phi)^2}{1+\phi+\phi^2} + \dfrac{1}{\sqrt{3}} \tan^{-1} \dfrac{2\phi-1}{\sqrt{3}} + \dfrac{\pi}{6\sqrt{3}} \right]} \qquad (2.5)$$

where $\phi = 1/[2.9(D/\nu)^{1/3}]$. The particle diffusivity, D can be given by the Einstein equation:

$$D = \frac{k_B \, T}{3 \, \pi \, \mu \, d_p} \qquad (2.6)$$

where k_B is Boltzman's constant (1.38×10^{-23} J/K) and T is the absolute gas temperature.

For $10^{-1} < \tau^* < 10$, which would represented particles 1 to 10 μm diameter in the case of common salt particles in air for example, the deposition follows a law termed the eddy diffusion-impaction regime by Gardner, [25].

It was proposed by Friedlander and Johnstone, [23], and Davies, [27], that the mechanism in this regime involved the particles acquiring velocities towards the surface induced by the turbulent eddies in the turbulent core and buffer layer, and then coasting across the viscous sub-layer to the surface as a result of their inertia (inertia coasting model).

Owen, [28], gave results of an analysis which was stated to be consistent with the concept of turbulent " bursts " which were observed by Kline et al., [29], to erupt sporadically from the viscous sub-layer. The particles would be carried to the wall in the " downward sweeps " of new fluid which follow the bursts. The law suggested by Owen is of the form

$$V^* = K_1 \, (\tau^*)^2 \qquad\qquad (2.7)$$

where K_1 is a constant. This expression agrees well with experimental data.

For $\tau^* \geq 10$, the results no longer follow the law of Owen, but tend to an almost constant value of being subject to a reduced rate of

transport across the turbulent core. This "particle inertia-moderate" regime has been considered by Hutchinson et al., [30], and by Reeks and Skyrme, [31].

§2.2. Mass Transfer Equation

The theoretical treatment has generally been based on the diffusion model in which the particle flux is expressed in terms of particle diffusivities and concentration gradient. Thus

$$N = (D + \varepsilon_p) \frac{dc}{dy} \qquad (2.8)$$

or in dimensionless form:

$$V^* = (\frac{D}{\nu} + \frac{\varepsilon_p}{\nu}) \frac{dc^*}{dy^*} \qquad (2.9)$$

where

$$V^* = \frac{V}{u_*} \quad ,$$

$$y^* = y \frac{u_*}{\nu} \quad ,$$

and

$$c^* = \frac{c}{c_0}$$

Friedlander and Johnstone, [23], were among the first to develop a major theory using this approach. They derived a free flight theory for particle deposition. The basic idea of their theory was that the turbulent eddies carry the particles in the radial direction in the pipe flow. These particles reach the region near the surface through tur-

bulent diffusion and are consequently projected through the relatively stagnant fluid next to the surface boundary independently of the fluid motion, having gained some specified initial velocity.

They introduced the concept of stopping distance: the distance a particle with a certain momentum will travel into the essentially laminar region with the help of the turbulent fluctuations. Thus the stopping distance, s, is given by

$$s = v_t \, \tau \tag{2.10}$$

and in dimensionless form it takes the form:

$$s^* = s \, \frac{u_*}{\nu} \tag{2.11}$$

The free flight particle velocity, v_t was assumed to be equal to the root mean square radial fluid velocity, for which they considered the experimental data of Laufer, [42], and assumed that it was independent of the position at which a particle was considered to start its free flight. In their analysis the assumed that $v_t^* = 0.9$ for all particle sizes.

Also Friedlander and Johnstone assumed that the turbulent diffusivity for the particles, ε_p is equal to that of the fluid, ε. The variation of ε/ν with the distance y from the surface was obtained for turbulent pipe flow by Lin et al., [33], for the viscous sub-layer and the buffer layer.

Considering the surface to be a perfect sink for the particles the final equations of their theory expressed in dimensionless form are:

$$\frac{1}{V^*} = \frac{1}{\sqrt{f/2}} + \frac{1525}{s^*} - 50.6 \qquad s^* < 5 \qquad (2.12)$$

$$\frac{1}{V^*} = \frac{1}{\sqrt{f/2}} - 13.75 + 5 \ln \frac{10.08}{s^* - 1.918} \qquad 5 \leqslant s^* \leqslant 30 \qquad (2.13)$$

$$\frac{1}{V^*} = \frac{1}{\sqrt{f/2}} \qquad s^* > 30 \qquad (2.14)$$

In this theory many original ideas were developed and it is widely used in design calculations even today. However, it has some deficiencies; such as:

i) It was implied that the free flight velocity starts at a distance $y^* = 80$ from the wall and the flow was assumed to be fully developed and turbulent. At that distance, the particles are still in the turbulent core and hence the constant value of v_t was unrealistic.

ii) The derivation of the deposition rate equation did not account for molecular particle diffusion.

iii) All the final equations of the theory are functions of the Fanning friction factor, f, suggesting that V^* increased with f. Hence V^* would be expected to increase as flow Reynolds number decreases, which is contrary to reality.

§2.3. Eddy Diffusivity

One of the basic assumption which Friedlander and Johnstone, [23], made was that the diffusivities of the particles and the fluid are identical. The turbulent eddy diffusivity, ε (which is an empirical parameter and, unlike other diffusivities, is a fluid property), varies

with the distance from the surface. According to Lin et al., [33], this variation follows different laws for the three parallel fluid layers with different turbulence characteristics, and is expressed in the following form:

$$\frac{\varepsilon}{\nu} = \left(\frac{y^*}{14.5}\right)^3 \qquad\qquad y^* \leqslant 5 \qquad (2.15)$$

$$\frac{\varepsilon}{\nu} = \frac{y^*}{5} - 0.959 \qquad\qquad 5 \leqslant y^* \leqslant 30 \qquad (2.16)$$

In the turbulent core, where $y^* > 30$, Friedlander and Johnstone, [23], used the Reynolds analogy, i.e. the mass flux divided by the concentration gradient is equal to the momentum flux divided by the velocity gradient. In symbolic form:

$$\frac{N}{(dc/dy)} = \frac{\tau_0 / \rho}{(du/dy)} \qquad\qquad (2.17)$$

Owen, [34], obtained the following expressions for the eddy diffusivity based on the data of Laufer, [32] :

$$\frac{\varepsilon}{\nu} = 0.001 \left(y^*\right)^3 \qquad\qquad 0 < y^* < 5 \qquad (2.18)$$

$$\frac{\varepsilon}{\nu} = 0.012 \left(y^* - 1.6\right)^2 \qquad\qquad 5 < y^* < 20 \qquad (2.19)$$

$$\frac{\varepsilon}{\nu} = 0.4 \left(y^* - 10\right) \qquad\qquad y^* > 20 \qquad (2.20)$$

Davies, [27], derived an empirical equation for the eddy diffusivity coefficient related to the distance from the tube surface in the following form:

$$\frac{\varepsilon}{\nu} = \frac{(y^*)^a}{10^3 \left(\frac{2.5 \times 10^7}{Re}\right)^b} \qquad (2.21)$$

where

$$a = 4.0 - (y^*)^{0.8}$$

$$b = \frac{y^*}{400 + y^*}$$

and is valid for

$$0.05 < y^* < 50000 \qquad\qquad Re = 10^6$$

$$0.05 < y^* < 500 \qquad\qquad Re = 10^4$$

Davies claimed that this equation gives values of turbulent eddy diffusivity close to those of the equations of Lin et al., [33], when y^* is small, and in agreement with the values of ε/ν calculated from the velocity measurements made by Laufer, [32], using hot wire anemometer over the ranges:

$$10 < y^* < 10000 \quad,$$

$$50000 < Re < 500$$

Davies questioned the validity of the assumption of Friedlander and Johnstone that the terminal velocity of the particle was constant. Within the laminar sub-layer it would rapidly decrease as the wall is approached. He represented the experimental data of Laufer, [32], for the r.m.s. radial air velocity by the expression:

27

$$v'^{*} = \frac{y^{*}}{10 + y^{*}} \qquad (2.22)$$

Thus Davies extended the concept by evaluating the terminal velocity v_t, at which the flight started, i.e. at $y = s + r_p$, which yields an implicit solution for the terminal velocity of the particle in the form:

$$v_t^{*} = \frac{1}{2}(1 - \frac{10 + r_p^{*}}{\tau^{*}}) + \sqrt{\frac{1}{4}(1 - \frac{10 + r_p^{*}}{\tau^{*}})^2 + \frac{r_p^{*}}{\tau^{*}}} \qquad (2.23)$$

Although the modified approach of Davies sounds logical, the resulting analysis and the experimental data showed a disagreement by at least two orders of magnitude for particles greater than 1.0 μm, but a quite good agreement for smaller particles. This fact has been remarked upon by Wells and Chamberlain, [22], and Beal, [35], although they compared Davies' theory with their own in which v_t^{*} was taken to be 0.9, the same as Friedlander and Johnstone.

Rouhiainen and Stachiewicz, [36], questioned the assumption that the particle diffusivity was the same as that of the fluid, and concluded that it is reasonable for sub-micron particles but becomes questionable for particle sizes for about 1 μm and is shown to be completely untenable for 30 μm particles.

Sehmel, [37], developed a theoretical model to describe effectively the turbulent deposition of particles by recalculating the particle eddy diffusivities and the free flight velocities from the available deposition data. He assumed that the particle transport is caused solely by effective eddy diffusivity, and correlated it as a function of y^{*} and τ^{*} as follows:

$$\frac{\varepsilon_p}{\nu} = 0.011 \, (y^*)^{1.1} \, (\tau^*)^{1.1} \qquad\qquad y^* < 20 \qquad\qquad (2.24)$$

$$\frac{\varepsilon_p}{\nu} = 0.4 \, y^* \qquad\qquad\qquad\qquad y^* > 20 \qquad\qquad (2.25)$$

and it *is* valid for vertical smooth surface for the range of

$$0.7 < d_p < 14 \quad \mu m$$

Also, he correlated the free flight velocity using a least squares method as:

$$v_t^* = 1.49 \, (\tau^*)^{-0.49} \tag{2.26}$$

The latter equation appears to contradict the intuitive idea that v_t^* should vary with τ^*, for as τ^* decreases one would expect the particle to detach itself from the eddy closer to the wall and consequently possess a smaller v_t^*.

Sehmel, [38], applied his method to horizontal duct flows considering the effect of gravity on the deposition and concluded that the effective particle diffusivity, ε_p/ν, to a horizontal smooth surface is greater than along a vertical one, and for both cases the particle effective eddy diffusivities are much greater than the air eddy diffusivity. Although Sehmel believed that these greater values of particle eddy diffusivities would reconcile the higher deposition velocities displayed by most authors, he also obtained with his limited experimental data the same scatter as before [12].

Liu and Ilori, [39], proposed a model for calculating the effective particle diffusivity, ε_p in the boundary layer of turbulent flow. Their model is based on the analogy between the diffusion of particles caused

by Brownian motion and that caused by fluid turbulence and calculated that:

$$\varepsilon_p = \varepsilon + v'^2 \tau \qquad (2.27)$$

where v' is the r.m.s. fluctuating velocity of the fluid in the direction normal to the wall and τ is the particle relaxation time. However, these differences seem to be important only in the particle inertia-moderated regime .

Kneen and Strauss, [40], made an analysis of the available theoretical and experimental results together with their correlations. It was concluded that the deposition rate of fine particles onto a smooth surface from a turbulent gas flow, in the absence of external forces acting on the particle, could be described by the equation in the following form:

$$V^* \propto (s^*)^2$$

where s^* is the dimensionless stopping distance.

They confirmed their predicted equation by experiments which indicated that the range of application was approximately from 0.5 to 50 μm particle diameter and the range of $0.3 < s^* < 8$. The corresponding ranges for other variables were not shown. To fit their scattered experimental results, they used the least squares criterion and expressed their predicted equation in the following form:

$$V^* = \frac{(s^*)^2}{2140} \qquad (2.28)$$

In an attempt to develop a comprehensive model to predict the deposition velocity in turbulent flow ranging from molecular size up to nearly 100 μm, Beal, [35], used equations(2.15), (2.16) and (2.17) with the assumption that the particle mass flux, N is varying linearly from the wall to the centre line of the channel or pipe,i.e.

$$N = N_0 \left(1 - \frac{2y}{d} \right) \tag{2.29}$$

where N_0 is the particle mass flux in the wall region.

He also postulated that the concentration at $y^* = s^* + r_p^*$ was not zero contrary to Friedlander and Johnstone's assumption. Considering that the radial velocity of particles consists of two parts, a component due to fluid motion normal to the wall and another due to Brownian motion of the particle itself, i.e.

$$v_t^* = v_f^* + v_B^* \tag{2.30}$$

Beal represented the first component from the data of Laufer, [32], by two straight lines:

$$v_f^* = 0.05 \, y^* \qquad\qquad 0 \leq y^* \leq 10 \qquad (2.31)$$
$$v_f^* = 0.5 + 0.0125 \, (y^* - 10) \qquad 10 \leq y^* \leq 30 \qquad (2.32)$$

and determined the Brownian motion velocity as

$$v_B^* = \left[\frac{k_B \, T}{2\pi m} \right]^{1/2} \Big/ u_* \tag{2.33}$$

Beal derived his model for three regions as follows:

$$0 \leq s^* \leq 5 ,$$

$$V^* = 14.5 \, Sc^{2/3} \, F(Sc,s^*) - \frac{(14.5)^2}{1.5 d_p^*} \, Sc^{1/3} \, G(Sc,s^*)$$

$$+ [5 + \frac{50}{Sc \, d_p^*} (1 - 0.959 \, Sc)] \, \ln(\frac{1 + 5.04 \, Sc}{1 + 0.04 \, Sc})$$

$$- \frac{250}{d_p^*} + \frac{1 - 13.73\sqrt{f/2}}{\sqrt{f/2}}]^{-1} \qquad (2.34)$$

$$5 \leq s^* \leq 30 ,$$

$$V^* = [5\{[1 + \frac{10}{Sc \, d_p^*} (1 - 0.959 \, Sc)] \, \ln \frac{1 + 5.04 \, Sc}{1 + Sc(\frac{s^*}{5} - 0.959)}$$

$$- \frac{10}{d_p^*}(6 - \frac{s^*}{5})\} + \frac{1 - 13.73\sqrt{f/2}}{\sqrt{f/2}}]^{-1} \qquad (2.35)$$

$$s^* \geq 30 ,$$

$$V^* = \frac{1}{1 - 13.73 \sqrt{f/2}} \qquad (2.36)$$

where

$$F(Sc,s^*) = \frac{1}{2} \, \ln \{ \frac{[1 + \frac{5}{14.5} \, Sc^{1/3}]^2}{1 - \frac{5}{14.5} \, Sc^{1/3} + (\frac{5}{14.5})^2 \, Sc^{2/3}} \}$$

$$- \frac{1}{2} \, \ln \{ \frac{[1 + \frac{s^*}{14.5} \, Sc^{1/3}]^2}{1 - \frac{s^*}{14.5} \, Sc^{1/3} + (\frac{s^*}{14.5})^2 \, Sc^{2/3}} \}$$

$$+ \sqrt{3} \, \tan^{-1} [\frac{\frac{10}{14.5} \, Sc^{1/3} - 1}{\sqrt{3}}]$$

$$- \sqrt{3} \, \tan^{-1} [\frac{\frac{2 s^*}{14.5} \, Sc^{1/3} - 1}{\sqrt{3}}]$$

and
$$G(Sc, s^*) = \frac{1}{2} \ln \left\{ \frac{1 - \frac{5}{14.5} Sc^{1/3} + (\frac{5}{14.5})^2 Sc^{2/3}}{[1 + \frac{5}{14.5} Sc^{1/3}]^2} \right\}$$

$$- \frac{1}{2} \ln \left\{ \frac{1 - \frac{s^*}{14.5} Sc^{1/3} + (\frac{s^*}{14.5})^2 Sc^{2/3}}{[1 + \frac{s^*}{14.5} Sc^{1/3}]^2} \right\}$$

$$+ \sqrt{3} \tan^{-1} \left[\frac{\frac{10}{14.5} Sc^{1/3} - 1}{\sqrt{3}} \right]$$

$$- \sqrt{3} \tan^{-1} \left[\frac{\frac{2 s^*}{14.5} Sc^{1/3} - 1}{\sqrt{3}} \right]$$

§2.4. Surface Roughness Considerations

Wells and Chamberlain, [22], and Chamberlain et al., [41], performed experimental deposition work onto both smooth and rough surfaces. Their results indicated that the deposition velocity was much greater for a rough surface than a smooth surface.

Browne, [42], was the first who developed a theoretical model in this subject taking into consideration the surface roughness effect. He presented a modification of Davies' approach to account for the surface roughness effect on the deposition of particles by adding extra distances to the particle-capture distance, $(s^* + r_p^*)$ and allowing for the displacement of the origin of the velocity profile resulting from the roughness, (Perry et al., [43], and Grass, [44]) to use the same equation for the radial velocity fluctuation.

33

He dealt with the friction velocity by using the empirical formula of Colebrook and White, [45], and expressed the equation of the deposition velocity in the form:

$$V^* = \cfrac{1}{\cfrac{1}{v_\Delta^*} + I}$$ (2.37)

where v_Δ^* is the radial fluctuation of velocity (dimensionless) at a distance Δ^* from the wall (dimensionless), (Δ is the new capture distance of the particle) and

$$I = \int_{\Delta^*}^{R^*} \cfrac{dy^*}{\cfrac{D}{v} + \cfrac{\varepsilon}{v}}$$ (2.38)

where R^* is the nondimension pipe radius. This integration is solved by using numerical analysis.

El-Shobokshy and Ismail, [46], derived a model of deposition onto rough surfaces similar to the one of Browne, [42]. They considered the effective particle eddy diffusivity as proposed by Liu and Ilori, [39], and used the equations of Lin et al., [3], for turbulent eddy diffusivity through the pipe. Also, they displayed a comparison between their model and the model of Browne. El-Shobokshy, [47], supported their model by experimental work covering a particle size range of 1.0 t0 6.2 µm.

In their model they examined, as Browne did, the effect of relative roughness, particle size, particle density and flow Reynolds number on the deposition velocity. It was concluded that the wall roughness has a large effect on the particle deposition velocity of a diameter less particles with

than 5 μm, this effect diminishes for particles of 10 μm, and for a given relative roughness and Reynolds number, the particle density has nearly no effect on deposition velocity of particles less than 0.1 μm in diameter.

Wood, [48], used the same idea of adding extra distances to the particle-capture distance and shifting the position of the origin of the velocity profile, but he used the approach of Lin et al., [33], by adopting their equations of the turbulent eddy diffusivity for the viscous sub-layer $(0 < y^* < 5)$ and the buffer layer $(5 < y^* < 30)$.

Wood put his model in the following expression:

$$V^* = \frac{1}{I_B + I_s} \tag{2.39}$$

where subscripts B and s represent the buffer and sub-layer respectively, and

$$I_B = \int_5^{30} \frac{dy^*}{\frac{D}{\nu} + \frac{\varepsilon}{\nu}}$$

$$I_s = \int_{\Delta^*}^{5} \frac{dy^*}{\frac{D}{\nu} + \frac{\varepsilon}{\nu}}$$

and if $\Delta^* > 5$, then $I_s = 0$ and

$$I_B = I_{B1} = \int_{\Delta^*}^{30} \frac{dy^*}{\frac{D}{\nu} + \frac{\varepsilon}{\nu}}$$

The analytical solution of Wood's equation are as follows:

$$I_s = \frac{14.5}{(\frac{D}{\nu})^{2/3}} [\ f(\phi) + g(\phi) - f(\phi_1) - g(\phi_1) \ ] \qquad (2.40)$$

where

$$f(\phi) = \frac{1}{6} \ln \frac{(1 + \phi)^2}{1 - \phi - \phi^2} \ ,$$

$$g(\phi) = \frac{1}{\sqrt{3}} \tan^{-1} (\frac{2\phi - 1}{\sqrt{3}}) \ ,$$

$$\phi = \frac{1}{2.9 \ (\frac{D}{\nu})^{1/3}} \ ,$$

and

$$\phi_1 = \frac{\Delta^*}{5} \ \phi$$

$$I_B = 24.2 \qquad\qquad \Delta^* < 5 \qquad\qquad (2.41)$$

$$I_{B1} = 5 \ln (\frac{25.2}{\Delta^* - 4.8}) \qquad\qquad \Delta^* \geq 5 \qquad\qquad (2.42)$$

Wood's theory has been restricted to roughness Reynolds number k^* less than approximately 5 by the use of the analytical expression of Lin et al. for eddy diffusivity. At the expense of the solutions obtained by Wood, Davies' universal expression of ε/ν for all values of y^*, used by Browne, could be adopted, necessitating a numerical solution. This expression displays a Reynolds number dependence.

Therefore, when the roughness is large, such that the concentration gradient occurs entirely within the turbulent core, the deposition velocity is a function of Reynolds number, as indicated by

Browne. The Reynolds number enters also through the limit of the integration.

Cleaver and Yates, [49], considered the suggestion of Owen, [28], and developed their model for deposition based on the idea that particles are convected to the wall by the "downsweeps" which have been described by Kline et al., [29]. They found after their analysis that

$$V^* = 0.084 \ Sc^{-2/3} \qquad\qquad (2.43)$$

which is similar to that equation expressed by Wells and Chamberlain, [22], i.e.

$$V^* = \frac{u_*}{U} \ Sc^{-2.3} \qquad\qquad (2.44)$$

Cleaver and Yates' model is critically dependent upon the exact form of the downsweeps and assumes that the solid surface is initially smooth, and remains, smooth.

Davies, [50], proposed a different theory with the postulate that the deposition occurs basically by particles being swept along the surface in the direction of flow until they impinge on roughness elements, which have been there either initially or have been produced by an early uneven deposition of some of the particles. The particles arrive in the region of the surface by a process of "jumping" across the streamlines in the laminar sub-layer.

Quantitatively, Davies, [51], deduced that for the deposition process when $\tau^* < 0.22$ for smooth surfaces

$$V^* = 0.075 \ Sc^{-2/3} \qquad (2.45)$$

while for rough surfaces

$$V^* = 0.08 \ Sc^{-1/2} \qquad (2.46)$$

and postulated that for $0.22 < \tau^* < 10$

$$V^* = C_1 \ \tau^* \ (1 + \tau^*) \ \frac{\rho}{\rho_p} \qquad (2.47)$$

where C_1 is a dimensionless constant related to the roughness geometry of the surface on which deposition is occurring. By fitting the above equation to published data for aerosol deposition onto polished brass, glass, aluminium and filter paper, Davies deduced values of C_1 ranging from 0.05 to 100.

A useful technique to calculate mass transfer rates between a solid boundary and a fluid is to draw an analogy with the rates of convective heat transfer under similar conditions. This technique is often known as the Chilton-Colburn analogy, or more simply, the Heat and Mass Transfer Analogy.

Kader and Yaglom, [52], used the available literature and expressed a correlation of deposition velocity for the case of two dimensional roughness elements, in the form:

$$\frac{1}{V^*} = 2.12\ln \ (\frac{X}{k_s}) + 3.2(k_s^*)^{1/4} \ (Sc^{2/3} + 0.3) + 4.0 \qquad (2.48)$$

where

X characteristic length of the flow,

k_s mean height of roughness element,

k_s^* dimensionless height of roughness element, $= (k_s u_*/\nu)$

and

Sc Schmidt number.

Hahn et al., [53], showed experimentally that the correlation of Kader and Yaglom can be used to predict rough wall deposition reasonably accurately for the entire range of particle from molecular size to 0.2 µm diameter and went to suggest that the equation can be further reduced such that the deposition velocity is given by

$$\frac{1}{V^*} = 3.2 \ (k_s^*)^{1/4} \ Sc^{2/3} \qquad\qquad (2.49)$$

Owen et al., [54], used the same technique and considered another empirical formulation for the convective heat transfer over a similar surface, (AGR fuel element surface), and described the mass transfer by convection:

$$Sh = 0.023 \ Re^{7/8} \ Sc^{1/3} \qquad\qquad (2.50)$$

where Sh is Sherwood number $= (\frac{V\ d_e}{D})$

Although a good agreement was shown between the two correlations and the results presented by Hahn et al., [33] Owen et al., [34], drew attention to an inherent weakness in this technique. It requires a complete similarity between the transport processes. For example,

the diffusivities of each should be of comparable magnitude. In the case of diffusing gases and vapours this is usually achieved. But in the case of sub-micron particles in gas streams, however, the ratio of Schmidt number to Prandtl number (Sc/Pr) can be of the order of 10^5 and such differences will result in the heat and mass transfer conditions changing by a factor of about 300.

Under circumstances such as these the heat and mass transfer analogy has to be applied with caution.

Considering the "Law-of-the wall" for the complete rough surface, where the friction factor is independent of the Reynolds number, Schack et al., [55], developed a general correlation for deposition of particles from a turbulent gas flow to a completely rough surface (where $k_s^* > 70$) in the following form:

$$Y = A X + B X^3 \tag{2.51}$$

where
$$Y = \frac{V d_p}{D}$$

$$X = \frac{d_p}{y_0} (y_0^*)^{1/2} Sc^{1/3}$$

y_0 called the roughness length, is the height at which the velocity $u(y)$ would vanish if the logarithmic form were actually valid up to the wall.

The two constants A and B depend on the shape and packing density of the roughness elements, and must be evaluated experimentally.

§2.5. External Forces Considerations

Taking into consideration the effect of additional external forces acting on the particles, Gardner, [25], derived a method for calculating the deposition velocity which he presented in two parts. The first concerns the diffusion and the eddy diffusion-impaction regimes with a superimposed equilibrium velocity u_E, which is the equilibrium velocity of a particle towards the surface obtained by a balance of viscous resistance to motion according to Stokes law and the external forces, say, thermophoretic, gravitational or electrostatic forces. The second concerns the turbulent impaction regime.

For the first part, He assumed that the particles have a velocity $(C_1 u_* + u_E)$ towards the surface at a distance $y^* = y_1^*$ from the surface, and this velocity decays to zero at $y^* = 0$ due to a Stokes law resistance. The assumption that part of the initial velocity is proportional to the friction velocity has been indicated by Owen, [28], to be compatible with the modern concept of turbulent bursts in the boundary layer.

Gardner assumed the expression of Lin et al., $[\varepsilon/\nu = (y^*/14.5)^3]$ for all stopping distances and expressed the deposition velocity in the following form:

$$V^* = \frac{u_E^*}{1 - (\frac{P_1}{Q_1})} \qquad (2.52)$$

with the assumption that the particle concentration at $y^* = y_1^*$ is sufficiently small to be equal to zero.

where

§2.5. External Forces Considerations

Taking into consideration the effect of additional external forces acting on the particles, Gardner, [25], derived a method for calculating the deposition velocity which he presented in two parts. The first concerns the diffusion and the eddy diffusion-impaction regimes with a superimposed equilibrium velocity u_E, which is the equilibrium velocity of a particle towards the surface obtained by a balance of viscous resistance to motion according to Stokes law and the external forces, say, thermophoretic, gravitational or electrostatic forces. The second concerns the turbulent impaction regime.

For the first part, He assumed that the particles have a velocity $(C_1 u_* + u_E)$ towards the surface at a distance $y^* = y_1^*$ from the surface, and this velocity decays to zero at $y^* = 0$ due to a Stokes law resistance. The assumption that part of the initial velocity is proportional to the friction velocity has been indicated by Owen, [28], to be compatible with the modern concept of turbulent bursts in the boundary layer.

Gardner assumed the expression of Lin et al., $[\varepsilon/\nu = (y^*/14.5)^3]$ for all stopping distances and expressed the deposition velocity in the following form:

$$V^* = \frac{u_E^*}{1 - (\frac{P_1}{Q_1})} \qquad (2.52)$$

with the assumption that the particle concentration at $y^* = y_1^*$ is sufficiently small to be equal to zero.

where

41

$$P_1 = \exp \left[\frac{\gamma}{\sqrt{3}} \tan^{-1} \left(\frac{2y_1^* - \beta}{\beta\sqrt{3}} - \frac{\pi}{2} \right) \right]$$

$$Q_1 = \left[\frac{(\beta + y_1^*)^2}{(\beta^2 - 2y_1^* + y_1^{*2})} \right]$$

$$\beta = 14.5 \left(\frac{D}{\nu} \right)^{1/3}$$

and

$$\gamma = \frac{\beta \, \nu \, u_E}{D}$$

He obtained the value of y_1^* by solving the equation of motion of particle in the boundary layer such that

$$y_1^* = \frac{C_1}{18} \left(\frac{\rho_p}{\rho} \right) (d_p^*)^2 \left[1 + \frac{u_E^*}{C_1} \right] \qquad (2.53)$$

The constant C_1 was chosen equal to 0.957 in agreement with the results of Liu and Agrawal, [24], for eddy diffusion-impaction regime.

§2.6. Thermophoresis

Thermophoresis is the term describing the phenomenon wherein particles such as soot particles, aerosols, dust or the like, when suspended in a gas in which there exists a temperature gradient, experience a force in the direction opposite to that gradient of temperature.

This phenomenon was first described by Tyndall, [56], who observed a dust free-zone in a dusty atmosphere around a hot body. The fundamental physical processes responsible for the phenomenon were first investigated by Maxwell, [57].

When the gas flow is contaminated with particles, an important non-dimensional parameter must be determined. This parameter is the Knudsen number, (Kn) which is defined as the ratio of the mean free path of gas molecules and the particle radius.

$$Kn = \frac{\lambda}{r_p} \qquad\qquad (2.54)$$

the mean free path the viscosity-based value is

$$\lambda = \frac{2\ \mu}{\rho\ \bar{c}} \qquad\qquad (2.55)$$

with $\bar{c} = \sqrt{(8\ \mathcal{R}T/\pi)}$, the mean molecular speed and $\mathcal{R}$ the specific gas constant.

Hidy and Brock, [58], introduced three regimes for the flow according to the values of $0 < Kn < \infty$:

a- For small values of Kn, the slip region is considered.

b- For $0.25 \leq Kn \leq 10$, it is defined by theoretical and experimental evidence as the transition region.

c- For $Kn > 10$, the free molecular regime is considered to describe the processes introducing only a small error.

§2.6.1 Theory of Thermophoresis

One of the earliest attempts to apply Maxwell's ideas to calculate the forces on spherical particles in a gas at rest in which there exists a temperature gradient is that introduced by Epstein, [59], who derived expressions for the thermophoretic force and the velocity acquired by the particle in the slip flow regime $(Kn \ll 1)$.

Epstein expressed the thermophoretic force in the from:

$$F_T = -9\pi\mu\nu r_p \frac{\nabla T}{T_0} \left(\frac{k_g}{k_p + 2k_g} \right)$$ (2.56)

and the corresponding thermophoretic velocity may be written as:

$$V_T = -\frac{3}{2}\nu \left(\frac{k_g}{k_p + 2k_g} \right) \frac{\nabla T}{T_0}$$ (2.57)

in which r_p is the particle radius, μ and ν are the gas dynamic and kinematic viscosities, T_0 the mean gas temperature in the vicinity of the particle, ∇T the temperature gradient in the gas and k_g and k_p the thermal conductivities of the gas and particle respectively.

Epstein's result has been found to be in reasonably good agreement with experiments for $Kn < 1$ for particles of low thermal conductivity such that $[(k_g/k_p) \sim 1]$. however it significantly underestimates the thermal force on particles of high thermal conductivity $(k_p \gg k_g)$.

A number of attempts have been made to improve upon the Epstien analysis in order to resolve the discrepancy between theory and experiment for high thermal conductivity particles.

A complete hydrodynamic analysis was first carried out by Brock, [60], who derived the velocity of thermophoresis for slip flow in the form:

$$V_T = -\frac{2 C_s \nu [(k_g/k_p) + C_t Kn] (\nabla T/T_0)}{(1 + 3C_m Kn) [1 + 2(k_g/k_p) + 2C_t Kn]}$$ (2.58)

where

44

C_s is the thermal slip coefficient,

C_m is the momentum exchange coefficient and

C_t is the thermal jump coefficient.

Brock chose reasonable values for C_m and C_t, the best kinetic theory values for complete accommodation appear to be C_m = 1.14 and C_t = 2.18, obtained by Loyalka and Ferziger, [61], and Loyalka, [62]. Brock also used the value C_s = 3/4, a value first obtained by Maxwell. However his results were found not to be in good agreement with experiment for particles of high thermal conductivity, although the discrepancy is much less than that obtained using Epstein's result.

More refined kinetic theory analysis by Ivchenkov and Yalamov, [63], yielded the result C_s = 1.17, for complete thermal accommodation, a value in substantial agreement with other kinetic theory analysis, [64].

Derjaguin and Yalamov, [65], claimed that there are two questionable points in the derivation of Maxwell's formula and, accordingly, in the work of Epstein and Brock:

1- The temperature stresses in the volume of the gas are neglected.

2- Use was made of a boundary condition, the derivation of which was based on the doubtful assumption that the gas molecules have the same velocity distribution before impacting the interface, as in the bulk of the gas.

However, a substantially different approach was developed by Derjaguin and Bakamov, [66], making allowance for the phenomena in

the bulk of gas and applying Onsager's principle. They derived the thermophretic velocity in the form:

$$V_T = - \frac{1}{2} \frac{\nu}{T_0} \left(\frac{8 \, k_g + k_p}{2 \, k_g + k_p} \right) \nabla T \qquad (2.59)$$

Derjaguin and Yalamov, [65], showed that when the temperature jump and the isothermal slip are taken into consideration, the thermophoretic velocity takes the following form:

$$V_T = - \frac{1}{2} \frac{\nu}{T_0} \frac{(8 \, k_g + k_p + 2 \, C_t \, k_p \, Kn)}{(2 \, k_g + k_p + 4 \, C_t \, k_p \, Kn)} \nabla T \qquad (2.60)$$

According to the comments of Byers and Calver, [67], Brock's equation, (2.58), was supported for slip flow regime, while Derjaguin and Yalamov, [65], gave overestimates of the thermal force by about 20 °/o , they suggested that the latter theory be adopted for quite large particles.

In the free molecular region the particle radius is very small with respect to the mean free path of the gas molecules. It has been considered that the particles have no effect on the velocity distribution of the gas molecules, and it has been assumed that this consideration is valid for Knudsen numbers greater than ten [68]. The forces acting on particles in this regime are coupled directly to non-uniformities in the suspending gas-gradients of concentration, temperature, etc. The free molecule theory for phoretic forces in a non-uniform gas has been treated by several workers. Perhaps best known are the calculation of Waldmann, [69], and those of Bakanov and Derjaguin, [70].

Waldmann, [69], obtained to a close approximation the following expression of the free-molecule thermal force, F_T^* for particles in monoatomic gases :

$$F_T^* = - \frac{32}{15} r_p^2 \left(\frac{k_g}{\bar{c}} \right) \nabla T \qquad (2.61)$$

where $\bar{c}$ is the mean molecular speed.

The particle thermal conductivity has become negligible in this equation, which is strictly valid when $r_p/\lambda \to 0$. However Jaccobsen and Brock, [71], claimed that comparison with experiments showed that it was not much in error for nonzero values of (r_p/λ). for example, it was in error by approximately $5^o/_o$ at $\lambda/r_p = 10$ and $10^o/_o$ at $\lambda/r_p = 5$.

The corresponding thermophoretic velocity was given by Waldmann and Schmidt, [72], and Hidy and Brock, [58], as:

$$V_T = - \frac{1}{5 \left(1 + \frac{\pi\alpha}{8} \right)} \frac{k_g}{p} \nabla T \qquad (2.62)$$

where p is the gas pressure and α is the coefficient of thermal reflection.

In the case of polyatomic gases, one should use the "translational" thermal conductivity, which in the simple kinetic theory is given by $(k_g = 15\mu \mathcal{R}/4)$ where μ is the dynamic gas viscosity and $\mathcal{R}$ is the specific gas constant [64].

Derjaguin and Balamov, [73], applied the method of calculation first suggested for diffusiophoresis, in which it was assumed that the ve-

locity distribution of the molecules impinging on a small particle is not disturbed by the presence of the later. Applying this to the thermophoresis of small particles, they derived the following formula for the velocity of thermophoresis:

$$V_T = - \frac{6}{a_1} \frac{\nu}{T_0} \nabla T \qquad (2.63)$$

in which a_1 is a constant equal to 8 on elastic rebound of molecules with diffuse scattering and on diffuse evaporation of the molecules from the surface, a_1 equals $8 + \pi$ [70].

In the transition region as collisions of gas molecules become important, the collisions have the effect of reducing the thermal force imparted by the gas molecules. Experimental studies of Schmitt, [74], and Schadt and Cadle, [75], of the thermal force in the transition region using the Millikan cell technique have found the following empirical relationship for the thermal force:

$$F_T = F_T^* \exp(- \frac{\tau}{Kn}) \qquad (2.64)$$

which is valid over the range $0 \le (r_p/\lambda) \le 5$.
Where

F_T^* is the free-molecule thermal force,

τ is a parameter for a particle aerosol system, and is independent on (r_p/λ) and observed experimentally.

$$\tau = f((k_g/k_p) , \alpha)$$

and

α   is accommodation coefficient.

Brock, [76], developed a theory of thermal force in the transition region based on that one of free molecule region. He expressed the thermal force for monatomic gases in the following form:

$$F_T = F_T^* \{1 - [0.06 + 0.09\alpha + 0.28\alpha(1 - \frac{\alpha k_g}{2k_p})] \frac{r_p}{\lambda} \} \qquad (2.65)$$

where F_T^* is the free molecule thermal force as mentioned before. It is seen that τ in equation (2.64) is a function of the thermal conductivity ratio (k_g/k_p) and the momentum accommodation coefficient α.

Talbot et al., [64], found that the theory of Brock, [60], with an improved value for the thermal slip coefficient, gave the best agreement with experiment for low Knudsen numbers, $Kn = O (10^{-1})$. Also they compared the available experimental data over a wide range of Knudsen numbers and proposed a fitting formula for the thermophoretic velocity useful over the entire range $0 \leq \lambda/r_p \leq \infty$ in the following form:

$$V_T = - \frac{2 C_s \nu [(k_g/k_p) + C_t Kn] C_c (\nabla T/T_0)}{(1 + 3C_m Kn) [1 + 2(k_g/k_p) + 2C_t Kn]} \qquad (2.66)$$

in which $C_s = 1.149$

and

C_c is the Cunningham correction factor expressed by

$$C_c = 1 + Kn[A + B \exp(-C/Kn)] \qquad (2.67)$$

where A,B and C are constant and usually take the values

A = 1.2

B = 0.41

C = 0.88

The calculated Knudsen numbers of the reactor and the experimental rig conditions are not the same and each one relates to a different region. For example Knudsen number along the fuel element in the reactor are in the range 0.05 to 0.08 which seem to be related to the slip flow region, but for the rig condition the Knudsen number in the range 0.6 to 2.26, which seem to be related to the transition region. For this reason the Talbot et al. fitting formula which was proposed for the entire range of Knudsen numbers is adopted to calculate the velocity of thermophoresis in the present theoretical work.

Kelly, [77], applied the model of Gardner, [25], to investigate the deposition of particles in the Windscale AGR channel taking into account the effect of the thermophoretic force, which was obtained from the expression of Talbot et al., [64]. He considered the temperature gradient to be the difference between the fuel clad temperature and the gas temperature divided by the laminar sub-layer thickness, and expressed the velocity of thermophoresis in the following form:

$$V_T^* = -1.2(\frac{k_g}{k_p} + Z)(\frac{T_c - T_g}{T_c + T_g}) \qquad (2.68)$$

and

$$Z = 5.03 \times 10^{-8}(\frac{T_c + T_g}{p\,d_p})$$

50

where p is the gas pressure in bar and T_c and T_g are the fuel clad temperature and the gas temperature respectively.

A more sensible treatment to calculate the temperature gradient has been derived by Im and Chung, [78], who considered it as the difference between the temperature of the gas at the laminar sub-layer and the temperature of the wall, divided by the laminar sub-layer thickness. Using the Reynolds analogy they obtained that difference in temperature as a function in the difference between the stream gas temperature and the surface temperature, i.e.

$$T_\ell - T_s = 5 \ (\sqrt{f}/2) \ (T_g - T_s) \tag{2.69}$$

CHAPTER 3

THEORETICAL APPROACH

§3.1 Introduction

The deposition of particles carried in a fluid stream onto a surface over which the stream is flowing, may be controlled by one or more of the following mechanisms:

1- molecular diffusion (Brownian diffusion),

2- turbulent diffusion (Eddy diffusion),

3- eddy diffusion-impaction,

4- inertial impaction,

5- sedimentation,

6- thermophoresis,

7- diffusiophoresis,

8- electric mobility.

The significant contribution of a certain mechanism in controlling the deposition process depends on various parameters, like the surface conditions, the fluid flow conditions as well as the particle diameter. For example, in the case of suspended particles in isothermal and stationary air, the sedimentation mechanism will control the deposition process. On the other hand, for particles suspended in air moving over a heated surfaces, the thermophoresis mechanism may have a greater contribution, and so on for the other mechanisms.

At the beginning of the study of the deposition of particles, it is important to determine the mechanisms which have a considerable effect on the deposition process. For the present study, the experiences of El-Shobokshy [11] and Davies [12] can be used. Also, it is convenient to review some factors which can effect on the deposition process.

§3.2 Particle-surface Collision Mechanisms

In the collision between projected particles and a surface, particles may be captured or there is a possibility of bouncing or re-entrainment. Dahneke, [79], in his study of the mechanism of particle-surface collision, found that there is a limiting value of incident velocity of the particle below which it can be expected that the particle will be captured by the surface and above which it will bounce. Dahneke assumed some conditions for his analysis, which are:

i) The viscous drag force near the surface is negligible,

ii) The particles are spherical and smooth,

iii) The surface is perfectly smooth, and

iv) The particles are projected normally to the surface.

§3.2.1 Critical Particle Incident Velocity

Considering the energies of particle before and after collision, Dahneke derived the critical incident velocity of particle in the following form:

$$V_{i.c} = \frac{1}{d_p} \sqrt{\frac{\bar{A} \left(1 - r_e^2 \right)}{\pi Z_o \rho_p r_e^2}} \tag{3.1}$$

where

$\bar{A}$ the Hamaker constant, is equal to 8×10^{-20} Joule for fluorescein particles,

53

r_e coefficient of restitution = V_i/V_r taken as 0.99,

V_i velocity of particles at incidence,

V_r velocity of particles at the rebound, and

Z_0 The equilibrium separation of sphere = 4 ^{o}A.

To test whether a particle will bounce or be captured upon touching the surface, the value of the velocity of particle at rebound (V_r) should compared with the value of critical incident velocity ($V_{i.c}$). If the particle rebounds with a velocity greater than $V_{i.c}$, then it will bounce, and if it rebounds with a velocity less than $V_{i.c}$, it will be captured.

§3.2.2 Normal Incident Velocity

According to Davies' theory, [26], which has been supported by Beal, [35], and used by Keen and Strauss, [40], for particles diameter less than 1 µm (the same range as this study) the normal velocity of the particle can be taken as the radial fluctuating velocity of the fluid flow near to the wall region. Davies correlated the experimental results of Laufer, [32], for the variation of the radial fluctuating velocity with the normal distance from the surface, in the following form:

$$v'^* = \frac{y^*}{10 + y^*} \qquad (3.2)$$

Considering the concept of the stopping distance, Davies derived the normal incident velocity of the particle as:

$$V_0^* = \frac{1}{2}(1 - \frac{10 + r_p^*}{\tau^*}) + \sqrt{\frac{1}{4}(1 - \frac{10 + r_p^*}{\tau^*})^2 + \frac{r_p^*}{\tau^*}} \qquad (3.3)$$

where

V_0^* dimensionless incidence velocity $= V_0/u_*$

V_0 normal incidence velocity

u_* shear velocity

r_p^* dimensionless particle radius $= r_p(u_*)^2/\nu$

τ^* dimensionless particle relaxation time $= \tau[(u_*)^2/\nu]$

τ particle relaxation time $= [\rho_p(d_p)^2/18\ \mu]$

ρ_p particle density $= 1700\ kg/m^3$, for Uranin particles, [16].

The derivations of equations (3.1) and (3.3) have been confirmed by El-Shabokshy, [11].

Although some authors have pointed out that the equation of Davies for normal incidence velocity is inaccurate for particles larger than 1.0 μm, it can be regarded as acceptable for the range of this study.

From equations (3.1) and (3.3) it can seen that $V_{i.c}$ depends on the particle diameter and its density, while V_0 also depends on the flow condition (shear velocity). Results of calculations of both equations for a set of flow condition which cover the expected range of the experimental work up to $u_* = 3.0$ m/s, are shown in Fig. 3.1.

The points of intersection of $V_{i.c}$ with the curves of V_0 determine the critical particle sizes for each flow condition (u_*). Below these points the particles will expected to be captured by the surface, while above them, the particles are most likely to rebound again.

The main conclusion from these results is that the range of sub-micron particles and flow conditions used in this study the particles will be captured on collision with the surface.

§3.3 Particle Re-entrainment

Based on the results of the particle-surface collision mechanism particles as large as 1 μm would be captured on collision with the surface for a flow friction velocity of 2 m/s. however the analysis of this mechanism considered only the energies of particles before and after collision without taking into account any consideration about the particles after their deposition. If the particles form any agglomerates over the test surface, they can be dislodged from it, depending on the flow condition and re-entrainment may possibly occur.

Most investigators consider the surface upon which particles would be deposited to be a "perfect sink", i.e. no removal of particles will occur. In experimental applications some workers of particle deposition have made the test surface sticky to avoid any possibility of re-entrainment. This is far from the real operating conditions.

In the present experimental work the natural rod surface, smooth or ribbed, was used to carry out the particle deposition test. It was therefore necessary to check whether or not there was re-entrainment during the experimental tests.

Corn and Silverman, [80], assumed that solid particle adhering to a surface will be removed when the drag and lift forces exceed the adhering force. For spherical particles the lift forces are negligible with respect to the drag forces, therefore the drag forces only would be compared with the adhering force. They concluded, experimentally that if the drag on a deposited particle is equal to or greater than 3.7×10^{-8} N, at least 75 $^o/_o$ of the particles will be removed.

The largest particle diameter which could be produced by the atomiser-impactor generator used in the present experiments, is 1 μm, and the electron micrographs showed that all the particles were smaller than this size. The calculations of the drag force which a 1 μm particle will be subject to, gives a value much less than 3.7×10^{-8} N, determined by Corn and Silverman. The calculations are provided in detail in Appendix B.

Therefore from the theoretical point of view, the model of the deposition of particles considers that test surface is a "perfect sink", i.e. no re-entrainment of the deposited particle will occur under the experimental flow conditions.

Taking into consideration the real surface, an experimental test was needed to support the belief that the surface is a perfect sink. Such experiments have been carried out and will be reported later; the results for both smooth and ribbed surfaces indicate that within 95 $^o/_o$ confidence limits there is no removal of particles after their deposition.

§3.4   Mechanisms of Deposition

The mechanisms of deposition of particles of concern in the present work will be discussed as follows:

§3.4.1   Molecular Diffusion

This is the mechanism by which particles within a purely laminar or stationary flow are brought to the surface under the action of fluid molecules interacting with the suspended particles. The motion of particles in such fluid was defined by Einstien, [15], as:

$$\overline{X}^2 = 2Dt \qquad\qquad (3.4)$$

where

$\overline{X}^2$ = the mean square displacement of particles,

t = the time required for this displacement,

D = diffusion coefficient of particle, expressed by:

$$D = \frac{k_B \, T}{3 \, \pi \, \mu \, d_p} \qquad\qquad (3.5)$$

in which

k_B = Boltzman's constant = 1.38×10^{-23} J/K

T = absolute gas temperature of fluid

μ = dynamic viscosity of fluid

d_p = diameter of particle.

The conditions under which the last equation is valid is that all external forces are absent, therefore, motion of the particles will be random. Brownian motion increases with decreasing particle size while it is negligible when Kn < 0.01 (i.e. in the continuum regime).

If a concentration gradient exists normal to the surface, particles will migrate from the higher concentration region to that of lower concentration. This migration due to the presence of a concentration gradient is known as diffusion. In a stationary or flowing gas contaminated with fine particles and adjacent to an adiabatic surface, diffusion leads to the deposition of particles onto the surface. This deposition maintains a concentration gradient with the concentration of particles being zero at the surface.

The rate of deposition of particles onto the surface due to this mechanism is equal to the product of Brownian diffusion coefficient and the particles concentration gradient near to the surface, namely:

$$N = D \frac{dc}{dy} \qquad (3.6)$$

The validity of this equation requires that no external forces act on the particles.

§3.4.2 Eddy Diffusion

When the fluid flow becomes turbulent, eddies which exist in the flow, act to speed up the diffusion process. The mass transfer process, therefore, becomes more complicated than that in the laminar or stagnant flow. The effect of eddies is represented by the eddy diffusion coefficient, which must be included in the mass transfer equation and takes the following form:

$$N = (D + \varepsilon_p) \frac{dc}{dy} \qquad (3.7)$$

and in dimensionless form it can be expressed as:

$$V^* = (\frac{D}{\nu} + \frac{\varepsilon_p}{\nu}) \frac{dc^*}{dy^*} \qquad (3.8)$$

where

$V^* = N/c_0 u_*$, dimensionless deposition velocity,

$c^* = c/c_0$, dimensionless concentration of particles,

ε_p = eddy diffusivity of particles.

For the range of sub-micron particles it is assumed, in usual practice, that the eddy diffusivity of the particles ε_p is the same value as the eddy diffusivity of the fluid. This assumption was discussed

by Rouhiainen and Stachiewicz, [36], and it was found to be reasonably acceptable for particles of diameter up to about 1.7 μm.

For a pipe flow, the radial turbulent diffusion coefficient can be estimated from the equations of Lin et al., [33], as follows:

$$\frac{\varepsilon}{\nu} = \left(\frac{y^*}{14.5}\right)^3 \qquad\qquad y^* \leqslant 5$$

$$\frac{\varepsilon}{\nu} = \frac{y^*}{5} - 0.959 \qquad\qquad 5 \leqslant y^* \leqslant 30$$

where y^* is the dimensionless normal distance from the surface, $y^* = y(u_*/\nu)$

It is assumed that for $y^* > 30$, well inside the turbulent core, uniform turbulent mixing is provided, so the diffusion in that region is usually neglected.

A single equation of the turbulent eddy diffusivity has been derived empirically by Davies, [27], for all values of y^*

$$\frac{\varepsilon}{\nu} = \frac{(y^*)^a}{10^3 \left(\dfrac{2.5 \times 10^7}{Re}\right)^b}$$

where

$$a = 4.0 - (y^*)^{0.8}$$

$$b = \frac{y^*}{400 + y^*}$$

§3.4.3 Eddy diffusion-impaction

For small particles near to the surface, where the effect of the eddies is small, the deposition process is assumed to be due to

Brownian diffusion. But large particles can possess sufficient inertia to be projected directly onto the surface. This is the concept of the eddy-impaction mechanism.

In this mechanism the molecular diffusion will be negligibly small and the mass transfer equation is expressed in the form:

$$N = \varepsilon_p \frac{dc}{dy} \tag{3.12}$$

and in dimensionless form it takes the form:

$$V^* = \frac{\varepsilon_p}{\nu} \frac{dc^*}{dy^*} \tag{3.13}$$

To estimate the particle eddy diffusivity, the concept of particle stopping distance corresponding to the velocity component normal to the surface may be employed. The velocity component of the particle will assumed to equal the normal velocity component of the fluid when the former penetrates the boundary layer. Thus the particle travels a certain distance, while the accompanying eddy is dissipated away. This distance is defined as stopping distance and is estimated by

$$s = V_0 \tau \tag{3.14}$$

where

$\quad V_0 \quad$ normal resolute of the turbulent velocity, and

$\quad \tau \quad$ particle relaxation time $= \dfrac{\rho_p d_p^2}{18 \mu}$

According to Liu and Ilori, [39], the additional diffusivity due to the particle itself, which is $(V_0)^2 \tau$, is analogous to that of Brownian

diffusivity $(D = (v_B)^2\tau)$. Given a fluid diffusivity ε, the effective particle diffusivity is then

$$\varepsilon_p = \varepsilon + (V_0)^2\tau \tag{3.15}$$

Distinguishing between molecular diffusion and eddy diffusion is not difficult and depends on the flow conditions. But the problem here lies in distinguishing between eddy diffusion and eddy diffusion-impaction mechanisms.

In the eddy diffusion mechanism, the deposition process is controlled by Brownian (molecular) diffusion and eddy diffusion. In the eddy diffusion-impaction mechanism, the deposition process is governed by the eddy diffusion and the inertia of the particle, while the Brownian diffusion is negligible. It is known that Brownian diffusion coefficient is significant for small particles, but it will be negligible for larger ones. The limit between these two sizes of particles must be known for a given flow condition in order to distinguish between these two mechanisms.

§3.4.4 Diffusion Layer Concept

El-Shobokshy, [11], followed by Davies, [12], used the concept of the "diffusion layer" to define a particle size limit below which eddy diffusion mechanism governs the particle deposition process, and above which eddy diffusion-impaction is responsible for the deposition process. The diffusion layer is just above the surface at a point where the Brownian diffusion becomes comparable with the eddy diffusivity.

At this point, for any particle size, D and ε can be approximately related according to

$$\varepsilon = 5D \qquad (3.16)$$

Substituting with value of eddy diffusivity form the equation of Lin et al., [33], then

$$(\frac{y_d^{*}}{14.5})^3 = 5 (\frac{D}{\nu}) \qquad (3.17)$$

where $(y_d)^{*}$ is the dimensionless diffusion layer thickness, expressed by

$$y_d^{*} = y_d \frac{u_{*}}{\nu}$$

hence,

$$y_d^{*} = 24.8 (\frac{D}{\nu})^{1/3} \qquad (3.18)$$

or

$$y_d = \frac{24.8 \, \nu}{u_{*}} (\frac{D}{\nu})^{1/3} \qquad (3.19)$$

y_d is the diffusion layer thickness, and it is a function of the Brownian diffusion coefficient which varies with the particle size. If the particle size increases the Brownian diffusion coefficient will decrease and consequently, the diffusion layer will also decrease.

From the definition of stopping distance and diffusion layer, it can be stated that if a particle is discarded by the eddies outside the diffusion layer, it will be projected directly to the surface by the influence of its inertia and will be deposited by eddy-impaction. If the particle is still accompanied by the eddy to the diffusion layer,

it will continue the deposition process by Brownian diffusion. If allowance is made for the particle radius, then the main conclusion can be expressed as follow

    (a) if $y_d > (s + r_p)$, then the mechanism is eddy-diffusion.

    (b) if $y_d < (s + r_p)$, it is eddy-diffusion-impaction.

Therefore, if the stopping distance and the diffusion layer are calculated for certain particle size under known flow conditions, it can predicted which mechanism will control the deposition process.

§3.4.5 Sedimentation of Aerosol Particles

A freely falling spherical particle acquires a constant or terminal velocity when the fluid dynamic drag balances with its weight.

To estimate the terminal or settling velocity for small particle due to gravity, it is assumed that the particle is rigid against the influence of gas molecules, falling independently free from external forces, slowly enough through viscous fluid such that Re_p ($V_s d_p/\nu$) will be smaller than unity and its size is much larger than the mean free path of the gas molecules, therefore, the motion will be according to Stokes' law. Hence the drag will be

$$F_D = 3\pi\mu V_s \, d_p \qquad\qquad\qquad (3.20)$$

where V_s is the terminal settling velocity. By balancing the drag and the buoyancy forces with the particle weight, then

$$3\pi\mu d_p V_s = \frac{\pi}{6} d_p^3 (\rho_p - \rho)g$$

and the terminal settling velocity becomes

$$V_s = \frac{(\rho_p - \rho) \, g \, d_p^2}{18 \, \mu} \qquad (3.21)$$

Since the particle density will normally be greater than the gas density, the terminal settling will be

$$V_s = \frac{\rho_p \, g \, d_p^2}{18 \, \mu} \qquad (3.22)$$

For particles of the size comparable with the mean free path of the gas molecules, the medium cannot be regarded as a continuum regime. The particles will move faster than predicted due to slip between them and the gas molecules. A Cunningham correction factor must be introduced to give allowance for slip flow, and the terminal settling velocity takes the final form

$$V_s = \frac{\rho_p \, g \, d_p^2}{18 \, \mu} \, C_c \qquad (3.23)$$

in which C_c is the Cunningham correction factor and equal to

$$C_c = 1 + Kn[A + B \exp(-C/Kn)] \qquad (3.24)$$

where A, B and C are constants usually take the values

A = 1.2, B = 0.42 and C = 0.88

$$Kn = \frac{\lambda}{r_p}$$

λ is the mean free path of the gas molecules and can be determined by

$$\lambda = \frac{1.2533 \, \mu}{\sqrt{p \, \rho}} \qquad (3.25)$$

in which p is the gas pressure (N/m^2), ρ is the gas density (Kg/m^3) and μ is the gas dynamic viscosity $(Kg/m.s)$.

A plot of setting velocity V_s is shown in Fig. 3.5 as a function of the particle diameter in air at 20 °C. Comparing between the values of the terminal velocity due to sedimentation and as a result of diffusion, indicates that in general, for sub-micron range of particles the contribution of the sedimentation mechanism to the deposition process is negligibly small with respect to that of eddy diffusion. But for large particles the effect of sedimentation must be considered. In the extreme case where the particle is quite large and the flow is stagnant, the deposition process would be governed mainly by the sedimentation mechanism.

§3.4.6 Thermophoresis

If a temperature gradient is set up in an aerosol, particles will move along the gradient under the influence of the molecular activity, where on the hotter side of the particle it will be greater than on the cooler side. This is the phenomena of thermophoresis, according to it the particles are driven away from hot surfaces and attracted towards cold surfaces.

The movement of particles in the presence of steep temperature gradient have been studied by a number of investigators such as Epstein, [59], Brock, [60], and Derjaguin and Yalamov, [65]. The resultant thermophoretic force and the velocity attained by the particles are described in chapter 2. But in general, the velocity of thermophoresis is a function of Knudsen number, which is the ratio of the gas molecules mean free path and the particle radius, the temperature of the gas, the temperature gradient as well as the thermal conductivity of the gas and that of the particle material.

According to Knudsen number, Kn, the flow is classified into three regions: for small values of Kn (less than 0.25) the slip flow region is considered, for $0.25 \leq Kn \leq 10$ it is defined by theoretical and experimental evidence as the transition region and for $Kn > 10$ the free molecular region is taken into account to describe the processes introducing only a small error.

The calculated Knudsen number of the reactor and the experimental work conditions are not the same and are related to different regions. For example, Knudsen number along the fuel element in the reactor conditions are in the range 0.05 to 0.08 which seem to be related to the slip flow region, but for the experimental work conditions, Knudsen numbers are in the range 0.54 to 2.8, which seem to be related to the transition region.

For this reason the fitting formula introduced by Talbot et al., [64], for the entire range of Knudsen numbers has been adopted to calculate the velocity of thermophoresis:

$$V_T = - \frac{2 C_s \nu [(k_g/k_p) + C_t Kn] C_c (\nabla T/T_0)}{(1 + 3C_m Kn) [1 + 2(k_g/k_p) + 2C_t Kn]} \qquad (3.26)$$

in which

C_s is the thermal slip coefficient, = 1.149,

C_m is the momentum exchange coefficient, = 1.14,

C_t is the thermal jump coefficient, = 2.18,

C_c is the Cunningham correction factor .

It should be emphasised that diffusiophoresis and electric mobility mechanisms are beyond the scope of this study. A neutraliser was used in the experiments to produce a highly concentrated sonic jet of positive and negative ions mixed with the aerosol cloud produced from the atomiser-impactor. Therefore, the electrostatic charge resulting from the atomiser process were neutralised. Furthermore, the test rod surface was earthed to avoid any electrostatic charging of the surface during the experimental time.

§3.4.7 Conclusions

The theoretical calculations have indicated that for the flow conditions and the size of particles concerned in the present work, the following prevail:

a- Any particle that collides with the surface must be captured.

b- Deposited particles on the surface are unlikely to be dislodged. Therefore, the re-entrainment of particles will not be considered.

c- The process of deposition of particles will be controlled by the eddy-diffusion mechanism, while the effect of the sedimentation mechanism and impaction is negligibly small.

d- In the case of hot surfaces, thermophoretic mechanisms will be be taken into account in addition to the eddy-diffusion mechanism using the fitting formula of Talbot et al, [64],for the entire range of Knudsen numbers.

§3.5   Deposition Model

§3.5.1 Isothermal Surfaces

1-   Ideal smooth surface

The theoretical treatment for this study has been based on an eddy-diffusion model in which the particle flux is expressed in terms of particle diffusivities and concentration gradient, thus

$$N_o = (D + \varepsilon_p) \frac{dc}{dy} \tag{3.7}$$

and in dimensionless form, it can be written as

$$V_o^* = (\frac{D}{\nu} + \frac{\varepsilon_p}{\nu}) \frac{dc^*}{dy^*} \tag{3.8}$$

where V_o^* is the dimensionless deposition velocity, $= (N_o/c_0 u_*)$.

The integration of equation (3.8) with boundary conditions

$$c^* = c_{s+r} \quad \text{at} \quad y^* = s^* + r_p^*$$

$$c^* = 1 \quad \text{at} \quad y^* = R^*$$

leads to

$$c_{s+r}^* = 1 - I.V_0^* \tag{3.27}$$

where

$$I = \int_{s^* + r_p^*}^{R^*} \frac{dy^*}{\frac{D}{\nu} + \frac{\varepsilon}{\nu}} \tag{3.28}$$

At the distance, $(s^* + r_p^*)$, from the wall surface, the terminal velocity of the particle due to free falling is assumed the same as the

69

radial component of the turbulent fluctuation velocity. Then the mass transfer equation may be written as

$$N_o = V_o \cdot c_{s+r_p} \qquad (3.29)$$

and in dimensionless form it will be

$$V_o^* = V_o^* \cdot c_{s+r_p}^* \qquad (3.30)$$

Substituting the value of $c_{s+r_p}^*$ from equation (3.30) into equation (3.27), the deposition velocity takes the following form:

$$V_o^* = \cfrac{1}{\cfrac{1}{V_o^*} + I} \qquad (3.31)$$

in which V_o^* is the dimensionless particle terminal velocity and can be obtained by

$$V_o^* = \frac{1}{2}(1 - \frac{10+r_p^*}{\tau^*}) + \sqrt{\frac{1}{4}(1 - \frac{10+r_p^*}{\tau^*})^2 + \frac{r_p^*}{\tau^*}} \qquad (3.3)$$

while the integration I, can be evaluated numerically.

2- The effect of surface roughness

To present an approach suitable for estimating rate of deposition of particles onto a rough surface, Browne's analysis, [42], is used. In this analysis, to take account of surface roughness, extra distances have been added to the particle-capture distance, and by shifting the position of the origin of the velocity particle, it has been possible to use the same equation as Davies, [26], for the radial velocity fluctuations. Thus,

$$V_0^* = \frac{\Delta^*}{10 + \Delta^*} \tag{3.32}$$

From the following figure
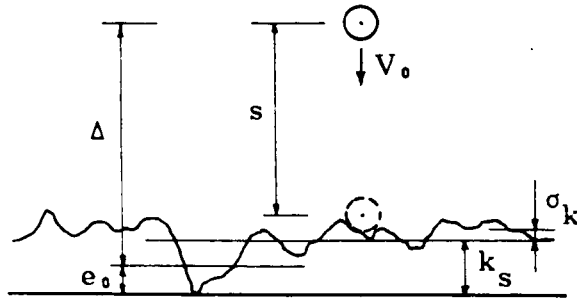
$$\Delta = s + r_p + k_s + \sigma_k - e_0 \tag{3.33}$$

or it takes the dimensionless form

$$\Delta^* = s^* + r_p^* + f(k_s^*) \tag{3.34}$$

where k_s equivalent surface roughness

σ_k standard deviation of average height of pipe surface roughness, $= 0.17\ k_s$

e_0 displacement in the origin of velocity profile, and is considered as $0.53\ k_s$.

The terminal velocity of the particle will be expressed by

$$V_0^* = \frac{1}{2}\left(1 - \frac{10+\phi^*}{\tau^*}\right) + \sqrt{\frac{1}{4}\left(1 - \frac{10+\phi^*}{\tau^*}\right)^2 + \frac{\phi^*}{\tau^*}} \tag{3.35}$$

in which

$$\phi^* = r_p^* + f(k_s^*)$$

71

Also the effect of surface roughness will be included into the integration where the lower limit will be Δ^* instead of $s^* + r_p^*$.

2.a Real smooth surface

To evaluate the role of roughness on the smooth rod, its surface topography was measured using a Talysurf. The average surface roughness, including the join between the sections was estimated statistically and found to be 1.5 μm.

2.b Regular ribbed surface

The analysis of Browne, [42], for the random rough surface, needs to be considered with some caution in calculation of the deposition rate of particles onto the regular roughness of the fuel rod surface.

The equivalent surface roughness of the regular ribbed surface is determined by assuming the additional area of cross-section produced by the rib was spread along the distance between the ribs, i.e for a square rib (e) on a pitch (p), the equivalent height of the roughness would be (e^2/p).

§3.5.2 Heated Surfaces

Considering the effect of thermophoresis with the eddy-diffusion mechanism, the mass transfer equation will be given by:

$$N_{th} = (D + \varepsilon) \frac{dc}{dy} + V_T c \qquad (3.36)$$

and in dimensionless form it will be written as

72

$$V_{th}^{*} = \left(\frac{D}{\nu} + \frac{\varepsilon}{\nu} \right) \frac{dc^{*}}{dy^{*}} + V_{T}^{*} c^{*} \qquad (3.37)$$

Taking into account the previous considerations for each surface, the final form of the dimensionless deposition velocity may be expressed by

$$V_{th}^{*} = \frac{V_{0}^{*} V_{T}^{*} \exp(I.V_{T}^{*})}{V_{T}^{*} + V_{0}^{*} [\exp(I.V_{T}^{*}) - 1]} \qquad (3.38)$$

§3.6 Thermal conductivity of particles

To apply the analysis of the theoretical consideration of the effect of thermophoresis phenomena on the deposition of particles, the value of the thermal conductivity of particle material, k_p must be known.

Because of that value for the sodium fluorescein (uranin) was not available in the published literature or the conventional sources , [81 - 83], Davies, [12], decided in his work to use the value of the thermal conductivity of a substance similar in nature to uranin. This substance was diatomaceous earth which has a thermal conductivity of about 0.242 W/mK. The decision of Davies was based on the fact that the preliminary calculations of the velocity of thermophoresis, V_T according to equation (2.64) indicated that V_T did not vary significantly for k_p/k_g < 100. For diatomaceous earth and air, k_p/k_g was less than 10.

Later Al-Azzawi and Owen, [84], have calculated experimentally the value of the thermal conductivity of the uranin (k_p). The experimental procedure was preparing test pieces of uranin produced from

strong solution of water and uranin which was left to dry out at room temperature. Then the pieces were exposed to one-dimensional steady state conduction by heating one surface using electrically heated copper elements. The experimental results gave a constant value of the thermal conductivity of uranin of about 0.43 W/mK.

In the theoretical calculations of the present work, the value of the thermal conductivity of the uranin was considered as that measured by Al-Azzawi and Owen.

CHAPTER 4

CHARACTERISTICS OF THE PIPE FLOW RIG

§4.1. Introduction

The deposition velocity of particles depends on the local wall shear stress and the relative roughness of the surface. It is, therefore, essential that the flow is carefully characterised before carrying out the required experimental work to determine the deposition of particles.

Mean velocity profiles allow the average Reynolds numbers to be determined and by using Clauser's method, estimates of the local skin friction coefficient could be made for the smooth surface. This was compared with measurements by means of the Preston tube technique.

A graphical method introduced by Perry and Joubert was applied to obtain the friction factor for the ribbed surface.

An electrical resistance technique was used for heating the test surface to assess the effect of thermophoresis on the deposition process.

§4.1.1 Clauser Chart

It has long been accepted that the velocity profile of turbulent boundary layers have inner layers for which the velocity scale is the friction velocity, u_*. These layers are the laminar sub-layer, adjacent

to the wall, the buffer region and logarithmic region. In most applications, the laminar sub-layer is too thin for its velocity profile to be determined accurately, so the logarithmic or the "law of the wall" region is used for comparing flows.

The skin-friction factor is derived by Clauser, [4], from measurements of the velocity profile in the following way:

For fully developed flow in a uniform pipe of radius r and with fluid velocity U_1 at the axis, a similarity defect law $[(U_1-u)/u_* = f(y/r)]$ is found to exist except in a thin layer adjoining the wall ($u_* = \sqrt{\tau_0/\rho}$, where τ_0 is the wall shear stress and ρ is the fluid density). A law of this form is also found to apply in zero-pressure-gradient boundary layers where r is replaced with δ, which is the boundary layer thickness and U_1 is the free stream velocity.

Close to the wall in both boundary layers and pipes, Prandtl's law of the wall is found to apply, i.e. $u/u_* = f(y\, u_*/v)$ even in the region of y where the defect law is applicable.

MilliKan, [85], pointed out that in the range of simultaneous validity of those two laws, the form of the function $f(y\, u_*/v)$ is mathematically restricted and given by:

$$\frac{u}{u_*} = A' \log y\, \frac{u_*}{v} + B' \qquad (4.1)$$

where A' and B' are universal constants . Equation (4.1) can be written as follows:

$$\frac{u}{U}\, \frac{U}{u_*} = A' \log y\, \frac{U}{v} + A' \log \frac{u_*}{U} + B' \qquad (4.2)$$

It can be seen from the above equation that on a (u/U) versus log (y U/ν) plot, a family of straight lines is produced, each line corresponding to a given value of friction factor, f. Thus a chart may be constructed and by plotting the experimental data on such a chart, the line upon which they fall gives the appropriate value of f. This value is dependent upon the value adopted for the constants A' and B'. Clauser choose the values $A' = 5.6$ and $B' = 4.9$.

§4.1.2 Preston Tube

The Preston tube method of measuring the skin-friction coefficient, which makes use of a simple Pitot tube lying on the surface, depends upon the assumption of a universal inner law common to boundary layers and fully developed pipe flow .

The difference between the pressure recorded by the Preston tube and undisturbed static pressure can be expressed in the non-dimensional form:

$$\left(\frac{\Delta p}{\rho\, u_*^2}\right) = f\left(\frac{u_*\, d_0}{\nu}\right) \qquad (4.3)$$

in which d_0 is the diameter of the Preston tube.

Alternatively, the non-dimensional relationship between the Preston tube reading and the skin-friction coefficient can be presented in the practically more convenient form given by Preston, [5], namely,

$$\left(\frac{\tau_0\, d_0^2}{4\, \rho\, \nu^2}\right) = F\left(\frac{\Delta p\, d_0^2}{4\, \rho\, \nu^2}\right) \qquad (4.4)$$

and the function F can readily be determined from measurements in fully developed pipe flow.

Patel, [86], has derived three formulae for three range of Preston tube Reynolds number $(d_0 u_* / 2 \nu)$ as follows:

in the range:

$$3.5 < \log_{10} (\tau_0 \, d_0{}^2 / 4 \, \rho \, \nu^2) < 5.3$$

$$55 < (d_0 u_* / 2 \nu) < 800$$

$$X_1 = Y_1 + 2 \log_{10} (1.95 \, Y_1 + 4.10) \qquad (4.5)$$

in the range:

$$1.5 < Y_1 < 3.5$$

$$5.6 < (d_0 u_* / 2 \nu) < 55$$

$$Y_1 = 0.8287 - 0.1381 \, X_1 + 0.1437 \, X_1{}^2 - \cdots \, X_1{}^{3} \qquad (4.6)$$

in the range:

$$Y_1 < 1.5$$

$$(d_0 u_* / 2 \nu) < 5.6$$

$$Y_1 = 0.5 \, X_1 + 0.037 \qquad (4.7)$$

Patel confirmed experimentally the results of Rechenberg, [87], which indicated that with a symmetrical bore for round Preston tubes the ratio of inside to outside diameter has a negligible effect on the calibration.

Recently, Lewkowicz et al., [88], confirmed the universal calibration relationship for Preston tubes and obtained a single equation formula which describes that function and covers the entire range of practical applications of Preston tubes and takes the following form:

$$Y_1 = 0.886X_1 - 1.45 + (23.64X_1^2 - 69.45X_1 + 64.40)(1 - \tanh X_1)$$

$$(4.8)$$

where

$$Y_1 = \log_{10}(\frac{u_*^2 \, d_0^2}{4 \, \nu^2})$$

and

$$X_1 = \log_{10}(\frac{\Delta p \, d_0^2}{4 \, \rho \, \nu^2})$$

§4.1.3 Hall's Transformation

Hall, [89], has derived a method to determine the friction factor for channels having rough and smooth surfaces. If the channel has inside and outside radius r_1 and r_2 respectively, from the velocity distribution, Hall assumed that the radius of maximum velocity, r_m defines a cylindrical surface at which there is no shear stress. Although he pointed out that this assumption is only strictly correct for non-turbulent flow, he applied a force balance on the region of the annular passage between the inner rough radius r_1 and the radius of no shear stress, r_m, and obtained the friction factor for the rough surface, f_1, which depends on the mean friction factor of the channel according to the following form:

$$f_1 = f \ \frac{d_{e_1}}{d_e} \ (\frac{A_1}{A})^2 \ \frac{\int_{r_1}^{r_2} \rho u r \ dr}{\int_{r_1}^{r_m} \rho u r \ dr} \ [\frac{\int_{r_1}^{r_2} u r \ dr}{\int_{r_1}^{r_m} u r \ dr}]^2 \qquad (4.9)$$

which can be evaluated from the measured velocity and temperature profiles across the channel, where:

d_e effective diameter of the channel,

d_{e_1} effective diameter of the passage bounded by r_1 and r_m,

A   cross-sectional area of the channel,

A_1 cross-section area of the passage bounded by r_1 and r_m.

§4.1.4 Perry and Joubert Method

Perry and Joubert, [6], developed a graphical method for determining the local rough wall boundary layer characteristics in adverse pressure gradients from each measured velocity distribution. The method could be considered as an extension of the method introduced by Clauser for smooth surfaces.

According to Clauser's technique, the value of friction factor, f, is confirmed only by the slope of the logarithmic line and not its position, and since roughness always increases turbulent skin-friction, the logarithmic line must shift to the right and downward because of the way that u_* occurs in the abscissae and ordinates. Clauser, [90], expressed the equation for the inner profile on a rough wall in the following form:

$$\frac{u}{u_*} = A' \ \log y \ \frac{u_*}{\nu} + B' - \frac{\Delta u}{u_*} \qquad (4.10)$$

where $\Delta u / u_*$ represents the vertical shift of the logarithmic curve caused by the roughness.

Perry and Joubert applied their method for ribbed surfaces, and for zero pressure gradient it can be summarised as follows:

For the velocity u let y_T be the distance measured above the crests of the elements and y be the distance from the logarithmic asymptote, this being located a distance ε_0 below the crests. From Clauser's equation it can be shown that

$$\frac{u}{U} = A'\sqrt{f/2} \, \log_{10}[(y_T + \varepsilon_0)\frac{U}{\nu}] + \sqrt{f/2} \, \{ A' \log_{10}\sqrt{f/2} + B' - \frac{\Delta u}{u_*} \}$$

$$(4.11)$$

This can be put into the more experimentally convenient form using Clauser's numerical values

$$\frac{u}{U} = 5.6 \, \sqrt{f/2} \, \log_{10} (y_T + \varepsilon_0) + P_1 \qquad (4.12)$$

where

$$P_1 = \sqrt{f/2} \, \{ 5.6 \, \log_{10}(\frac{U}{\nu} \sqrt{f/2}) + 4.9 - \frac{\Delta u}{u_*} \}$$

Representing the experimental points on a semilogarithmic plot of (u/U) versus $\log_{10} y_T$ and by addition of a chosen value of ε_0, from several attempts of trail and error, to each experimental point, a curve of (u/U) versus $\log_{10} (y_T + \varepsilon_0)$ could be drawn on the same semi-logarithmic plot. From equation (4.12), the slope of the asymptote, of the curve which comes close the experimental points, gives the value of $5.6\sqrt{f/2}$.

§4.1.5   The Entry Length

For fluid flowing in a pipe, turbulence is not necessarily established very close to the inlet, in general, the eddy structure is established only at a distance, the so called entry length, downstream from the entrance to the pipe. Only after this point is the characteristic turbulence developed at the centre of the pipe, and only after this point are the mean velocities (in given regions of the pipe) independent of the distance along the pipe.

According to Welty et al., [91], there is no relation available to predict the entry length for a fully developed turbulent velocity profile, but in general, due to experiments of Deissler, [92], a greater distance is required for a rounded entrance than for a sharp-edged entrance, since in the former the initial portion of the boundary layer is laminar and a laminar boundary layer increases in thickness more slowly than a turbulent one.

Schiller and Kirsten, [93], observed that for turbulent flow at $Re > 10^4$, $L_e > 50 d$ were generally necessary for the formation of a fully developed turbulent velocity profile.

Later Davies, [94], derived the following equation to calculate the entry length for turbulent flow in smooth pipe

$$L_e = 1.41 \ d \ Re^{0.25} \qquad\qquad (4.13)$$

and claimed that it can be safety assumed for smooth pipes that (L_e/d) approaches 100. Rough pipes, bent pipes, or pipes with sharp

edges have (L_e/d) values usually much smaller than 100, e.g. as low as 30 or even less.

The use of roughness to reduce the entry length, L_e may be illustrated by the device of Rube, [95], to reduce the inlet length. He introduced an initial section of length (5d) with severe roughness; a stable turbulent profile then develops in the otherwise smooth pipe within a total distance of (15d) from the inlet point.

More recently, calculations by Walklate[96], have shown that in a highly turbulent duct flow, the boundary layers develop quickly and usually interfere at 15 to 20 diameter downstream of the inlet, [97].

Kelly, [77], calculated the entry length required for the flow in the channel of the reactor to become fully developed turbulent flow according to the following equation :

$$L_e = 1.35 \ d_e \ Re^{0.25} \qquad \qquad (4.14)$$

where d_e is the effective diameter of the channel.

§4.2 Performance of The Channel

§4.2.1 The Flow Rig

A circular cross-section pipe was designed and constructed to carry out the required experiments for studying the deposition of sub-micron particles onto the fuel rod surface.

The working section was located at a position where the flow is fully developed and was chosen on the basis that the entry length must be at least equal to that introduced by Kelly, [77], using:

$$L_e = 1.35 \ d_e \ Re^{0.25} \tag{4.14}$$

Dummy fuel rods were inserted in the entry length of the pipe before the working section to make sure that the flow was fully developed.

A suction fan was used via a butterfly valve with six openings to obtain the required Reynolds number of the air flow similar to those found in the Windscale gas cooled reactor; about 3×10^5, [2].

Air flow was drawn from room conditions through a big wooden box $(1 \times 1 \times 2 \ m)$, which was provided with an absolute filter to prevent any dust or undesirable particles entering the flow rig.

Davies, [26], pointed out that swirl must be avoided in experiments of this sort, honeycomb flow straighteners were therefore used in two positions. One at the inlet of the channel with another before the butterfly valve, to prevent any swirl formation in the flow.

The layout of the experimental rig is shown in Fig. 4.1.a.

The fuel rod surface is divided into a number of sections, each 4.8 cm long and containing the same number of ribs. These sections were assembled together by using a tie-rod and means of specially manufactured ferrules between the individual sections the rod was re-assembled to its original form. Fig. 4.1.b shows the method of assembly. The ability to break down the test rod into smaller sections

meant that after the tests, the deposition on each section could be measured individually to obtain the spatial distribution of deposit.

For purpose of comparison, a smooth rod with the same diameter was used as a parallel case to measure the corresponding deposition rate onto smooth surfaces. As with the ribbed rod, the smooth rod was divided into sections each 5 cm long but a slightly different technique was used for assembling the sections. Because the smooth rod had a considerable thickness, the ends of each section was machined to form a spigot which fitted neatly into the mating piece. This technique of assembly is shown in Fig. 4.1.c.

In both cases the rods were earthed to avoid any electrostatic effects on the experimental deposition results.

§4.2.2   Pressure Distribution along the Channel

It was assumed that the pressure is constant in the radial direction through the pipe flow rig. A set of four static pressure tapping were fixed at positions upstream and downstream of the working section and at another two positions before the working section. The aim of fixing these pressure tapping was to get the mean static pressure along the channel by using a micro-manometer. It was found that there was no difference between the readings of the manometer when the smooth rod was replaced by the ribbed surface rod. This is because the rods have a much small diameter than the pipe.

The pressure distribution along the channel is shown in Fig. 4.2, for the fifth position of the butterfly valve which gave a Reynolds

number of the flow of about 3×10^5. From the figure, it can be considered that the flow through the working section is fully developed. This consideration may be supported by the formula of Latzko, [98], which predicted the entry length required for the friction factor to be constant. This formula determined the length by:

$$L_e = 0.623 \ d_e \ Re^{0.25} \qquad (4.15)$$

and has a good agreement with the theoretical results of Deissler, [99], for turbulent friction factors for flow in the entrance section of circular tubes. These results show that at a distance of about 10 diameters from the entrance, the static pressure gradient becomes constant. While the local friction factor which is $[\tau_0 \ / \ \frac{1}{2}\rho U^2]$, becomes constant in a distance of about 6 diameters indicating that the velocity profile adjacent to the wall becomes established in a short distance.

§4.2.3   Velocity Distribution through the Working Section

A DISA hot wire anemometer type 55D01 was used to measure the mean velocity and the turbulence intensity in the working section. The anemometer was connected, after its calibration using a Pitot tube and micro-manometer, with a lineariser which was connected to a digital voltmeter to read the instantaneous mean velocity corresponding to the radial position.   Also a RMS voltmeter was connected with the lineariser to read the corresponding velocity fluctuation.

The probe used for these measurements was a hot wire type 55P11 5 μm diameter platinum plated tungsten wire. This probe was traversed in the radial direction by using a fine traversing mechanism. These

measurements were carried out at positions upstream and downstream of the working section.

Six velocity distributions were obtained for the smooth rod and for the ribbed rod at both positions. The velocity profiles are shown in Figs. (4.3 - 4.6), in which the instantaneous mean velocity is plotted against the radius r^*, which is defined as

$$r^* = \frac{r - r_1}{r_2 - r_1} \qquad (4.16)$$

where

r_1 the radius of the inside rod,

r_2 the radius of the outside pipe,

r the radius at which the velocity was measured.

The value of the mean velocity is calculated according to

$$U = \frac{\int_{r_1}^{r_2} ur\, dr}{\int_{r_1}^{r_2} r\, dr} \qquad (4.17)$$

where u is the instantaneous mean velocity.

The values of the mean velocity and the corresponding Reynolds numbers and the mass flow rate are shown in Tables 4.1 and 4.2.

The effect of the surface roughness displaces the velocity profile slightly towards the smooth wall without changing the value of the mean velocity.

§4.2.4 Skin Friction Coefficient

A different probe, a boundary layer hot-wire type 55P15, was used to measure the instantaneous mean velocity close to the surface. Using a fine traverse mechanism, twenty readings were recorded within 1 cm above the surface. These measurements were taken on the smooth rod at the upstream and downstream positions.

A Clauser chart was constructed, using the computer facilities, from equation (4.2), to determine the skin-friction coefficient. Next the experimental measurements were plotted and the value of the skin-friction factor was determined by matching the experimental data to the theoretical curves. Twelve charts were drawn to determine the value of the skin-friction factor at the upstream and downstream stations for the six available positions of the butterfly valve. Fig. 4.7 shows Clauser's method applied at the downstream position.

The Preston tube method was used as another technique to determine the skin-friction factor for the smooth rod surface. The readings of the manometer were recorded for both upstream and downstream positions, then the corresponding skin-friction factor was calculated using the equation obtained by Lewkowicz et al., [88].

Lee, [100], has summarised the experimental and empirical friction velocity equations for fluid flow through a pipe. Two common equations have been chosen for comparison with the skin-friction factor determined in the present work. First is the equation of Reichardt, [101], for any value of $y^* > 0$

$$u^* = 2.5 \ln(1 + 0.4\, y^*) + 7.8\, [\,1 - e^{-\frac{y^*}{11}} - \frac{y^*}{11}\, e^{-0.33 y^*}\,] \qquad (4.18)$$

the second equation of Deissler, [102], for $y^* > 26$

$$u^* = 2.78 \ln y^* + 3.8 \qquad\qquad (4.19)$$

where

$$u^* = \frac{u}{u_*}$$

$$y^* = y \frac{u_*}{\nu}$$

For purpose of verification, the above two equations were drawn using the computer facilities. The corresponding friction velocities were calculated and the experimental points were plotted for each case. The final graphs are shown in Fig. 4.8, which show a reasonable agreement between the last two equations and the experimental measurements.

§4.2.5   Friction Factor for Rough Fuel Rod

Hall's method, [89], which determines the friction factor for channels having rough and smooth surfaces, as in the pipe flow rig, depends on the mean friction factor of the channel. Because of the fuel rod is so small with respect to the size of the channel, the difference in average pressure gradient was not measurable when the rough and smooth rods were interchanged.

The method of Perry and Joubert, [6], was chosen in which the slope of the asymptote line is equal to $5.6 \sqrt{f/2}$. The representation of this method at downstream position of the working section is shown in Fig. 4.9.

It is difficult to find a similar type of rough surface having the same dimensions as the channel to obtain a suitable comparison, but, in general, it was found that the friction factor obtained by Perry and Joubert was in the same range as that correlated experimentally by Winkel, [103], which is

$$f = 0.165 \; Re^{-0.2} \qquad (4.20)$$

and with the experimental data shown by Wilkie, [1].

§4.3 Air Flow over Heated Rods

It was described earlier (Section 2.6) that thermophoresis is the phenomenon that occurs at a surface as a result of the temperature gradient which exists due to a difference in the temperature of the surface and that of the gas flow. An electrical resistance heating technique was used to heat the test surfaces.

This technique for heating was decided upon in preference to other methods of heating (hot air, steam or direct electrical heating), because of its convenience. Firstly, the test rods were divided into sections for deposition tests requirements, therefore, using a hot fluid flow to heat the test rods would effect on the deposition test due to the leakage which would occur at the joins of the individual sections. Secondly, the diameter of the test rod is small (about 1.6 cm), and therefore, so, would be the mass flow rate of the hot fluid; it would therefore be necessary to heat the fluid employed in the heating process to a high temperature or the resultant surface temperature would be too low. Thirdly, any contamination in the heating fluid

would be deposited onto the inside surface of the test rod, which would effect the final deposition measurements.

For the electrical resistance heating technique, it is not possible to use the test surface directly because of the joins between the individual sections, which would suffer from localised heating. Instead, the tie-rod which was used for assembling of the sections, was heated after being electrically insulated from the test surface and the supporting flanges using a monolux-500 insulation material.

§4.3.1 Electrical Resistance Heating Circuit

The electrical resistance heating system is shown in **Fig. 4.10,** in which the electrical power required for the heating process is supplied to the tie-rod from a 240 volt, 60-cycle power transformer through a variable auto-transformer. The low-voltage leads from the transformer were connected to the ends of the tie-rod by flexible copper cables using copper bus bars.

A voltmeter and an ammeter with a current transformer were provided to the circuit for measuring the power input to the heating process after equilibrium conditions had been attained.

Two springs were used at the end of the tie-rod to apply a continuous axial compression on the assembled sections of the test rod to compensate for any effect of expansion due to heating. Also to allow the expansion of the tie-rod without any bending or buckling during the experimental time three fine stainless steel wires (about 0.2 mm) were used to carry the rod at three different positions.

§4.3.2 Surface Temperature Measurements

Thirteen copper-constantan thermocouples were distributed along the test rod surface at thirteen sections, in order to measure the temperature distribution along the surface. After getting the steady state operation conditions which took about 25 minutes, and by using the variable auto-transformer, it was possible to obtain approximately the same surface temperature profiles at a flow Reynolds number of 3×10^5 for both the smooth and the ribbed surfaces, as shown in Fig. 4.11 and Fig. 4.12. Figures 4.13 and 4.14 show the higher surface temperature distribution which could also be approximately obtained at another different flow Reynolds numbers (6×10^4 and 5×10^3) for both surfaces.

§4.3.3 Heat Transfer Calculations on the Rod Surface

The heat transfer equation of the test surface can be presented in the following form:

$$\frac{d^2 \theta}{dx^2} - m^2 \theta + \frac{q^o}{k} = 0 \tag{4.21}$$

in which

$$m^2 = \frac{h\ P}{k\ A}$$

where

θ the temperature difference ($T_s - T_a$),

q^o heat generation per unit volume of the test surface,

h heat transfer coefficient by convection,

k thermal conductivity of the surface material,

A cross-sectional area of the test surface, and

P   perimeter of the test surface.

A finite difference method can be used to solve the previous equation (4.21) using the recorded data of surface temperature, air temperature and the reading of the voltmeter and the ammeter after equilibrium conditions had been attained. However, since the heat transfer by conduction through the test surface in the axial direction is so small with respect to that transferred by convection from the surface to the flowing air, a simple calculation can be made by considering only the heat transfer by convection from the surface.

The calculated heat transfer coefficients for each case are shown in Figs. (4.15) and (4.16) for both smooth and ribbed surfaces at flow Reynolds numbers 3×10^5, 6×10^4 and 5×10^3. Fig. 4.17 shows a comparison of the corresponding Stanton number, St of smooth and ribbed surfaces for flow Reynolds number of 3×10^5, with the formulae introduced by Burgoyne et al., [104], and Rapier, [105]. Also the values of Stanton number, St, seem in the same range obtained experimentally by Wilkie, [1].

CHAPTER 5

EXPERIMENTAL INVESTIGATION OF PARTICLE DEPOSITION

ONTO RIBBED AND SMOOTH SURFACES

§5.1. Introduction

The work described in this chapter is the experimental part which complements the theoretical approach described in chapter 3.

The first step in this work was the design and construction of the pipe flow rig; the performance of the pipe flow was established in chapter 4.

Since the main purpose of this chapter is to study the deposition of particles onto AGR fuel rod surface, the particle generator was calibrated to produce particles with diameters similar to those which were thought to exist in the AGR, as described in chapter 1. Mass median diameters of 0.25 µm and 0.05 µm were successfully obtained from different uranin solution strengths of 5 $^o/_o$ and 0.2 $^o/_o$. The geometric standard deviations of the particle diameters were 1.64 and 1.47 respectively.

The deposition tests were carried out using an AGR fuel rod, with its ribbed surface, and a hydraulically smooth rod. This enabled a comparison to be made between the deposition rates onto the ribbed surface and those onto the smooth surface. The smooth surface data could then also be used to compare the present study with the pub-

lished data. The thermophoretic study was also carried out using ribbed and smooth surfaces. For experimental purposes each type of rod was divided into equal sections which could then be re-assembled over a tie-rod as described in section 4.2.1.

The deposition rate is usually characterised by the deposition velocity, V which, as its name suggests, has the dimensions of velocity and is the mass deposition rate per unit area of the surface per unit time, N, divided by the free stream concentration, c_0, i.e.

$$V = \frac{N}{c_0} \qquad\qquad (5.1)$$

§5.2 Particle Concentration Measurements

The particle concentration in the free stream flow over the surface must be known to calculate the deposition velocity. The concentration of a particulate cloud can be found by collecting a sample of the free stream flow and measuring the mass of particulate material in that sample.

The probe as shown in Fig. 5.1 was designed to obtain the required samples for each deposition test. It consists of a suction tube bent to face the direction of the flow stream. The top of this tube is covered fit by a brass cap which has a thin thickness and its top end is conical at small angle and grounded into a knife-edge according to the recommendation of Parker, [106], in order to minimise the disturbance in the flow due to the presence of the probe.

El-Shobokshy, [11], and Davies, [12], used isokinetic sampling for measuring the free stream particle concentration, in which the velocity

of sampling must be equal to that of the free stream. If the velocity of sampling is greater than the free stream, some larger particles will fail to be diverted into the orifice of the probe and the measured concentration may be less than the true one. On the other hand, if the sampling velocity is smaller than the free stream velocity, the larger particles will tend to cut across the streamlines and be carried into the orifice, so that the measured concentration may be exceed than the true particle concentration.

In practice, very small particles, as in the present case, have low inertia and follow deflections of the streamlines, due to the presence of the probe and particles in the suspending medium are drawn into the probe in the correct proportions. This can be concluded from the work of Watson, [107], for particles in atmospheric air in which the concentration measurements were found to be constant for particles having mass median diameter below 4 μm, for sampling velocity in the range 0.5 to 2.0 times the free stream velocity.

The sampling procedure begins by cutting the millipore filter paper to a size equal to the outside diameter of the top end of the suction tube using a clean knife-edged wad puch. For each experiment the millipore filter paper was placed over the top of the suction tube and the cap fitted over it. The probe was inserted through the pipe wall into the flow facing upstream and left there for a certain interval of time. After this period the probe was removed and the filter paper was immersed in a known amount of de-ionized water and the resulting solution for each sample analysed in the fluorimeter. Using a flowmeter connected between the suction tube and the vacuum pump the flow

rate and hence the total volume of the air drawn was known. The concentration of the particles in the free stream could then be calculated.

§5.3 Deposition Experiments

The experimental technique which has been used previously by several investigators in this kind of work was based on the preparation of a reception surface using an aluminium foil tape which covered the real surface and upon which the particles could deposit. After the deposition run the tape was cut into sections, then each was removed in turn and wrapped around a glass rod. The glass rod was placed into a test tube containing a certain amount of de-ionzed water. After the particles had dissolved into the water the resulting solutions were analysed using the fluorimeter and the mass deposited thereon could be found.

In the present work the situation is different where the AGR fuel rod has a regular ribbed surface; therefore the technique established previously was not suitable. Instead, the real surface was used directly for measuring the deposition of particles. The technique for assembling the individual sections of the rod is described in section 4.2.1. It was decided to use the real surface of the smooth rod to make a comparison between the deposition results for smooth and ribbed surfaces under a similar conditions. The same experimental technique for measuring the deposition rates were used for both the unheated and heated surfaces.

§5.3.1 Experiments on Isothermal Surfaces

The procedure for carrying out the deposition tests at normal laboratory temperatures was as follows:

1- It was necessary to make sure that the atomisers contained sufficient solution to complete the experimental run. This was made possible by filling the jars of at the beginning of each run up to the maximum permitted level.

2- It was important to ensure that the sections of the rod and the connecting ferrules were absolutely clean by carrying out the following washing procedure:

Washing and boiling the sections and ferrules using detergent and tap water to remove any substances remaining from previous deposit. The solution is then drained and the sections washed under running tap water. After rinsing, the sections are put in a basin containing de-ionized water for washing again. The water is then drained and the sections again put into fresh de-ionized water and reboiled. After boiling for a few minutes, the sections are transferred to a rack and kept in a desiccator containing silica gel. The sections are kept in the desiccator overnight before using, no force drying should be applied.

3- The necessary glassware for the experiment was also prepared by applying the above procedure. After drying in the desiccator the test tubes were filled with a measured amount of de-ionized water to be ready for the free stream samples.

4- The tie-rod was cleaned with ethanol before assembling the individual sections over it. The assembly process was carried out using

fine tweezers. Then the assembled rod was mounted in its place within the working section.

5- The compressor was switched on and the receiver was charged to a pressure of 120 psi. Compressed air at 40 psi (about 2.8 bar) was supplied to the atomisers via a regulator. A two-way valve, installed between the holding chamber and the flow rig , was used to divert the aerosol out of the laboratory while the atomisers were settling down to the steady operations.

6- The fan of the pipe flow rig was switched on, then the control valve was adjusted to allow the particles to enter the pipe flow rig through the inlet wooden box to commence the test.

7- At the same time, the vacuum pump was switched on and during the one-hour test, samples were extraced at regular intervals of time depending on the flow Reynolds number and the size of the particles being produced by the particle generator. For example, when the flow Reynolds number was 3×10^5 and the particle size was 0.25 μm, the interval of time during which samples were extracted was five minutes, whilst for the same particles the interval of time was three minutes when the flow Reynolds number was 5×10^3. Also the amount of de-ionized water used to produce the solution for analysis in the first case was five mℓ whilst for the second case was twenty mℓ.

8- At the end of the one-hour run, the butterfly valve was closed. Immediately, the pipe flow rig, the particle generator and the compressor were switched off. The test tubes were filled with known amount of de-ionized water for dissolving the deposited particles.

The lid of the working section was taken off and the rod was carefully taken out without touching the surface. The rod was dis-assembled using fine tweezers and each individual section of the rod was placed in the appropriate labelled test tube.

9- All the test tubes of the free stream samples and the individual sections of the rod were transferred to the fluorimeter room for analysis.

From preliminary measurements of the deposition rate it was found that the values of the deposition rate were not constant along the rod. Therefore it was decided to repeat each experiment three times under the same conditions to obtain more data from which the mean value could be calculated.

Because of the possibility of contamination of the the inlet air flow, where the efficiency of the absolute fitter at the inlet could be limited, a background test was carried out as recommended by previous workers in this field. The background test was carried out following the previous procedure described above but without injecting any particles, i.e. the particle generator was switched off. The net values of the deposition rate of particles along the rod was calculated by reduced the measuring values by a value equal to the ratio of the mean background value to the mean value of the measurements along the rod.

§5.3.2 Duration of Test

In previous work at Liverpool relating to sub-micron particulate deposition investigators carried out the deposition tests over a period of one hour; it was accepted that this length of time was sufficient for the pattern of deposition to be established. It was also assumed that no particle re-entrainment would occur. In the present study some preliminary experiments were carried out to test these assumptions.

Consequently, experiments were carried out over periods of one, two and three hours for the particle size of 0.25 μm and with the smooth and ribbed unheated surfaces for the flow Reynolds number of 3×10^5. Each experiment was carried out three times, [The relevant results for each test run are shown in figures 5.2, 5.3 and 5.4 for smooth surface and in figures 5.5, 5.6 and 5.7 for ribbed surface] and the mean value of the deposition velocity to the surface was calculated together with the error based at the 95 $\%$ confidence limits

$$95 \text{ } \% \text{ confidence limits} = P \pm 1.96 \text{ } \bar{\sigma} \qquad (5.2)$$

where

P the mean value of individual readings, $= \dfrac{1}{n} \sum P_i$

P_i the individual reading,

n the number of readings,

$\bar{\sigma}$ the standard deviation of the mean, $= \dfrac{\sigma}{\sqrt{n}}$

σ the standard deviation of the readings, $= \sqrt{\dfrac{\sum (P - P_i)^2}{n}}$

The mean deposition values and their 95 % confidence limits were plotted against the corresponding time of the experiment for both the smooth and ribbed surfaces. as shown in Fig. 5.8 and Fig 5.9. The linear increase in the level of deposition indicates that the test period of one hour is adequate. It also suggests that particle removal is not occurring.

§5.3.3   Particle Re-entrainment

It was mentioned earlier in section 3.3 that the assumption that the surface behaves as a perfect sink (i.e. no deposited particles are re-entrained) should be examined. The deposition tests for different periods of time, outlined above, suggest that the assumption is valid. The assumption can be further tested by carrying a "blow -off" test. This was achieved using the smooth rod, the 0.25 µm particles and the highest flow Reynolds number since these conditions were assumed to be the most likely to cause re-entrainment in the present exper- iments.

The particle deposition test was carried out as described earlier for a one hour-run. After this time the pipe flow rig, the particle generator and the vacuum pump were switched off and the rod was taken out of the working section and dis-assembled. Alternate sections of the rod were taken for analysis and replaced with clean sections. The rod was again re-assembled and put back into the working sec- tion. The air flow was then switched on but this time no particles were injected. After a further one hour the remaining sections of the ori- ginal rod assembly were removed for analysis.

§5.3.4 Experiments on Heated Surfaces

The deposition tests were carried out using heated rods to investigate the effect of thermophoresis on the deposition of particles. The test procedure for the heated rod was the same as for the unheated rod using a one hour run as described in section section 5.3.1. To apply the heating, after the assembled rod had been mounted in the working section, the two ends of the tie-rod were connected to the low-voltage leads of a transformer via flexible copper cables using copper bus bars. Before the particles were injected into the pipe flow rig, the steady state surface temperature had been obtained for each case using a variable auto-transformer.

A thermocouple was fixed to the section in the middle of the rod and connected to a digital thermometer and was used through out the experimental period as a monitor to check the temperature of the surface. Therefore this section was not used for the deposition measurements. From the earlier heat transfer experiments it was possible to deduce the overall temperature profile based on the single monitored temperature reading.

After the one-hour run all the apparatus was switched off and the rod was left to cool. Following this period the rod was dis-assembled and analysed as before.

As for the isothermal tests, regular background readings were taken for the tests of heated surfaces

§5.4. General Precautions observed during the experiments

Perfectly clean conditions must be maintained during the experiments of deposition of sub-micron particles. Therefore general precautions must be taken into consideration, some of these were learned following the experience of previous investigators, [11]. The precautions which have been carefully considered in this work are as follows:

a- The glass slides for electron microscope analysis were cleaned using an ultra-sonic apparatus after they had been subjected to a concentrated washing process. Also the slide was cleaned by an air-dust spray before it was inserted into the output table from the particles generator, to receive the deposited particles. The specimens were always kept in the desiccator.

b- The sections of rods, the glassware and the cuvettes used in the fluorimeter analysis were always kept in a big desiccator after they had been subjected to a concentrated washing process, and they were only taken out just before use.

c- The millipore filters which were used for measuring the free steam particle concentration were always placed in a special clean glass casing and kept in a clean cupboard. Also any tool used in the test was kept in that cupboard after it had been cleaned by ethanol.

d- Using the aerosol generator occasionally involved handling the jars of the atomisers, which contained the fluorescine solution. Due to the pressure inside the jars and the strength of the sol-

ution bubbles were produced inside the jars, so a leakage of bubbles occasionally occurred. Also the drain of the impactors had to be removed from time to time. Therefore from the beginning of the test, hands were carefully washed after any equipment of the aerosol generator had been touched to avoid any contamination.

e- Considering the chemical instability of the uranin solution, only the necessary amount was prepared for carrying out the one deposition test (about 3 litres), and reference solution from which the standards were prepared, was not kept in the jars more than one month without renewal. Also the atomisers, the impactors and the connection tubes were cleaned occasionally to maintain the aerosol generator in a good working condition. Failure to do this can result in blockage of the holes of the atomiser or those of the impactor plates, also dry uranin can cover the inside wall of the connection tube to reduce the flow of the produced aerosol.

f- The working section of the pipe was always cleaned using a large piece of tissue wetted by ethanol and left to dry before the test rod was mounted to prevent any aggregation of particles from earlier tests.

g- After the deposition and background runs the test tubes containing the sections of the test rod, were kept in a clean cupboard during the dissolving process which has been recommended to be not less than 10 minutes.

h- The fluorimeter, having very sensitive interior parts, should

be kept in a cool and clean place to prevent any contamination from airborne particles reaching its sensitive interior parts. Also, the fluorimeter must be switched on to warm up for 60 minutes to be ready for use. The heat generated from the mercury lamp may cause air borne particles to deposit on the three main filters inside the instrument. Therefore, the filters were cleaned before the analysis as any surface deposited particles might alter their optical characteristics.

i- Since the florimetric analysis may take more than 1 hour after warming up, the heat generated by the fluorimeter can affect sensitive internal parts as well as the characteristics of the standard solutions hence readings were repeated twice to obtain a mean value.

j- The reference solution and the standard solutions used in the fluorimeter analysis were very weak (reference solution was 10 μg/mℓ and standard solutions were 0.01 to 0.5 μg/mℓ). It was reported that fluorescine sodium solutions of low strength such as those in the present analysis are very sensitive to temperature and unstable from the chemical point of view and their charac-teristics can change within a period of a few days. Therefore the solutions were kept in a cool and clean place renewed after about ten days. Whilst the standard solutions were kept for not more than two days.

k- For all of the deposition experiments, the tests were repeated three times to achieve a better accuracy in the final results.

§5.5 Experimental Results

The experimental study of the particle deposition can be classified into two main groups corresponding to the cases of the heated and unheated surfaces. Within each of these groups the experimental study investigated the effects on the deposition rate of surface roughness, flow Reynolds number and particle size.

The graphical results presented in this section also include theoretically predicted data. To avoid confusion these should be overlooked for now but will be returned to late in chapter 6.

§5.5.1 Deposition Results for isothermal surfaces

In accordance with the experimental procedure described in section 5.3.1, a set of deposition tests were carried out for particles having mass-median diameters of 0.25 and 0.05 μm at three different flow Reynolds numbers (3×10^5, 6×10^4 and 5×10^3) on isothermal smooth and ribbed (AGR) surfaces.

The experimental results were first plotted as a histogram form, where each interval represented the length of the corresponding section of the test rod. Then, for purpose of clarity it was decided that the mid-points of the intervals could be used to represent the position along the test rod.

Figs. 5.2, 5.3 and 5.4 show the deposition velocity of the 0.25 μm particles along the axial distance of the smooth rod when the Reynolds number was 3×10^5 for a test run of 1, 2, and 3 hours respectively. Each graph represents three repeated tests and thus illustrates the typical experimental scatter.

Figs. 5.5, 5.6 and 5.7 show the deposition velocity for the same conditions but along the ribbed rod.

The mean value of the mass deposited per unit area and the corresponding 95 % confidence limits for all the tests carried out under the same conditions have been calculated using equation (5.2). Figs. 5.8 and 5.9 show the calculated values for the smooth and the ribbed rod respectively.

The mean value of the deposition velocities for all the experimental data for the 1, 2 and 3 hour runs was calculated together with the corresponding 95 % confidence limits. The final results for the smooth rod are shown in Fig. 5.10, while the results for the ribbed rod are shown in Fig. 5.11.

Fig. 5.12.a shows the deposition velocities of three experiments of the blow-off tests for 0.25 μm diameter particles on smooth rod where the flow Reynolds number was 3×10^5. The mean value of the deposition velocity before and after the blow-off test and the corresponding 95 % confidence limits are compared in Fig. 5.12.b.

To investigate the effect of the flow Reynolds number on the deposition velocity, the deposition test of 0.25 μm particles was carried out for another two flow Reynolds numbers of 6×10^4 and 5×10^3. The mean value of the deposition velocity along the axial distance of the test rod for three experiments were calculated. Fig. 5.13 shows the deposition velocity for the smooth rod and the ribbed rods at different Reynolds numbers.

Fig. 5.14 shows the deposition velocity for the 0.05 µm particles onto the smooth rod after one hours run with a flow Reynolds number of 3 × 10^5. Fig. 5.15 shows the deposition velocity along the ribbed rod surface for the same conditions.

For the 0.05 µm particles, the deposition velocities along the smooth rod for flow Reynolds number 5 × 10^3 are shown in Fig. 5.16, whilst the deposition velocities under the same conditions for the ribbed rod are shown in Fig. 5.17.

§5.5.2 Deposition Results for Heated surfaces

As described earlier in section 4.3.2 it was possible to obtain approximately the same surface temperature profiles at flow Reynolds number of 3 × 10^5 for both the smooth and the ribbed rods. For each of the surface temperature profiles shown in Figs. 4.11 and 4.12, deposition tests were carried out for the smooth and the ribbed rods for one hour runs. Also each test was repeated three times as for the isothermal tests.

The deposition velocity for each test was calculated and to show the effect of thermophoresis, it was decided to represent the experimental data as a ratio of the local deposition velocity of the heated rod (V_{th}) to the mean value of the deposition velocity of the isothermal one (V_o).

Figs. 5.18, 5.19 and 5.20 show the deposition velocity along the axial distance of the smooth rod, for the three surface temperature profiles of Fig. 4.11. The percentage ratio of V_{th}/V_o along the ribbed

rod having the three temperature profiles of Fig. 4.12 are shown together in Fig. 5.21.

The deposition tests were carried out and repeated three times for one hour runs for flow Reynolds numbers of 6×10^4 and 5×10^3 at higher surface temperature profiles (as shown in Figs. 4.13 and 4.14) for both the smooth and the ribbed rod. Figs. 5.22 and 5.23 show the percentage ratio of V_{th}/V_o for the smooth heated rod whilst Figs. 5.24 and 5.25 show the effect of thermophoresis for the ribbed heated rod under the same conditions.

To investigate the effect of thermophoresis on the deposition velocity for the different size particles, the deposition tests were repeated for the 0.05 µm particles for both the smooth and the ribbed rods for the flow Reynolds numbers 3×10^5 and 5×10^3.

Figs. 5.26 and 5.27 show the percentage ratio of V_{th}/V_o for the smooth heated and the ribbed rods respectively when the flow Reynolds numbers was 3×10^5. For flow Reynolds numbers 5×10^3 the corresponding results are shown in Figs. 5.28 and 5.29 respectively.

§5.6 Discussions of the Experimental Results

§5.6.1 Results for Isothermal surfaces

The primary results show a variation of the deposition velocity along the test rods although the fluid flow within the working section was examined and calculated to be fully developed turbulent flow as described in chapter 4. This variation is typical of that found in

aerosol deposition experiments . Each experimental test was repeated three times to obtain a large number of measurements. Then the mean deposition velocity and the corresponding 95 $^o/_o$ confidence limits were estimated which gave consistent values as shown in Fig. 5.11 and Fig. 5.12, for example.

From Figs. 5.2 to 5.7 and Figs. 5.14 to 5.17, a comparison between the results of the smooth rod and those of the ribbed one show clearly the effect of the surface roughness on the deposition velocity. The deposition velocity increased due to the surface roughness for the range of particles used in this experiments (0.05 - 0.25 μm). This effect is greater at higher Reynolds number, for example the deposition velocity for the ribbed rod increases four fold at Re = 5 × 10^3 and up to twenty fold at Re = 3 × 10^5, compared with the corresponding values for the smooth rod. The increased deposition for the ribbed surface is due to the increased turbulence at the surface which in turn increases the turbulent diffusivity.

Fig. 5.13 shows that for smooth and ribbed rods the deposition velocity increases as the flow Reynolds number increases. This is due to the increase in the friction velocity which again promotes the turbulent diffusivity.

Comparison of the experimental results for the two particle sizes shows that the deposition velocities for the smaller particles are higher than those for the larger ones.This is because as the particle size increases the corresponding Brownian diffusion coefficient decreases which leads to a decrease in the value of the deposition velocity where the particle's inertial influence is still negligible. This is true up to

a certain size of particle after which the inertial effects begin to dominate, then the deposition velocity increases again with the particle size.

This effect of particle diameter on the deposition velocity is important for the smooth rod, and also for the ribbed rod, only at low Reynolds number. This can be seen from the data of Figs. 5.2 to 5.4, Fig. 5.13 and Figs. 5.14, 5.16 and 5.17. For the ribbed rod at high Reynolds number the particle diameter has nearly lost its effect on the deposition velocity where its value is about the same for the 0.25 μm and the 0.05 μm particles, as shown in Figs. 5.5 to 5.7 and Fig. 5.15.

The results of the time variation and the blow-off tests show that there is no evidence of re-entrainment of the deposited particles for both the smooth rod and the ribbed rod. Figs. 5.8 and 5.9 indicate that the mass of particles deposited per unit surface area can be considered to be a linear relationship with the experimental time within 95 $^{\circ}/_{\circ}$ confidence limits for 1, 2 and three hour runs. Furthermore, the deposition velocity can be regarded as unchanged before and after the blow-off test, within $95^{\circ}/_{\circ}$ confidence limits, for each case as shown in Fig. 5.12.b.

§5.6.2 Results for Heated surfaces

Generally speaking, all the results show that the deposition velocities of particles onto the heated rods are less than the corresponding ones onto the isothermal rods. This indicates the effect of themophoresis on the deposition mechanisms. Considering the effect

of thermophoresis in more detail, the process is also influenced by the other parameters studied, i.e. :

1- particle diameter.

2- surface temperature.

3- flow Reynolds number.

4- surface roughness.

Comparisons between the results in Figs. 5.18 and 5.28 and those in Figs. 5.21 and 5.29 show that the percentage ratio of the deposition velocity onto the heated rod to that onto the isothermal rod (V_{th}/V_o) for the 0.25 μm particles is less than that of the 0.05 μm particles, at the same surface temperatures and flow Reynolds numbers. In other words, the effect of thermophoresis on the smaller particles (0.05 μm) is less than that on the larger ones (0.25 μm), due to the fact that smaller particles will have smaller temperature difference across them which, in turn leads to a lower molecular imbalance. This effect of thermophoresis is the same for both the smooth rod and the ribbed rod. It is also generally accepted that for particles larger than about 0.25 μm the thermophoretic effect reduces as the particle size increases. This is due to the increasing inertia of the particles which overcomes the thermophoretic force. This feature has been observed by Wood, [108], Owen, [109] and Owen et al., [110]. Thus the particle sizes considered in the present work are those most susceptible to thermophoresis.

For a given particle diameter and flow Reynolds number Figs. 5.21 and 5.29 show that the percentage ratio of V_{th}/V_o decreases as the surface temperature increases. This can be seen from Figs. 5.18 to

5.20 for the smooth rod and Fig. 5.21 for the ribbed rod. As the surface temperature increases, the temperature gradient near to the surface also increases and this leads to an increase in the thermophoretic force acting on the particles. As the flow Reynolds number is increased the effect of thermophoresis reduces, for the same surface temperature. Figs. 5.22, 5.23 and 5.24 for the smooth rod and Figs. 5.25, 5.26 and 5.27 for the ribbed show that the percentage ratio of V_{th}/V_o for the higher Reynolds numbers is greater than that for the lower Reynolds numbers. This is a reflection of the higher friction velocity and greater turbulent energy which promotes the deposition of particles by overcoming the effect of thermophoresis.

Finally, from the results of the same particle diameter, surface temperatures and the flow Reynolds numbers it can be seen that the effects of thermophoresis are reduced over the ribbed rods compared with its effect over the smooth rods. For example Figs. 5.18, 5.19 and 5.20 compared with Fig. 5.21 show that the percentage ratio of V_{th}/V_o over the ribbed rod are higher than the corresponding values over the smooth rod. This is again due to the enhanced turbulence near to the ribbed surface.

§5.7 Comparison of the Experimental Results with those of other
Investigators

To make a reasonable comparison between two experimental results it is necessary to achieve equality of certain parameters such as the particle size, the fluid flow conditions and the test surface conditions. In practice, equality of such factors at the same time is difficult. This problem has been approached by plotting the deposition velocity in its

dimensionless form, V^*, against the dimensionless particle relaxation time, τ^*, where

$$V^* = \frac{V}{u_*}$$ (5.3)

and

$$\tau^* = \tau \frac{u_*^2}{\nu}$$ (5.4)

These two parameters V^* and τ^* include the previous factors for any particle deposition test.

Montgomery and Corn, [111], introduced some selected data of Wells and Chamberlain, [22], Sehmel, [112] and Friedlander and Johnstone, [23] as well as their own data. Fig. 5.32 shows these data and the mean values of the present experiments for the isothermal smooth rods, from which it can be seen that the present results are consistent with these earlier studies.

Fig. 5.33 shows the experimental measurements of the present work for the isothermal ribbed rods compared with the results of Chamberlain, [113] for very rough surfaces collected by Davies, [50]. Davies considered that for τ^* less than 0.22, the deposition process is that of diffusion whilst for dimensionless relaxation times greater than this value, the deposition process becomes influenced by impaction. On this basis Fig. 5.33 shows that the dominant mechanism of deposition in the present work is that of diffusion as was concluded from the theoretical considerations of section 3.4.7. Also Fig. 5.33 shows that the present experimental results are in the same range of those obtained by Chamberlain, [102].

Also, Davies plotted the data of Wells and Chamberlain, [22], and that of Chamberlain, [113], when τ^* was less than 0.22, in an attempt to validate two deposition equations for that range, where

$$V^* = 0.075 \ Sc^{-2/3} \tag{5.5}$$

for smooth surfaces, and

$$V^* = 0.08 \ Sc^{-1/2} \tag{5.6}$$

for rough surfaces.

Fig. 5.34 shows these equations compared with the experimental results of the present work for the smooth and the ribbed rods.

Fig. 5.35 shows the present results for the isothermal smooth rods compared with the experimental results of Chamberlain et al., [41] for smooth surfaces. Fig. 5.36 shows the results of the isothermal ribbed rods of this work compared with those of Chamberlain et al., [41] for repeated ribbed surfaces also but with different pitch to height ratio. Again it can be seen that the results of the present work are in good agreement with work of Chamberlain et al., [41]

Schack et al., [55], introduced the data of Sehmel and Sutler, [55], to verify their general correlation for deposition of particles from turbulent gases to completely rough surfaces. The roughness length, y_0 was calculated according to the procedure of Chamberlain et al., [41], as shown in Fig. 5.37. The resultant y_0^* (y u_*/ν) from the graph satisfied the condition of Schack et al., which was that for $y_0^* > 7$ to 14 the surface can be considered as "rough", when the flow Reynolds number was 3×10^5

Fig. 5.3$\S$ shows the present results for the ribbed isothermal rod for both particle sizes at Re = 3 $\times$ 10^5 compared with those of Sehmel and Sutler, [114] Again, the agreement is good.

Returning to Fig. 5.1$\S$, the present data is compared with that of Wells and Chamberlain, [22], for different Reynolds numbers. Although the particles used by Wells and Chamberlain were larger (0.65 μm compared with 0.25 μm in the present data), the deposition rates over the smooth surfaces are similar those measured in the present work. The same is not true for the rough surfaces, however, where the deposition velocities for the larger particles are greater, showing that the surface generated turbulence has a greater influence in the eddy diffusion of the larger particles than of the smaller particles. Similar results have been obtained before by Chamberlain et al., [41], who indicated experimentally that the aerodynamically smooth filter-paper surface was more efficient in capturing particles than the aerodynamically rough AGR type surface, as can be seen by comparing their results in Fig. 5.35 with those in Fig. 5.36.

It should be mentioned that the experimentally measured results for the 0.25 μm particles and isothermal ribbed rod of the present work were found to be eighteen times greater than the experimental value of Hahn et al., [53], for 0.2 μm. Hahn's data is at odds with the data presented above although the test surfaces used by Hahn also had two dimensional roughness elements and the flow Reynolds number in the same range as the present work.

Although El-Shobokshy, [11], and Davies, [12], stated that there was no evidence of particle re-entrainment in their work, their re-

entrainment tests were carried out in different way. Their procedure was to repeat the deposition tests for different flow velocities for the same run time (one hour). Their conclusions were based on the observation that the deposition rate increased as the flow velocity increased. It is believed that the procedure of the present tests used for studying re-entrainment is more convincing. Furthermore, there was a significant difference between the results of El-Shobokshy and Davies although the range of the flow conditions were the same.

O'Brien et al., [115], studied the deposition of particles onto a heated and unheated cylinder. Their experimental results show that the percentage ratio of the deposition velocity onto a 40 °C heated cylinder (V_{th}) to that onto the unheated cylinder (V_o) was about 85 % for 0.06 μm diameter particles and a Reynolds number of 9.6 × 10^4. The percentage ratio of V_{th}/V_o was about 30 % for when the cylinder surface temperature was 60 °C for the same flow conditions. Comparison between these results and those of Fig. 5.28, indicate that O'Brien et al. obtained a greater thermophoretic effect than the present study even at a lower surface temperature. This could be due to the very different boundary layer conditions.

CHAPTER 6

EVALUATION OF THE THEORETICAL MODEL AND SCALING

TO THE REACTOR CONDITIONS

§6.1. Introduction

As mentioned earlier, the main purpose of the present work is to study the deposition of sub-micron particles onto an AGR fuel rod. To fulfil this it is necessary to apply the proposed theoretical approach to the reactor conditions. Many experimental data have been obtained for the reactor operating conditions, each condition has a different temperature distribution of the fuel rod surface and in the coolant (CO_2) along the channel. Also, each data has different mass flow rate of the coolant used in the reactor.

Typical data relating to the level of deposit and the corresponding temperature profiles have been obtained by Johnson, [2]. However, before applying the theoretical model to the conditions in the reactor it must first be compared with the experimental data presented in the previous chapter.

§6.2. Comparison of the Experimental Results with the Proposed Theoretical Model

§6.2.1 Results for the Isothermal surfaces

Although the experimental results showed good agreement with the available data of other investigators, as described in section 5.7, the theoretical model described in section 3.5 produced results which were significantly different to those measured experimentally along the smooth isothermal rod. For example the deposition measured along the smooth rod for the 0.25 μm diameter particles and a flow Reynolds number of 3×10^5 was about twice that predicted. Although differences of this magnitude are not unusual in aerosol studies it was considered to be unsatisfactory.

Similar differences between experimental results and theoretical models have been declared in the work of Whurr and White, [116], Owen, [109] and O'Brien et al., [115]. For example the theoretical values of O'Brien et al. are just one percent of the experimentally determined deposition rate on an unheated cylinder when the theoretical model proposed by Davies, [12], was used.

To obtain a better agreement between the theoretical calculations and the experimental results for the smooth rod, the surface roughness was taken into consideration where the roughness average was measured using a Talysurf. The measurement consisted of 100 readings including the joint between the individual sections. The resultant value of the roughness average was about 1.5 μm. This would normally be considered to be hydraulically smooth.

The theoretical deposition velocity considering the real surface of the smooth rod achieved a good agreement with the mean value of the experimental results especially at the higher flow Reynolds number. Fig. 5.11 shows the theoretical value of the deposition velocity compared with the mean value of the experimental results and its 95 $^o/_o$ confidence limits for 0.25 µm particles and a Reynolds number of 3 × 10^5 over a smooth "real" surface. In Fig. 5.16 the effect of including the smooth surface roughness for a Reynolds number of 3 × 10^5 and for 0.05 µm particles is clearly seen.

In Figs. 5.2, 5.3, 5.4, 5.10.a, 5.13 and 5.15, the theoretically predicted deposition velocities are shown together with the experimentally measured values. These have all been calculated by substituting roughness into equation (3.33).

For the ribbed rod, the calculation of the equivalent roughness by the method described in section 3.5.1 failed to achieve a good agreement between the theoretical calculation of the deposition velocity and the experimental results. Also, it is difficult to relate the roughness associated with the ribs to the random roughness model used in the theory. For this reason it was decided to use a scaling factor to fit the theoretical values of the deposition velocity with those of the experimental results. The scaling factor (α) was chosen by multiplying $f(k_s^*)$ in equation (3.34) by α and adjusting its value until a reasonable fit was obtained. This decision to place faith in the experimental data was based mainly on the good agreement of the experimental results with the data of other investigators, as described

in section 5.7, and the good agreement achieved for the smooth rod when the surface roughness was included in the calculations.

The factor (α) required for scaling the equivalent roughness to align the experimental data with the theoretical calculation was 0.1 as shown in Fig. 5.13, and it was decided to use this value in all of the analyses. The resulting theoretical prediction and the mean value of the experimental results and its 95 $^o/_o$ confidence limits are shown in Fig. 5.12 for the 0.25 μm particles and flow Reynolds number of 3 × 10^5. The resulting theoretical calculation for each deposition test is shown, together with the relative experimental data in Figs. 5.5, 5.6, 5.7, 5.15 and 5.17.

§6.2.2 Results for the Heated surfaces

The results for the heated rods show that the theory underpredicts the deposition velocity of particles, i.e. overstates the influence of the thermophoresis. The greatest discrepancy was seen in the case of particles having 0.25 μm diameter where the maximum difference was about eight orders of magnitude for the smooth heated rod.

Again this huge discrepancy between the theoretical calculations of the deposition velocity and the experimentally measured results for heated surfaces has been declared in the work of previous investigators. The theoretical results of Whurr and White, [116], were about 300 times smaller than the experimentally measured ones. This difference in the work of Owen, [109], was up to two orders, while in the work of O'Brien et al, [115], the theoretical value for points around the test cylinder were found to be practically zero for both 40 °C and

60 °C mean surface temperature while the experimental deposition was found to be present.

This exaggerated theoretical effect of the thermophoresis has been declared before by Ryley and Al-Azzawi, [117], for example, who show that if the internal steam heating were applied to the guide blades of a low pressure steam turbine then a temperature difference of just 20 °C would be sufficient to repel fog droplets away from the surface of the blade. On the other hand El-Shobokshy, [118], showed that a 30 °C temperature difference is sufficient to prevent the deposition of particles less than 1 μm in a turbulent pipe flow.

The reason for this discrepancy between the theoretically predicted values and the experimentally measured results could be due to the presence of the eddies of turbulence in the flow penetrating through into the laminar sub-layer in a manner described by Kline et al., [29]. The particles would be expected to be captured by the surface in the downward sweep of new fluid which follow the bursts without being affected by the mean temperature gradient. An isolated eddy can contain large numbers of particles and will have its own temperature gradient which will have no relation to the mean gradient. Furthermore, the experimental measurements which support the theoretical expressions of the thermophoretic velocity were carried out in a quiescent flow condition where the effects of the eddies of turbulence were absent.

The relevant equation of the deposition velocity, used in the present work, is an exponential function and very sensitive in particular to the calculated value of the velocity of themophoresis, V_T.

The themophoretic velocity itself is derived from the expression due to a fitting formula of Talbot et al., [64]. They claimed that their formula was found to agree within 20 %, with the majority of the available data. Unfortunately, these errors would accumulate and magnified by the exponential function used in the calculations of the deposition velocity in the presence of thermophoresis.

In an attempt to overcome this discrepancy between the theoretical predictions and the experimentally measured deposition velocity, attention was drawn to the expression for the thermophoretic velocity where the suspect parameter is the temperature gradient. A correction factor was therefore used to scale the temperature gradient to align the experimentally measured results with the theoretically predicted values. The resulting scaling factor, (β) was found to be 0.2. Fig. 6.1 shows the deposition velocity for the 0.25 μm particles with a flow Reynolds number of 3×10^5 for the smooth rod heated to about 95 °C. No physical model is presented to justify factoring the temperature gradient other than the observation that the actual gradient present under deposition conditions may well be less than the average thermal gradient at the surface. The theoretically predicted values of V_{th}/V_o are shown together with the relevant experimentally measured results, in Figs. 5.18 to 5.31.

Fig. 6.2 shows the calculated deposition velocity as a function of particle size for the ribbed AGR fuel rod and for the hydraulically smooth rod used in the experiments. The calculation for the ribbed rod includes the roughness scaling factor, α, whilst the calculation for the smooth rod includes the measured roughness of 1.5 μm.

Fig. 6.3 shows the effect of thermophoresis for 0.25 μm particles, a flow Reynolds number of 3×10^5 and with surface to air temperature differences of +/- 300 °C.

§6.3 Deposition Calculations for Typical AGR Operating Conditions

Comparison of the theoretical predictions with the experimentally measured deposition indicated that the equivalent ribs height (e^2/p) had to be scaled by a factor of 0.1. Furthermore, the surface temperature gradient had to be scaled by a factor of 0.2 to match the thermophoretic data. To achieve the required similarity between the experimental laboratory conditions and the reactor operating conditions, it was suggested that since the deposition is controlled by the surface condition rather than the bulk flow conditions, the scaling should be made on the equivalence of the rib-based Reynolds number. Using this criterion the equivalent roughness used in the deposition calculation becomes

$$\text{equivalent random roughness in the reactor case} = 0.1 \left(\frac{e^2}{p}\right) \left[\frac{\nu_{CO_2}}{\nu_{air}} \ \frac{u_{*air}}{u_{*CO_2}} \right] \tag{6.1}$$

Since the terms in the large brackets are of order 0.1, then the height of the random roughness substituted into the theoretical model was taken as 0.01 times e^2/p for the reactor case. The scaling factor needed for the temperature gradient to be used in the expression of Talbot et al., [64], for the thermophoresis velocity was 0.2, as used for the laboratory conditions. Based on the previous considerations the deposition velocity was calculated for the typical operating conditions of the AGR obtained by Johnson, [2].

A distinctive feature of all channel flows is the entry length effect. Deissler, [105], showed that the friction factor takes a finite length to reach its fully developed value and this variation with the distance, x, along a channel with a hydraulic equivalent diameter, d_e, is fitted by the following equation:

$$\frac{f_e}{f_d} = 1.09 + 0.502 \left(\frac{d_e}{x}\right) \qquad (6.2)$$

where f_e is the friction factor through the entry and f_d is the fully developed value of the friction factor through the channel.

The fully developed value of the friction factor of the reactor channel used in the theoretical calculation is given by the formula of Rapier, [105], and takes the form

$$f_d = 0.0115 + 1.325 \left(\frac{e}{d_e}\right) + 0.265 \left(\frac{e}{2\,r}\right) \qquad (6.3)$$

The temperature gradient, ∇T needed to calculate the velocity of thermophoresis was considered as

$$\nabla T = \frac{Nu}{d_e} (T_s - T_g) \qquad (6.4)$$

and the Nusselt number obtained by

$$Nu = St \cdot Re \cdot Pr \qquad (6.5)$$

According to Rapier, [105], the Stanton number for the fuel pin surface was found experimentally to be

$$\frac{St}{St_s} = 2.4 + 20 \left(\frac{e}{d_e}\right) + 8 \left(\frac{e}{2\,r}\right) \qquad (6.6)$$

where the smooth Stanton number, St_s, is given by:

$$St_s = 8.26 \times 10^{-4} + 7.6125 \times 10^{-2}\, Re^{-0.32} \qquad (6.7)$$

The main condition for the correlation of Rapier is that

$$(e \; \frac{u_*}{\nu}) > 40.$$

Fig. 6.4 shows the calculated deposition velocity of 0.2 μm particles along the axial distance of the fuel rod. Due to the higher friction velocity and the lower temperature difference between the fuel pin surface and the coolant at the inlet of the channel, (see Fig.1.2), the deposition velocity curve starts with its maximum value. The effect of the thermophoresis is clearly seen. As the surface temperature increases the temperature gradient increases so the deposition velocity consequently decreases. At the end of the channel the surface temperature of the fuel rod gradually decreases whereas the gas temperature continues to increase, the deposition velocity therefore increases as a reflection of the decreasing temperature gradient in this region.

For sixty days operating cycle and with the assumption of a free stream concentration of 10 μg/m^3, the thickness of the deposition layer was estimated by calculation and is shown in Fig. 6.5. This thickness of the deposition layer is obviously dependent on the operating time, the unknown free stream concentration as well as the possibility of the re-entrainment of the deposited particles. Due to the thickness of the deposition layer, there is a possibility of aerodynamic particle removal from the surface. This removal will mainly depend on the surface shear stress.

Fig. 6.6 shows the distribution of the removal wall shear stress along the axial distance of the channel according to equations (6.2) and (6.3) for the friction factor for the entrance and for the fully

developed regions. The surface shear stress starts with a high value at the beginning of the entrance length, decreasing rapidly to a minimum value and then increases gradually along the length of the channel.

Cleaver, [119], represented data from wide range of experimental and theoretical studies relating to the removal of the particles as shown in Fig. 6.7, which indicates the critical wall shear stress at which particles of a given diameter are expected to be removed.

Using the wall shear stress distribution of Fig. 6.6 with the data presented by Cleaver, the deposition layer may take the final form as shown in Fig. 6.8. The high shear stress in the entry length is high enough to remove the deposited layer in this region, also the high value of the shear stress may also contribute to the removal of the deposited layer at the end of the channel. In the middle of the channel the deposition layer is thinner, as a reflection of thermophoretic effect, and the wall shear stress is insufficiently high to cause removal.

The final predicted shape of the deposition layer, in general terms, agrees with the observed trends of the reactor operating conditions as indicated, for example, by Skyrme and Reeks, [120]. The predictions can only be qualitative since the free stream concentration is unknown.

CHAPTER 7

CONCLUSION AND FUTURE WORK

§7.1. General Summary

A study of the deposition of sub-micron particles has been carried out in an attempt to investigate the possible mechanisms of particle deposition on the fuel elements of advanced Gas-cooled Reactors. The main results of the deposition of such particles are that the deposited material acts as an insulating layer and in time the benefits of roughening the surface, to increase the heat transfer to the coolant, are lost. The output of the power station can be significantly reduced.

Modelling of the deposition was achieved by using sub-micron uranin particles in a full scale laboratory flow rig using air instead of carbon dioxide. The particles were produced by a well established atomiser-impactor method.

Electron microscope analysis was used to determine the diameter of the particles produced by the atomizer-impactor generator. The particles produced were moderately monodispersed, statistical methods were undertaken to determine the mass-median diameter and the geometric standard deviation. Particles having 0.25 μm and 0.05 μm mass-median diameters with 1.64 and 1.47 geometric standard deviation respectively, could be produced from two different solution of uranine of 5 °/ₒ and 0.2 °/ₒ respectively.

A general survey of the available particle deposition models and of the formulae of thermophoretic velocity, was carried out. A deposition model introduced by Browne, [42], was chosen for application to the present study because it considered the effect of the surface roughness; it is an extension of the theory of Davies, [27], which appears to be logical and has achieved good agreement for sub-micron particles, [22]. The fitting formula obtained by Talbot et al., [64], for the velocity of thermophoresis was adopted for considering the effect of themophoretic forces on the deposition process of particles in the case of heated rods.

Some aspects of particle behaviour were studied and the theoretical model assumed the following :

a- Any particle that collides with the surface must be captured.

b- After the deposition process has taken place, no re-entrainment of particles will occur.

c- The mechanism which is mainly responsible for the deposition process is eddy-diffusion, resisted by the thermophoretic force in the case of heated surfaces.

The thermal conductivity of the particle material was taken as the value measured by Al-Azzawi and Owen, [84], about 0.43 W/mK, while the density of the particle material was taken as 1700 kg/m^3 as given by Parker and Ryley, [9].

A pipe flow rig was designed and constructed to carry out the required experimental part of this study. The working section was located at a position where the flow becomes fully developed turbulent flow where the ratio of the entry length to the equivalent hydraulic

diameter was greater than 30. The flow was characterised for six different Reynolds number; the deposition tests were carried out for three of them, viz. 3×10^5, 6×10^4 and 5×10^3

The skin friction factor for the smooth rod was measured using the technique of Clauser, [4], and by using a Preston tube. The single equation of Lewkowicz et al., [88], was used for the Preston tube calculations. The resulting values of the corresponding friction velocity were compared with the equation of Reichardt, [101], and that of Deissler, [102].

The friction factor for the ribbed surface was determined using the graphical method of Perry and Joubert, [6]. The calculated values of the friction factor were compared with the equation introduced by Winkel, [103], and the measured values of Wilkie, [1], for a similar surface.

To assess the effect of thermophoresis on the deposition of particles an electrical resistance heating technique was used for heating the test surface. The tie-rod was used as a resistance heating element which was already electrically insulated from the test rod and the supporting flanges using an insulating material of monolux 500. It was possible to obtain approximately the same three surface temperature distributions for both the smooth rod and the ribbed rod at flow Reynolds number of 3×10^5. The higher surface temperature distribution could be obtained for the flow Reynolds number of 6×10^4 and 5×10^3 for both surfaces.

The heat transfer coefficient relevant to each case was calculated. McAdams formula was used for comparison with the results for the smooth rod. Also the corresponding Stanton numbers for smooth and ribbed rods were compared with the formulae introduced by Burgoyne et al., [104], and Rapier, [105], and the values obtained experimentally by Wilkie, [1].

A fluorimetric analysis technique was used to measure the deposition rate of particles and the free stream particle concentration. The basic idea of this technique is that after dissolving the particles deposited onto the test surface into a known amount of de-ionized water, the concentration of the resulting solution is measured and compared with a standard (known) solution of the particle material. The same method was applied for the free stream concentration where samples were extracted using a vacuum pump. A millipore filter paper was used to capture the particles from the sample; knowing the total volume of the extracted air the concentration of the particles in the free stream can then be calculated. The deposition velocity of the particles was calculated as a ratio of the deposition rate of particles to the free stream concentration, whilst the nondimensional value of the deposition velocity could be obtained by referring it to the value of the friction velocity.

Due to the variation of the deposition velocity measured along the surfaces in the initial tests, the deposition tests were repeated three times under the same conditions; statistical methods were then used to obtain the value along the test rod and the corresponding 95 $^{\circ}/_{\circ}$ confidence limits.

Time variation effects were studied experimentally for particles of 0.25 μm diameter at a flow Reynolds number of 3×10^5 for both the smooth rod and the ribbed one. Also the blow-off tests were carried out for the smooth rod under the same conditions.

The deposition tests were carried out for isothermal smooth and ribbed rods at flow Reynolds numbers of 3×10^5, 6×10^4 and 5×10^3 for a particle size of 0.25 μm mass-median diameter. Also the deposition tests were repeated for a particle size of 0.05 μm at 3×10^5 and 5×10^3 flow Reynolds number.

To investigate the effect of surface temperature , the deposition tests were carried out for both the surfaces at the same flow Reynolds number (3×10^5) and different surface temperature distributions. The effect of flow Reynolds number was investigated by carrying out the tests for both surfaces at the same surface temperature distribution for different flow Reynolds number, which was 5×10^3.

To study the effect of particle diameter on the thermophoretic deposition results, the deposition tests were also carried out using particles having 0.05 μm mass-median diameter at the higher surface temperature for the flow Reynolds numbers 3×10^5 and 5×10^3

Considering the possible contamination of the ambient air, a background test was carried out for each case of the deposition tests.

The experimentally measured results have been discussed and the compared with those of other investigators, such as Montgomery and Corn, [111], Wells and Chamberlain, [22], Sehmel, [112], Friedlander and Johnstone, [23], Chamberlain, [113], Sehmel and Sutler, [114],

Hahn et al., [53], El-Shobokshy, [11], Davies, [12], and O'Brien et al., [115]. Also, comparisons between the proposed theoretical model and the experimentally measured results have been made. Finally the theoretical model was applied to typical AGR data obtained by Johnson, [1].

§7.2. Conclusions

The main conclusions from the investigations may be summarised as follows :

1) The atomizer-impactor technique can be used successfully for generating moderately monodispersed sub-micron particles. The compressed air needed for the atomisation process was maintained at 40 psi (about 2.8 bar) while the gap of the impactor plate was adjusted to be 1.8 mm. The particles produced from the uranin solution of 5 $^o/_o$ and 0.2 $^o/_o$ had mass-median diameters of 0.25 µm and 0.05 µm with geometric standard deviation of 1.64 and 1.47. respectively.

2) The fully developed turbulent friction factor was established through the working section of the pipe flow rig, which was located at a position where $L_e \simeq 32 \ d_e$. This agrees with the equation of Latzko, [98], and the theoretical results of Deissler, [99], for the entry length needed for the friction factor to be fully developed.

Also the velocity profiles indicated that fully developed turbulent flow was established through the working section. This agrees with the formula of Kelly, [77], rather than the calculations of Walklate, [96].

3) The skin friction factor for a smooth surface can be measured using the technique of Clauser, [4], and the equation of Lewkowicz, [88], with a Preston tube. The typical values of the skin friction factor were in the range of 4.5×10^{-3} to 0.011. The relevant friction velocity agrees with the equation of Reichardt, [101], and that of Deissler, [102]. The transformation method introduced by Hall, [89], could not be used to determine the friction factor for the ribbed surface because the fuel element rod size is so small with respect to the size of the channel while the graphical method of Perry and Joubert, [6], could be applied. The calculated values of the friction factor were found to be the same range as the correlation of Winkel, [103], and the experimental data shown by Wilkie, [1], and were typically in the range of 0.012 to 0.018.

4) The heat transfer equation of the test surface could be solved by a finite difference method. The calculated heat transfer coefficient for the smooth rod agrees with the formula of McAdams, [120]. Also the corresponding Stanton number agrees with the correlation of Burgoyne et al., [104], and that of Rapier, [105]. The Stanton number for the ribbed surface agrees with the data of Wilkie, [1]. The typical values of Stanton number for the smooth rod was about 2.9×10^{-3} whilst for the ribbed rod was about 4.6×10^{-3} at flow Reynolds number of 3×10^{5}.

5) The theoretical considerations and the experimentally measured results confirm that there is no evidence for particle re-entrainment during the deposition tests for sub-micron particles for the condition of this study. Also the experimental deposition tests show that the total mass deposited during the test period increases linearly.

6) The good agreement between the theoretical calculations and the experimentally measured results of the deposition velocity for the "real" smooth surface verifies the following :

a- The roughness of the surface, whatever it is, must be considered for the deposition of the sub-micron particles.

b- The deposition model introduced by Browne, [42], when supplied with the true surface roughness, adequately predicts the rate of the deposition.

c- The eddy-diffusion mechanism controls the deposition process for particles such as those used in this study, the effect of inertia and sedimentation can be neglected.

d- For the deposition process of sub-micron particles, the eddy diffusivity of the particle can be taken as that of the fluid eddy diffusivity. This agrees with the analysis of Rouhianen and Stachiewicz, [36].

e- Particles can be accurately defined by their mass-median diameter if they are moderately monodispersed.

f- Ion generator technique and earthing of the test surface can overcome problems of electrostatic charge in the deposition tests.

7) The theoretical calculations and the experimentally measured results show that :

i- As the flow Reynolds number is increased the deposition velocity increases. This a reflection of increasing the friction velocity which promotes the turbulent diffusivity.

ii- The deposition velocity for smaller particles (0.05 µm) is higher than that for larger ones (0.25 µm). This is because increasing the particle size decreases the Brownian diffusion coefficient without a sensible increase in the inertial effect, this leads to decrease the final deposition velocity.

8) For the ribbed surface, the equivalent roughness obtained by assuming that additional area of the cross-section produced by the rib was spread along the distance between the ribs proved to be inadequate. The theoretical calculation based on this definition failed to achieve a good agreement with the experimentally measured results. It proved necessary use a factor of 0.1 on the equivalent rib height to align the theoretical calculations with the experimental results for isothermal ribbed rod. The faith in the experimental data was based on the good agreement of the experimental results with those of other investigators.

The deposition velocity for the ribbed rod is much higher than for the smooth rod, especially at higher flow Reynolds numbers, this can be up to twenty fold at flow Reynolds number of 3 × 10^5. Using the scaling factor, the theoretical calculations agree with the experimentally measured results that as the flow Reynolds

number is increased the deposition velocity increases (as for the smooth rod). In the sub-micron range the effect of particle diameter on the deposition rate is only seen at low flow Reynolds numbers; at higher flow Reynolds numbers the deposition velocity is independent of the particle diameter.

9) For hot surfaces, thermophoretic effects must be taken into account in the deposition of sub-micron particles. The deposition velocity is less than that for an isothermal surfaces as a reflection of the temperature gradient developed at the surface which forms a thermophoretic force to drive the particles away. It has been necessary to use another scaling factor to align the theoretical calculations of the deposition velocity with thermophoresis, with the experimentally measured results. This factor was found to be 0.2 which gives good agreement particularly at the higher surface temperature and higher flow Reynolds number. For both the smooth rod and the ribbed rod as the surface temperature is increased the deposition velocity consequently decreases. This is due to the increasing thermophoretic forces which drive the particles away from the surface. Also, as the flow Reynolds number is increased the effect of thermophoresis reduces for the same surface temperature. This is a reflection of the higher friction velocity and greater turbulent energy which promotes the deposition of particles by overcoming the effect of thermophoresis. The effect of thermophoresis on the smaller particles (0.05 μm) is less than that on the larger ones (0.25 μm). This is due to the fact that the smaller particles have a smaller temperature difference across them, which in turn leads to a lower molecular imbalance. Also the effect

138

of thermophoresis over the rib ribbed surface is less than over the smooth surface, this is due to the enhanced turbulence near to the ribbed surface which increases the deposition of particles.

§7.3. Future Work

The deposition tests in the present study were carried out for single smooth and ribbed rods mounted axially in the working section of the pipe flow flow rig, which is not the real shape of the reactor channel. So, it is suggested that the deposition test be repeated for more a realistic configuration where a number of fuel elements are mounted in the working section. Also the heating of the elements around the test rod must be applied.

The experimental work must be extended to obtain a compete picture of the deposition velocity under the influence of the following parameters :

    a- the particle diameter in the sub-micron range.

    b- the flow Reynolds number.

    c- the temperature of the test surface.

New models need to be developed which take account of the effect of turbulence on the temperature field around the particles.

Although sub-micron particles cannot be removed by fluid dynamic forces it is likely that after substantial agglomeration on the surface, where each particle loses its own identity, that removal will occur.

In many industrial situations the surface is colder than the gas stream e.g., internally cooled gas turbine blades and boiler tubes.

Under these circumstances the thermophoretic forces will be assisting the deposition process. Given the inadequacy of the models used to predict thermophoretically reduced deposition, it is recommended that the inverse situation, with a cooled surface, be studied.

REFERENCES

[1]- Wilkie,D. (1966)

"Forced convection heat transfer from surfaces roughened by transverse ribs"

Paper No. 1, 3rd Int. Heat Transfer Conference, Chigago, Augst.

[2]- Johnson, P. A. V. (1985)

UKAEA Private Communication.

[3]- Kelly, B. T. (1984)

"A particulate model for low temperature deposition in Advanced Gas-cooled Reactors"

UKAEA Report ND-M-2537(s).

[4]- Clauser, F. H. (1954)

"Turbulent boundary layers in adverse pressure gradients"

J. Aeronaut. Sci., 21, 2, 91-108.

[5]- Preston, J. H. (1953)

"The determination of turbulent skin friction factor by means of Pilot tubes"

J. R. Aeronaut. Soc., 58, 109-121.

[6]- Perry, A. E. and Joubert, P. N. (1963)

"Rough-wall boundary layers in adverse pressure gradients"

J. Fluid Mech., 17, 193-211.

[7]- Wohers, H. C., Kass, T. E. and Johnson, K. R. (1959)

"Fluorescent dyes as airborne tracer material"

A.S.T.M. Tech. Publ., 281, 15-22.

[8]- Whitby, K. T., Lundgrem, D. A. and Peterson, C. N. (1965)

"Homogeneous aerosol generators"

Int. J. Air Wat. Poll. Pergamon Press, 9, 263-277.

[9]- Parker, G. J. and Ryley, D. J. (1969-70)

"Equipment and techniques for studying the deposition of sub-micron

particles on turbine blades"

Proc. Instn. Mech. Engrs., 184, 3c, 43-51.

[10]- Parker, G. J. and Lee, P. (1972)

"Studies of the deposition of sub-micron particles on turbine blades"

Proc. Instn. Mech. Engrs., 186, 519-526.

[11]- El-Shobokshy, M. S. (1975)

"Diffusional Deposition of fog droplets onto low-pressure steam turbine

guide blades at off-design conditions"

Ph.D. Thesis, Mech. Eng. Dept., University of Liverpool.

[12]- Davies, J. B. (1980)

"The effect of thermophoresis on the deposit of fog droplets on low-

pressure turbine fixed blades"

Ph.D. Thesis, Mech. Eng. Dept., University of Liverpool.

[13]- Al-Azzawi, H. K. (1984)

"Studies on the internally-heated steam turbine fixed blade and its

influence on the cost of replacing eroded blades"

Ph.D. Thesis, Mech. Eng. Dept., University of Liverpool.

[14]- Fuchs, N. A. and Sutugin, A. G. (1966)

"Generation and use of monodisperse aerosols"

Aerosol Science, Academic Press, (edited by Davies, C.N.).

[15]- Green, H. L. and Lane, W. R. (1964)

"Particulate Clouds: Dusts, Smokes and Mists"

General and Industrial Chemistry Series, (edited by Bunbury,H.M.).

[16]- Bergland, R. N. and Liu, B. Y. H. (1973)

"Generation of monodisperse aerosol standards"

Envirom. Sci. Technol., 7, 2, 147-153.

[17]- Whitby, K. T. (1961)

"Generation for producing high concentrations of small ions"

Rev. Sci. Instrum., 32, 1351-1355.

[18]- Drinker, P. (1925)

"The size-frequency and identification of certain phogocytosd Dusts"

J. Ind. Hyg., 7, 305-

[19]- Loveland, R. P. and Trivelli, A. P. H. (1927)

"Mathematical methods of frequency analysis of size of particles"

J. Franklin Inst., 204 (2), 193-217.

[20]- Drinker.P and Hatch, T. F. (1936)

"Industrial dust"

1st. Ed., McGraw-Hill, New York .

[21]- Hatch, T. and Choate, S. P. (1925)

"Statistical distribution of the size properties of non-uniform

particulate substances"

J.Franklin Inst., 207, 369-387.

[22] Wells, A. C. and Chamberlain, A. C. (1967)

"Transport of small particles to vertical surfaces"

Br. J. App. Phy., 18, 1793-1799.

[23] Frindlander, S. K. and Johnstone, H. F. (1957)

"Deposition of Suspended Particles From Turbulent Gas Streams"

Ind. Eng. Chem., 49, 1151-1156.

[24] Liu, B. Y. H. and Agramal, J. K. (1974)

"Experimental observation of aerosol deposition in turbulent flow"

Aerosol Sci., 5, 144-155.

[25] Gardner, G. C. (1975)

"Deposition of particles from a gas flowing parallel to a surface"

Int. J. Mult. Flow, 2, 213-246.

[26] Davies, C. N. (1966)

"Deposition of aerosols from turbulent flow through pipes"

Proc. Roy. Sco. A, 289, 235-318.

[27] Davies, C. N. (1966)

"Deposition from moving aerosols"

"In: Aerosol Science, Editor Davies, C. N., Academic Press, London.

[28] Owen, P. R. (1969)

"Pneumatic transport"

"J. Fluid Mech., 39 (2), 407-432.

[29] Kline, S. J., Reynolds, W. C., Schraub, F. A. and
    Runstadler, P. W. (1967)
"The structure of turbulent boundary layers"
"J. Fluid Mech., 30 (4), 741-773.

[30] Hutchinson, P., Hewitt, G. F. and Dukler, A. E. (1971)
"Deposition of liquid or solid dispersions from turbulent gas streams:
a stochastic model"
"Chem. Engng. Sci., 26, 419-439.

[31] Reeks, M. W. and Skyrme, G. (1976)
"The dependence of particle deposition velocity on particle inertia in-
ertia in turbulent pipe flow"
"J. Aerosol Sci., 7, 485-495.

[32] Laufer, J. (1954)
"The structure of turbulence in fully developed pipe flow"
NACA Report 1174.

[33] Lin, C. S., Moulton, R. W. and Putnam, G. L. (1951)
" Mass transfer between solid wall and fluid streams"
"Mechanism and eddy distribution relationships in turbulent flow"
Ind. Engng. Chem., 45, 637-646.

[34] Owen, P. R. (1960)
"Dust deposition from a turbulent air stream"
"In: Aerodynamic capture of particles (Pergman Press, Oxford).

[35] Beal, S. K. (1970)
"Deposition of particles in turbulent flow on channel of pipe walls"

Nucl. Sci. Eng., 40, 1-11.

[36] Rouhiainen, P. O. and Stachiewicz, J. W. (1970)
"On the deposition of small particles from turbulent streams"
J. Heat Trans., 92, 169-177.

[37] Sehmel, G. A. (1970)
"Particle deposition from turbulent air flow"
J. Geophys. Res., 75 (9), 1766-1781.

[38] Sehmel, G. A. (1971)
"Particle diffusivities and deposition velocities over a horizontal smooth
surface"
J. Colloid and Interface Sci., 37 (4), 891-906.

[39] Liu, B. Y. H. and Ilori, T. A. (1973)
"Inertial deposition of aerosol particles in turbulent pipe flow"
ASME Symp on Flow Studies in Air and Water Pollution, Atlanta.
Georgia. USA, 103-113.

[40] Kneen, T. and Strauss, W. (1969)
"Deposition of dust from turbulent gas streams"
Atmo. Enviro., 3, 55-67.

[41] Chamberlain, A. C., Garland, J. A. and Wells, A. C. (1984)
"Transport of gases and particles to surfaces with widely spaced
roughness elements"
B.L. Meteorology, 29, 343-360.

[42] Browne, L. W. B. (1974)

"Deposition of particles on rough surfaces during turbulent gas-flow in a pipe"

Atmo. Enviro., 8, 801-816.

[43] Perry, A. E., Schofield, W. H. and Joubert, P. N. (1969)

"Rough wall turbulent boundary layers"

J. Fluid Mech., 37 (2), 386-387.

[44] Grass, A. J., (1971)

"Structural features of turbulent flow over smooth and rough boundaries"

J. Fluid Mech., 50 (2), 233-255.

[45] Colebrook, C. F. and White, C. M. (1937)

"Experiments with fluid friction in roughened pipes"

Proc. Roy. Soc. A 161, 367-381.

[46] El-Shabokshy, M. S. and Ismail, I. A. (1980)

"Deposition of aerosol particles from turbulent flow onto rough pipe wall"

Atmo. Enviro.,14, 297-304.

[47] El-Shabokshy, M. S. (1983)

"Experimental measurements of aerosol deposition to smooth and rough surfaces"

Atmo. Enviro.,17 (3), 639-644.

[48] Woods, N. B. (1981)

"A simple method for the calculation of turbulent deposition to smooth and rough surfaces"

Aerosol Sci., 12 (3), 275-290.

[49] Cleaver, J. W. and Yates, B. (1975)

"A sub-layer model for the deposition of particles from a turbulent flow"

Chem. Engng. Sci., 30, 983-992.

[50] Davies, J. T. (1983)

"A new theory of the deposition of colloidal particles from turbulent fluids"

Ann. N. Y. Acad. Sci., 404, 313-326.

[51] Davies, J. T. (1983)

"A new theory of aerosol deposition from turbulent fluids"

Chem. Engng. Sci., 38,135-139.

[52] Kader, B. A. and Yaglom, A. M. (1977)

"Turbulent heat and mass transfer from a wall with parallel roughness ridges"

Int. J. Heat Mass Trans., 20, 345-357.

[53] Hahn, L. A., Stukel, J. J., Leong, K. H. and
    Hopke, P. K. (1985)

"Turbulent deposition of sub-micron particles on rough walls"

J. Aerosol Sci., 16 (1), 81-86.

[54] Owen, I., El-Kady, A. A. and Cleaver, J. W. (1985)

"A note comparing the rates of deposition of submicron particles with the rates of heat transfer for ribbed surfaces exposed to turbulent gas streams"

J. Aerosol Sci., 17 (2), 145-148.

[55] Schack, C. J., JR, Pratsinis, S. E. and
Friedlander, S. K. (1985)
"A general correlation for deposition of suspended particles from turbulent gases to completely rough surfaces"
Atmo. Enviro., 19 (6), 953-960.

[56] Tyndall, J. (1870)
"On dust and disease"
Proc. Roy. Inst., 6, 1-

[57] Maxwell, J. C. (1879)
"On stresses in rarified gases arising from inequalities of temperature"
Phil. Trans. Roy. Sco. London, 170 (1), 231-256.

[58] Hidy, G. M. and Brock, J. R. (1970)
"The dynamics of aerocolloidal systems"
Pergman Press. Oxford.

[59] Epstein, P. S. (1929)
"Zur theorie des radiometers"
Z. Phys., 54, 537-563.

[60] Brock, J. R. (1962)
"On the theory of thermal forces acting on aerosol particles"
J. Colloid, Sci., 17, 768-780.

[61] Loyallka, S. K. and Ferziger, J. H. (1967)
"Model dependence of the slip coefficient"
Phys. Fluids, 10, 1833-1839.

[62] Loyallka, S. K. (1968)

"Momentum and temperature-slip coefficients with arbitrary accomodation at the surface"

J. Chem. Phys., 48, 5432-5436.

[63] Ivchenkov, I. N. and Yalamov, Ya. I. (1971)

"A hydrodynamic method for the calculation of the rate of thermophoresis of moderately large involatile aerosol particles"

Russian J. Phys. Chem., 45 (3), 317-319.

[64] Talbot, L., Cheng, R. K., Schefer, R. W. and
      Willis, D. R. (1980)

"Thermophoresis of particles in a heated boundary layer"

J. Fluid Mech., 101 (4), 737-758.

[65] Derjagiun, B. V. and Yalamov, Ya. I. (1965)

"Theory of thermophoresis of large aerosol particles"

J. Colloid Sci., 20, 555-570.

[66] Derjagiun, B. V. and Bakanov, S. P. (1961)

"The theory of the slipping of a gas along a rigid surface under the action of a temperature gradient"

Dokl. Akad. Nauk. SSSR 141, 384-386.

[67] Byers, R. L. and Calvert, S. (1969)

"Particle deposition from turbulent streams by means of thermal force"

I & EC Fund., 8 (4), 646-655.

[68] Tong, T. N. and Bird, G. A. (1971)

"The thermal force in the low density limit"

J. Colloid and Interface Sci, 35 (3), 403-408.

[69] Waldmann, L. (1959)

"Uber die kraft eines inhomogenen gases auf kliene suspendierte"

Z. Naturforsch, 14 A, 588-599.

[70] Bakanov, S. and Derjagiun, B. V. (1960)

"The motion of a small particle in a non-uniform gas mixture"

Disc. Faraday Soc., 30, 130-138.

[71] Jacobsen, S. and Brock, J. R. (1965)

"The thermal force on spherical sodium choride"

J. Colloid Sci., 20, 544-554.

[72] Waldmann, L. and Schmitt, K. H. (1966)

"Thermophoresis and diffusiophoresis of aerosols"

In: Aerosol Science, (Editor Davies, C.N.) Academic Press, London.

[73] Derjagiun, B. V. and Bakannov, S. P. (1957)

"The theory of the movement of small aerosol particles in a diffusing field"

Dokl. Akad. Nauk. SSSR, 117, 959-962.

[74] Schmitt, K.H. (1959)

"Untersuchungen an schwebstoffteilchen im temperaturfeld"

Z. Naturforsch, 14 A, 870-881.

[75] Schadt, C. F. and Cadle, R. D. (1961)

"Theermal forces on aerosol particles"

J. Phys. Chem., 65 (2), 1689-1694.

[76] Brock, J. R. (1967)

"The thermal force in the transition region"

J. Colloid and Interface Sci, 23, 448-452.

[77] Kelly, B. T. (1984)

"A particulate model of low temperature carbon deposition in the windscale AGR"

UKAEA Report ND-M-2762 (s).

[78] Im, K. H., and Chung, R. M. (1983)

"Pariculate deposition from turbulent parallel streams"

AICHE, J., 29 (3), 489-505.

[79] Dahneke, B. (1971)

"The capture of aerosol particles by surfaces"

J. Colloid Interface Sci., 37 (2), 342-353.

[80] Corn, M. and Silverman, L. (1965)

"Removal of solid particles from solid surface by Turbulent air stream"

J. Amr. Ind. Hyg. Assoc., 22, 337-347.

[81] C. R. C. Limited, (1978-1979)

"Handbook of Chemistry and Physics"

Published by C. R. C. Press, 59th edition.

[82] Kayes, G. W. C. and Laby, T. H. (1973)

"Tables of physical and chemical constants and mathematical functions"

Longman Group Ltd., London.

[83] B. D. H. Chemical Limited (1985)

"Private Communications".

[84] Al-Azzawi, H. K. and Owen, I. (1984)

"Measuring the thermal conductivity of uranine"

Int. J. Heat and Fluid Flow, 5, 1, 57-59.

[85] Millikan, C. D. (1939)

"Turbulent flows in channels and circular tubes"

Pro. fifth Int. Congr. Appl. Mechanisms, 386-392.

[86] Patel, V. C. (1965)

"Calibration of the Preston tube and limitations on its use in preasure

gradients"

J. Fluid Mech., 23, 1, 185-208.

[87] Rechenberg, I. (1963)

"Messung der turbulenten Wandschubspannung"

A. Flugwiss, 11, 429-

[88] Lewkowicz, A. K., Ming, X. and Meier, H. U. (1981)

"New Data and a single equation calibration formula for Preston tubes"

DFVLAR IB 222, 81A17.

[89] Hall, W. B. (1981)

"Heat transfer in channels having rough and smooth surfaces"

J. Mech. Eng. Sci., 4, 3, 287-291.

[90] Clauser, F. H. (1956)

"The turbulent boundary Layer".

Appl. Mech., 4, 1-51.

[91] Welty, J. R., Wicks, C. E. and Wilson, R. E. (1969)

"Fundamental of momentum, hear and mass transfer"

John Wily & Sons, Inc.

[92] Deissler, R. G. (1955)

"Turbulent heat transfer and friction in the entrance regions of smooth passages"

Trans. ASME, 77, 1221-1233.

[93] Schiller, L. and Kirsten, H. (1929)

Z.Tech.Phys., 10, 268.

[94] Davies, J. T. (1972)

"Turbulance Phenomena"

Academic Press, New York.

[95] Rubes, J. H. (1962)

Jet Propulsion Lab. Tech. Ref. No. 32-207.

[96] Walklate, P. J. (1976)

"A comparative study of theoretical modles of turbulence for the numerical prediction of boundary-layer flows"

Victoria Univ. of Manchester, Ph.D. Thesis.

[97] Walklate, P. J. (1981)

"A Holographic technique for the study of heat transfer from a Rib-Roughened surface"

AERE-R 10172.

[98] Latzko, H. (1921)

" Der warmenbergang an einen turbulent flussigkeits oder gasstrom"

Z. Angew. Math. Mech., 1, 268-290.

[99] Deissler, R.G. (1953)

"Analysis of turbulent heat transfer and flow in the entrance regions of smooth passages"

NACA TN 3016.

[100] Lee, Y. (1964)

"Turbulent flow and heat transfer in concentric and eccentric annuli"

Ph.D Thesis, Mech. Eng. Dept., University of Liverpool.

[101] Reichardt, H. (1940)

"Die Warmeubertragung in turbulent Reibungschichten".

Z. Angew. Math. Mech., 20, 297-

[102] Deisser, R. G. (1950)

"Analytical and experimental investigation of adiabatic turbulent flow in smooth tubes"

NACA TN 2138.

[103] Winkel, R. (1923)

"Die wasserbewegung in leitungen mit ringspalt-durchflubquerschnilt"

Z. Angew. Math. u. Mech., 3, 251-257.

[104] Burgoyne, T. B., Burnett, P. and Wilkie, D. (1964)

"Forced convection hear transfer from surfaces roughened by transverse Ribs"

UKAEA TRG Report 781(W).

[105] Rapier, A. C. (1977)

"A correction of flow and heat transfer data for surfaces roughened with transverse square ribes of pitch to height ratio of 7.2"

UKAEA Report ND-R-63(W).

[106] Parker, G. J. (1968)

"Some factors govering the design of probes for sampling in particle and drop-laden streams"

UKAEA Report ND-R-63(W).

[107] Watson, H. H. (1954)

"Errors dut to anisokimetic sampling of aerosols"

Amer. Ind. Hyg. Ass. Quart., 1, 21-25.

[108] Wood, N. B. (1981)

"The mass transfer of particles and acid vapour to cooled surfaces"

J. of the Institute of Energy, 76, 76-93.

[109] Owen, I. (1984)

"The diffusion of sub-micron aerosols through hydrodynamic and thermal boundary layers"

Internal Report, August, Mech. Eng. Dept., University of Liverpool"

[110] Owen, I., El-Kady, A. A. and Cleaver, J. W. (1987)

"Fine particle fouling of roughened heat transfer surfaces"

Proc. ASME-JSME Thermal Engineering Cof., Hawaii, March, 3, 95-102.

[111] Montgomery, T. L. and Corn, M. (1970)

"Aerosol deposition in a pipe with turbulent air flow"

Aerosol Science, 1, 185-213.

[112] Sehmel, G. A. (1966)

Battelle Memorial Institute Publication BNWL-578, Richland, Washington.

[113] Chamberlain, A. C. (1967)

"Transport of Lycopodium spores and other small particles"

Proc. Roy. Soc., A 296, 45-70.

[114] Sehmel, G. A. and Sutler, S. L. (1974)

"Particle deposition rates on a water surface as a function of particle diameter and air velocity"

J. Reach. Atmos., 8, 911-920.

[115] O'Brien, T. P., O'Donnell, L. J. and Opone, M. (1985)

"Sub-micron deposition on a heated and unheated cylinder"

Final year project, Mech. Eng. Dept., University of Liverpool.

[116] Whurr, J. R. and White, A. (1984)

"The effect of thermophoresis on the deposition of Sub-micron particles on low pressure turbine fixed blades"

Final year project, TE 4, April, Eng. Dept., University of Liverpool.

[117] Ryley, D. J. and Al-Azzawi, H. K. (1983)

"Suppresion of the deposition of nucleated fog droplets on steam turbine stator blades by blade heating"

Int. J. Heat and Fluid Flow, 4 (4), 207-216.

[119] Cleaver, J. W. (1986)

"Particulate fouling in turbulent flow"

Internal Report, Mech. Eng. Dept., University of Liverpool.

[120] Skyrme, G. and Reeks, M. W. (1986)

"An examination of a recent particle transport theory for the low temperature deposition of carbon on AGR fuel pins"

CEGB Report, Tprd/B/Pc/0239/M86.

[121] McAdams, L. H. (1954)

"Heat transmission"

McGraw-Hill Book Company, New York.

TABLE 1.1 Determination of median diameters for 5 °/o uranin solution.

range of size (µm)	d	n_i	n_i log d	°/o in range	°/o cumulative	log d - log dg	n_i (log d - log dg)^2	n_i d^3	°/o in range	°/o cumulative
0.005-0.055	0.030	23.0	-35.026	5.056	5.06	-0.7445	12.74990	0.001	0.006	0.006
0.055-0.105	0.080	74.0	-81.171	11.718	16.77	-0.3186	7.51021	0.038	0.375	0.381
0.105-0.155	0.130	289.0	-256.070	36.966	53.74	-0.1077	3.35347	0.635	6.277	6.658
0.155-0.205	0.180	202.0	-150.435	21.717	75.46	0.0336	0.22817	1.178	11.647	18.305
0.205-0.255	0.230	163.0	-104.038	15.019	90.48	0.1401	3.19772	1.983	19.607	37.912
0.255-0.305	0.280	55.0	-30.406	4.389	94.86	0.2255	2.79662	1.207	11.937	49.849
0.305-0.355	0.330	39.0	-18.778	2.711	97.58	0.2969	3.43668	1.402	13.856	63.705
0.355-0.405	0.380	21.0	-8.825	1.274	98.85	0.3581	2.69325	1.152	11.392	75.097
0.405-0.455	0.430	12.0	-4.398	0.635	99.48	0.4118	2.03500	0.954	9.433	84.530
0.455-0.505	0.480	7.0	-2.231	0.322	99.81	0.4596	1.47848	0.774	7.654	92.184
0.505-0.555	0.530	4.0	-1.103	0.159	99.97	0.5026	1.01048	0.596	5.887	98.071
0.555-0.605	0.580	1.0	-0.237	0.034	100.00	0.5418	0.29351	0.195	1.929	100.000
		890.0	-692.719				40.7835	10.115		

TABLE 1.2 Frequency distribution for 5 °/o uranin solution.

d (μm)	f(d)	f(d) × ln d_2/d_1	°/o in range	°/o cumulative
0.0550	57.5190	56.4163	6.2786	6.2786
0.1050	464.6098	225.5717	25.1040	31.3826
0.1550	712.6647	231.9171	25.8102	57.1928
0.2050	659.2906	161.6069	17.9853	75.1782
0.2550	496.1027	97.5885	10.8607	86.0389
0.3050	339.3689	55.7593	6.2055	92.2444
0.3550	221.8051	31.2920	3.4825	95.7269
0.4050	141.9882	17.5517	1.9533	97.6802
0.4550	90.2175	9.9240	1.1044	98.7847
0.5050	57.3221	5.6801	0.6321	99.4168
0.5550	36.5763	3.2974	0.3670	99.7838
0.6050	23.4959	1.9429	0.2162	100.0000
		898.5480		

TABLE 1.3 Determination of median diameters for 0.2 % uranin solution.

range of size (µm)	d	n_i	$n_i \log d$	% in range	% cumulative	$\log d - \log dg$	$n_i (\log d - \log dg)^2$	$n_i d^3$	% in range	% cumulative
0.005-0.015	0.010	2.0	-4.000	2.583	2.58	-0.5660	0.64061	0.000002	0.021	0.021
0.015-0.015	0.020	13.0	-22.087	14.261	16.84	-0.2649	0.91241	0.000104	1.091	1.112
0.025-0.035	0.030	26.0	-39.595	25.565	42.41	-0.0888	0.20518	0.000702	7.363	8.475
0.035-0.045	0.040	38.0	-53.122	34.299	76.71	0.0361	0.04954	0.002432	25.509	33.984
0.045-0.055	0.050	16.0	-20.816	13.441	90.15	0.1330	0.28309	0.002000	20.978	54.961
0.055-0.065	0.060	7.0	-8.553	5.522	95.67	0.2122	0.31519	0.001512	15.859	70.820
0.065-0.075	0.070	3.0	-3.465	2.237	97.91	0.2791	0.23376	0.001029	10.793	81.613
0.075-0.085	0.080	2.0	-2.194	1.416	99.32	0.3371	0.22732	0.001024	10.741	92.354
0.085-0.095	0.090	1.0	-1.046	0.675	100.00	0.3883	0.15077	0.000729	7.646	100.000
		108.0	-154.877				3.01786	0.009534		

TABLE 1.4 Frequency distribution for 0.2 °/o uranin solution.

d (μm)	f(d)	f(d) × ln d_2/d_1	°/o in range	°/o cumulative
0.0150	7.3762	5.1128	4.7425	4.7425
0.0250	67.5479	27.3883	25.4050	30.1475
0.0350	110.9834	31.9279	29.6158	59.7634
0.0450	97.6815	21.7970	20.2186	79.9819
0.0550	64.9531	11.8424	10.9848	90.9667
0.0650	37.5869	5.7940	5.3745	96.3412
0.0750	20.2527	2.7044	2.5085	98.8497
0.0850	10.5288	1.2401	1.1503	100.0000
		107.8069		

TABLE 4.1 Flow parameters for the smooth rod.

| valve position | friction factor | friction velocity | | mean velocity m/s | Reynolds number |
| | | Clauser tecnique | Preston tube | | |
		m/s			
1	0.0110	0.032	-----	0.429	5.0×10^3
2	0.0085	0.336	0.13	5.150	6.0×10^4
3	0.0070	0.703	0.726	11.883	1.6×10^5
4	0.0055	1.014	1.014	19.350	2.4×10^5
5	0.0045	1.202	1.195	25.512	3.0×10^5
6	0.0045	1.260	1.224	26.574	3.2×10^5

TABLE 4.2 Flow parameters for the ribbed rod.

valve position	friction factor	friction velocity m/s	mean velocity m/s	Reynolds number
1	0.018	0.041	0.429	5.0×10^3
2	0.012	0.399	5.150	6.0×10^4
3	0.012	0.921	11.883	1.6×10^5
4	0.012	1.499	19.350	2.4×10^5
5	0.012	1.964	25.512	3.0×10^5
6	0.012	2.058	26.574	3.2×10^5
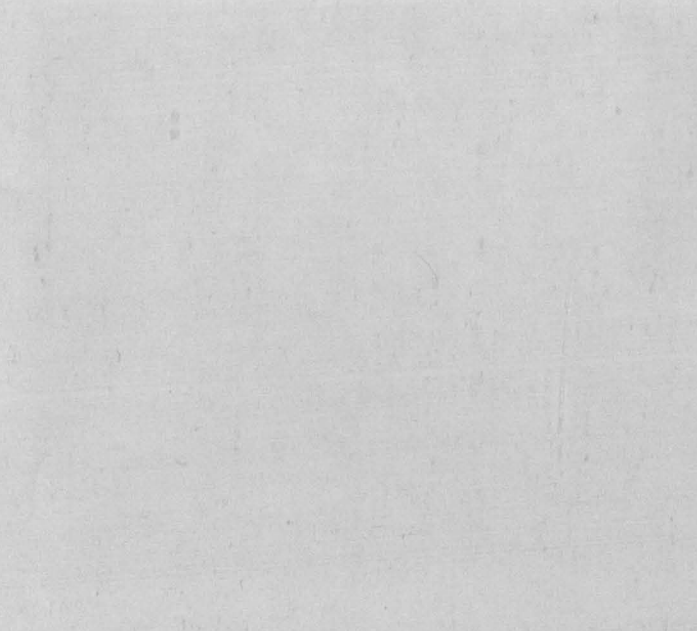
Plate 1 Electron microscope photograph of
particles produced from 5 % uranin
solution (magnification = × 6000).
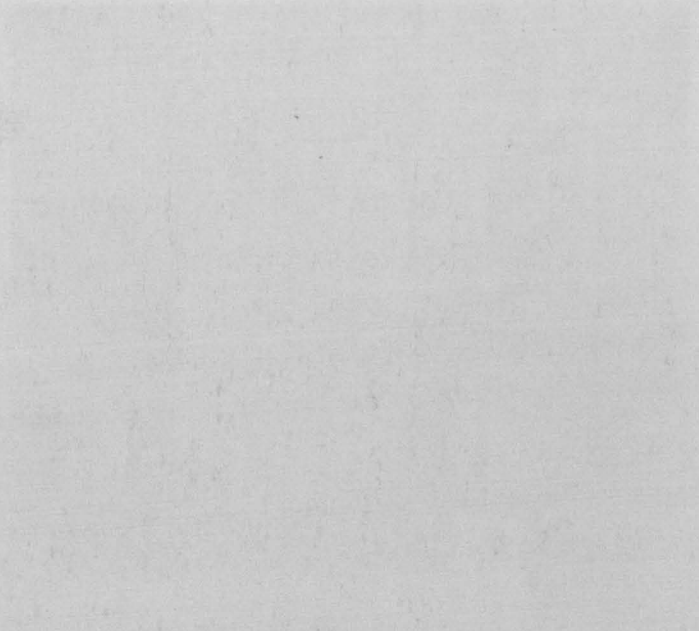
Plate 2 Electron microscope photograph of
particles produced from 0.2 % uranin
solution (magnification = × 46000).
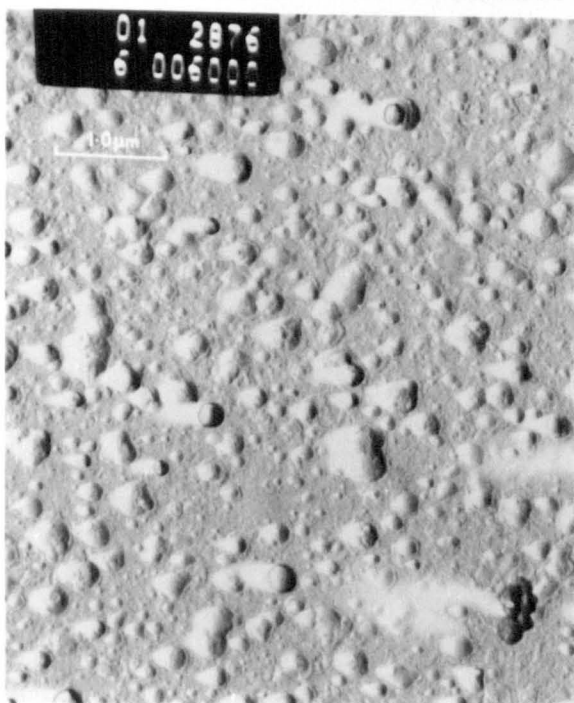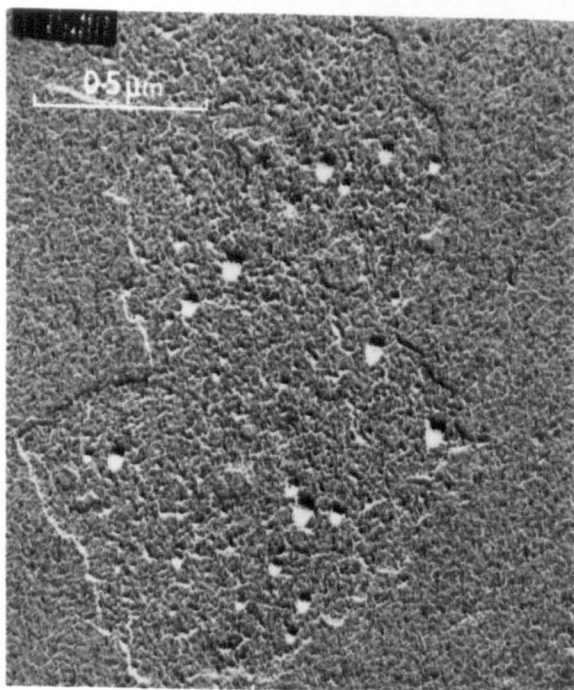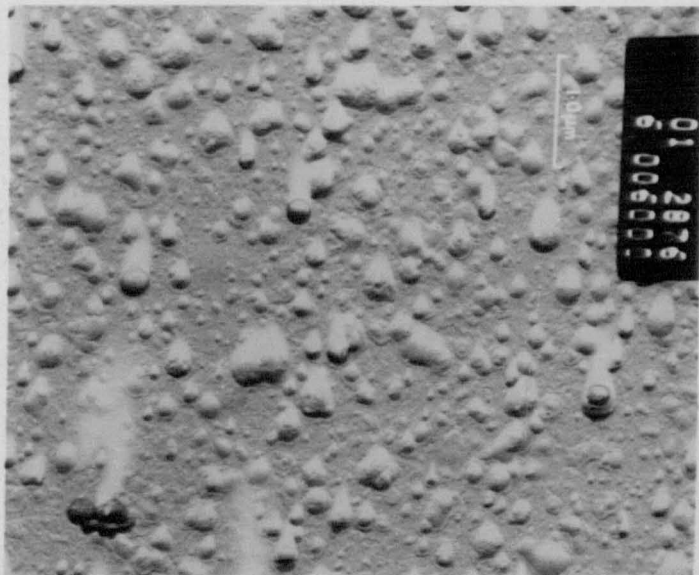
Plate 1 Electron microscope photograph of particles produced from 5 % uranin solution (magnification = × 6000).
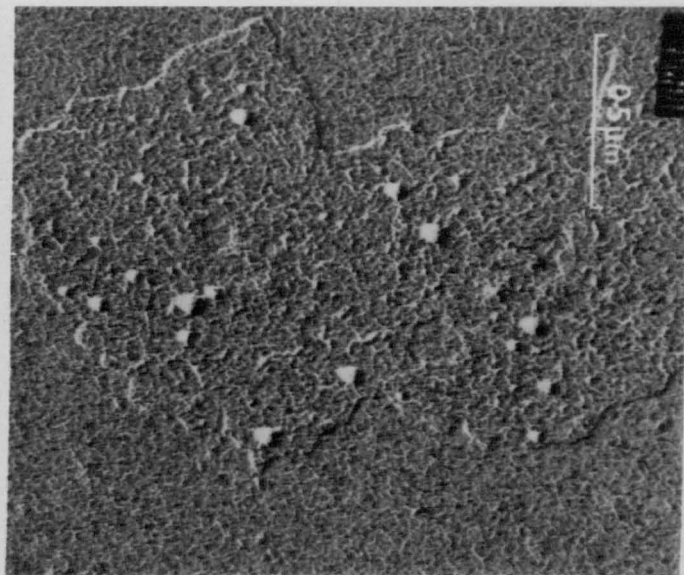
Plate 2 Electron microscope photograph of particles produced from 0.2 % uranin solution (magnification = × 46000).

Figures

Graghite sleeve

36 fuel pins
15.8 mm diameter

p

e
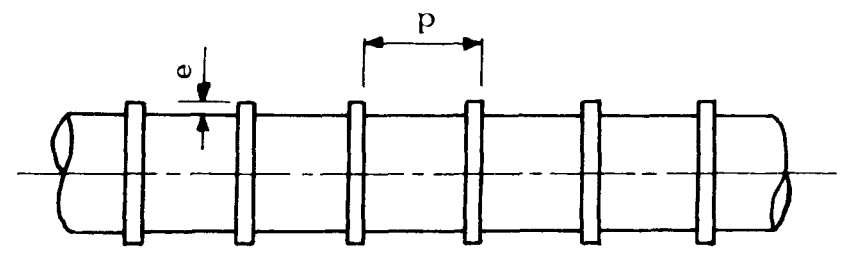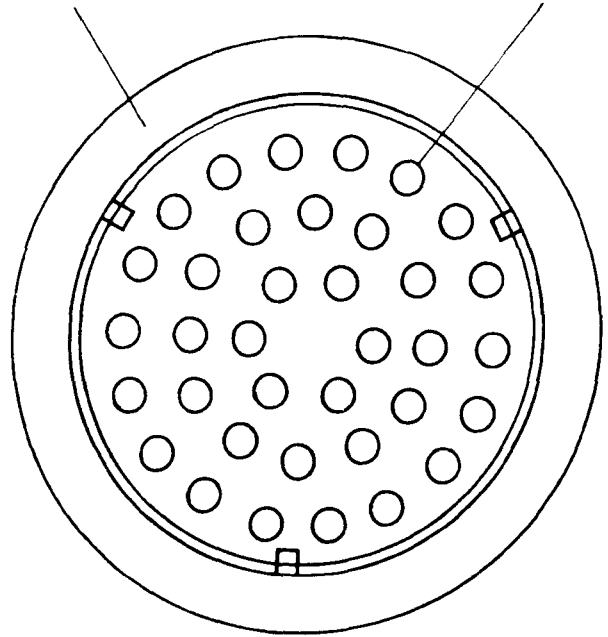
Individual fuel pin 7.2 pitch to height ratio

Fig. 1.1 Cross-section of flow channel in commercial AGR.
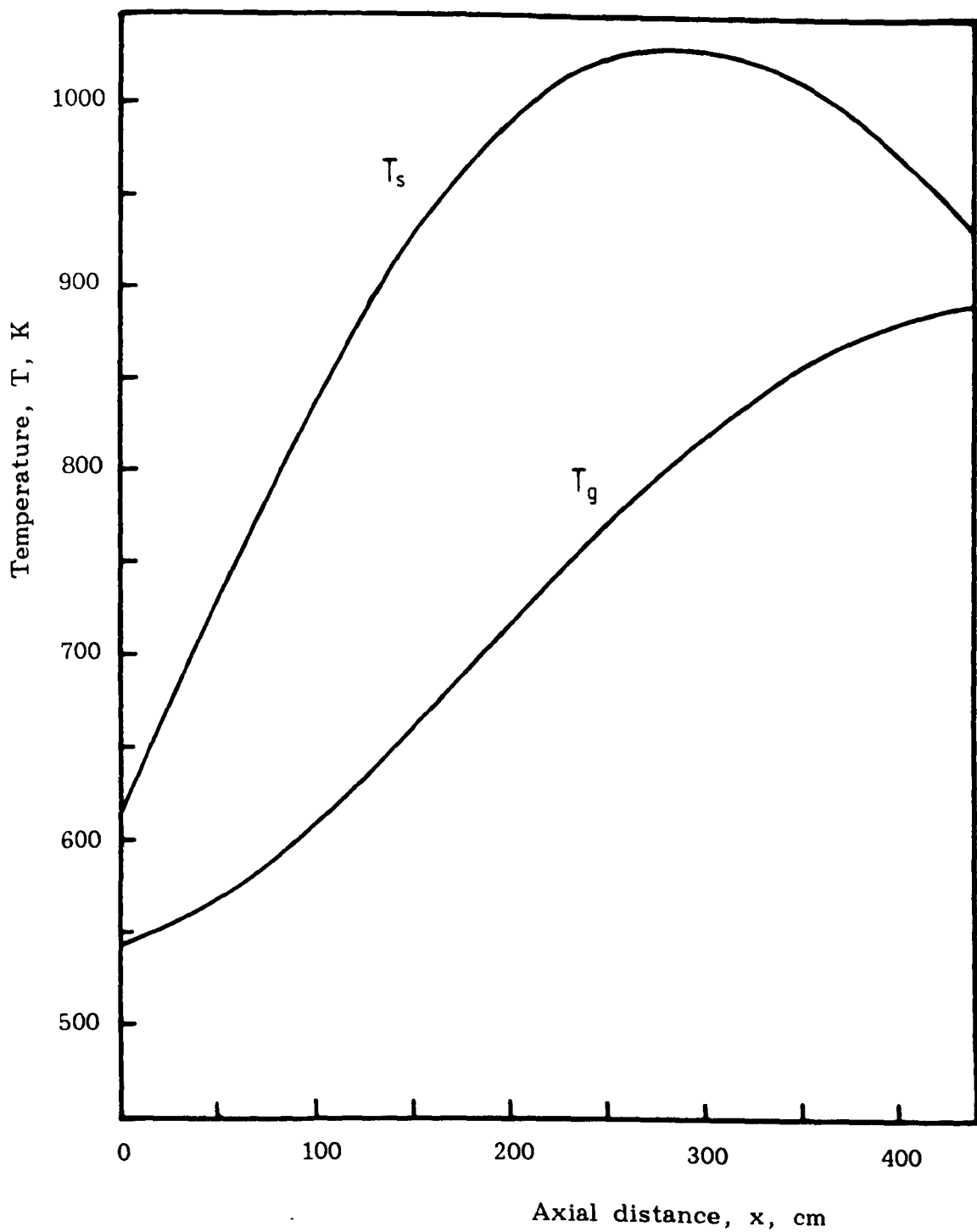
Fig. 1.2 Clad and fuel temperatue distribution along the fuel element.
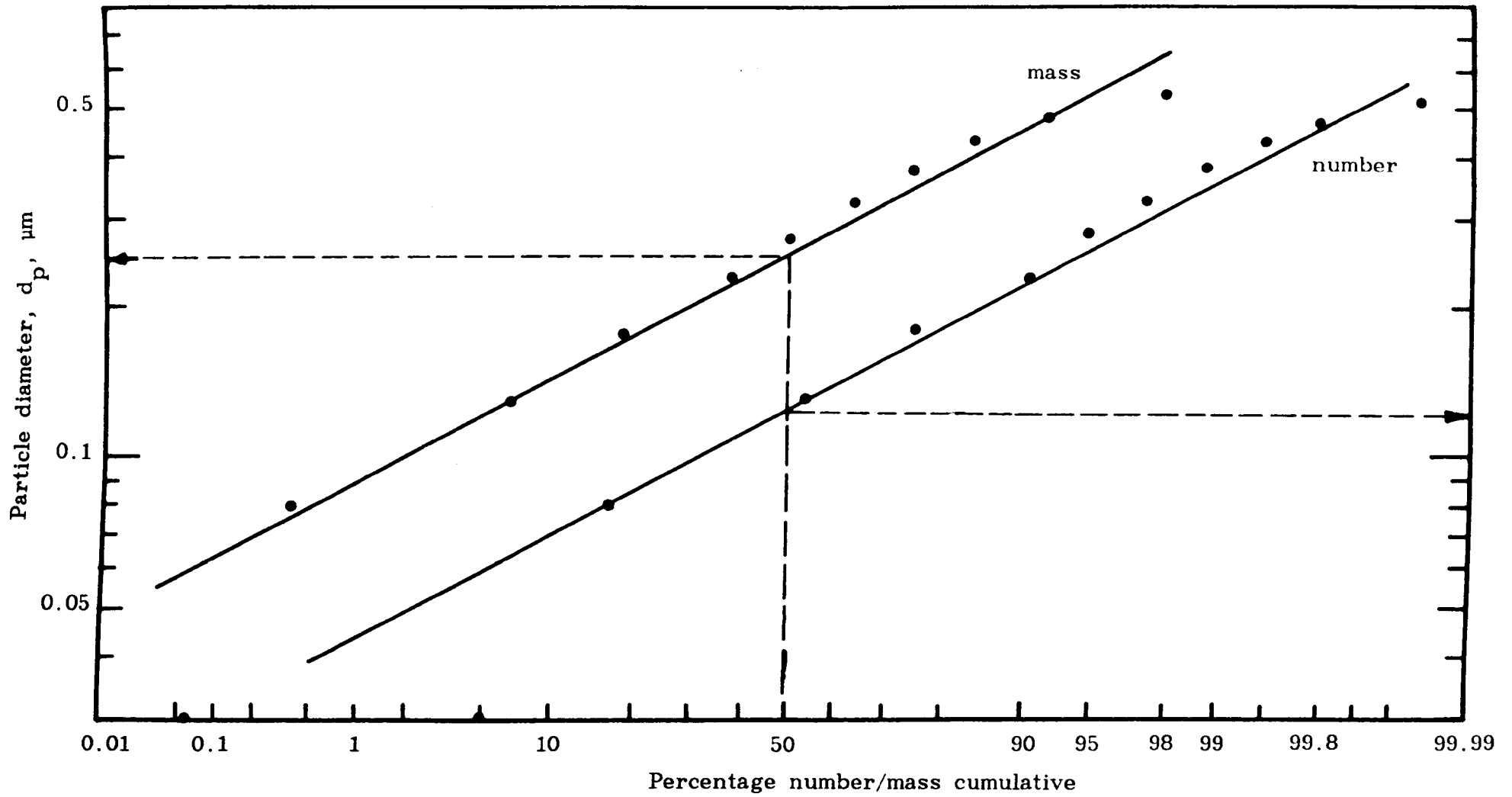
Fig. 1.3 Determination of mass/geometric median diameter for 5 °/o uranine solution.
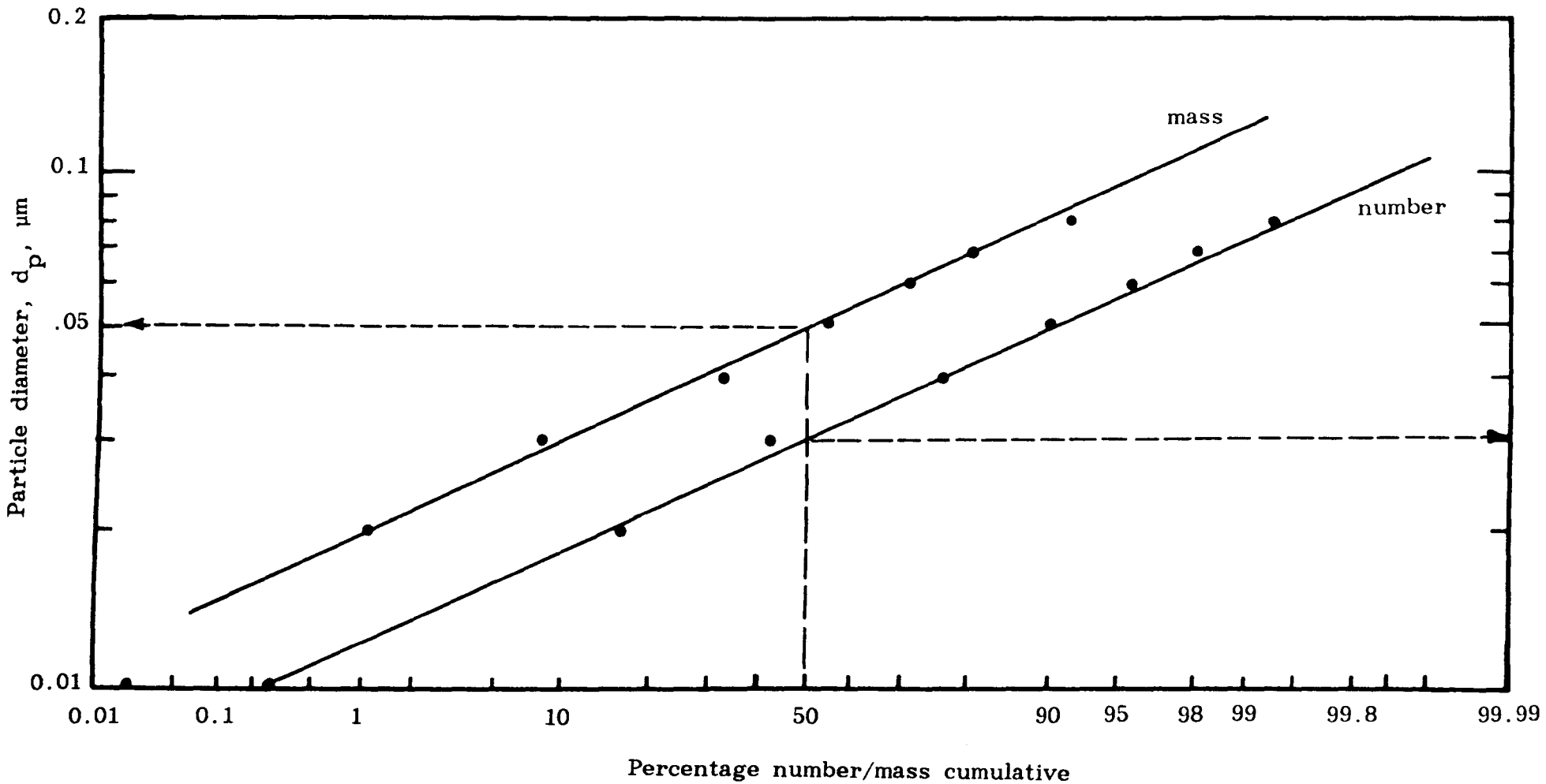
Fig. 1.4 Determination of mass/geometric median diameter for 0.2 °/o uranine solution.
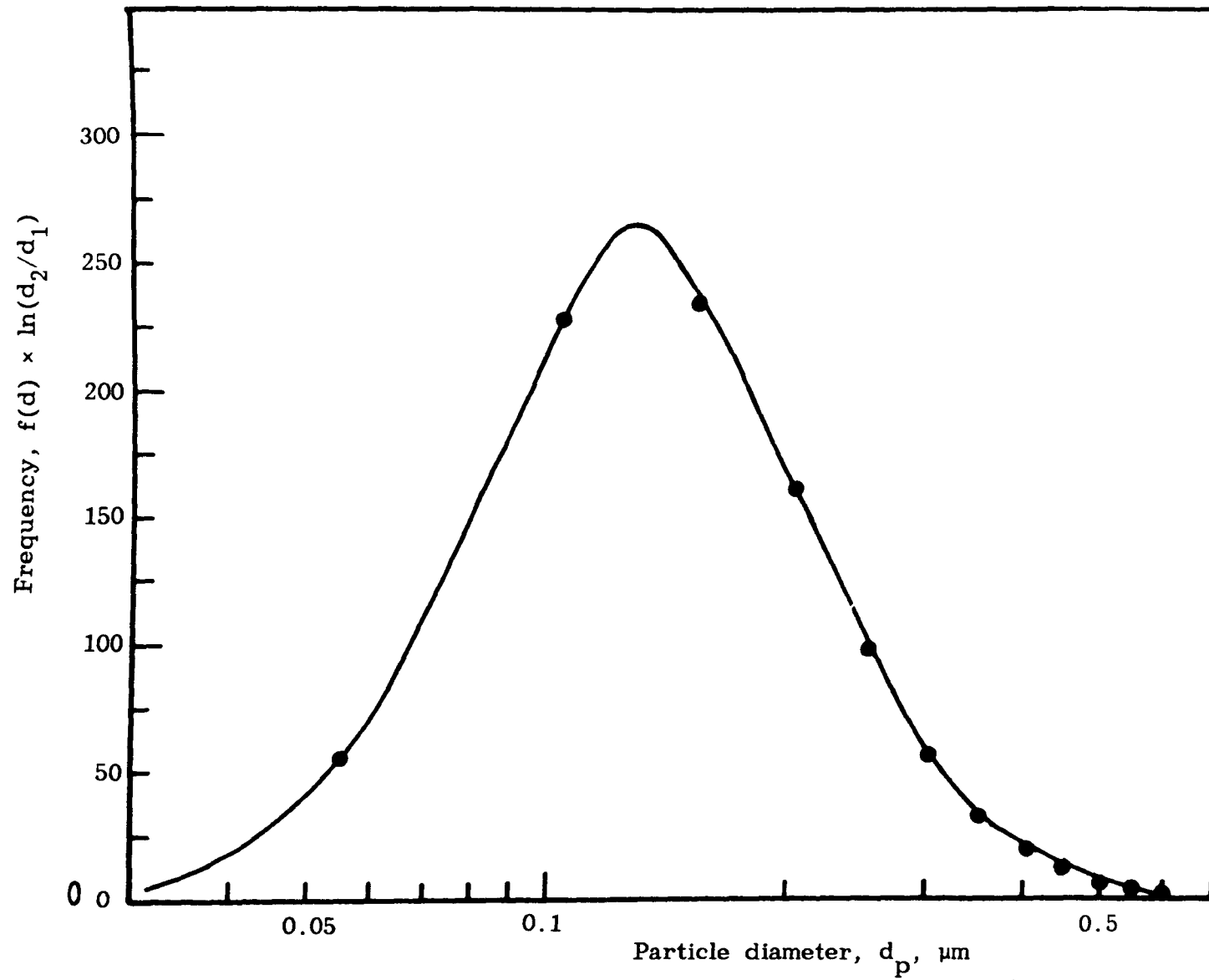
Fig. 1.5 Frequency distribution for 5 °/o uranine solution.
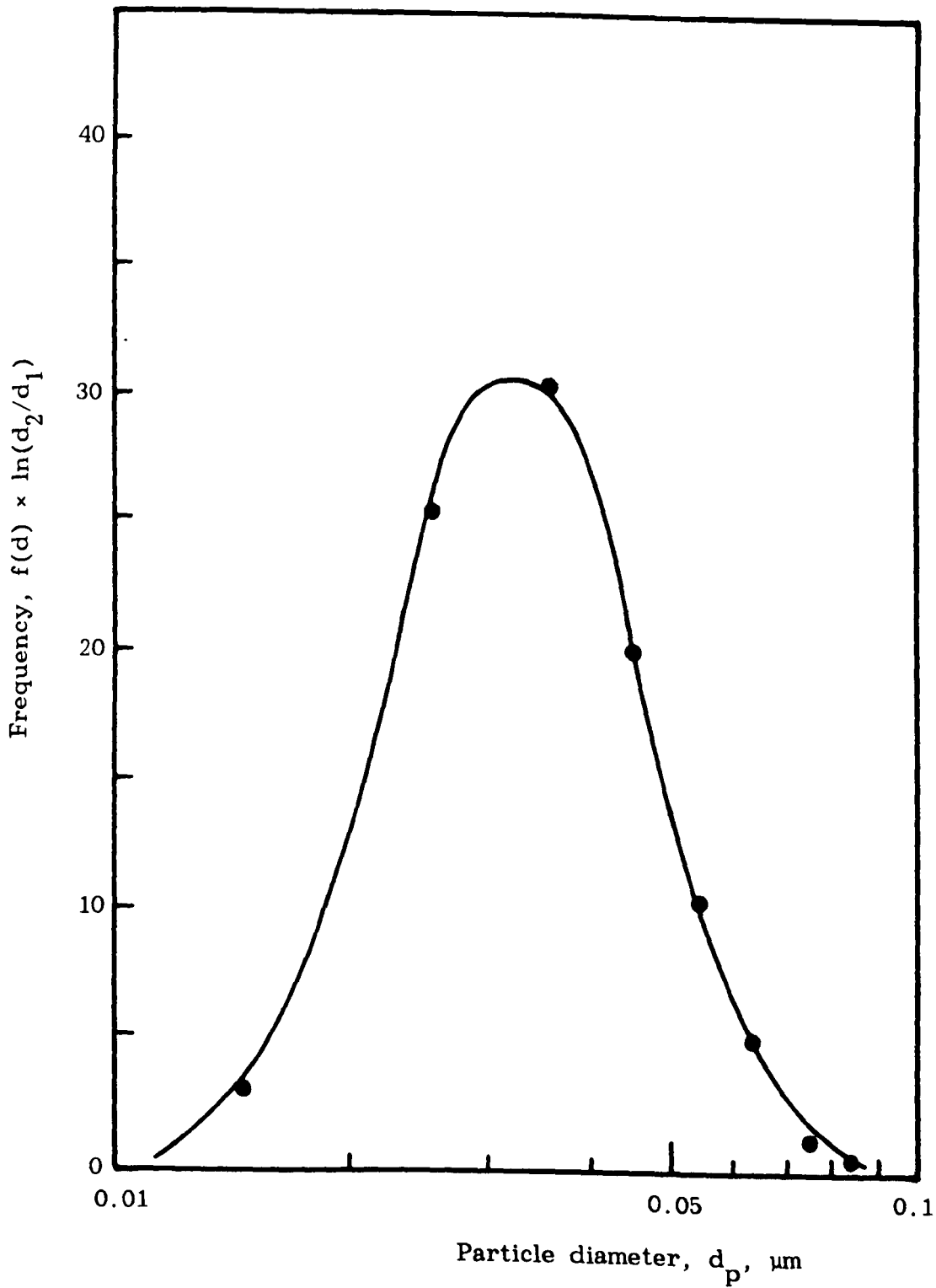
Fig. 1.6 Frequency distribution for 0.2 °/o uranine solution.
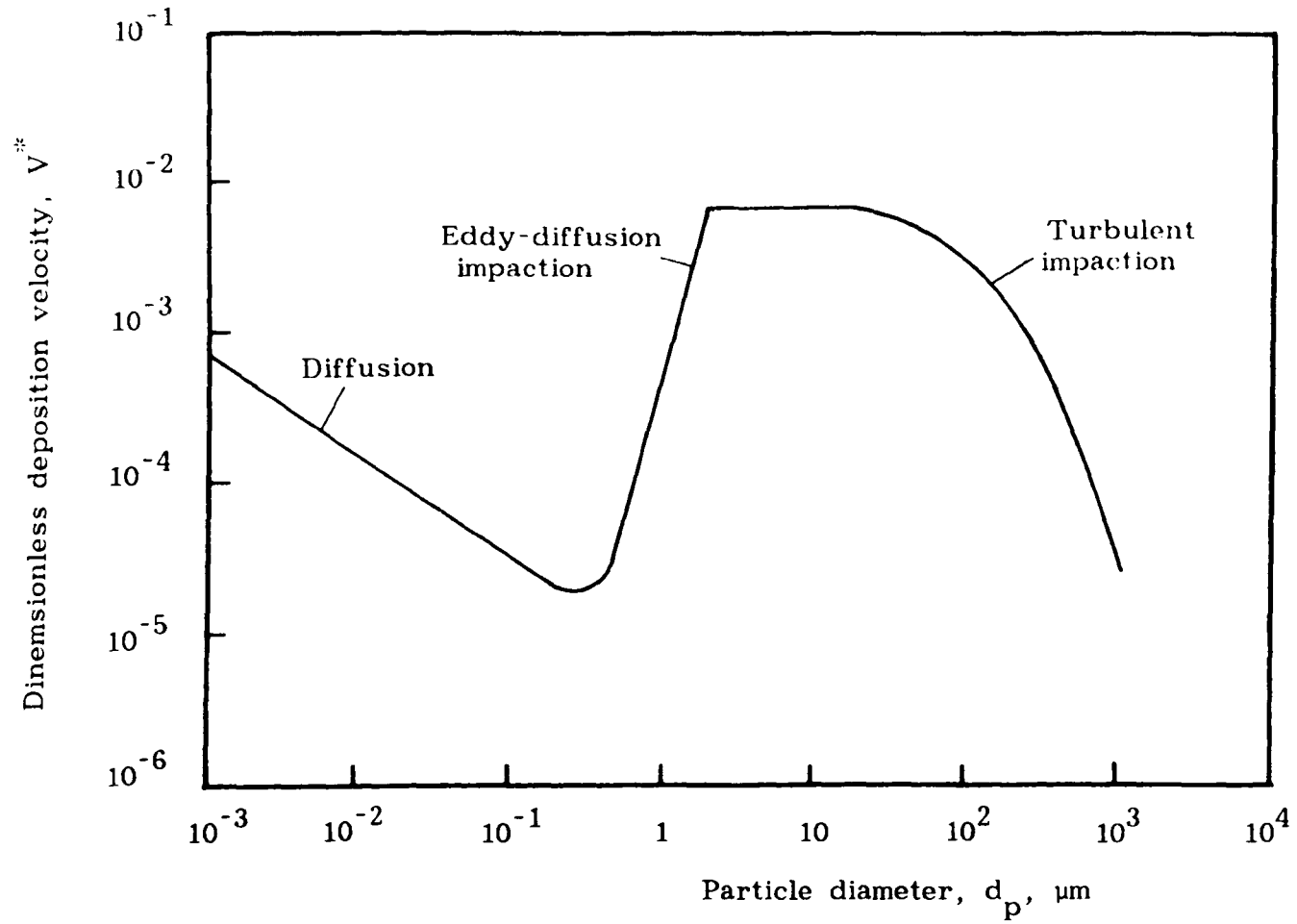
Fig. 2.1 Variation of the deposition velocity with particle diameter.
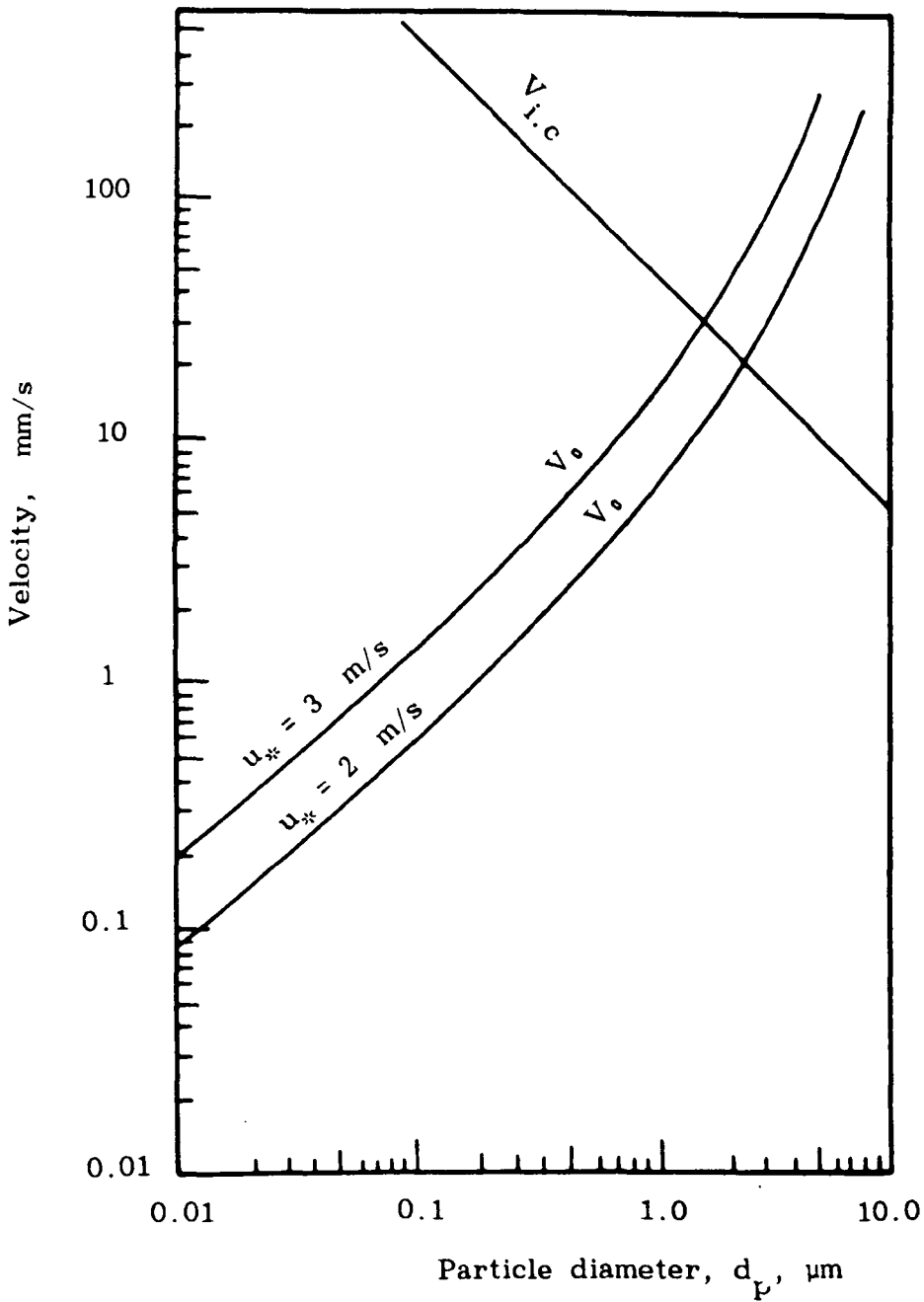
Fig. 3.1 Variation of incidence velocity and critical
incidence velocity with particle diameter.
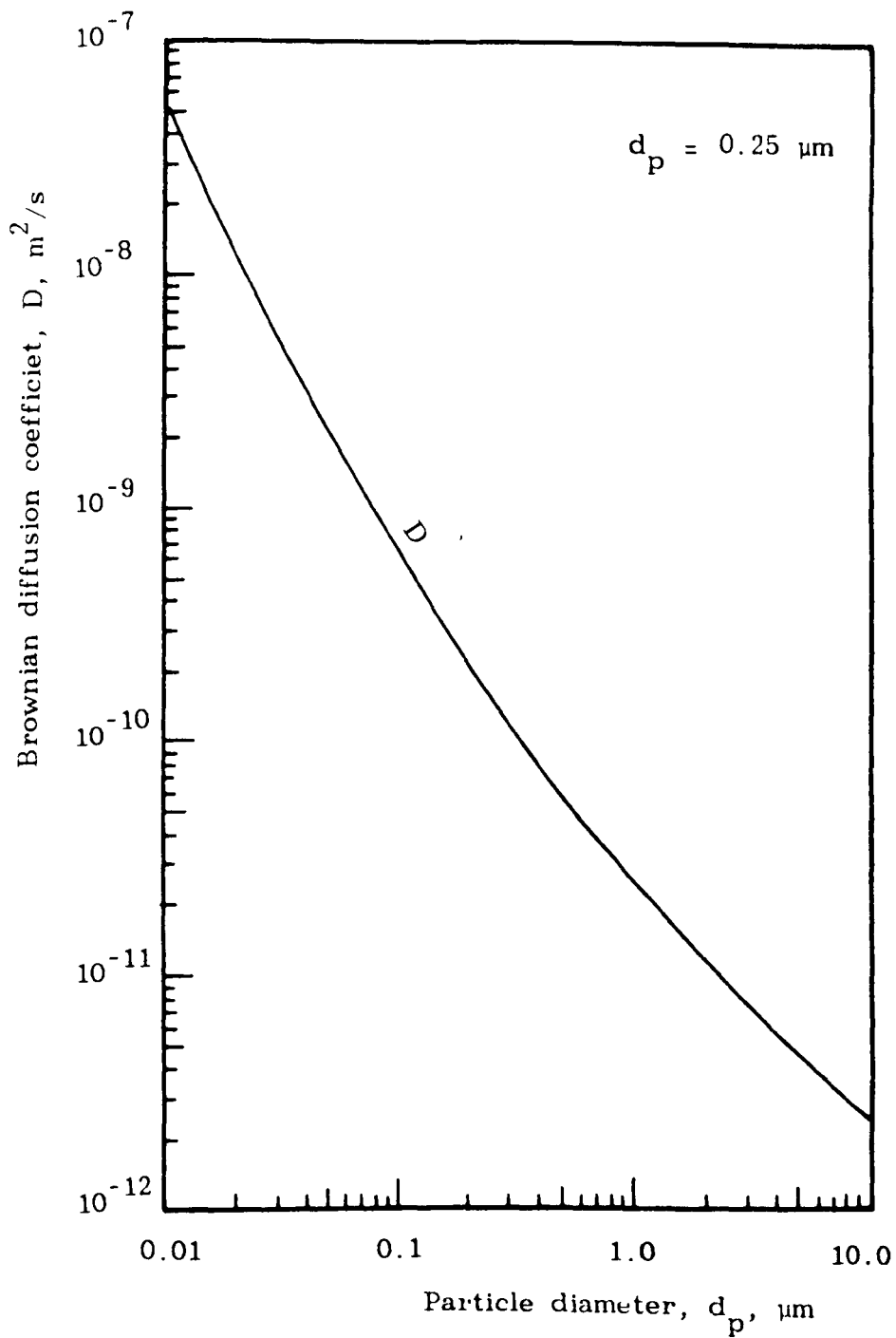
Fig. 3.2 Variation of Brownian diffusion coefficiet of aerosol particles in ambient air temperature.
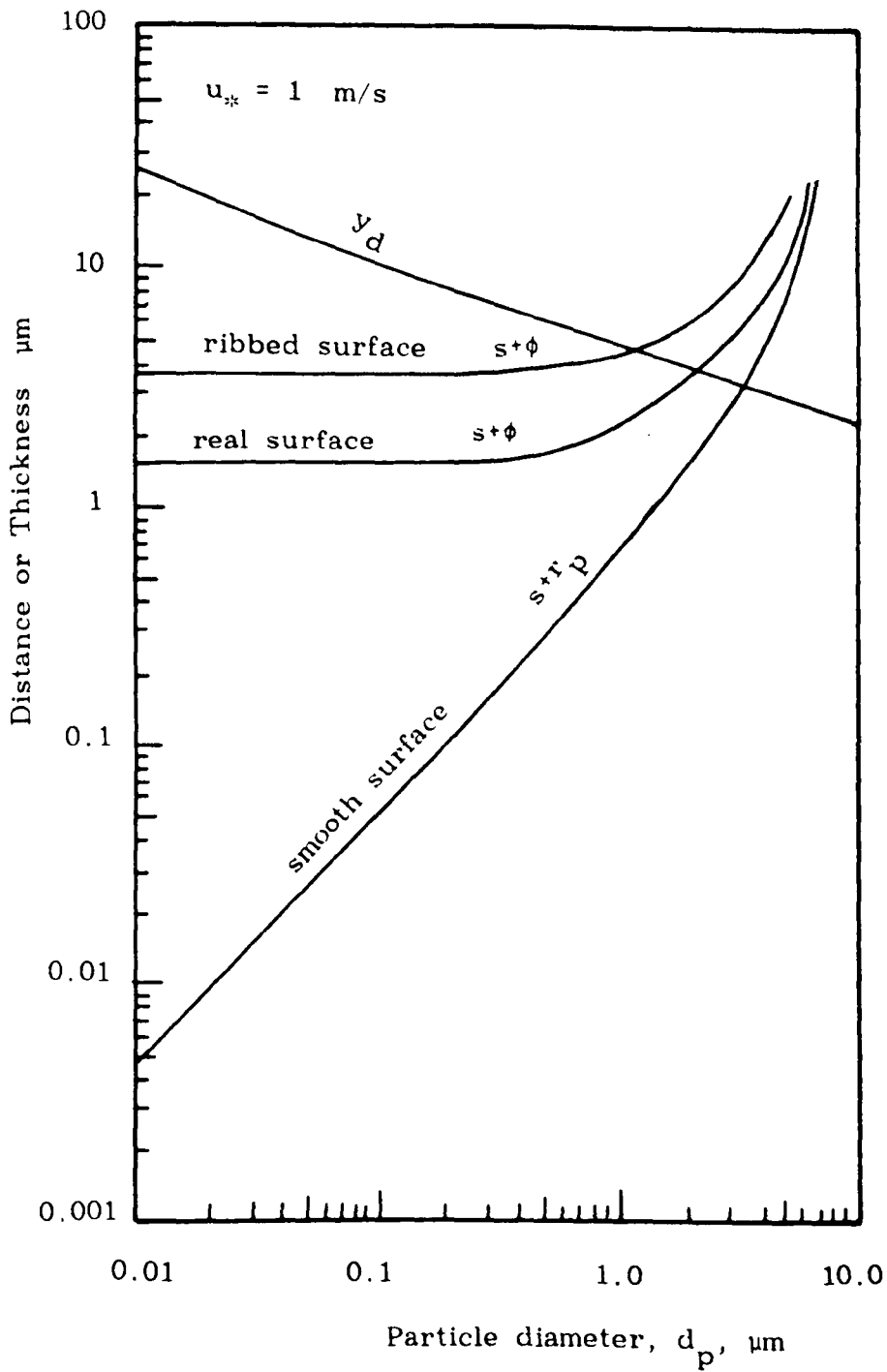
Fig. 3.3 Variation of diffusion layer thickness and capture distace with particle diameter.
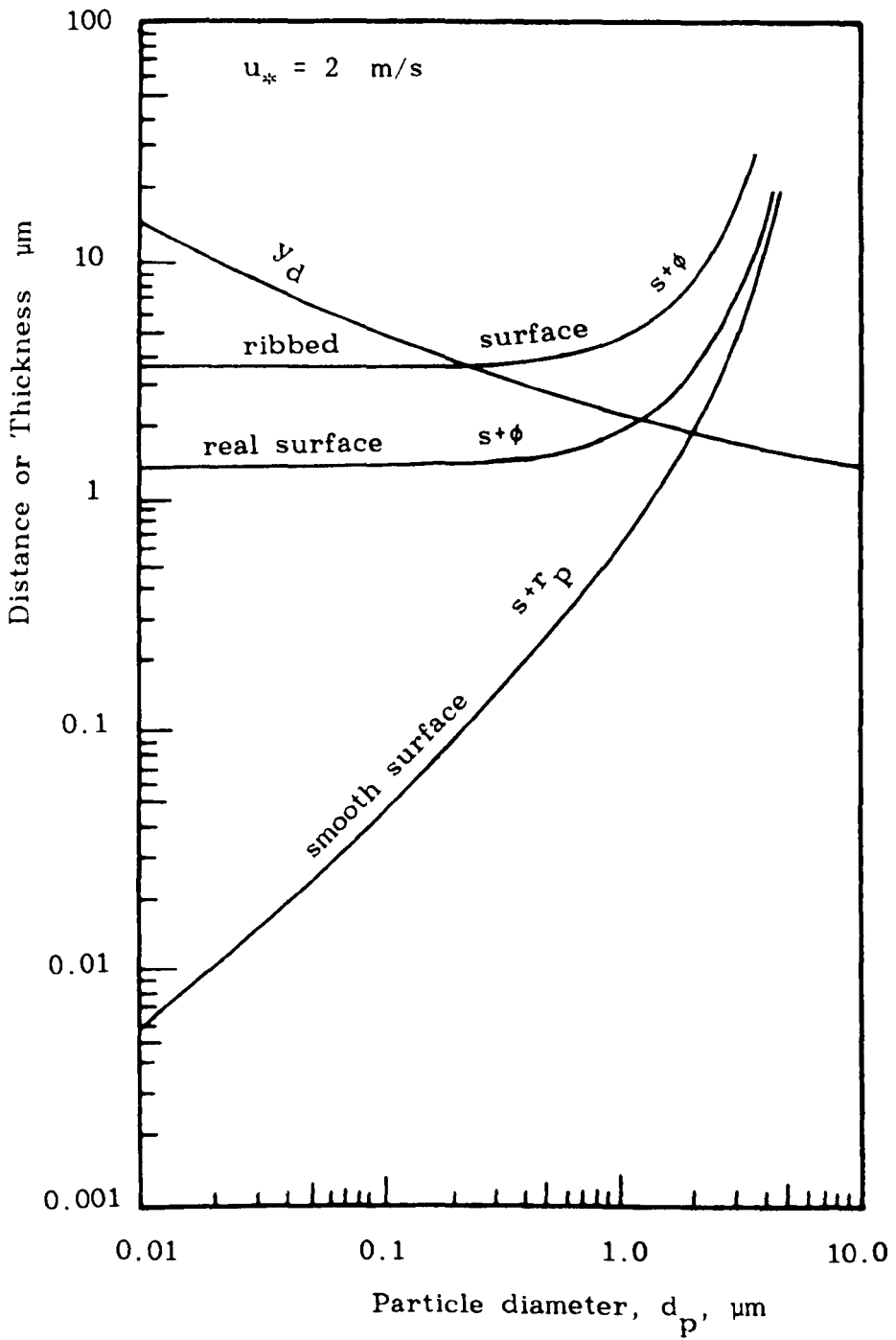
Fig. 3.4 Variation of diffusion layer thickness and capture distace with particle diameter.
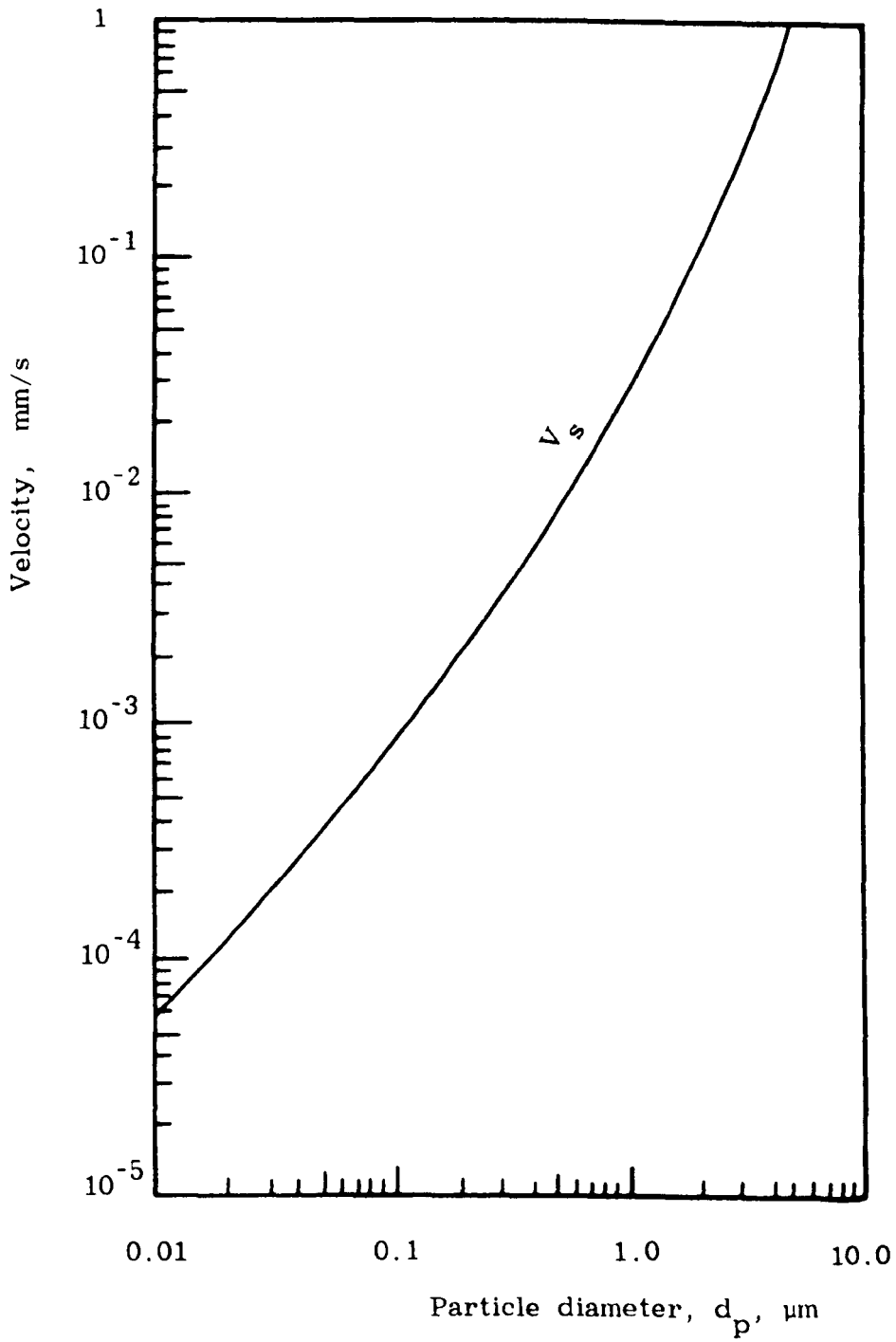
Fig. 3.5 Variation of sedimentation velocity with
particle diameter.
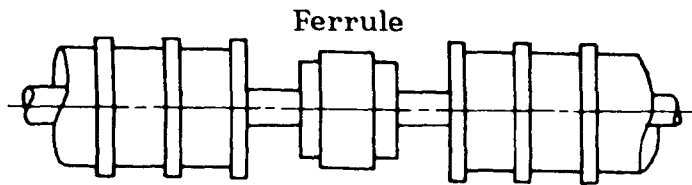
Fig. 1.4.b Regular ribbed sections assembly.
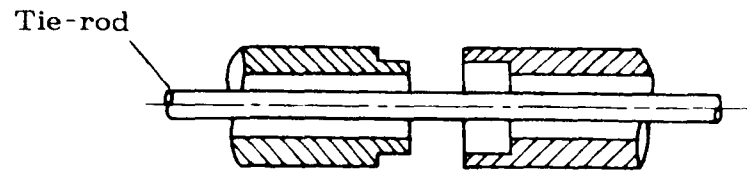
Fig. 1.4.c Smooth sections assembly.
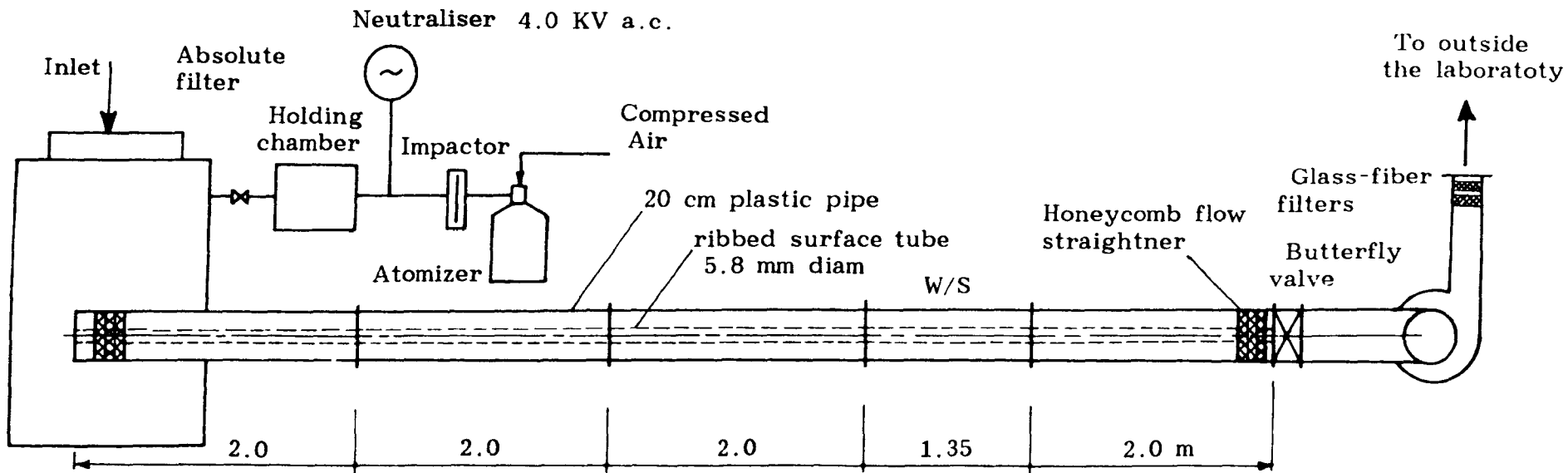
Fig. 4.1.a Layout of the experimental rig.
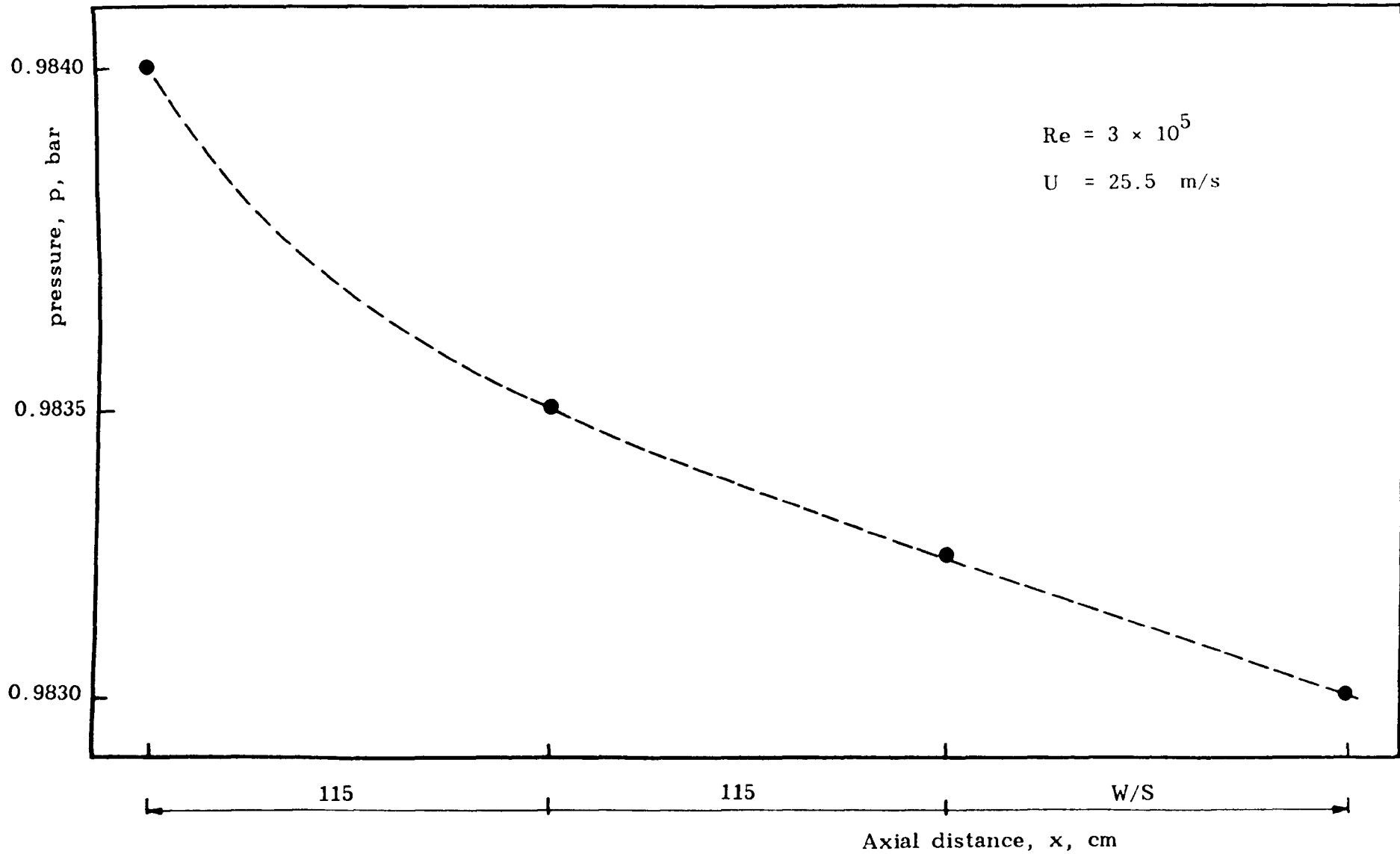
Fig. 4.2 Pressure distribution along the channel.
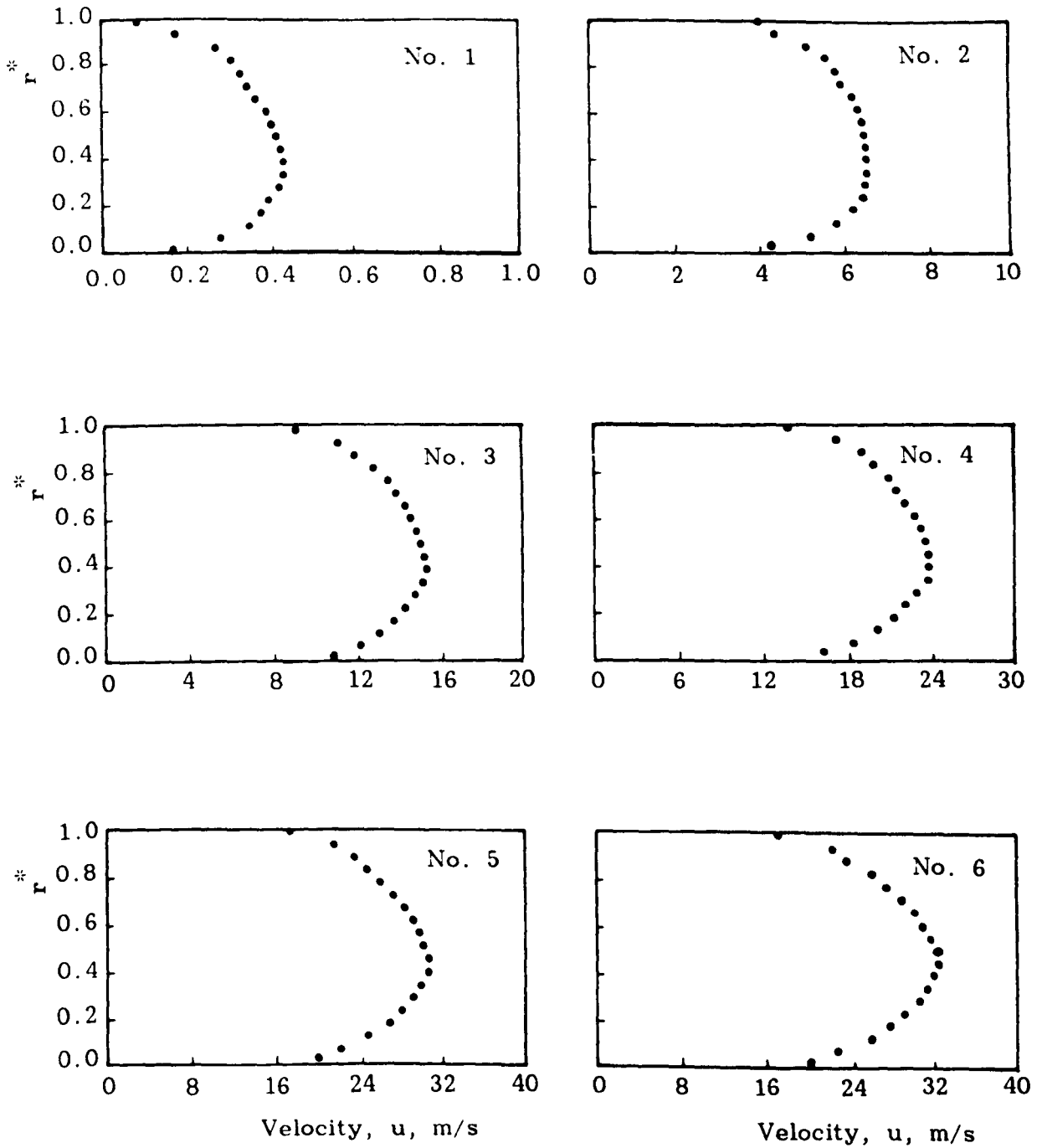
Fig. 4.3 Velocity profiles through the rig (smooth - upstream).
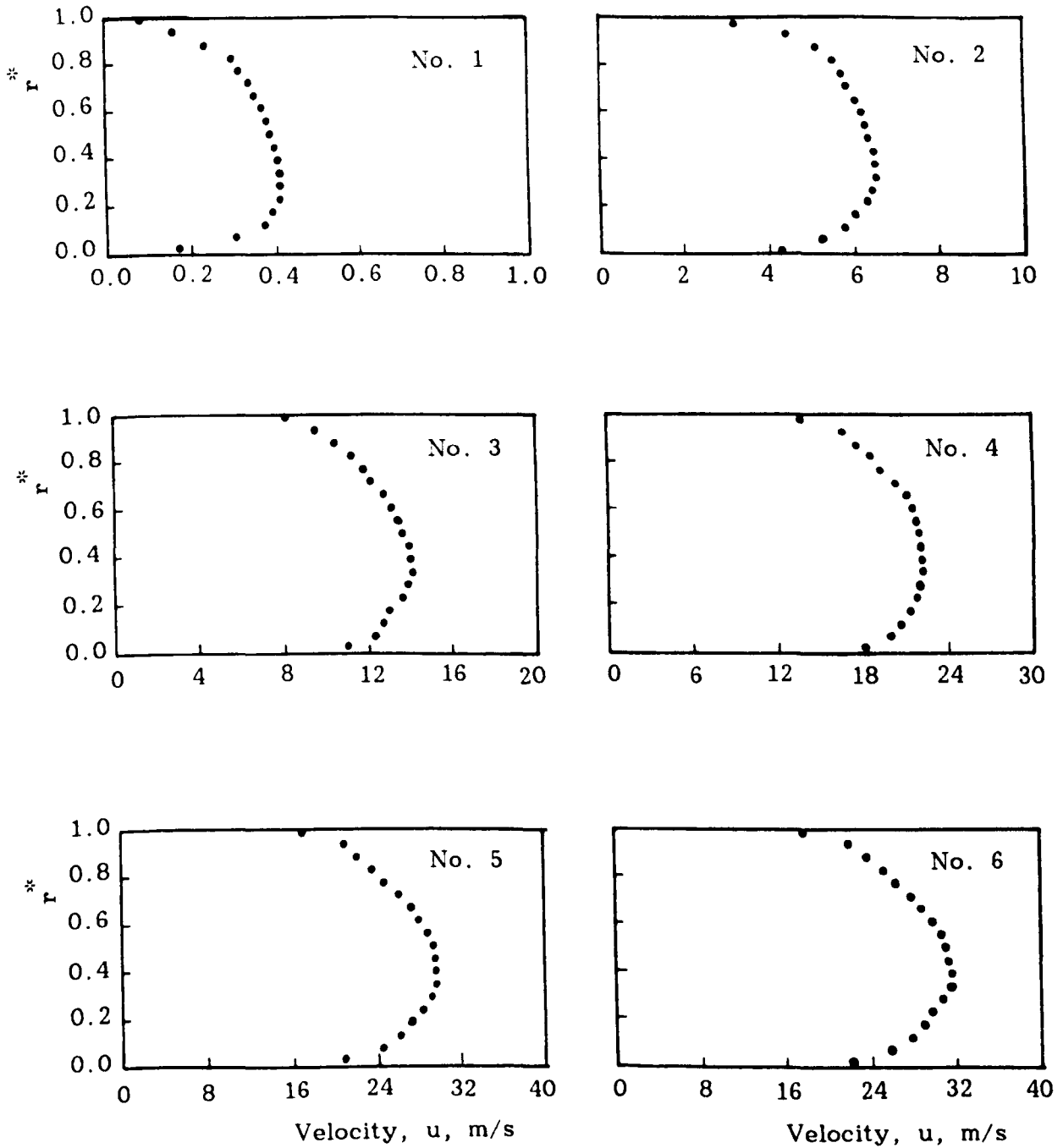
Fig. 4.4 Velocity profiles through the rig (smooth - downstream).
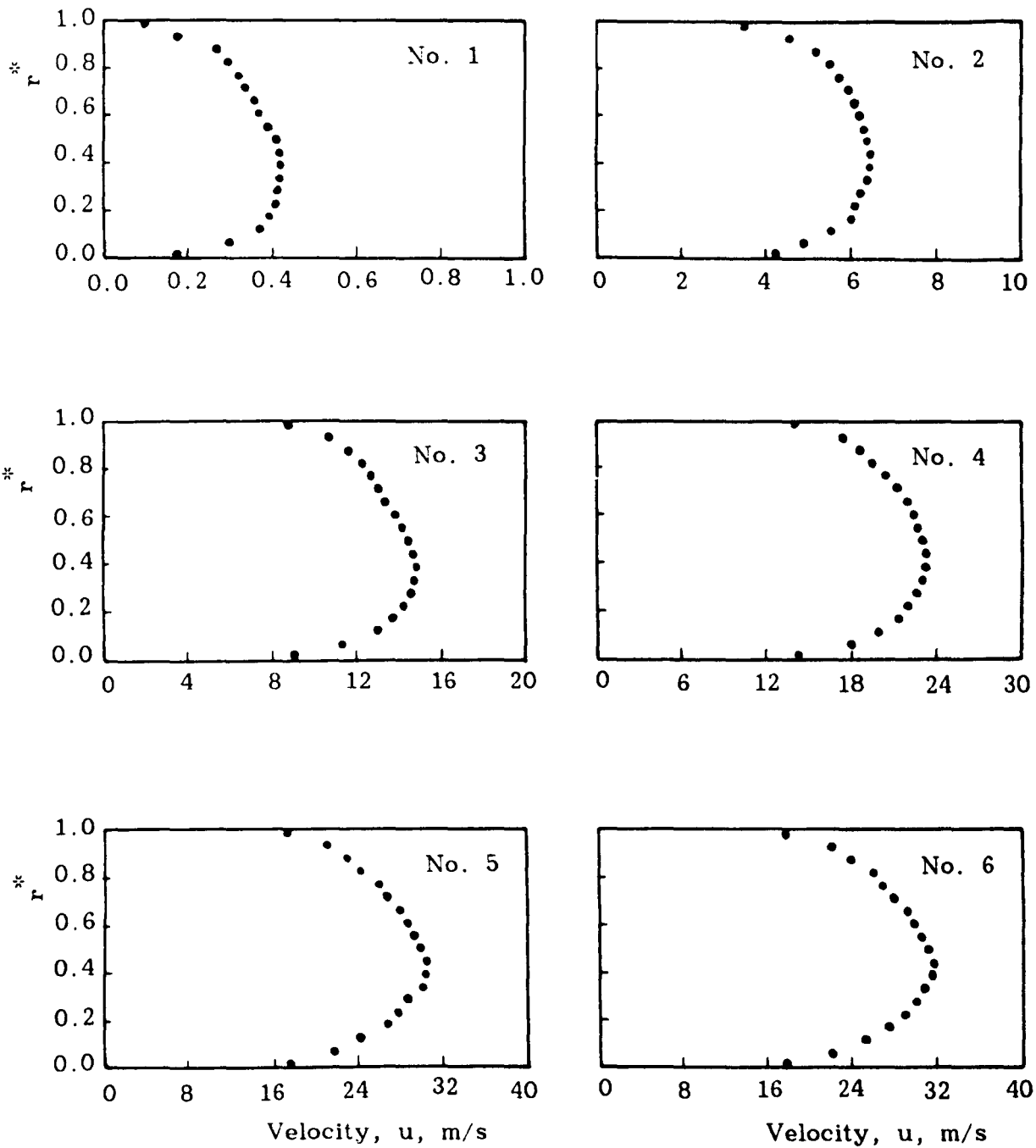
Fig. 4.5 Velocity profiles through the rig (rough - upstream).
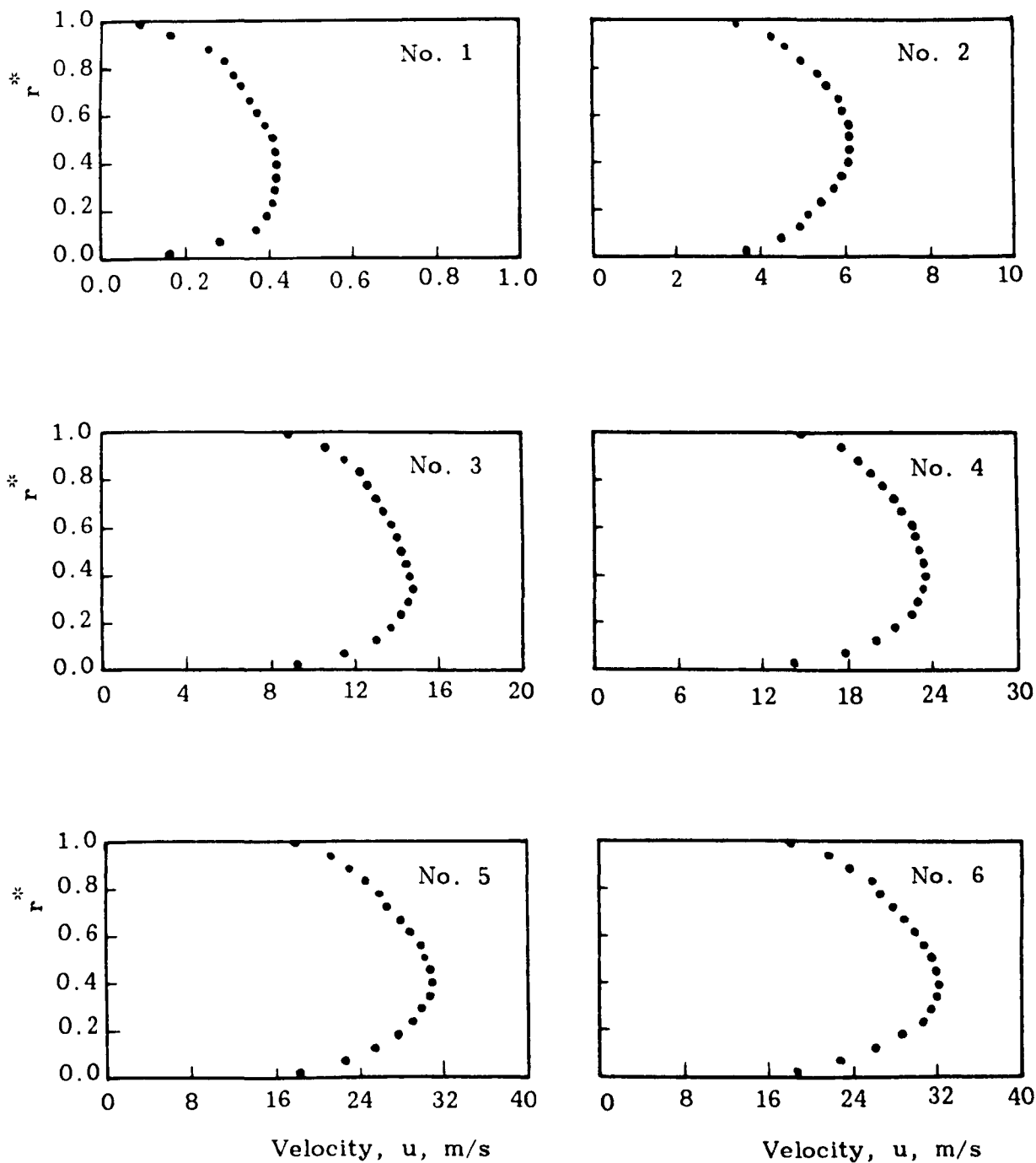
Fig. 4.6 Velocity profiles through the rig (rough - downstream).
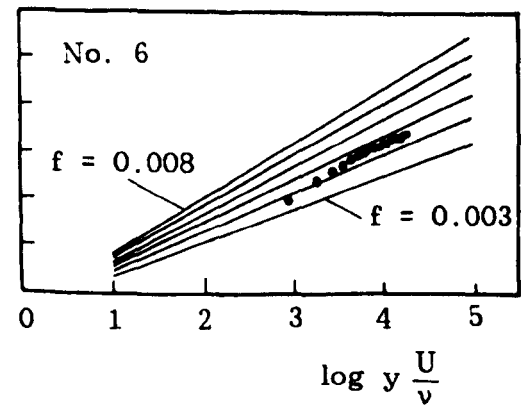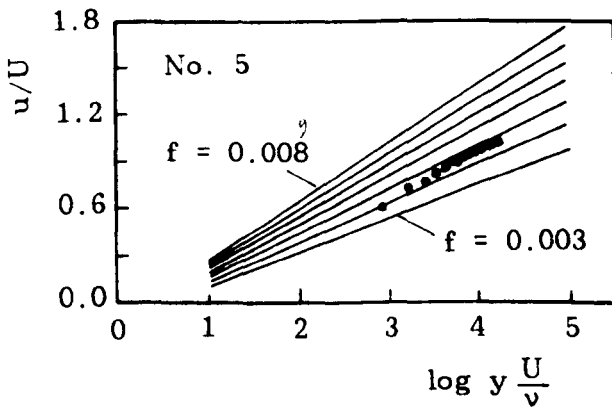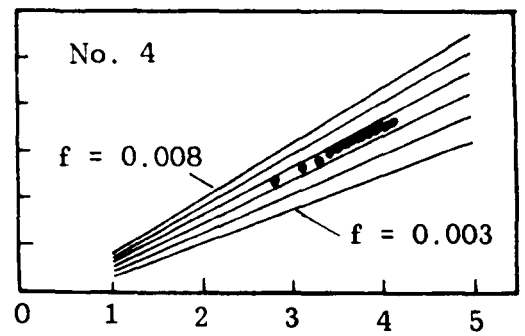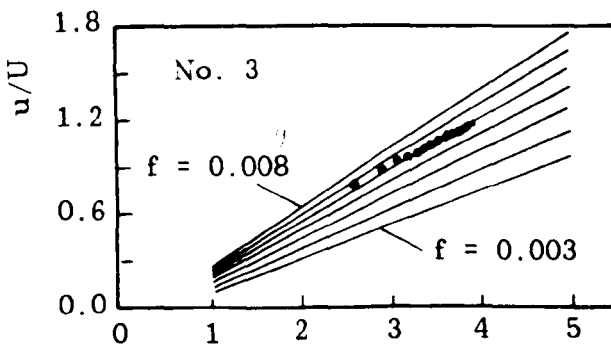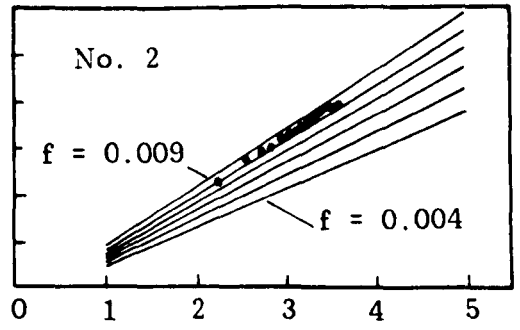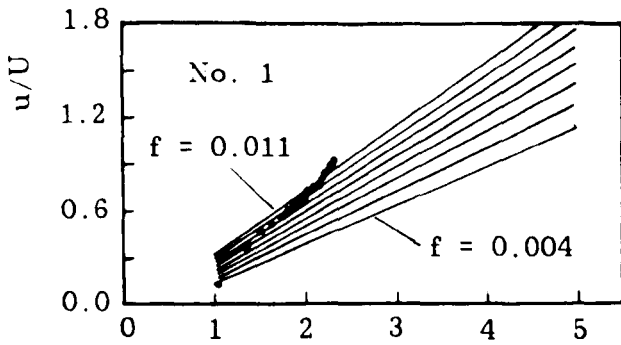
Fig. 4.7 Clauser chart method to calculate friction factor.
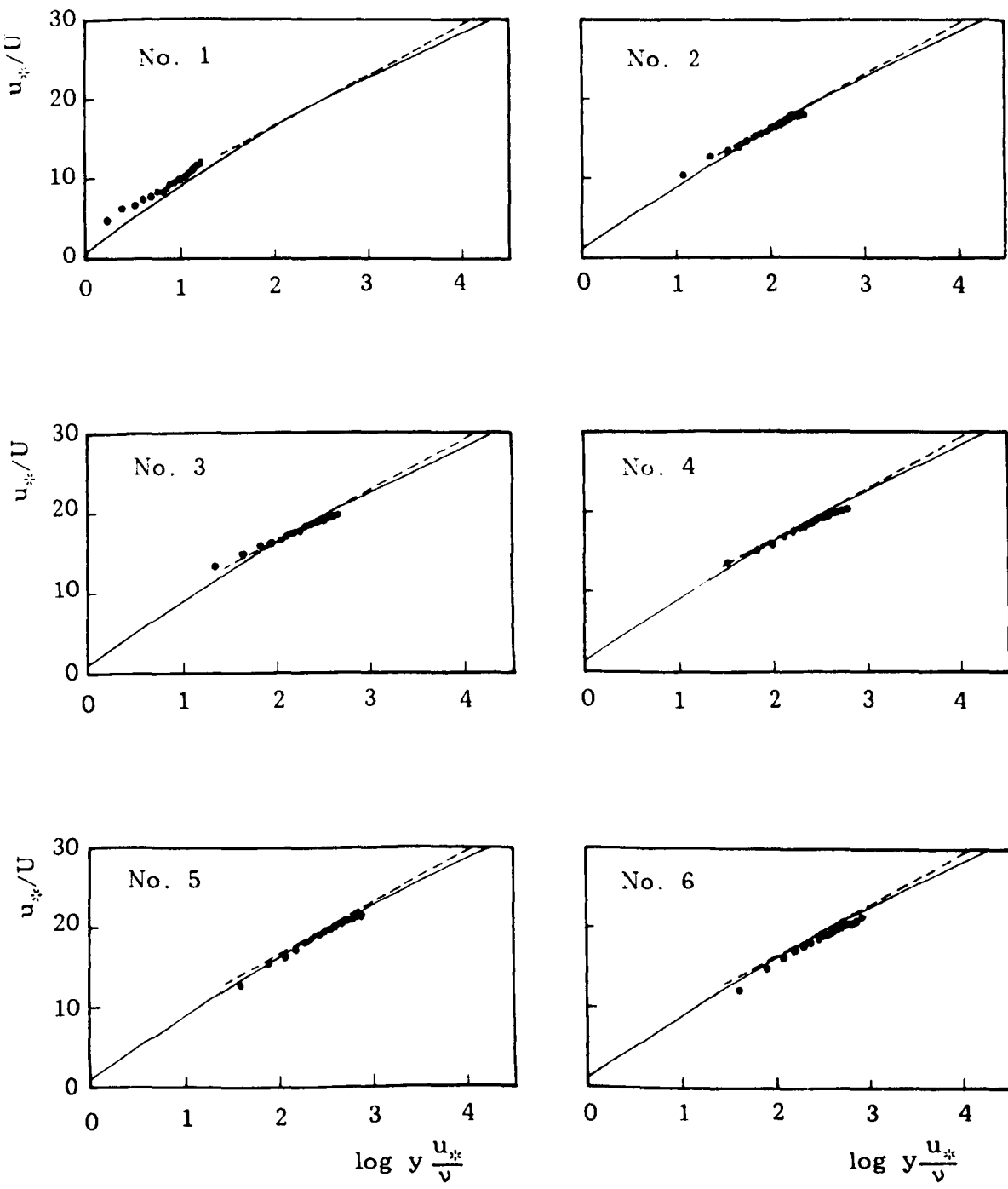
Fig. 4.8 Friction velocity compared with equations of Reichardt and Deissler.
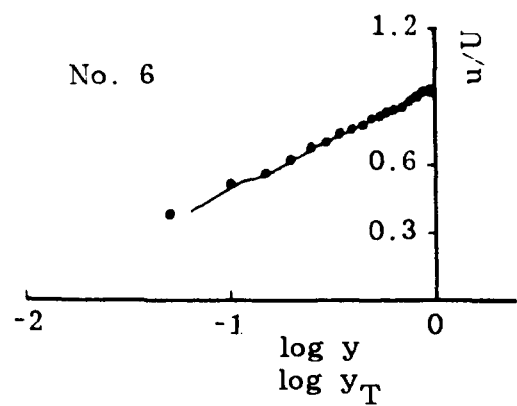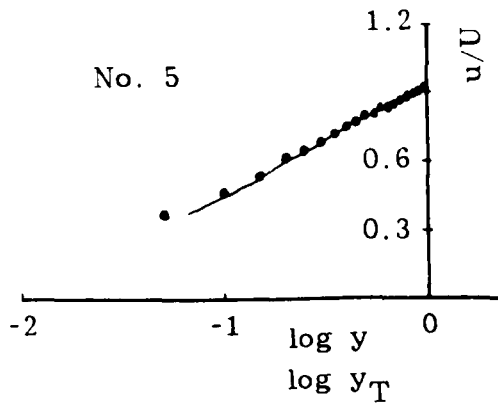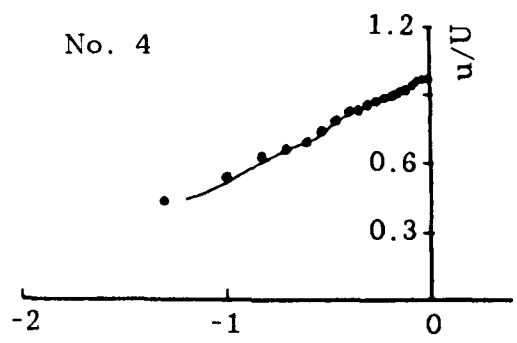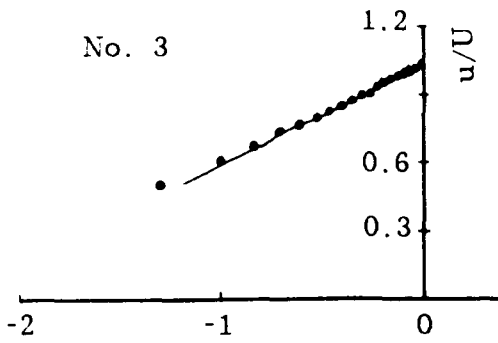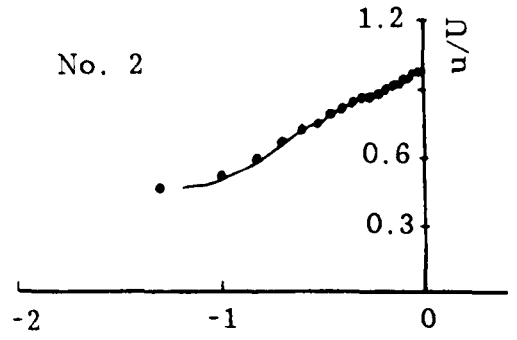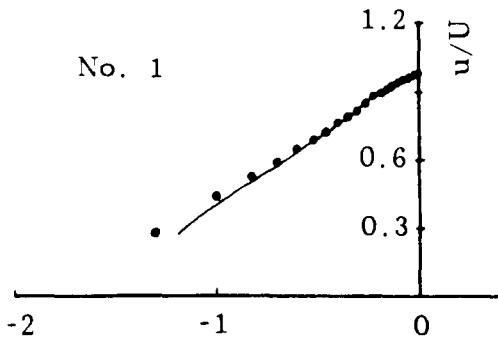
Fig. 4.9 Perry and Joubert method for calculation friction
factor for ribbed surface.

Fig. 4.10 Layout of the heating system.
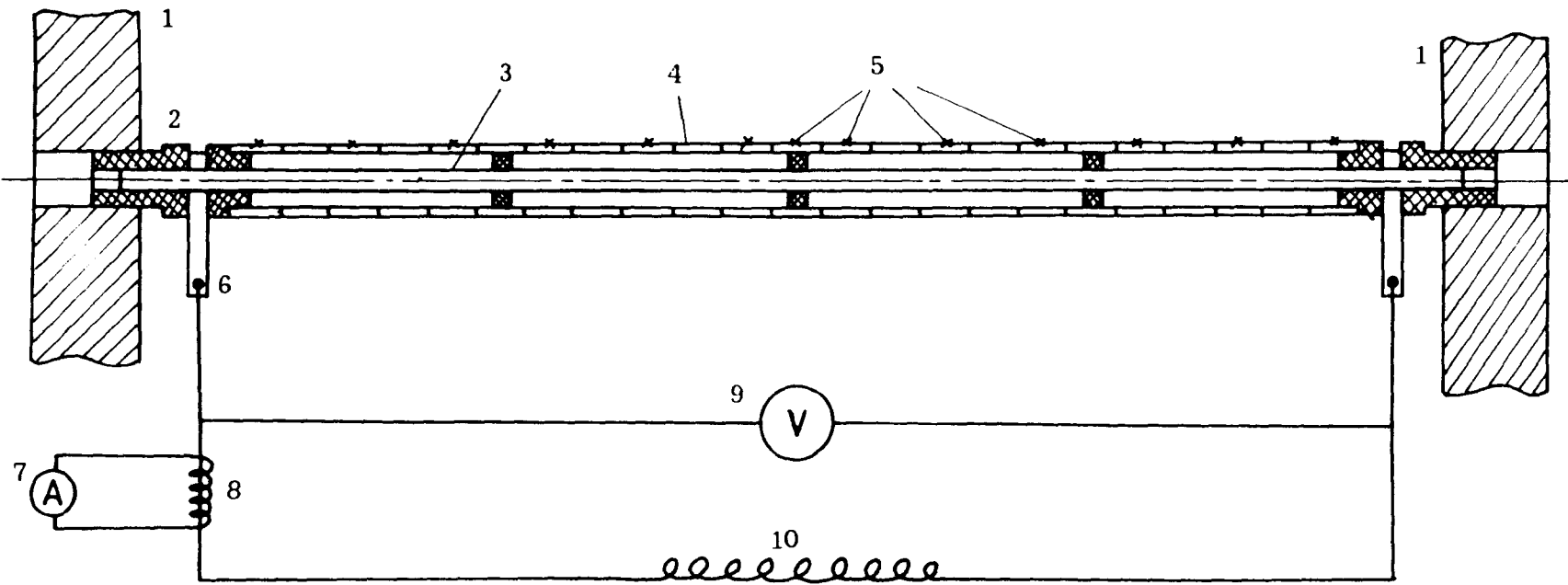
1- Supported flanges.

2- Monolux 500 insulator material.

3- Tie-rod.

4- Tested surface.

5- Thermocouple.

6- Copper busbar.

7- Ammeter.

8- Current transformer.

9- Voltmeter.

10- Power transformer.

11- Variable auto-transformer.

240 v
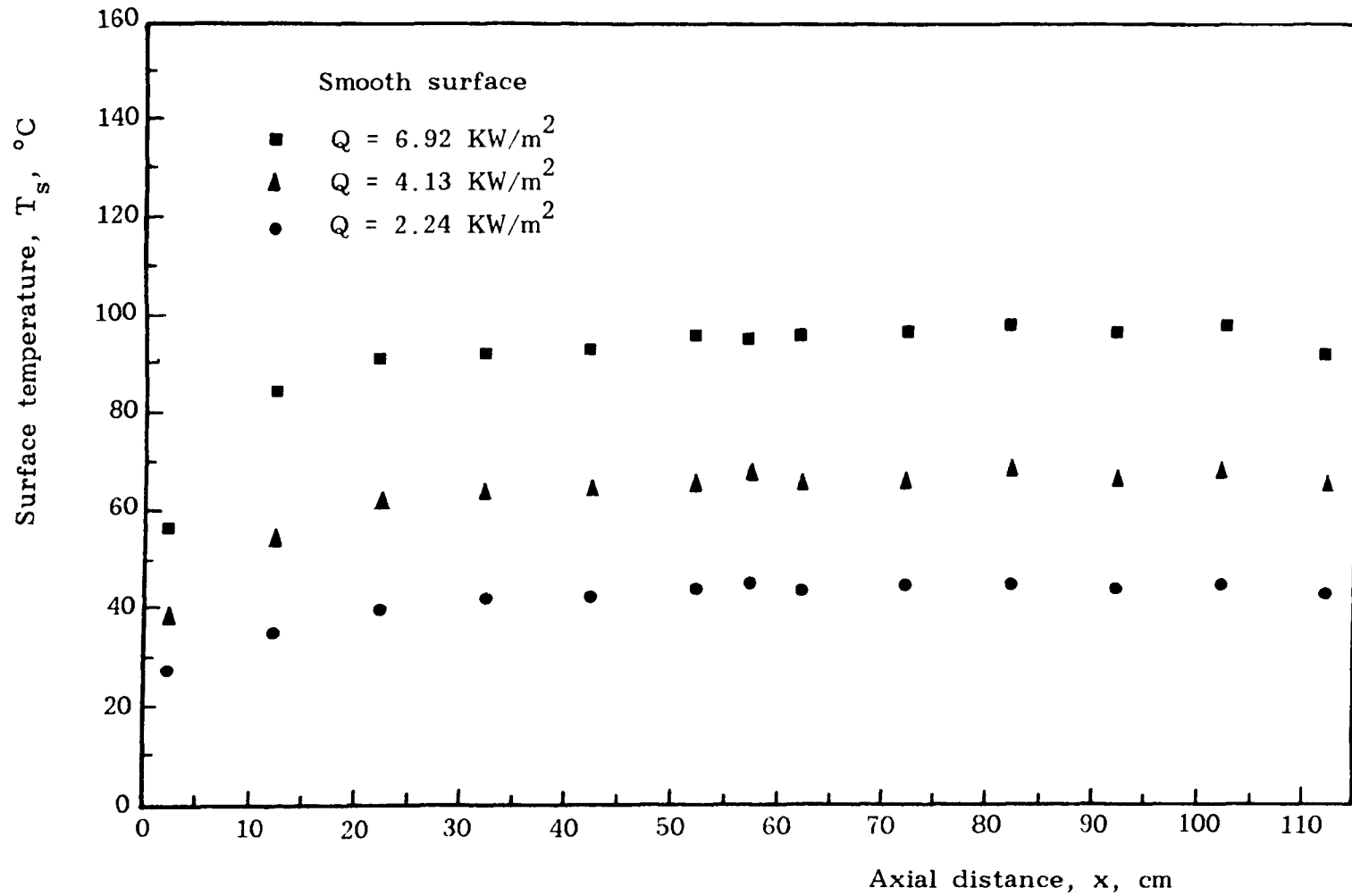
Fig. 4.11 Three surface temperature distributions along the rod.
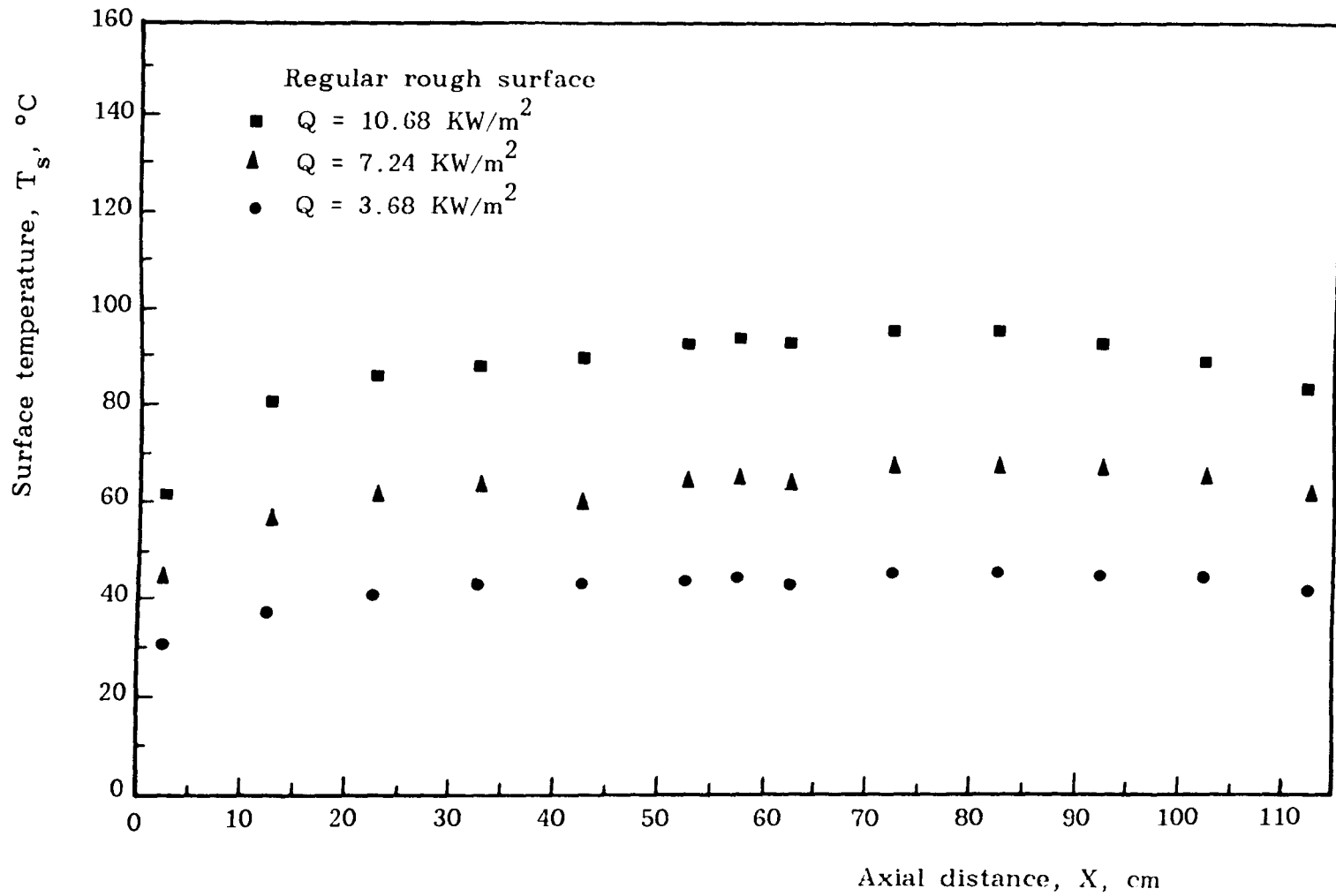
Fig. 4.12 Three surface temperature distributions along the rod.
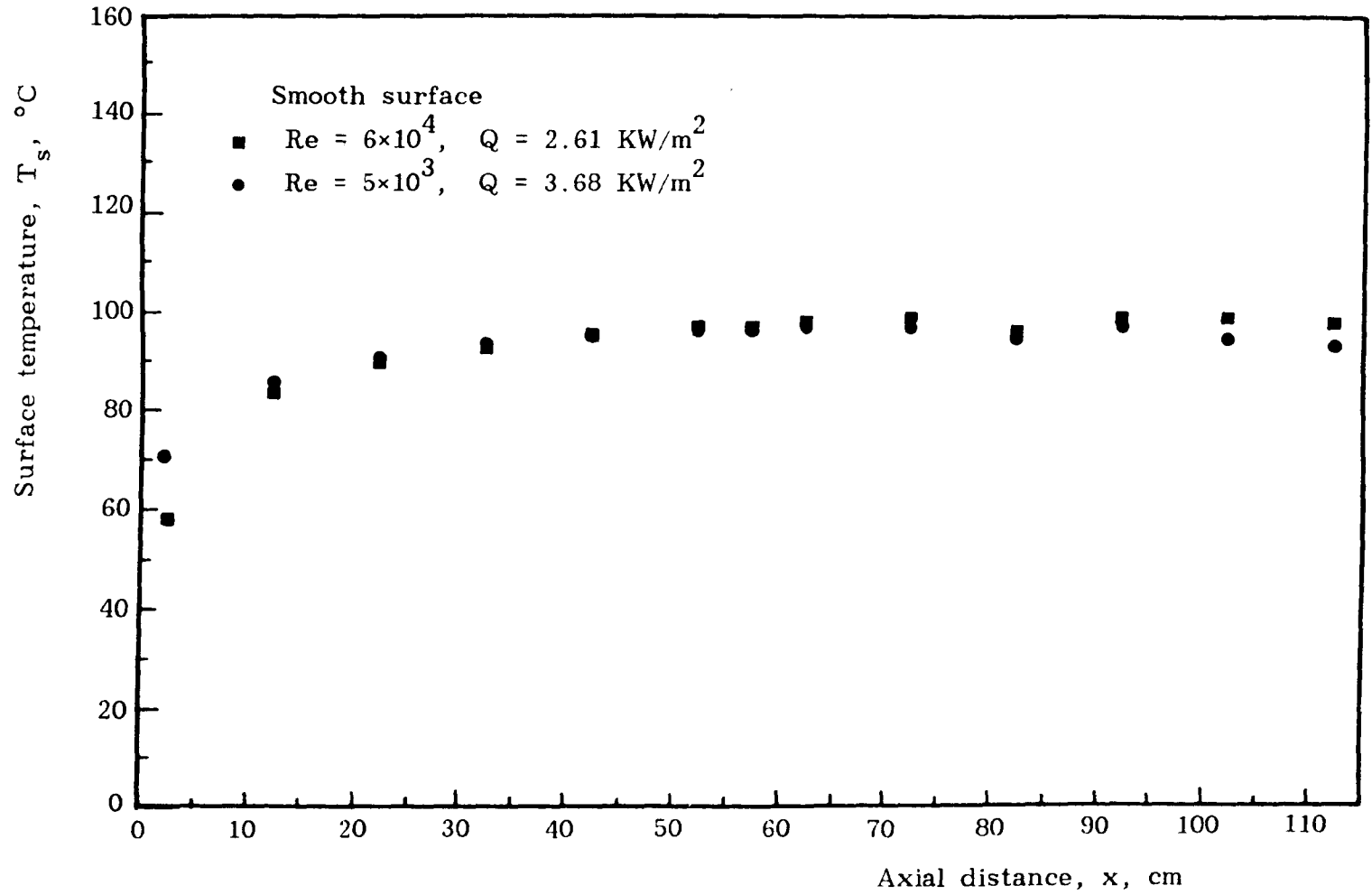
Fig. 4.13 Three surface temperature distributions along the rod.
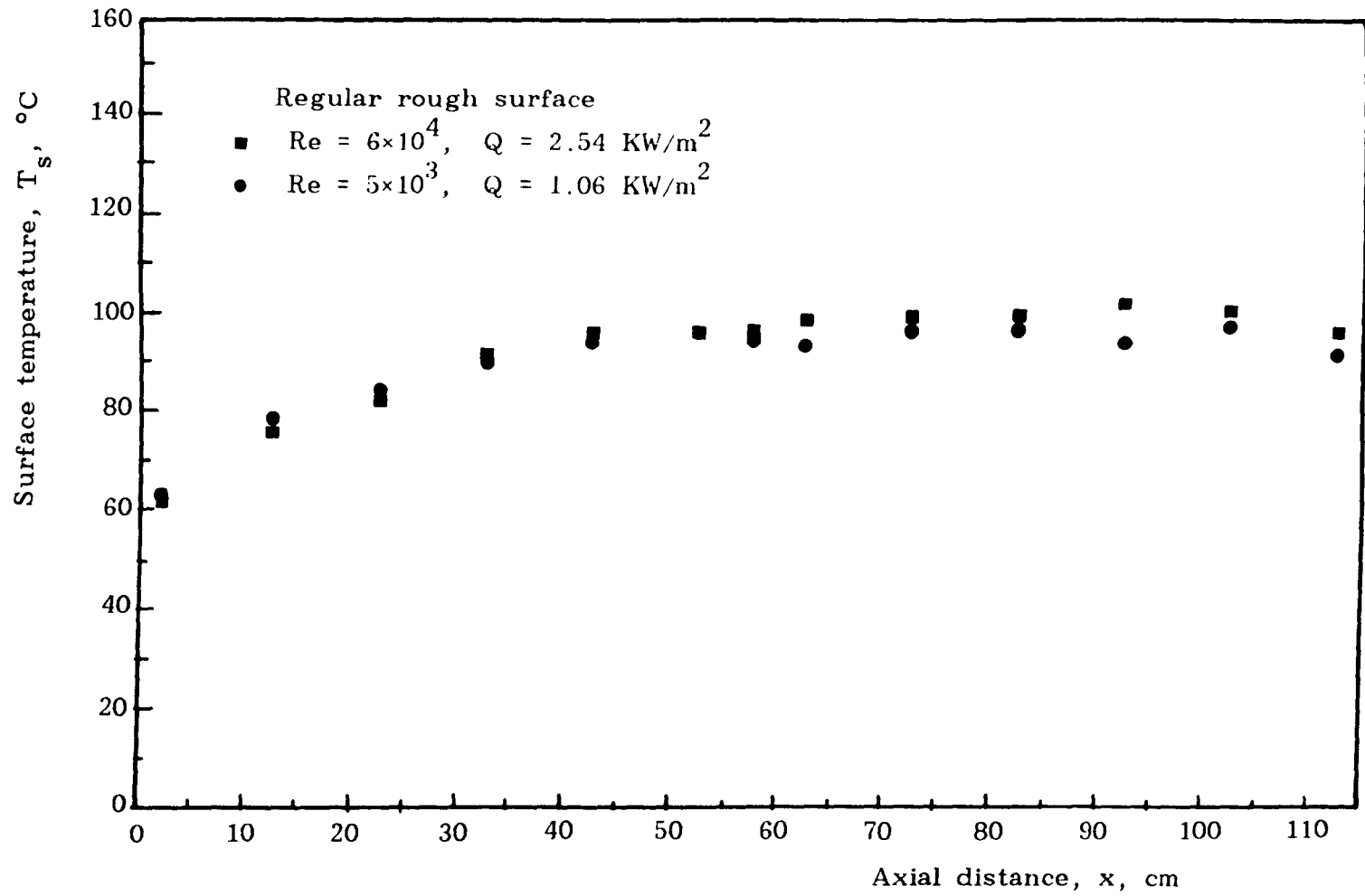
Fig. 4.14 Three surface temperature distributions along the rod.
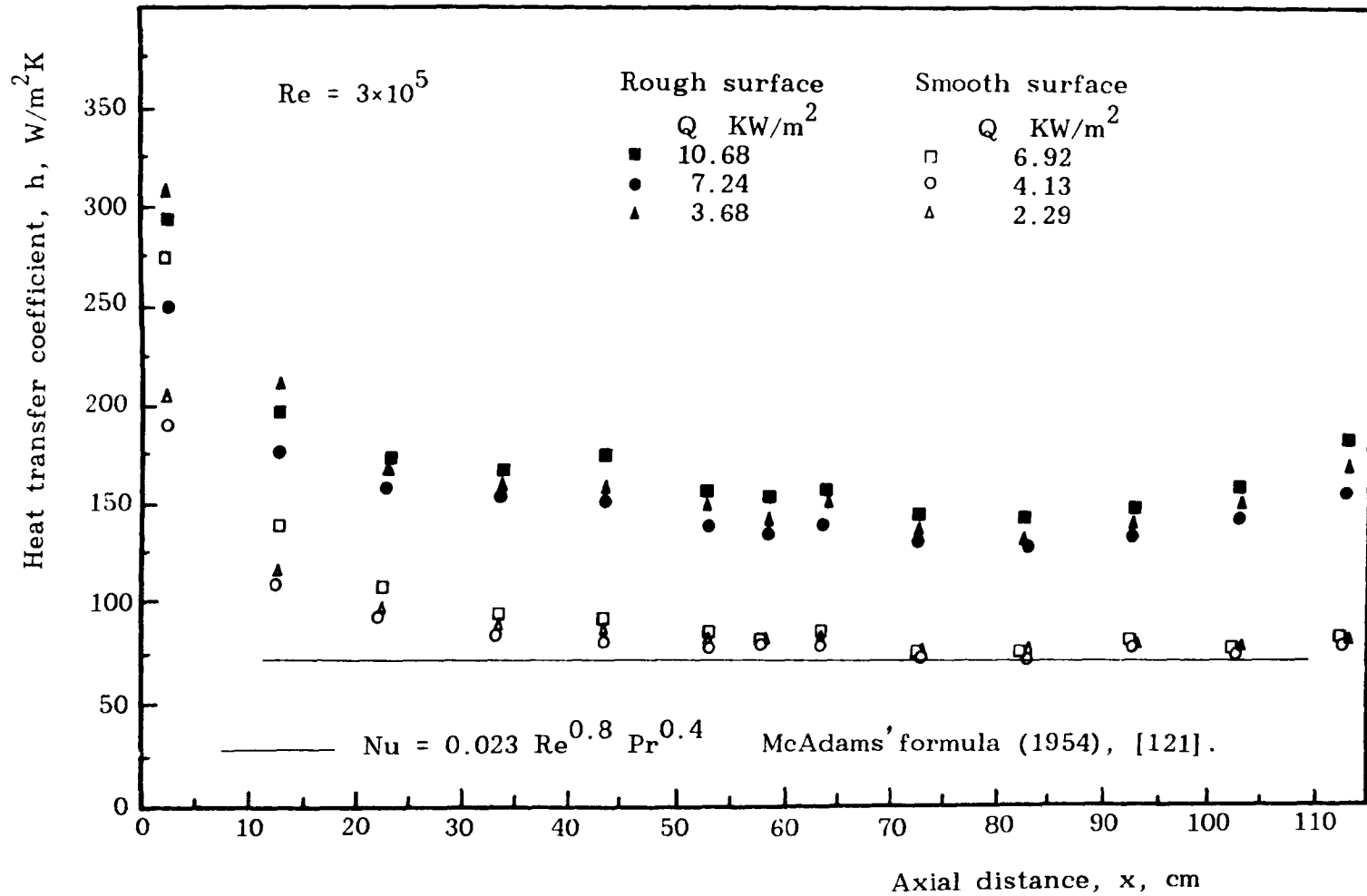
Fig. 4.15 Heat transfer coefficient along the rods.
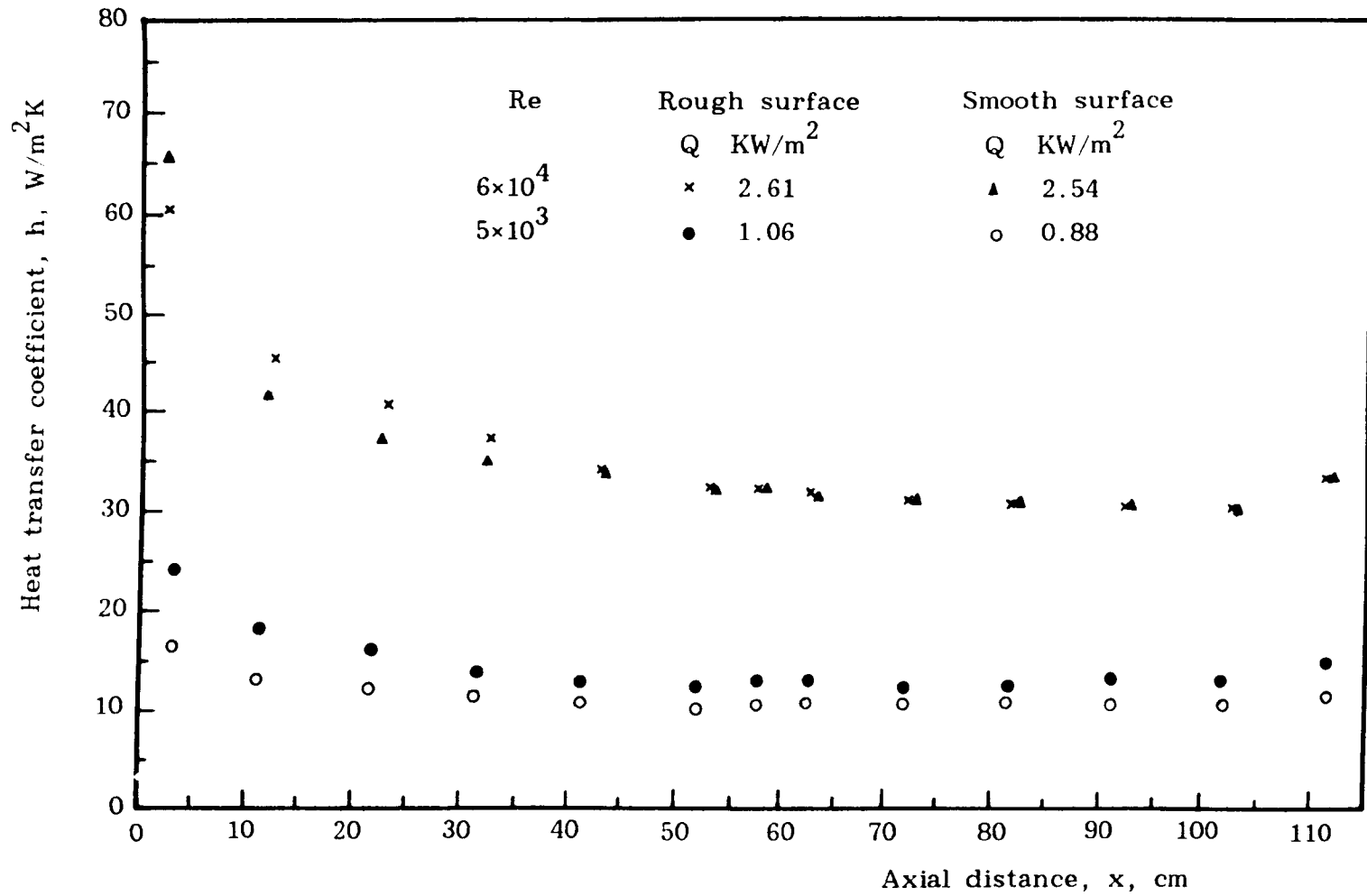
Fig. 4.16 Heat transfer coefficient along the rods.
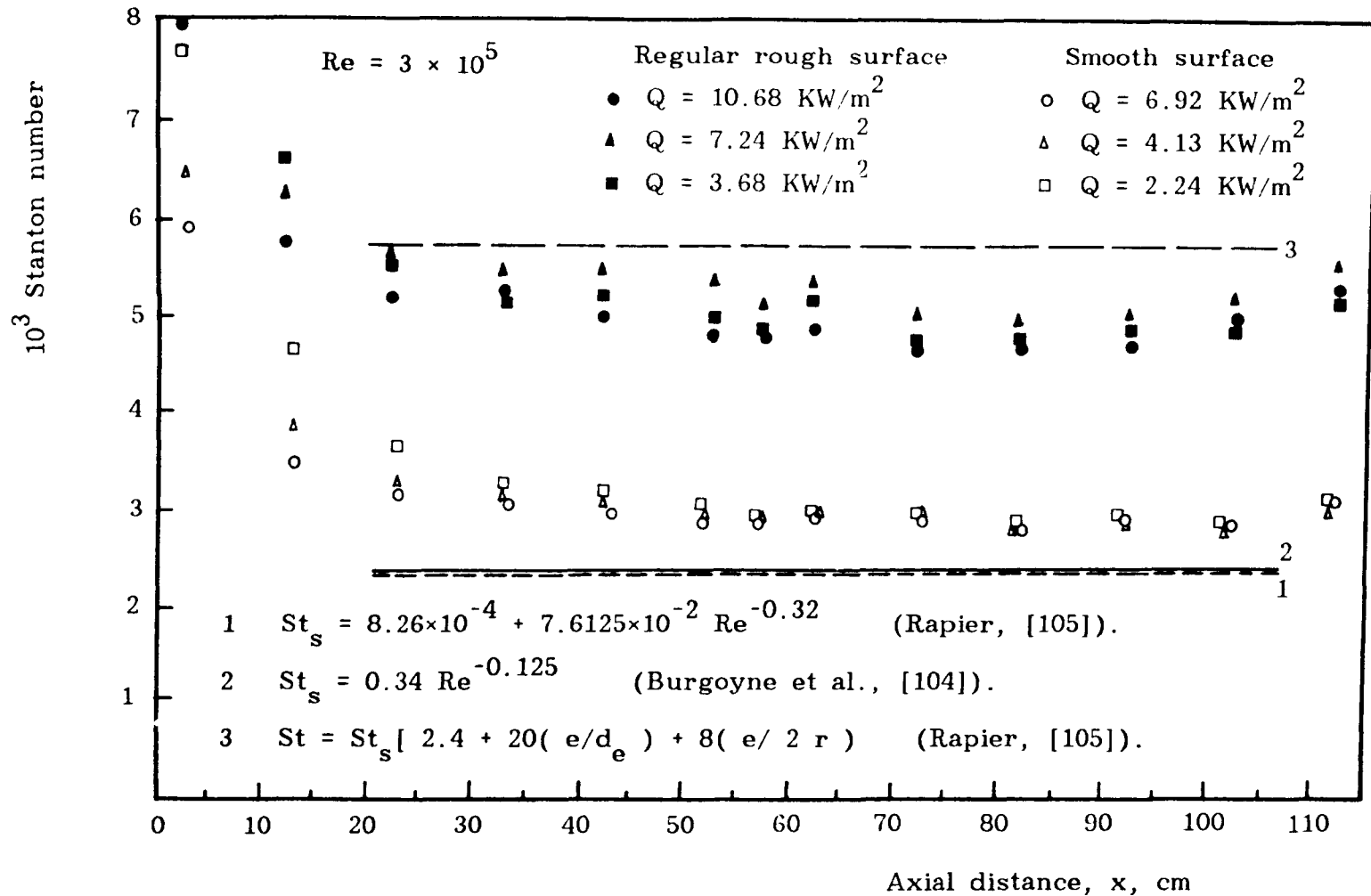
Fig. 4.17 Stanton number, St, along the test rods.

7.5

10

15

9.5

Brass "cap"

Air flow

8.5

Section at A – A

8.2

5

65

9.5
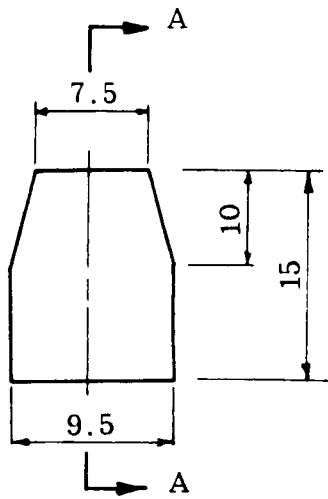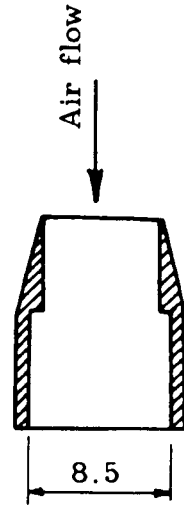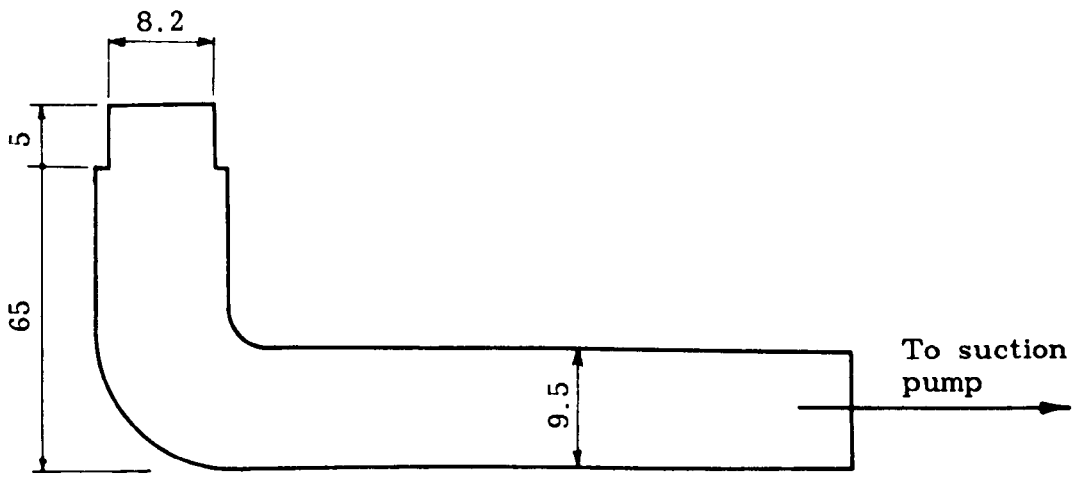
To suction
pump

Suction tube

Dimensions in mms.

Fig. 5.1 Probe for measuring free stream concentration
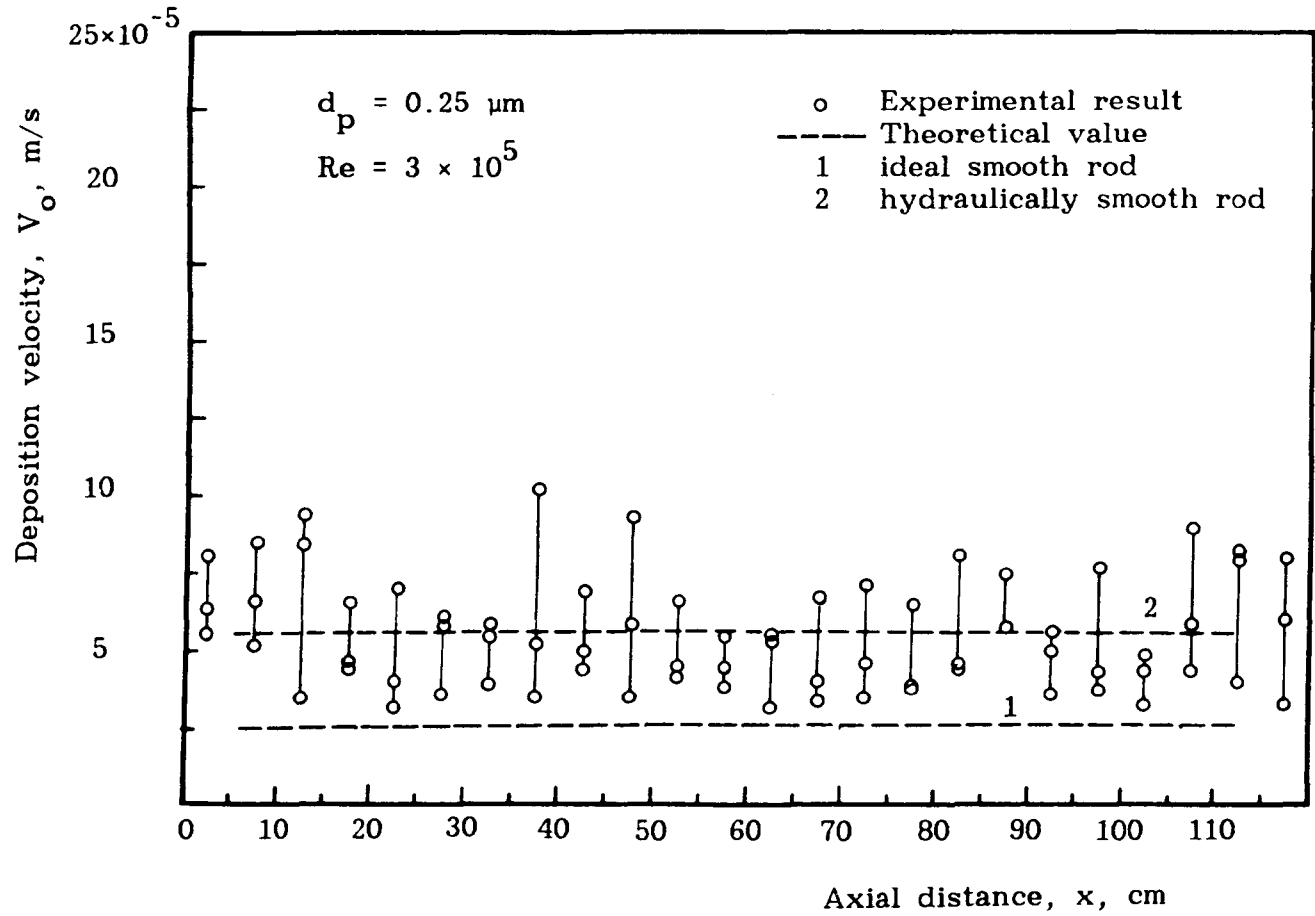
Fig. 5.2 Deposition velocity along cold smooth rod after 1 hour.
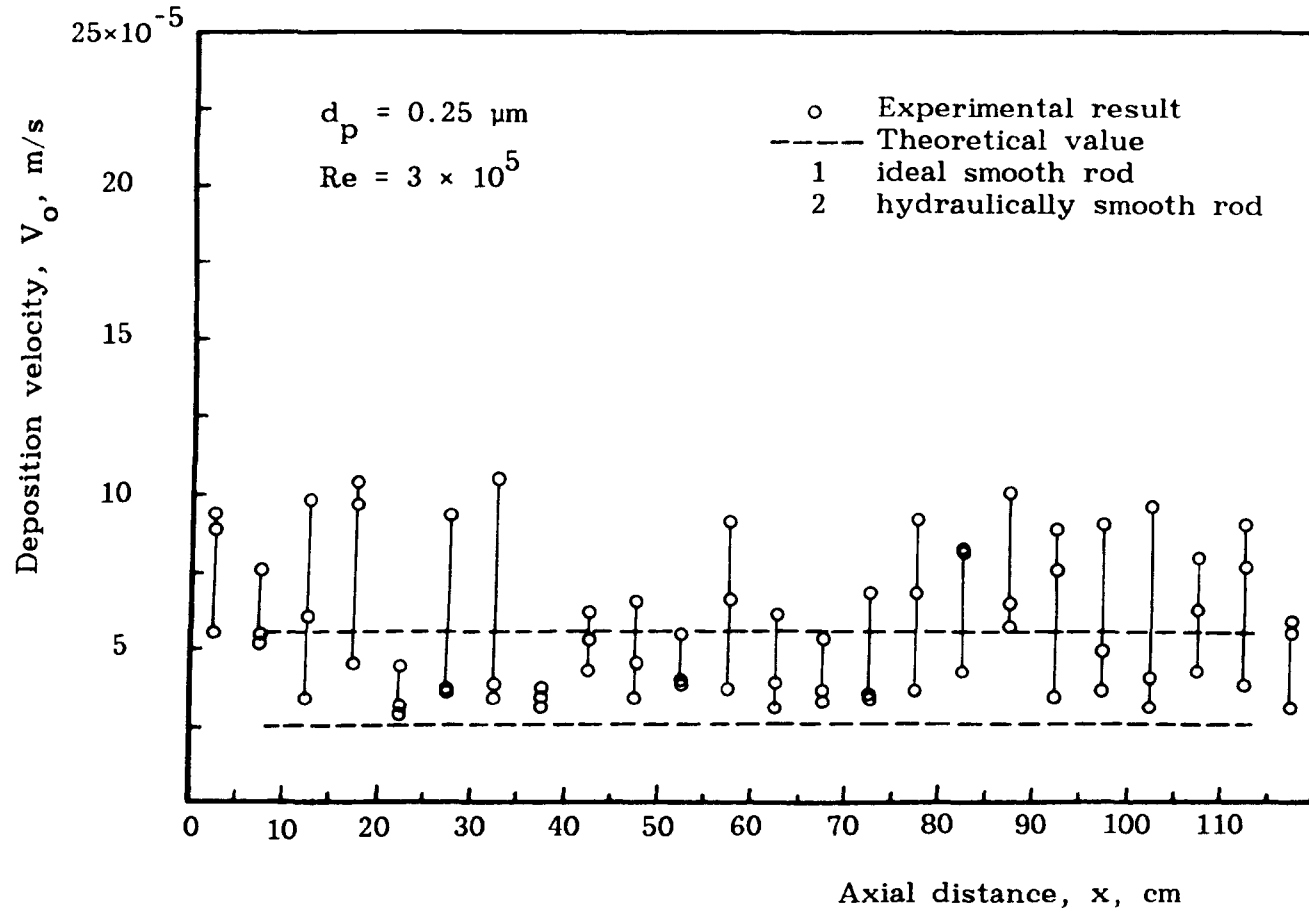
Fig. 5.3 Deposition velocity along cold smooth rod after 2 hours.
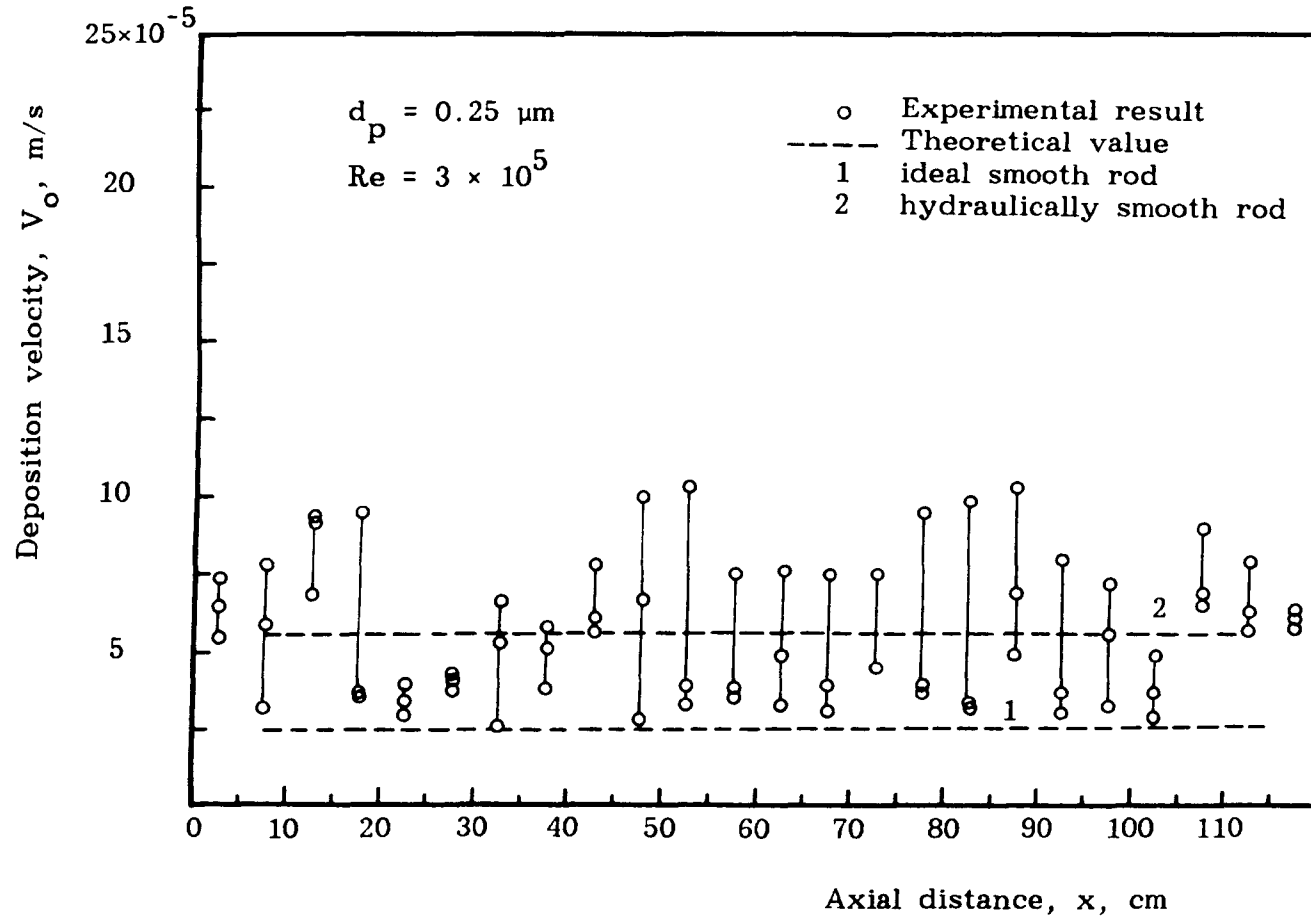
Fig. 5.4 Deposition velocity along cold smooth rod after 3 hours.
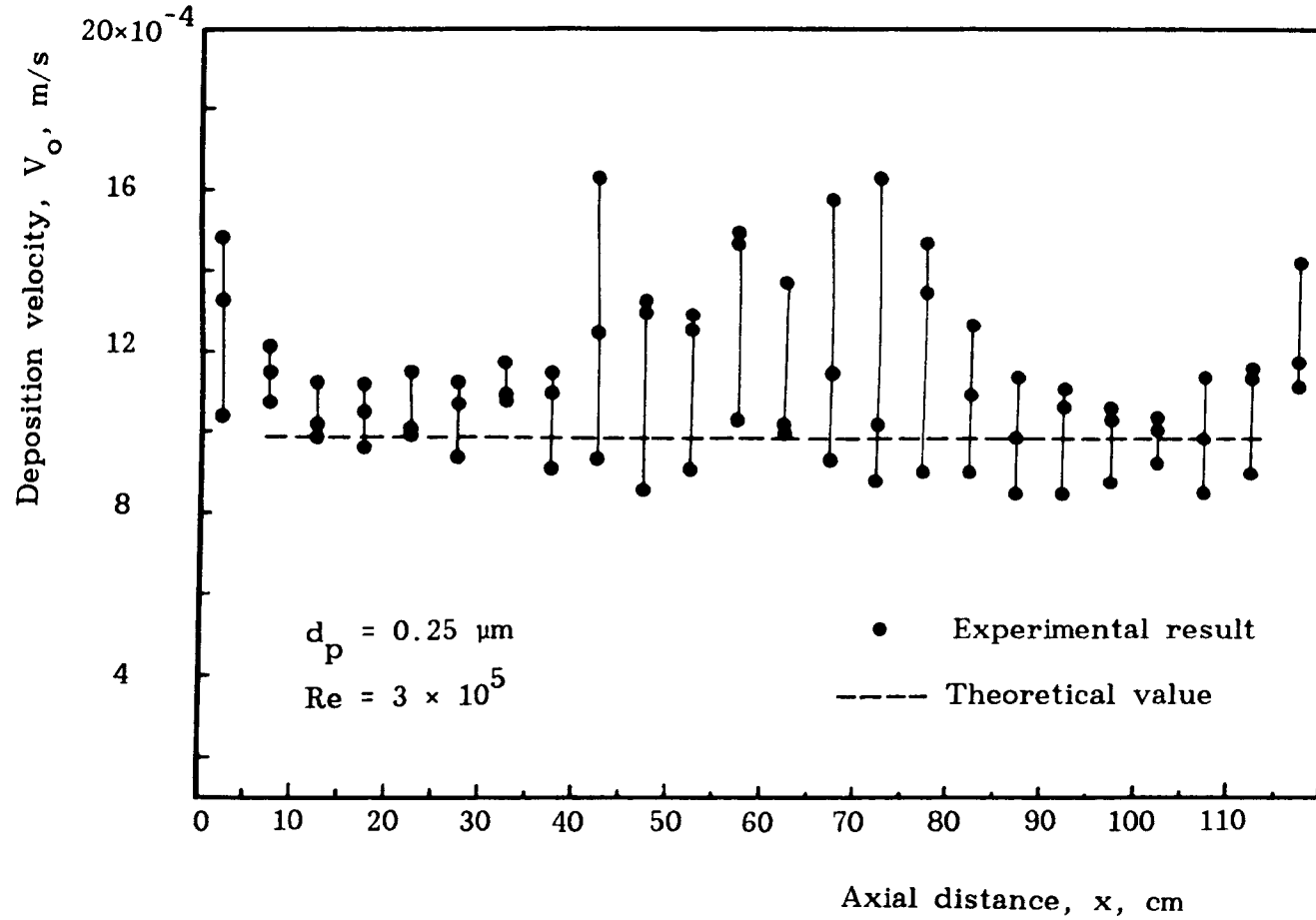
Fig. 5.5 Deposition velocity along cold ribbed rod after 1 hour.
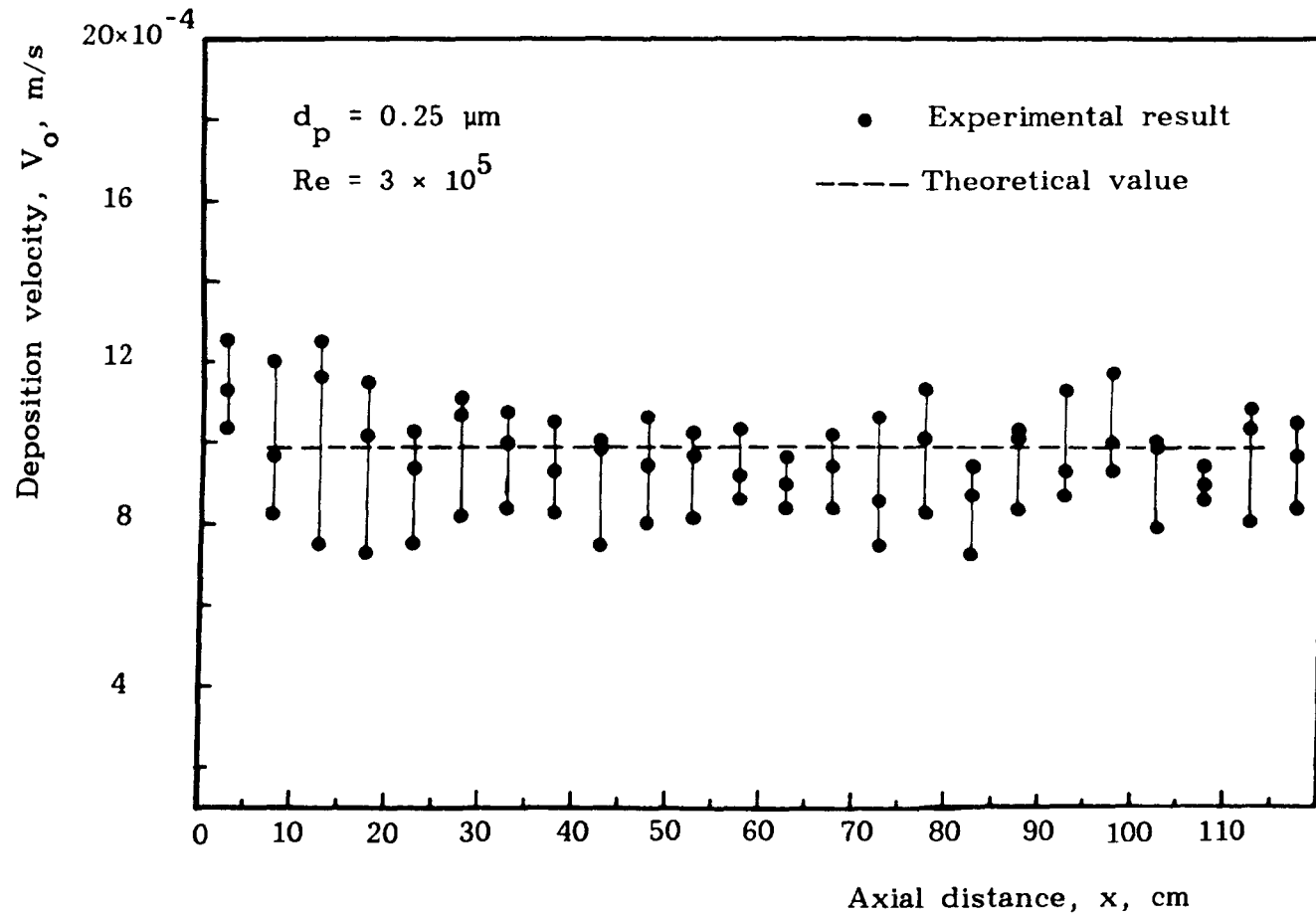
Fig. 5.6 Deposition velocity along cold ribbed rod after 2 hours.
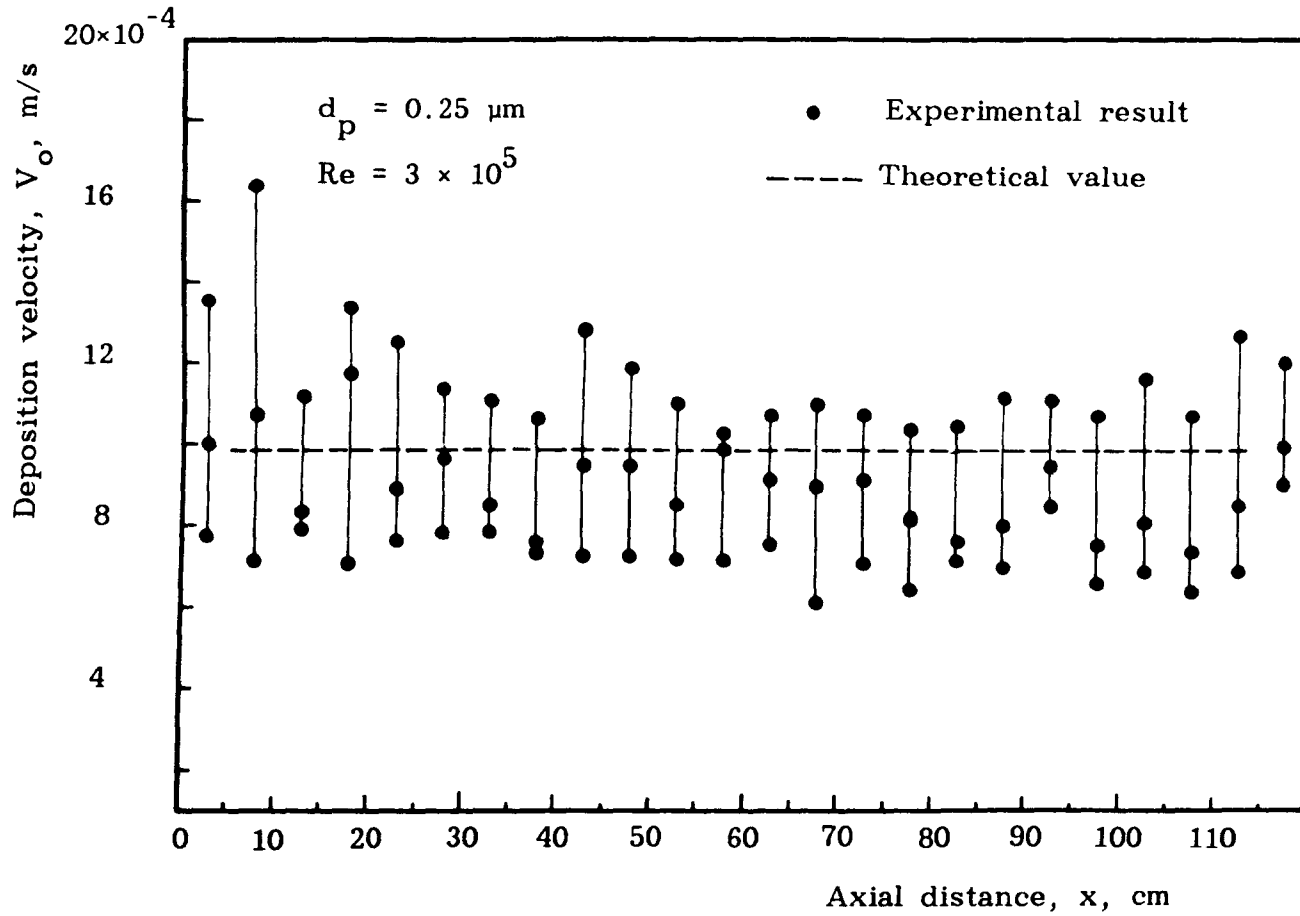
Fig. 5.7 Deposition velocity along cold ribbed rod after 3 hours
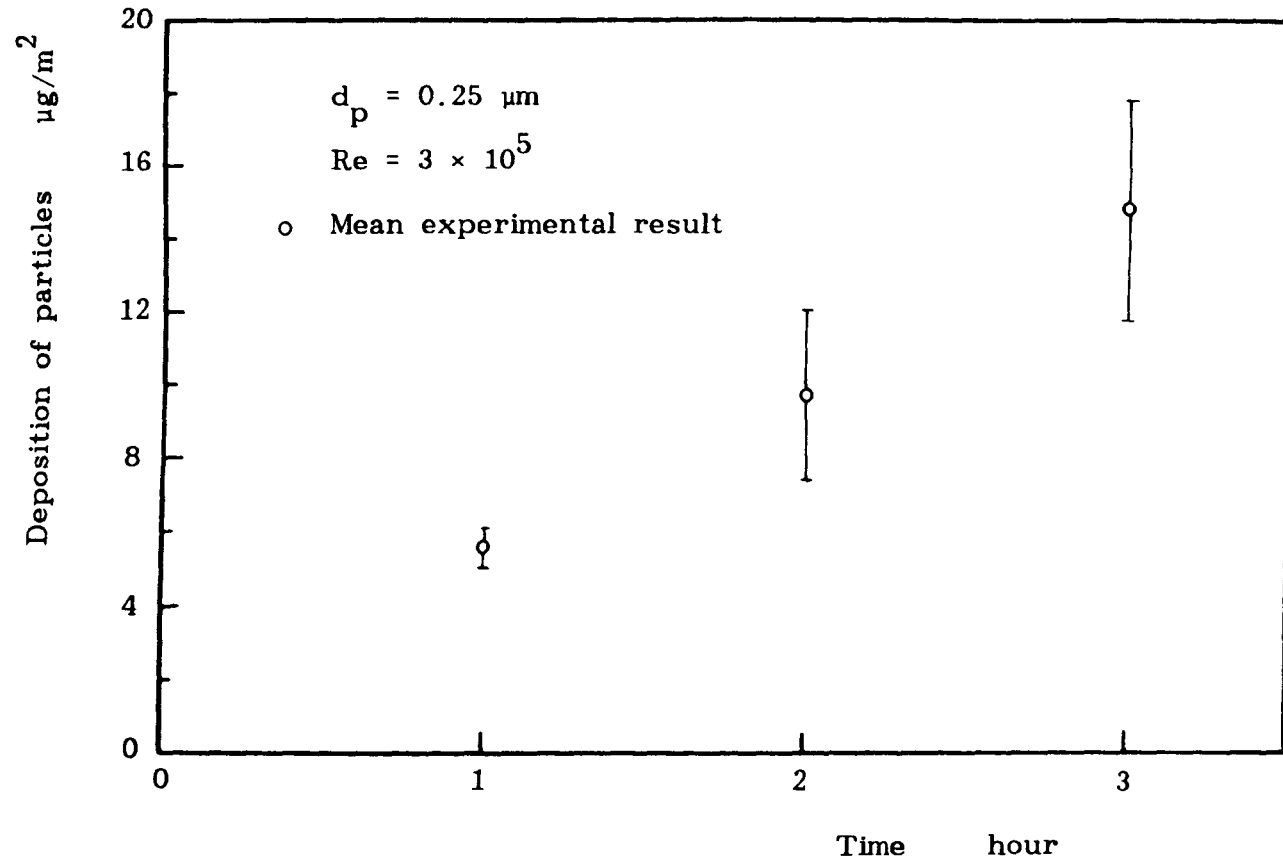
Fig. 5.8 Deposition of particles onto smooth cold rod after 1, 2 and 3 hours.
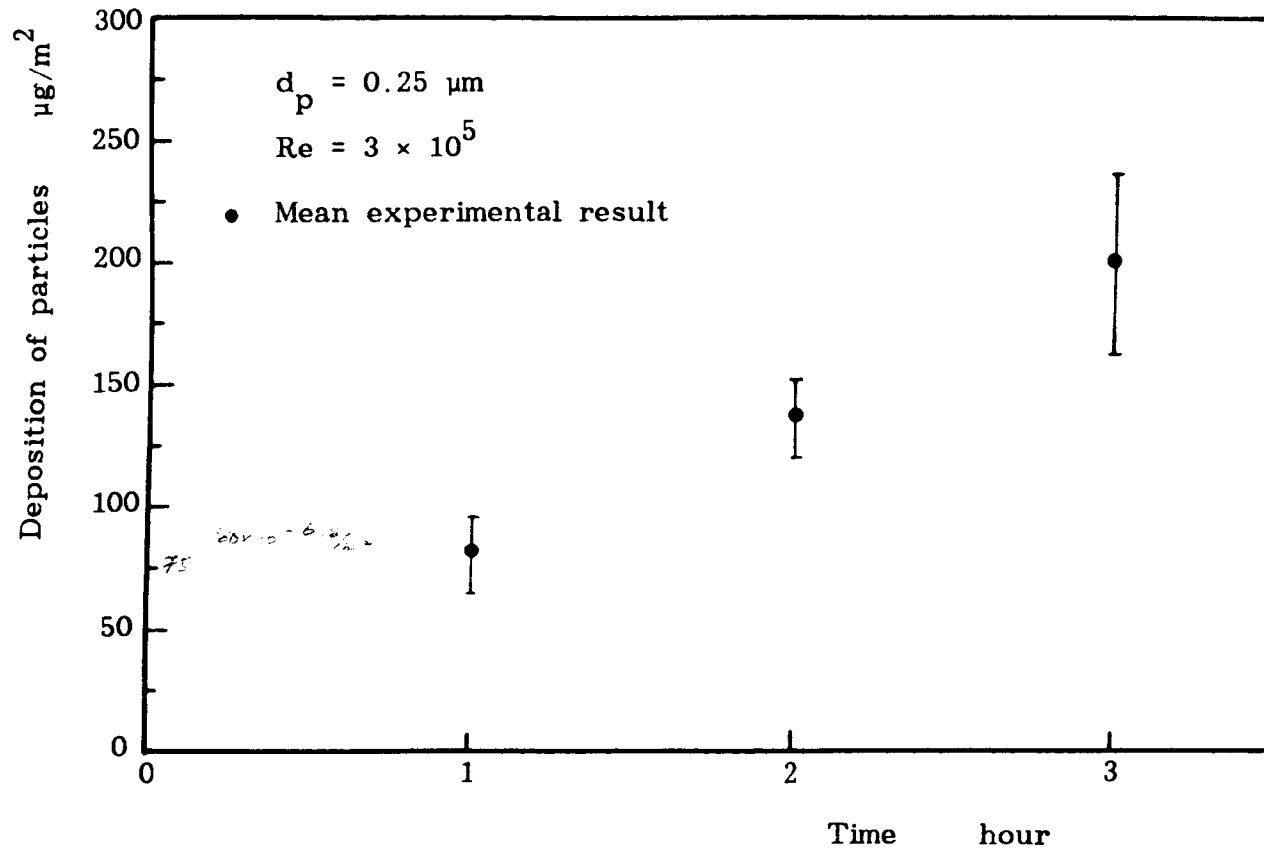
Fig. 5.9 Deposition of particles onto ribbed cold rod after 1, 2 and 3 hours.
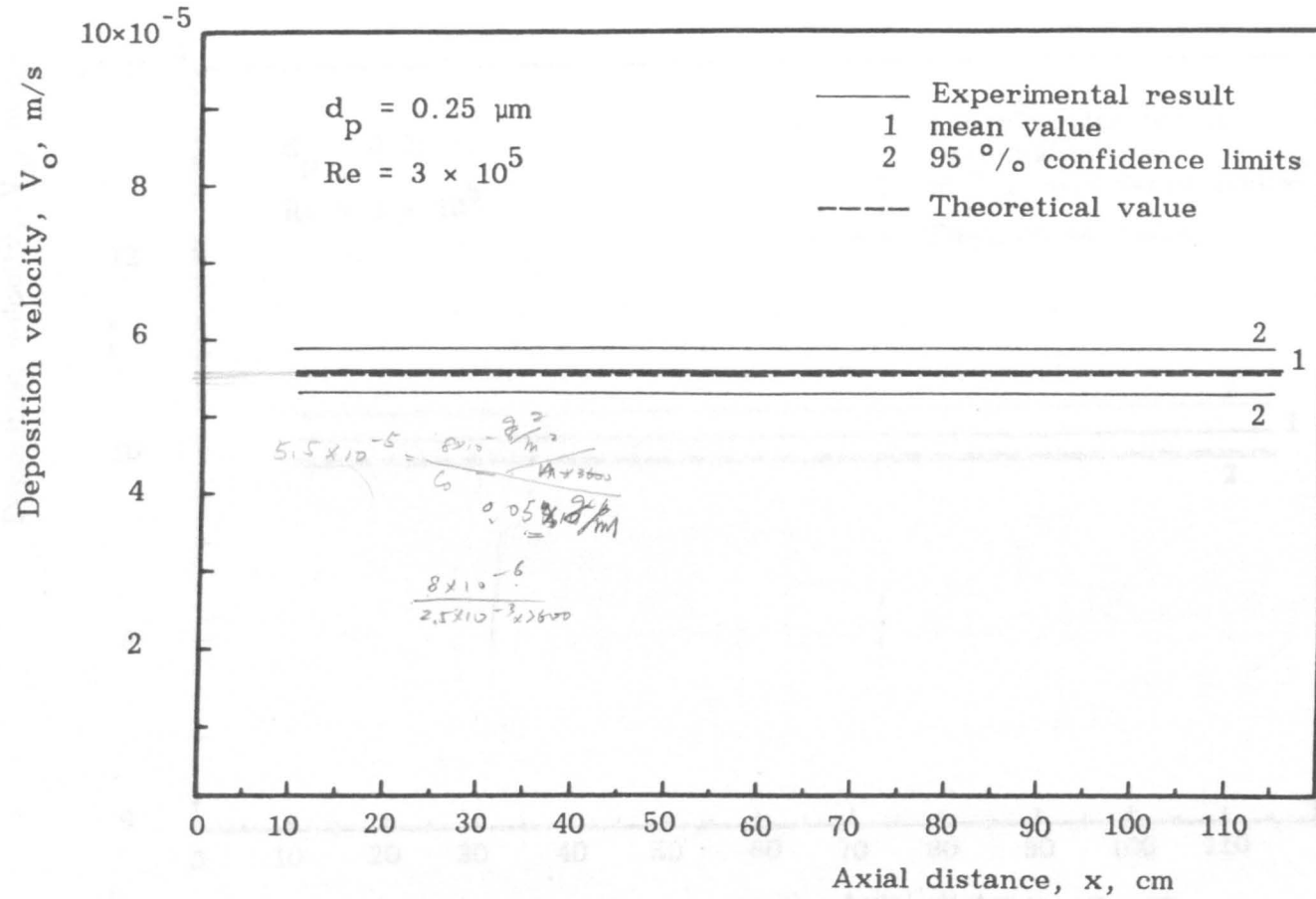
Fig. 5.10 Deposition velocity along cold smooth rod.
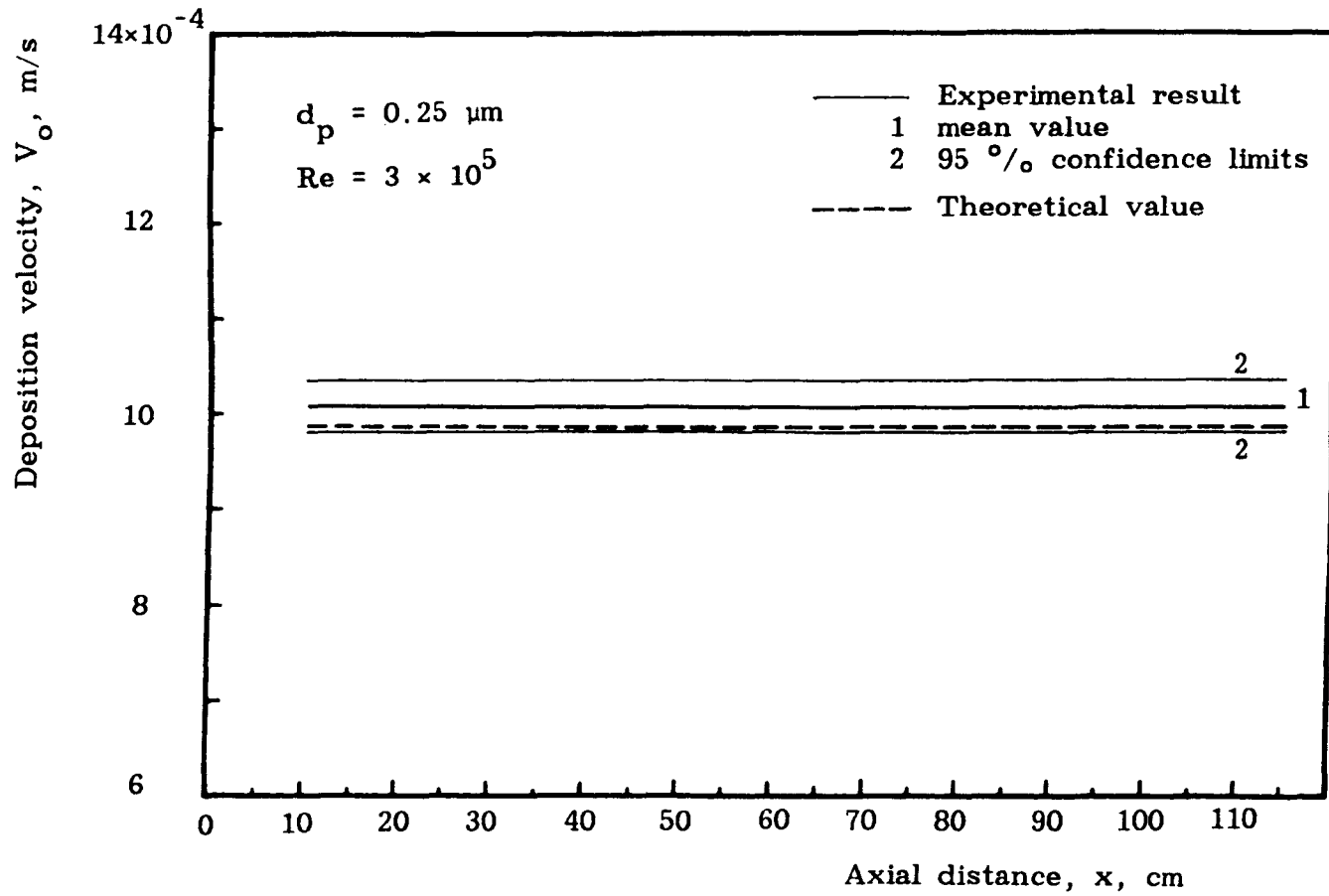
Fig. 5.11 Deposition velocity along cold ribbed fuel rod.
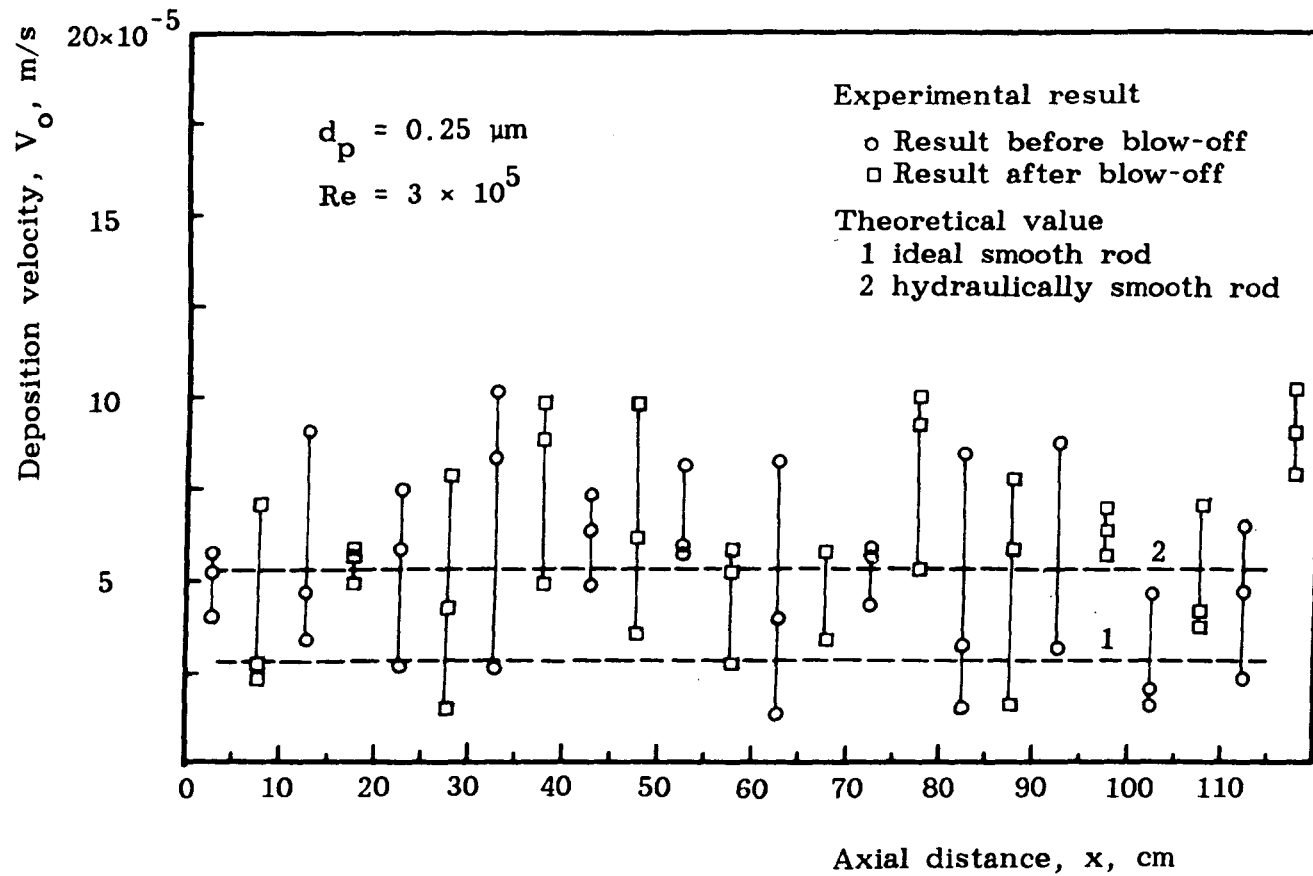
Fig. 5.12.a Deposition velocity along cold smooth rod before and after blow-off test.
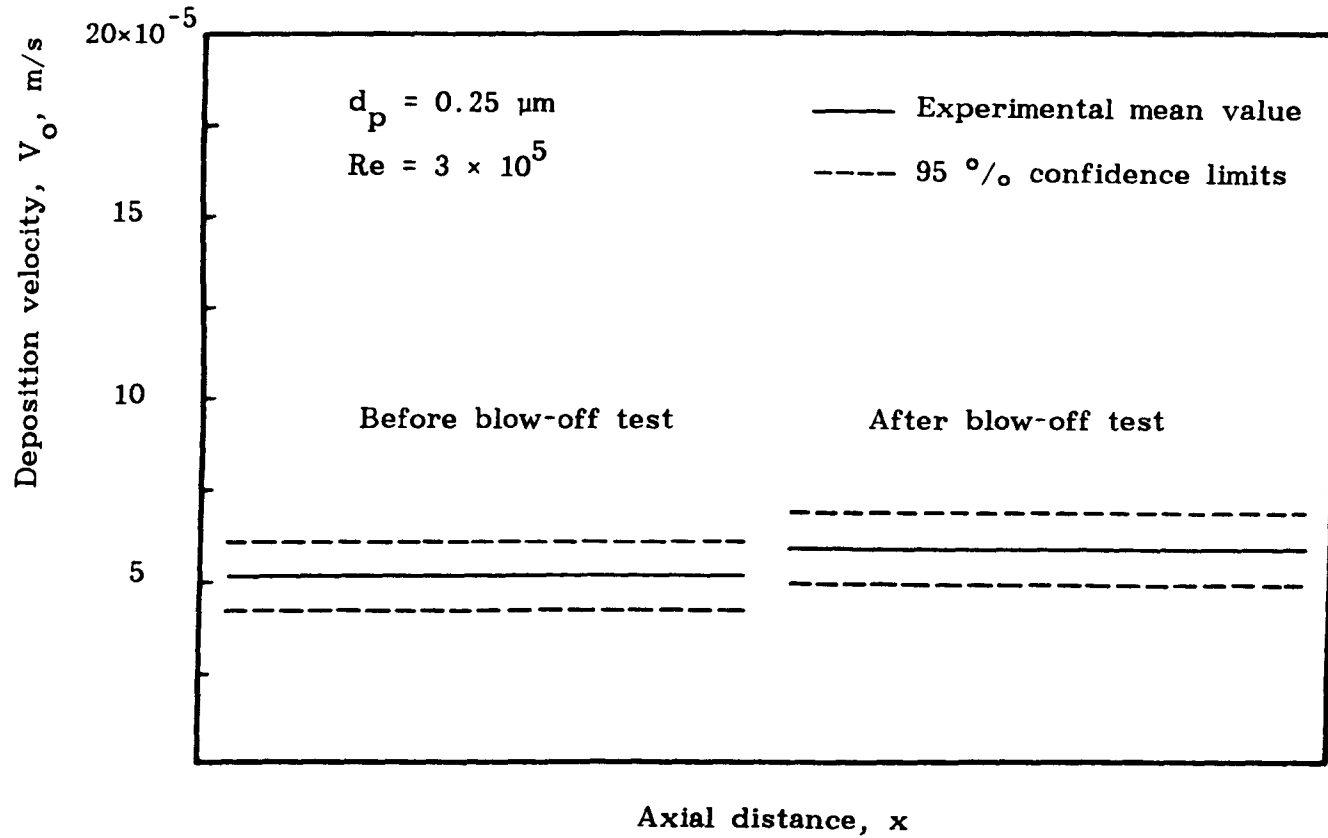
Fig. 5.12.b Deposition velocity along cold smooth rod before and after blow-off test.
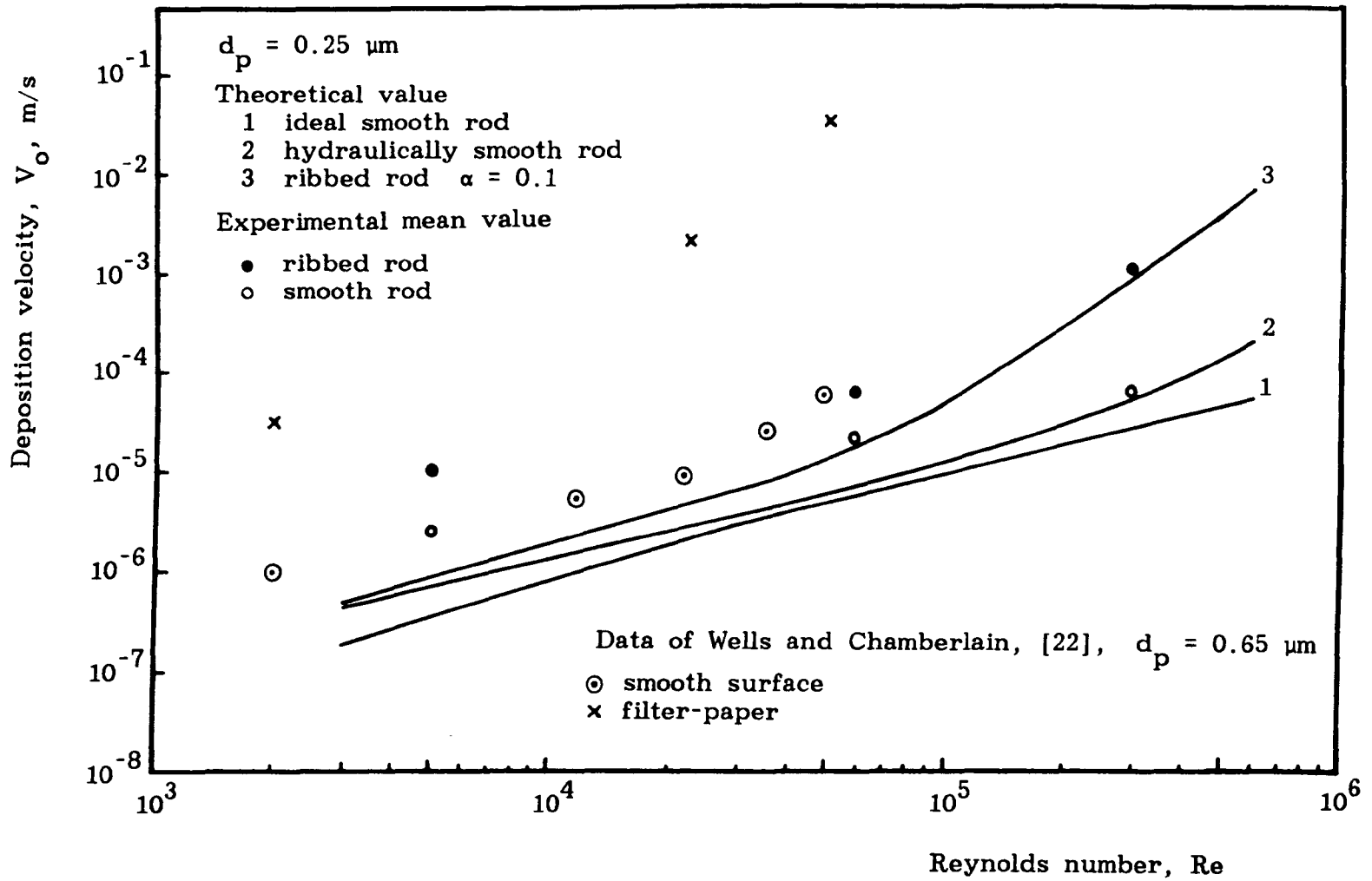
Fig. 5.13 Deposition velocity as a function of Reynolds number.
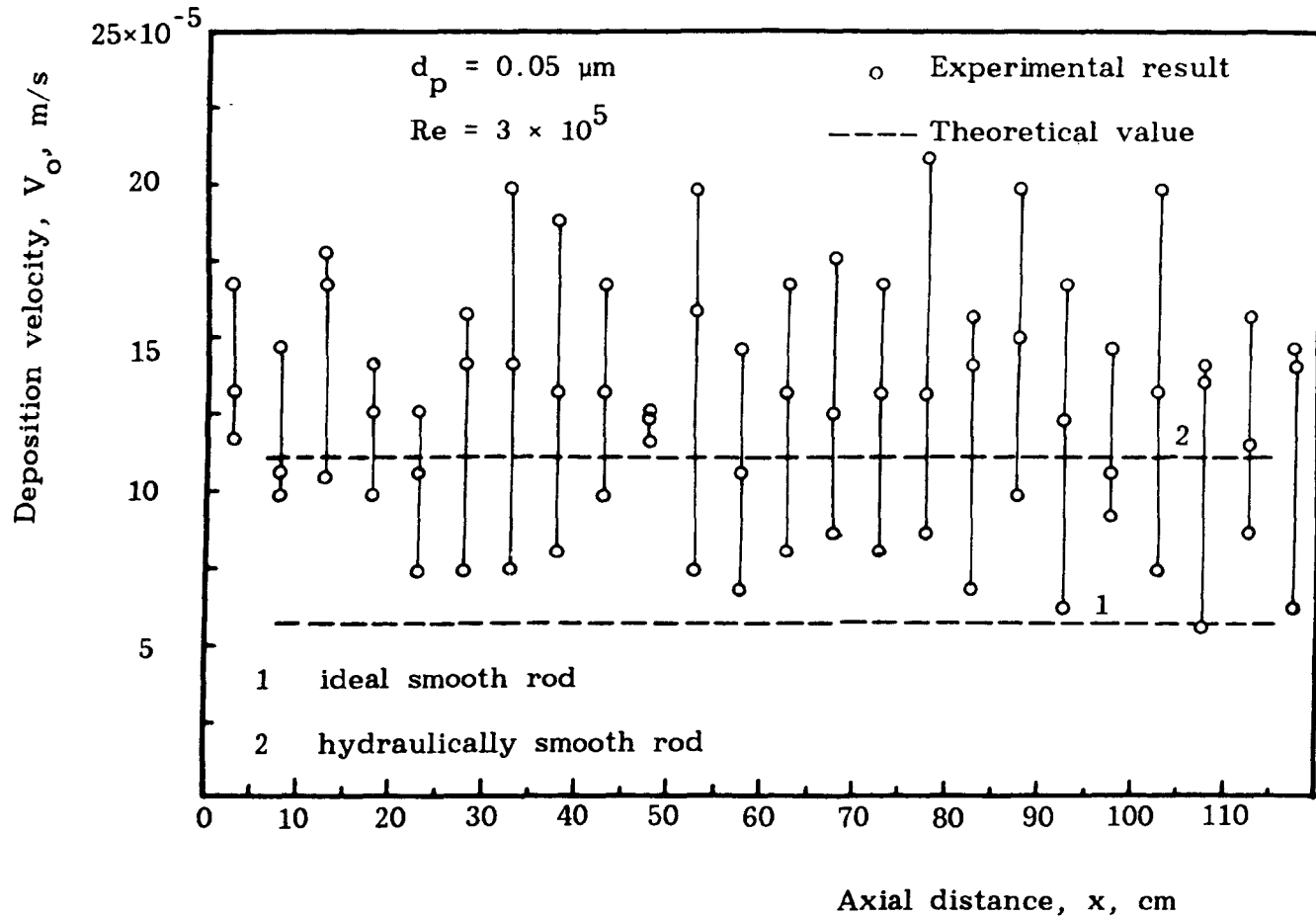
Fig. 5.14 Deposition velocity along cold smooth rod after 1 hour.
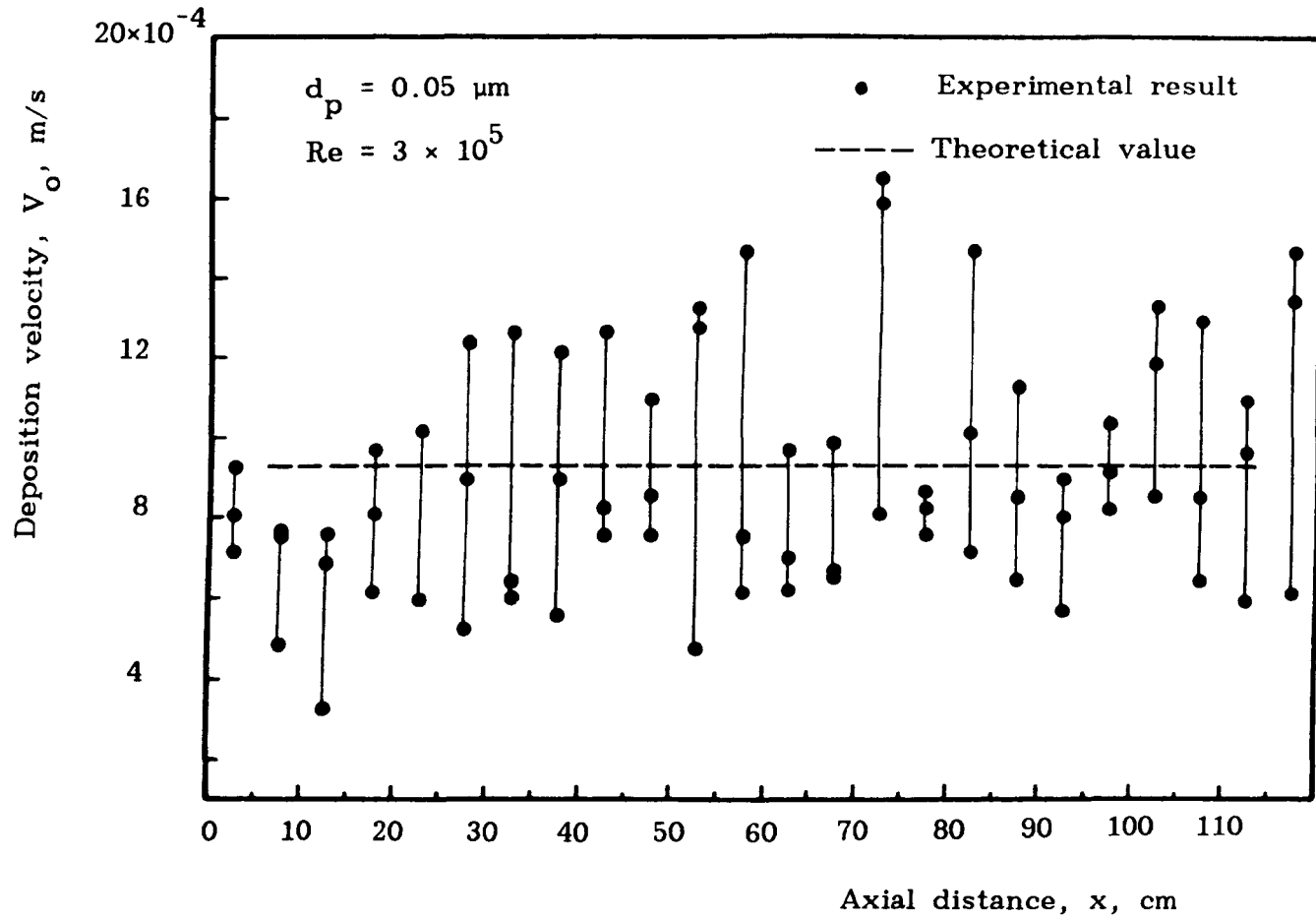
Fig. 5.15 Deposition velocity along cold ribbed rod after 1 hour.
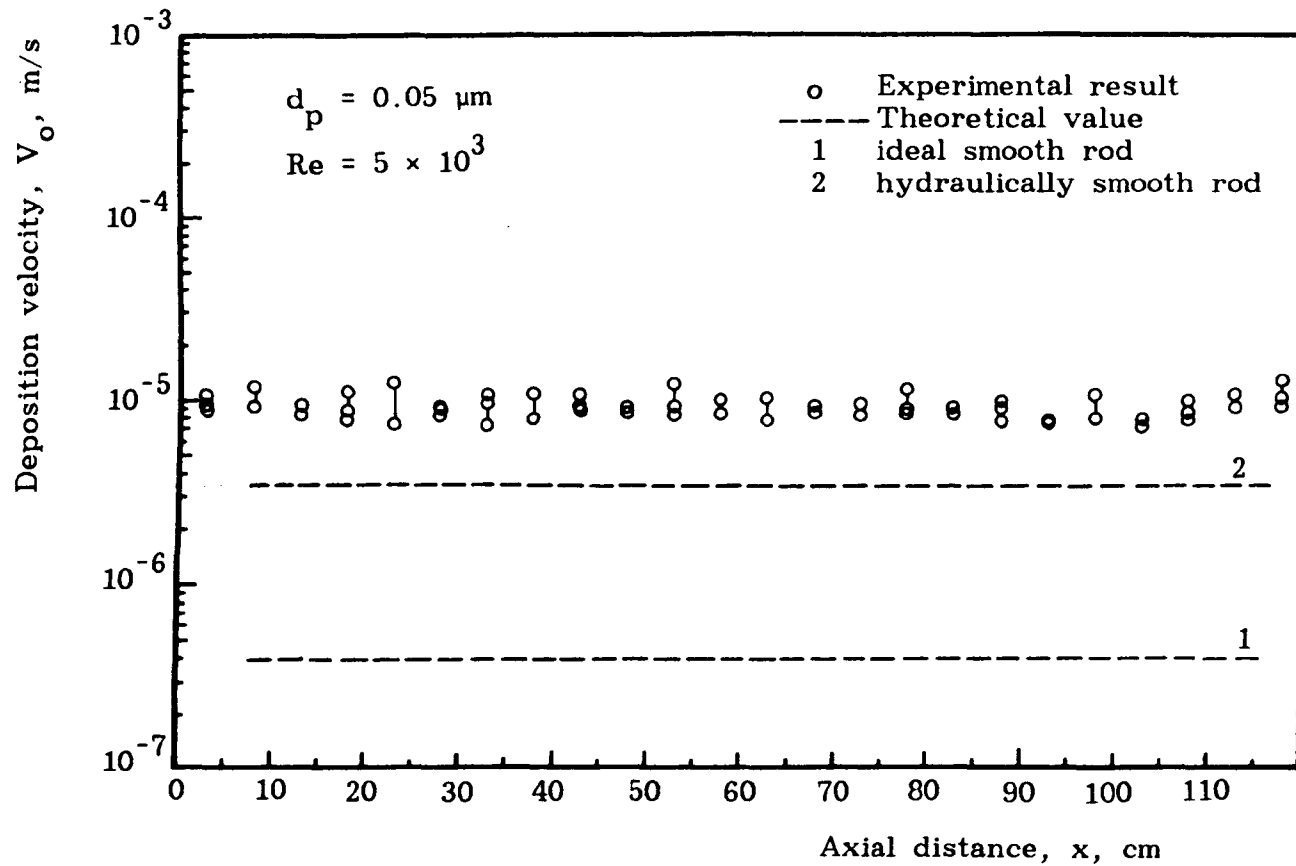
Fig. 5.16 Deposition velocity along cold smooth rod after 1 hour.
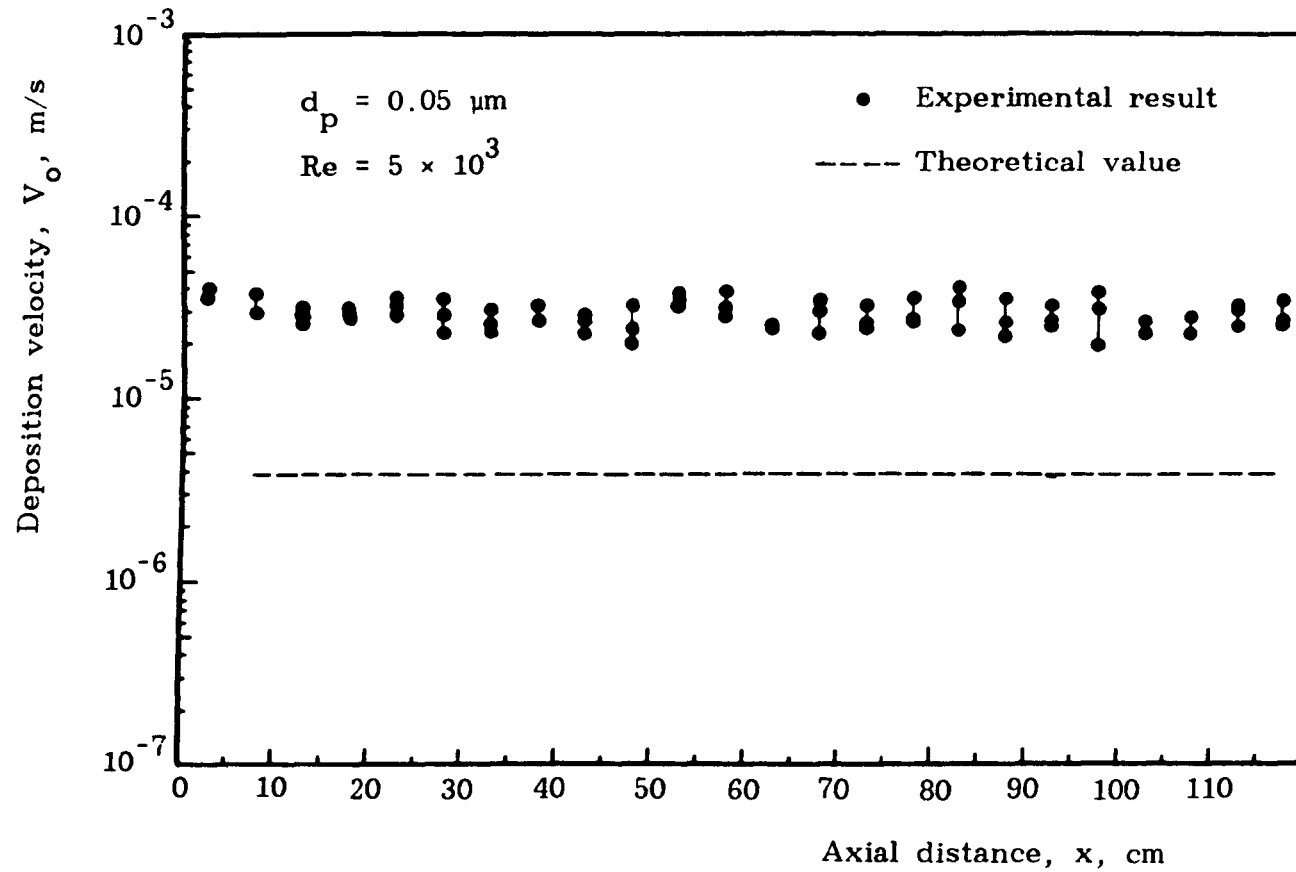
Fig. 5.17 Deposition velocity along cold ribbed rod after 1 hour.
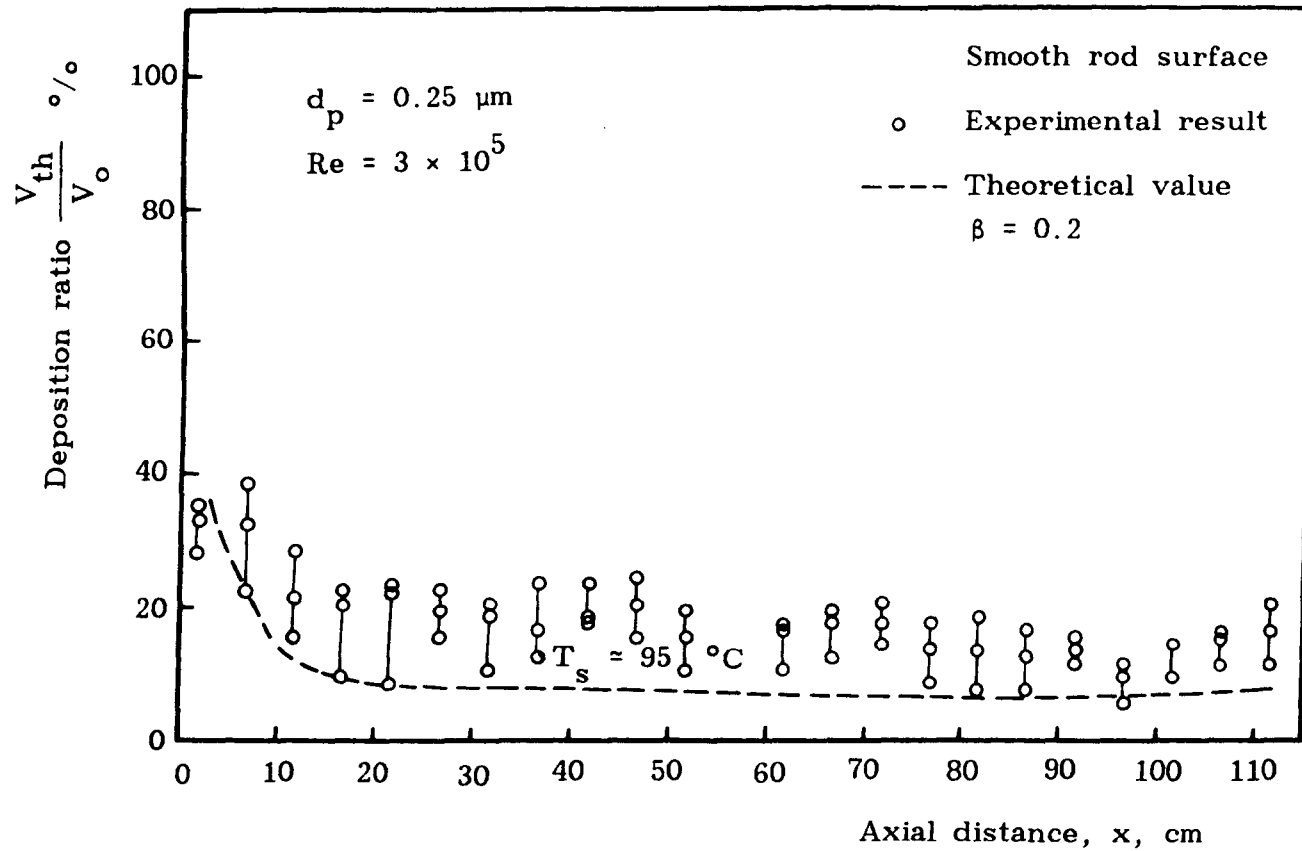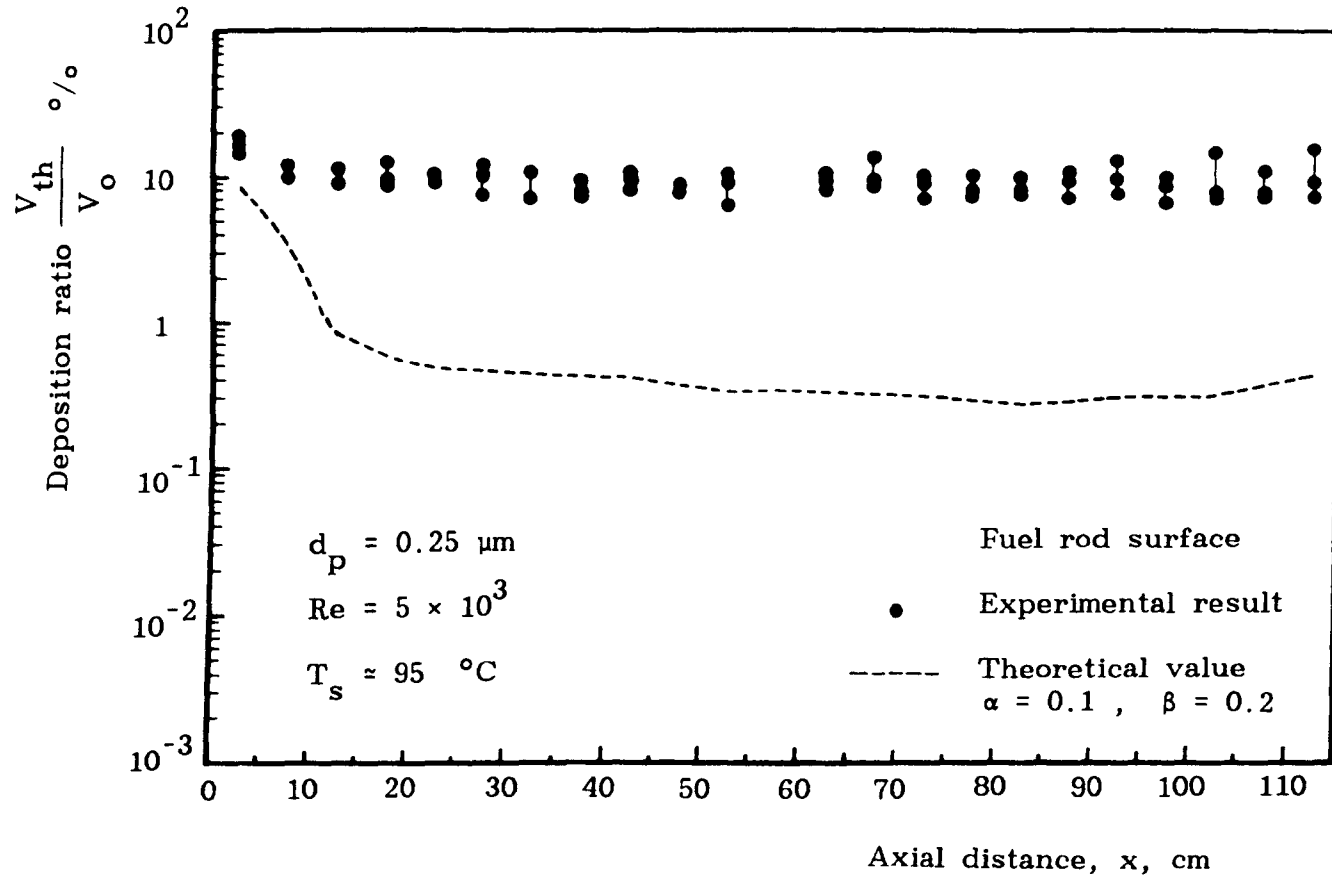
Fig. 5.18 Percentage ratio of the deposition velocity with thermophoresis (V_{th}) to the deposition velocity without thermophoresis (V_o).
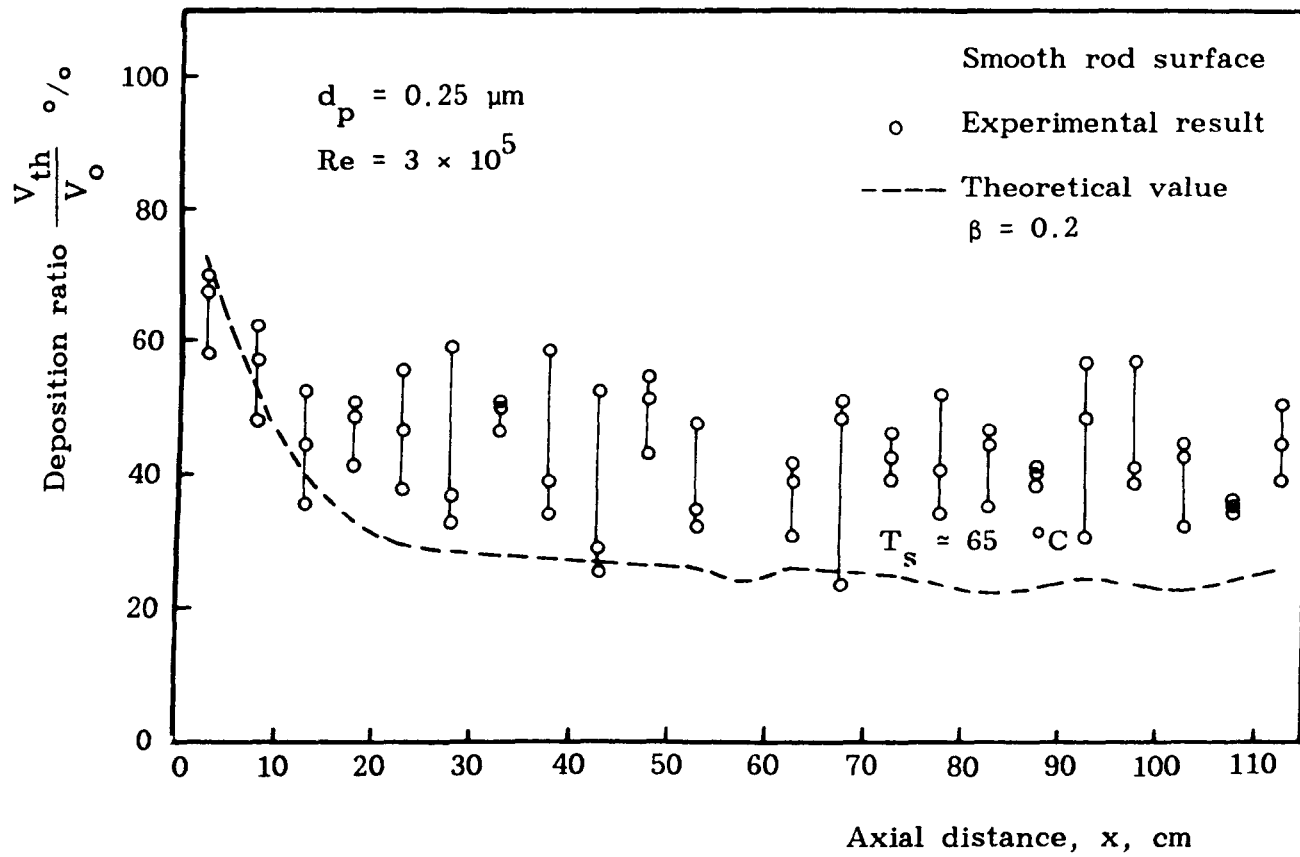
Fig. 5.19 Percentage ratio of the deposition velocity with thermophoresis (V_{th}) to the deposition velocity without thermophoresis (V_o).
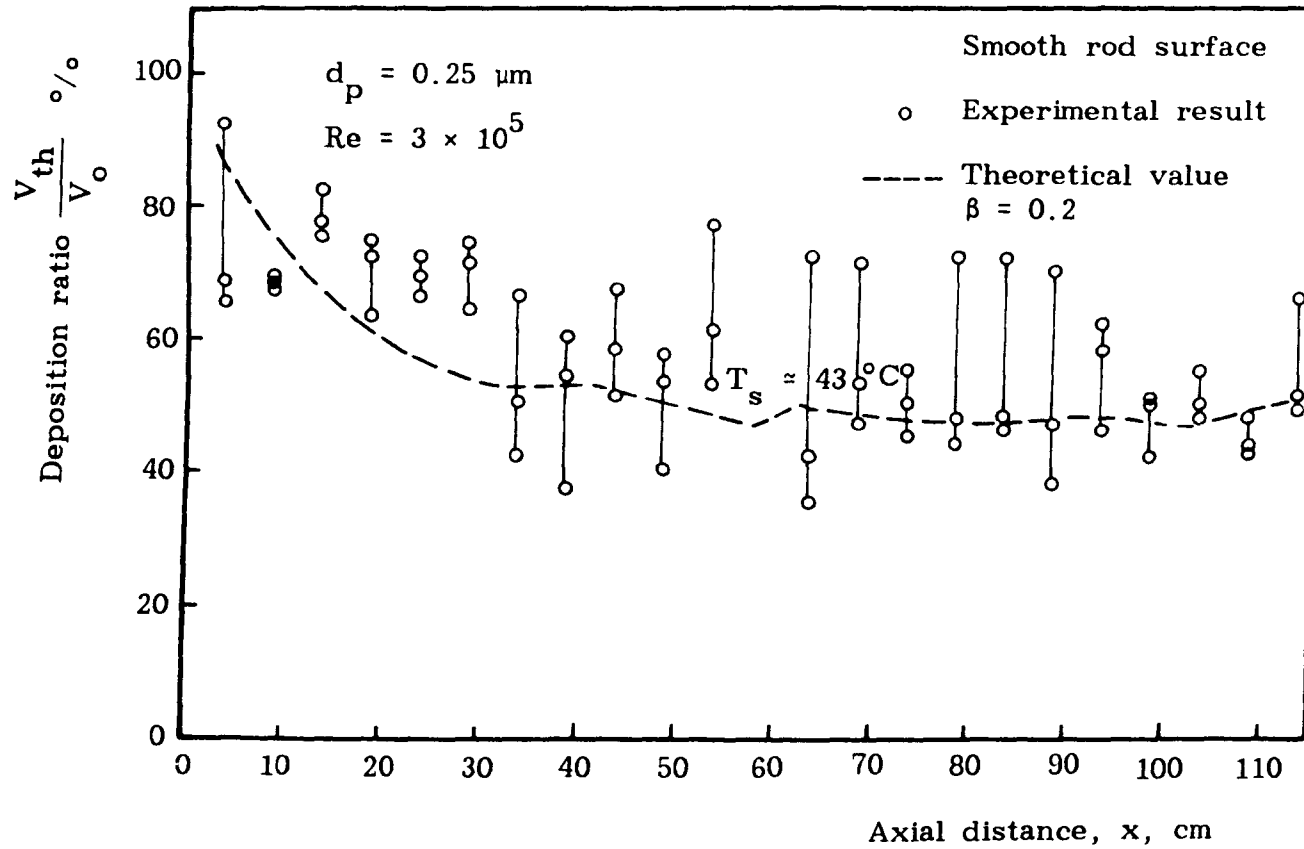
Fig. 5.20 Percentage ratio of the deposition velocity with thermophoresis (V_{th})
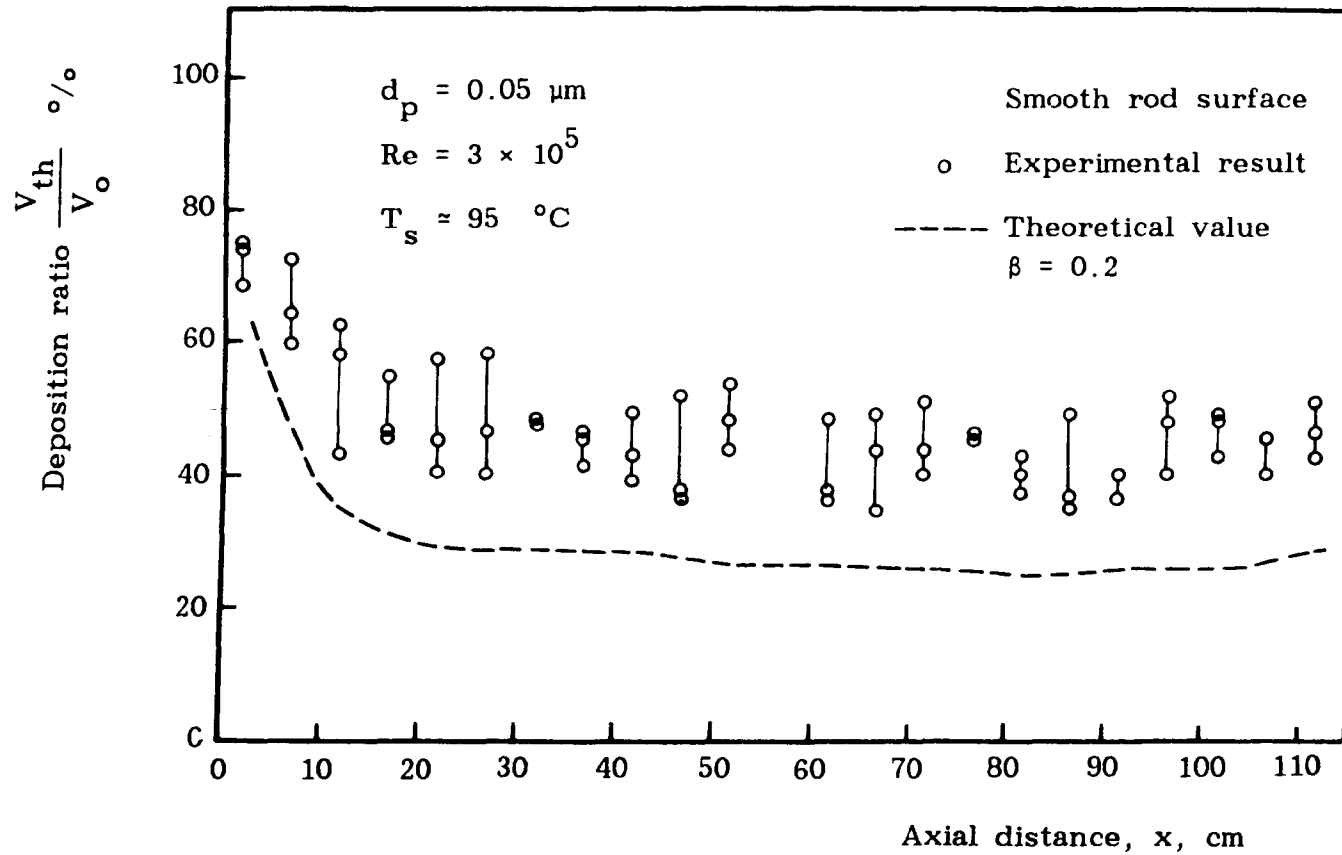
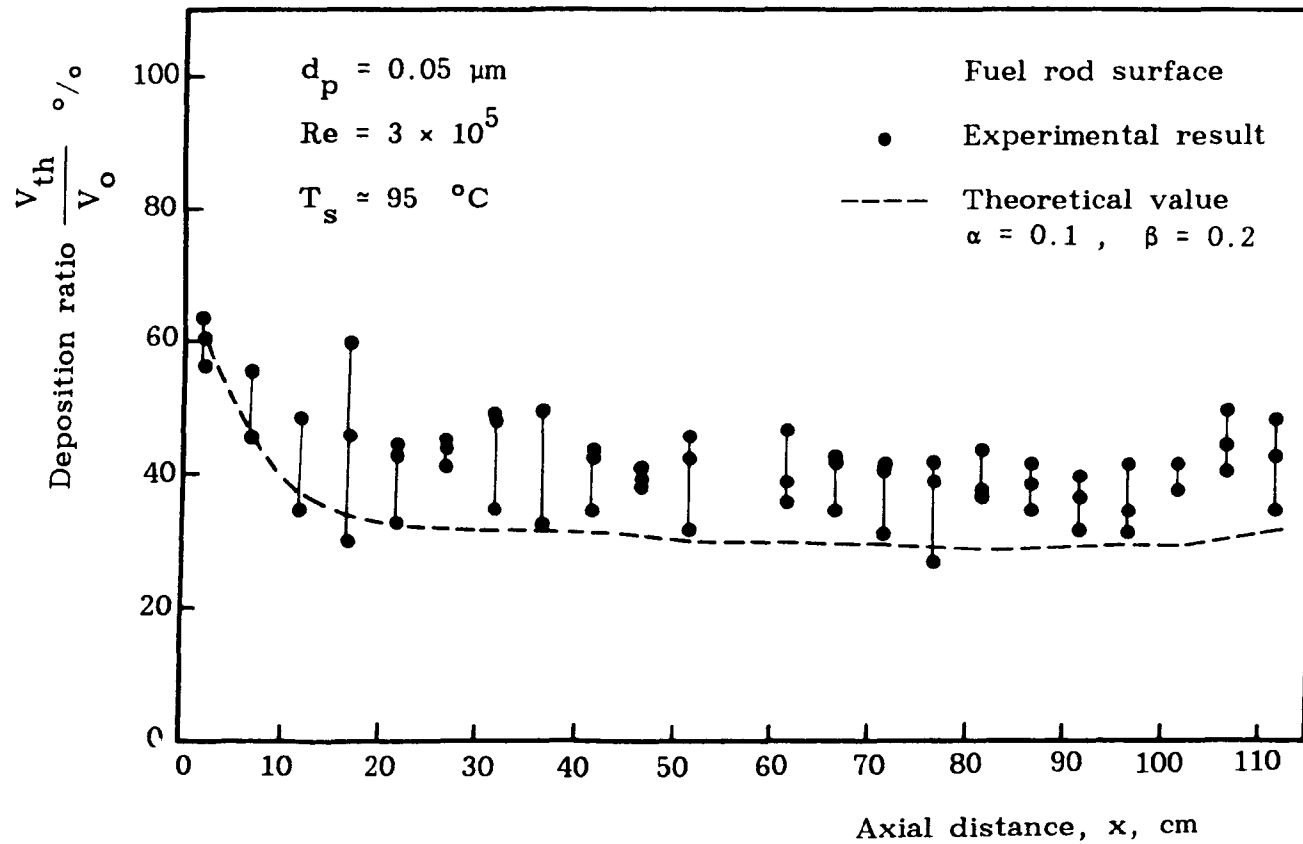to the deposition velocity without thermophoresis (V_o).
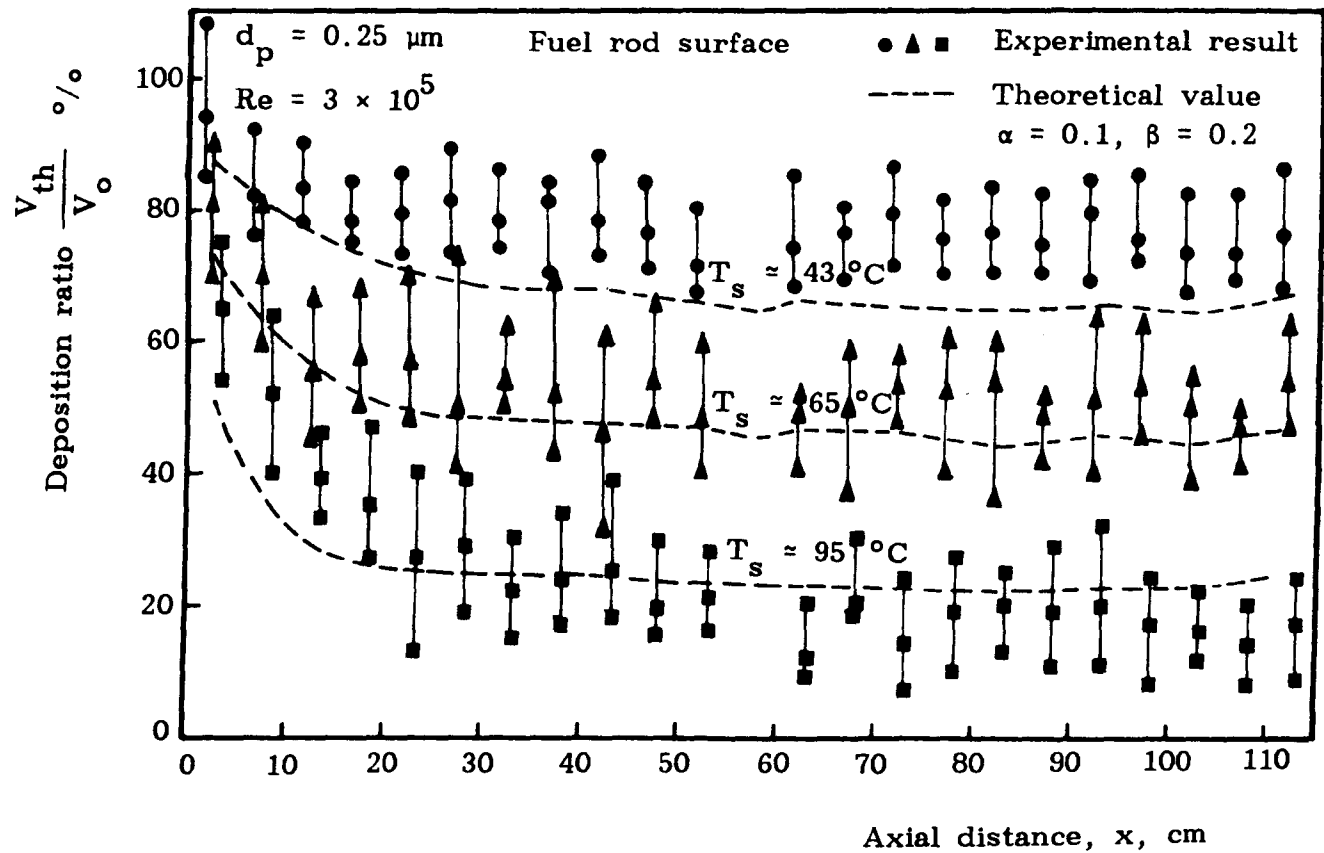
Fig. 5.21 Percentage ratio of the deposition velocity with thermophoresis (V_{th}) to the deposition velocity without thermophoresis (V_{o}).
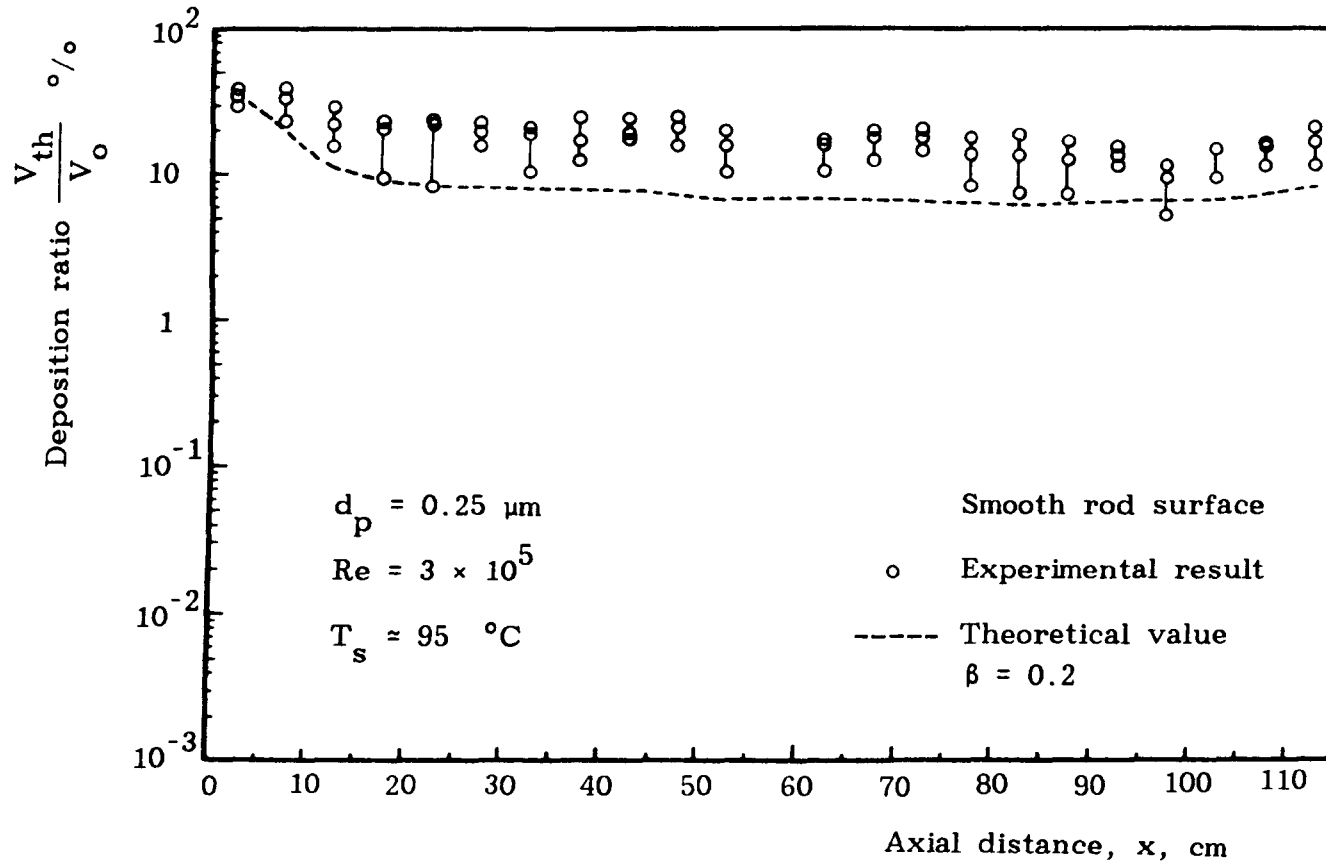
Fig. 5.22 Percentage ratio of the deposition velocity with thermophoresis (V_{th}) to the deposition velocity without thermophoresis (V_o).
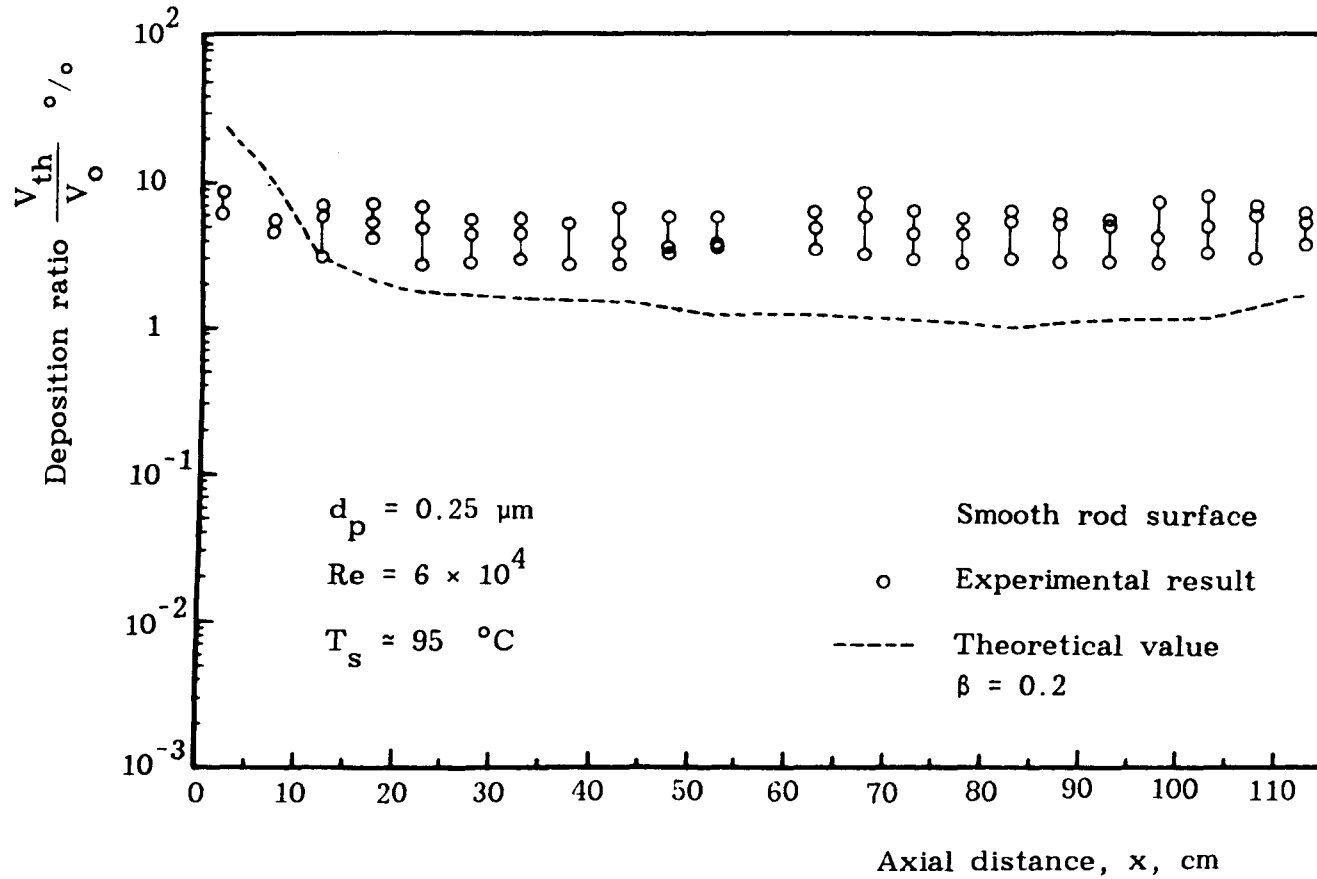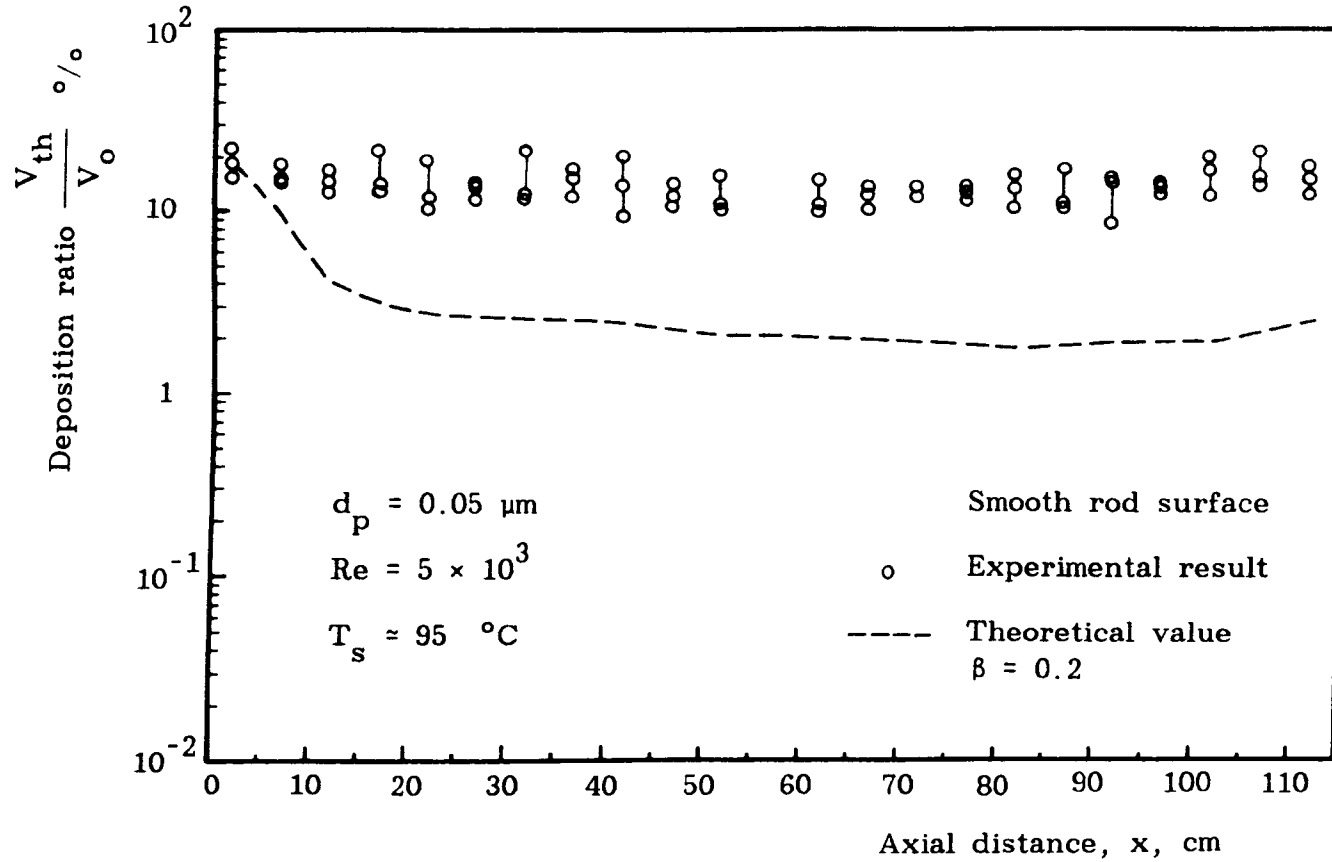
Fig. 5.23 Percentage ratio of the deposition velocity with thermophoresis (V_{th}) to the deposition velocity without thermophoresis (V_o).
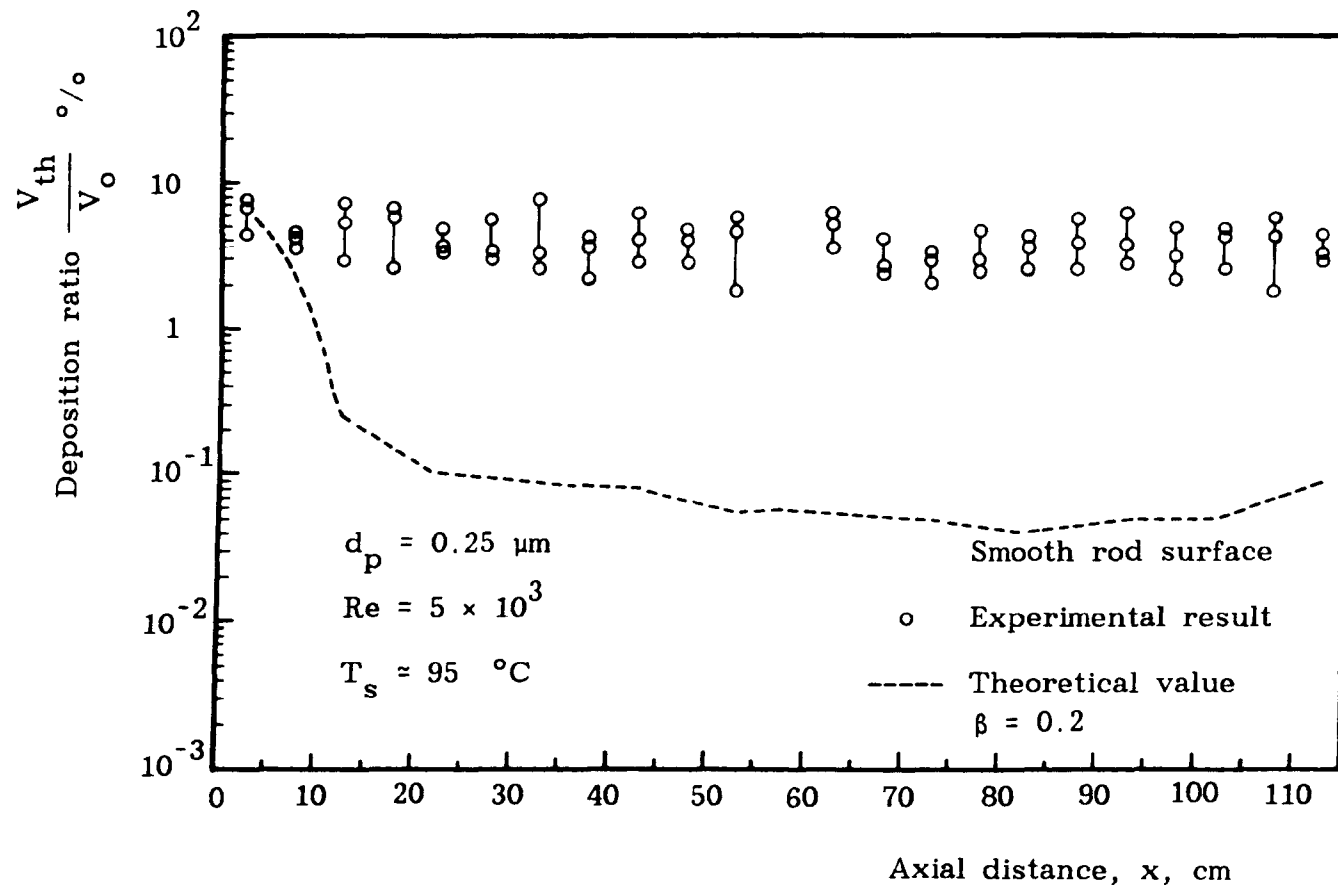
Fig. 5.24 Percentage ratio of the deposition velocity with thermophoresis (V_{th})

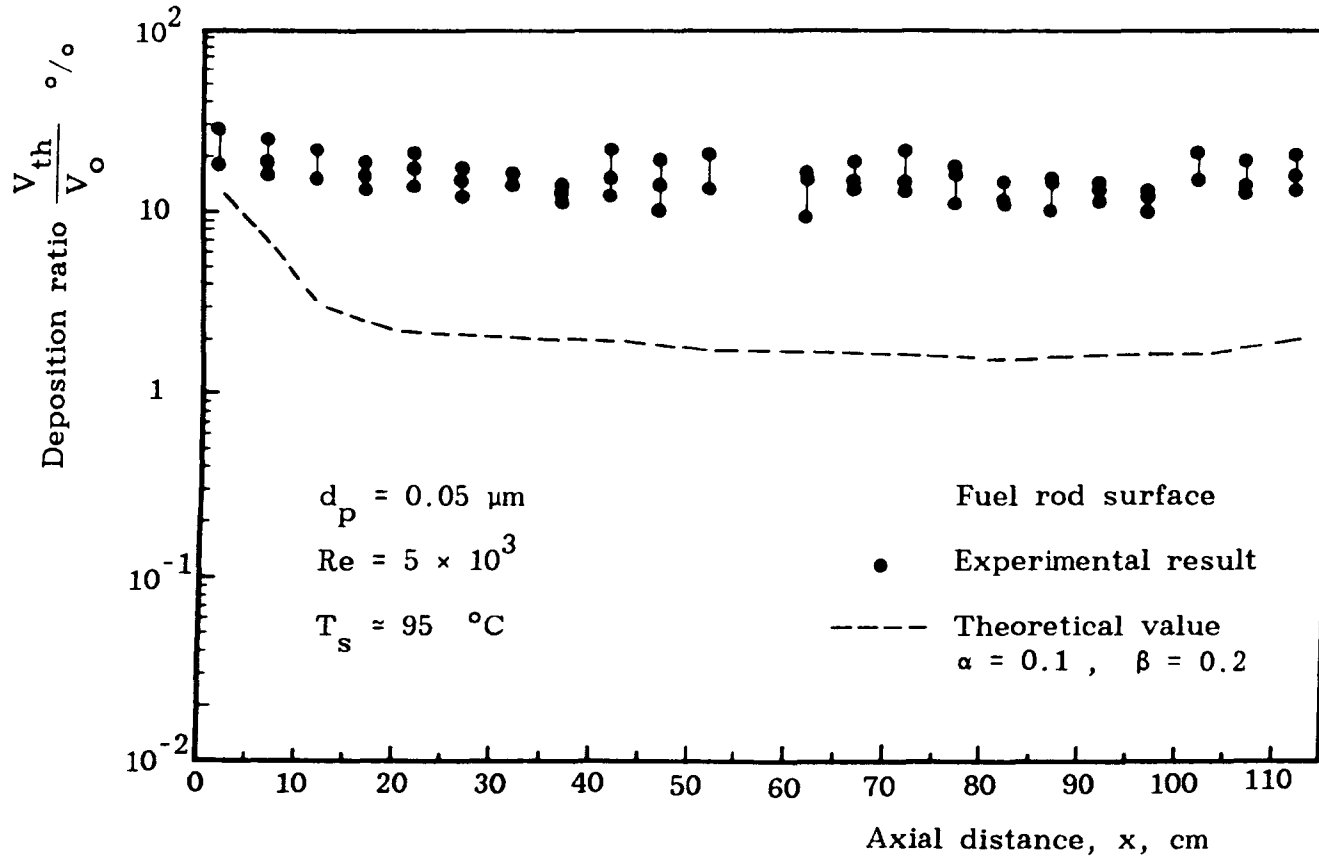to the deposition velocity without thermophoresis (V_o).
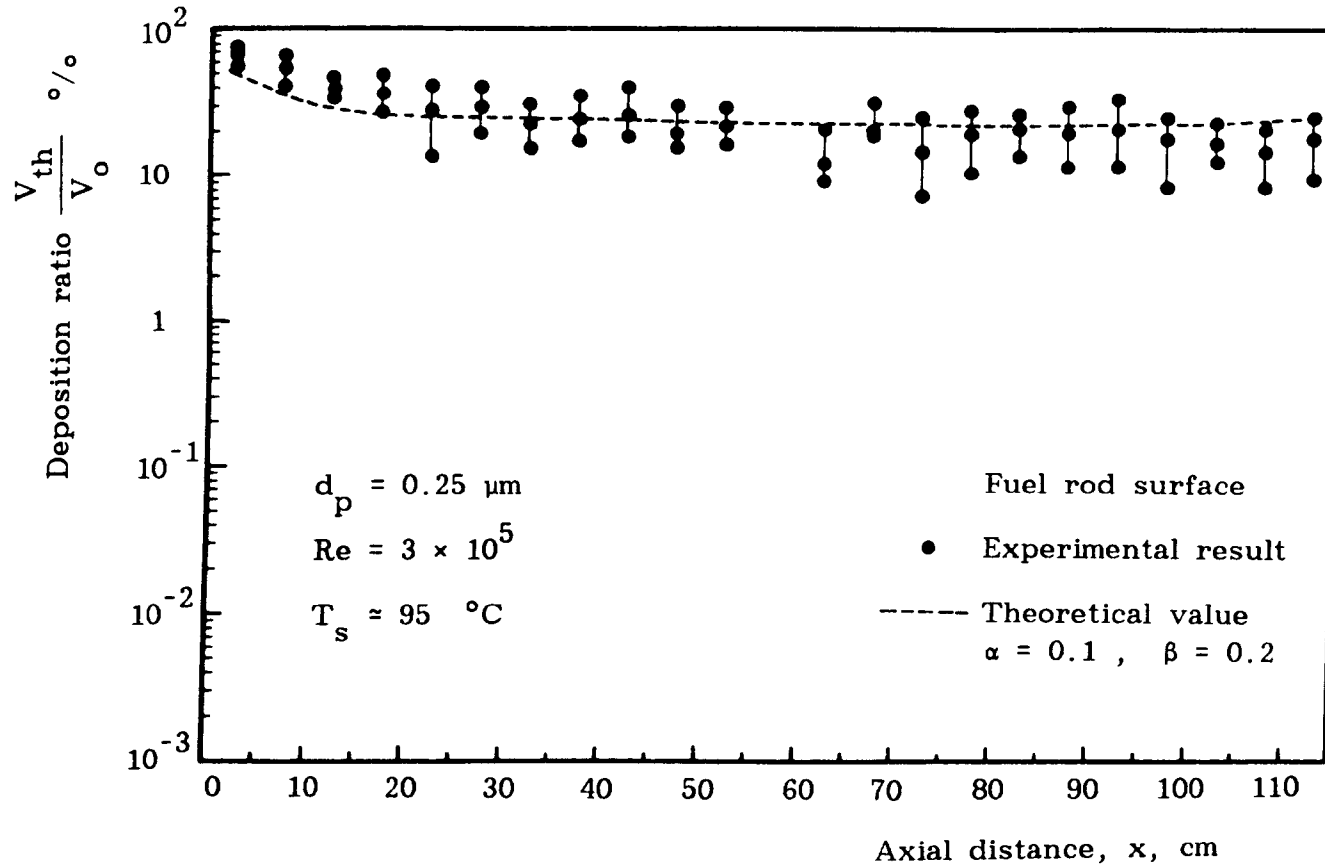
Fig. 5.25 Percentage ratio of the deposition velocity with thermophoresis (V_{th}) to the deposition velocity without thermophoresis (V_o).
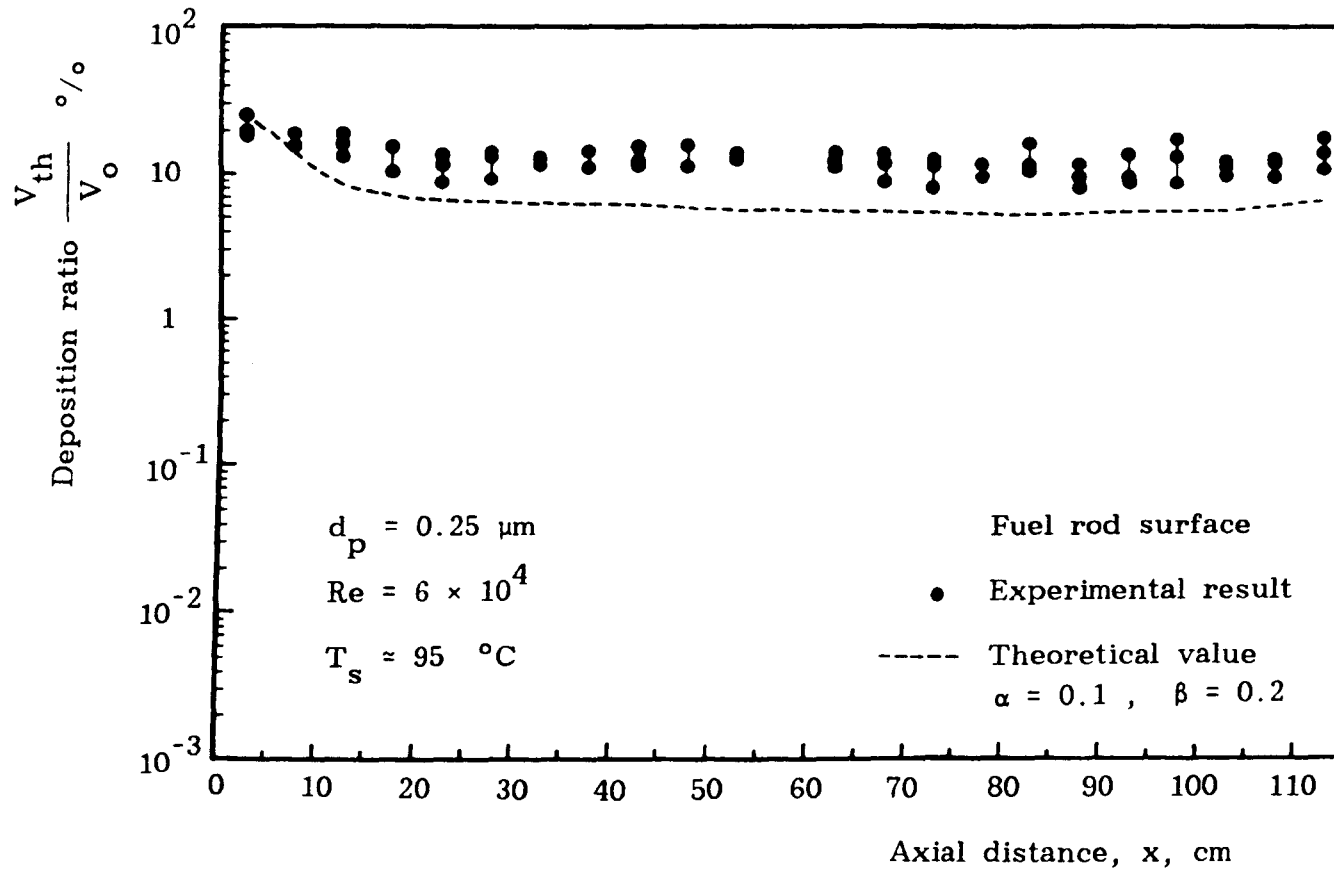
Fig. 5.26 Percentage ratio of the deposition velocity with thermophoresis (V_{th}) to the deposition velocity without thermophoresis (V_o).

Fig. 5.27 Percentage ratio of the deposition velocity with thermophoresis (V_{th})

to the deposition velocity without thermophoresis (V_o).

Fig. 5.28 Percentage ratio of the deposition velocity with thermophoresis (V_{th}) to the deposition velocity without thermophoresis (V_o).

Fig. 5.29 Percentage ratio of the deposition velocity with thermophoresis (V_{th})

to the deposition velocity without thermophoresis (V_o).

Fig. 5.30 Percentage ratio of the deposition velocity with thermophoresis (V_{th}) to the deposition velocity without thermophoresis (V_o).

Fig. 5.31 Percentage ratio of the deposition velocity with thermophoresis (V_{th})

to the deposition velocity without thermophoresis (V_o).
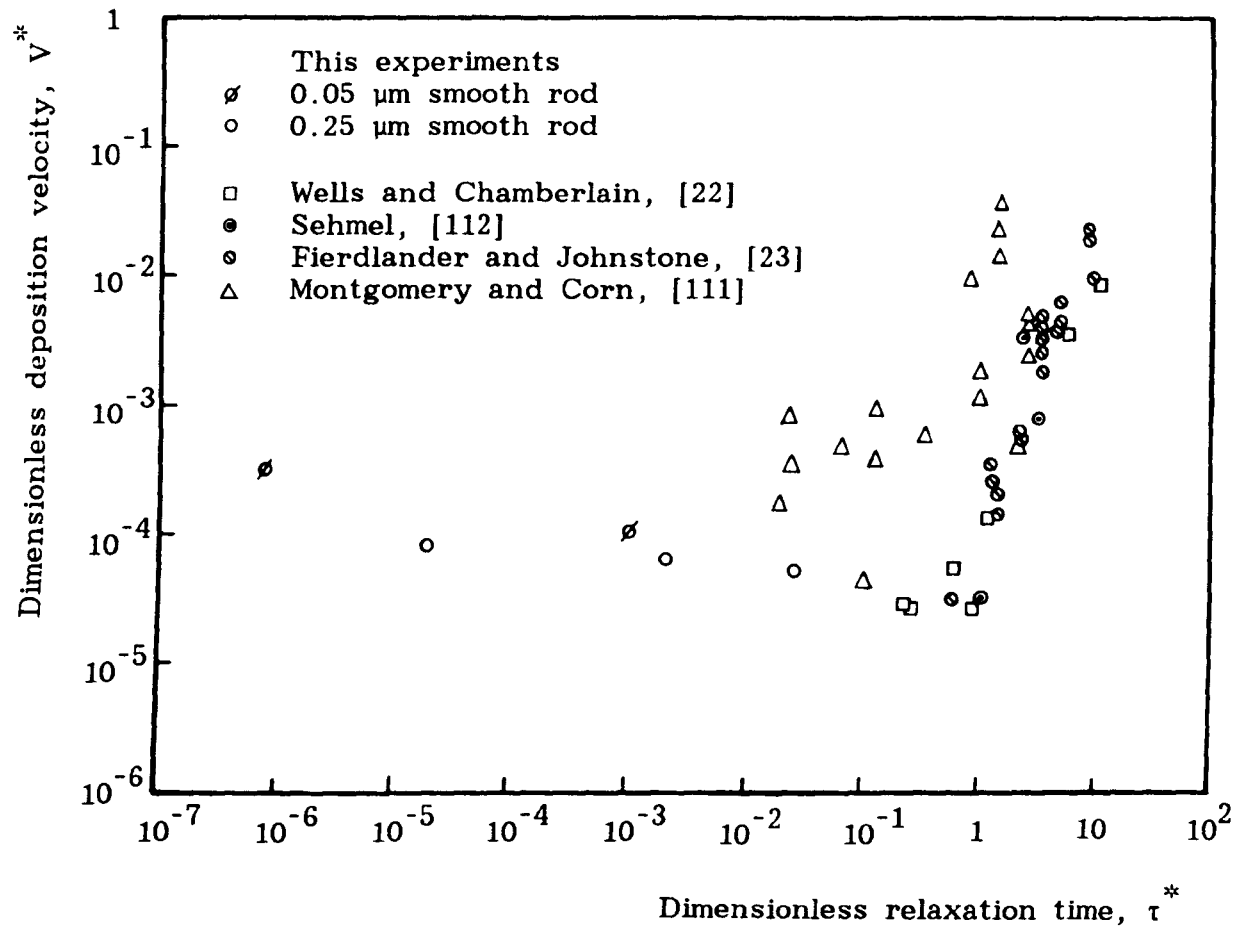
Fig. 5.32 Comparison of data of this work with those of other investigators.
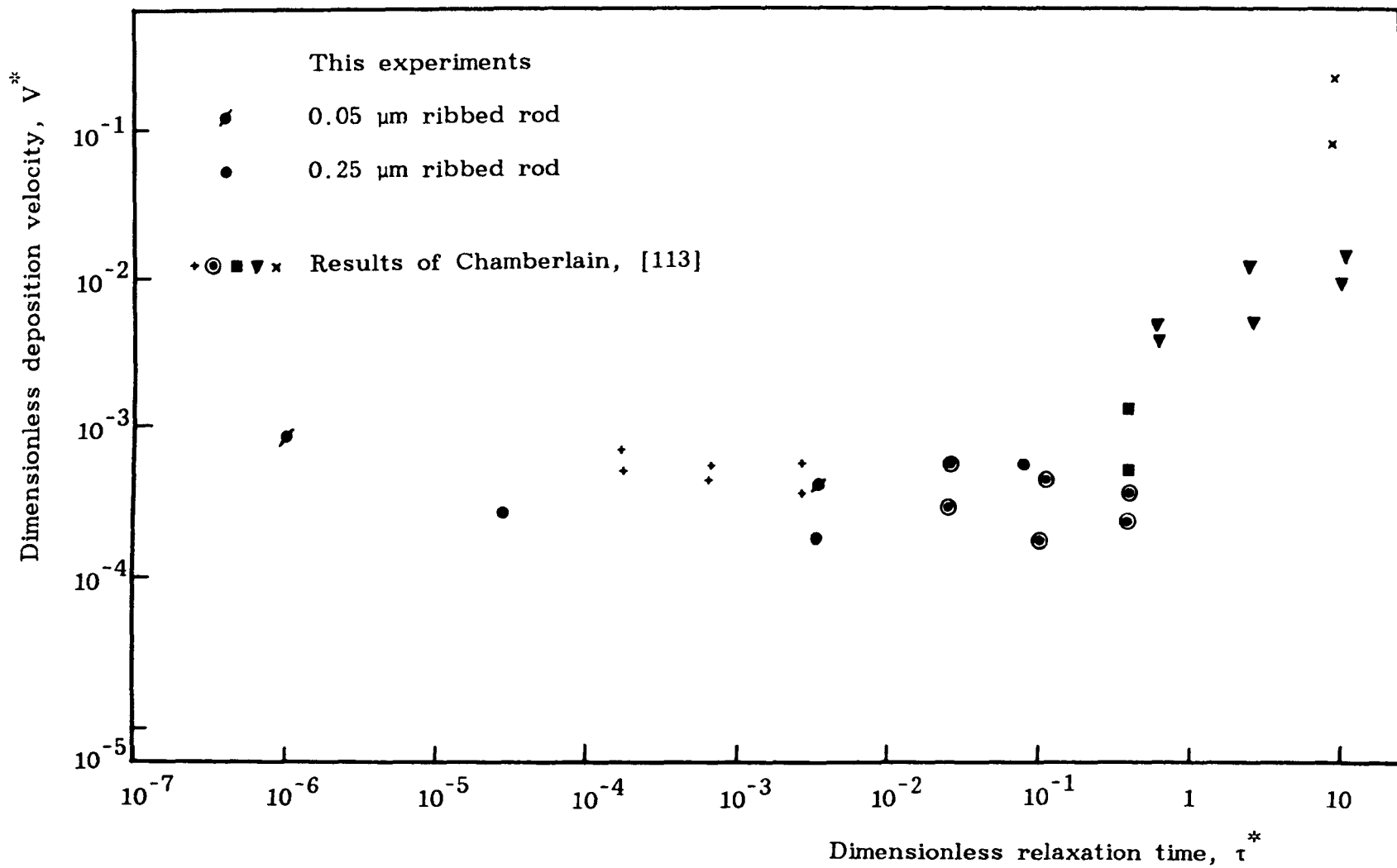
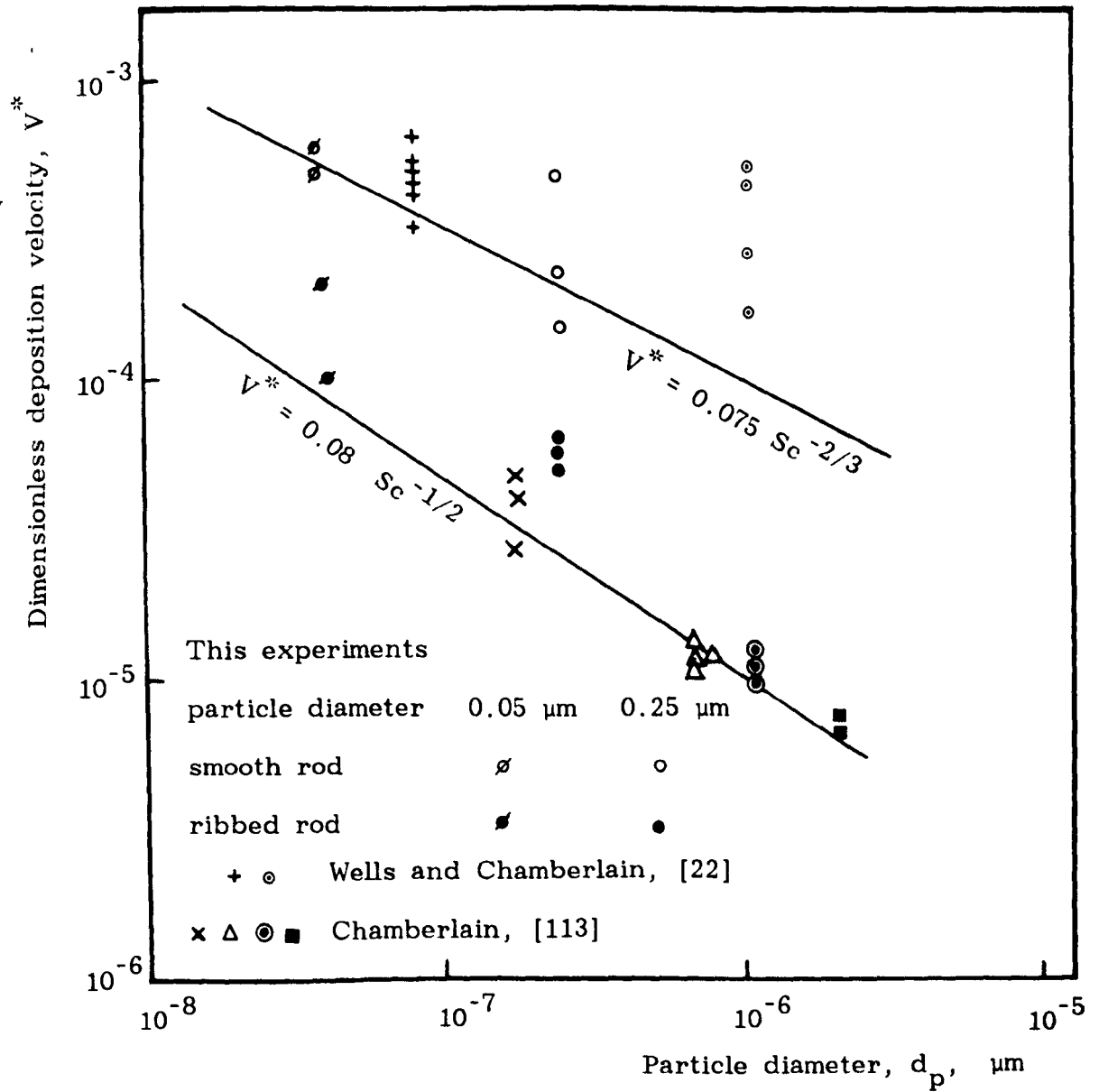Fig. 5.33 Comparison of the ribbed rod results with the data of Chamberlain.

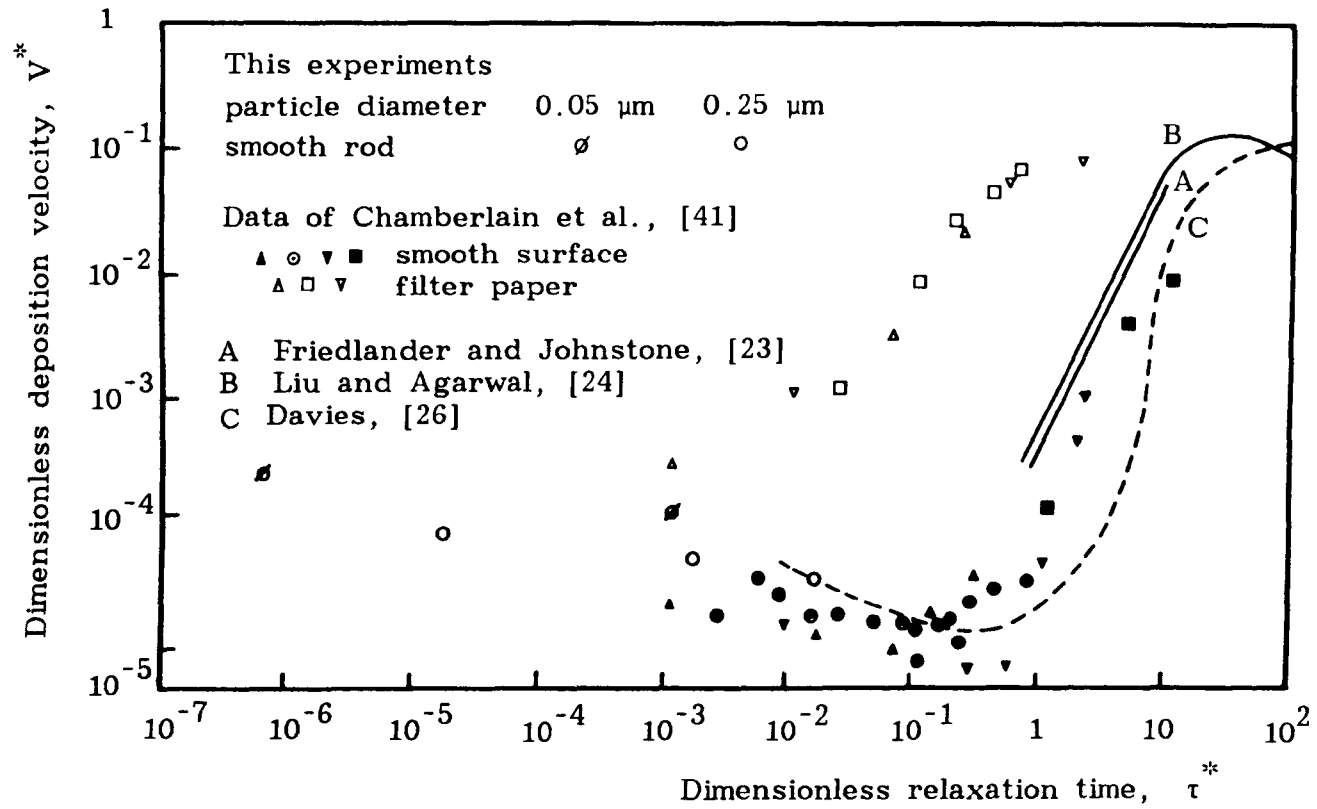Fig. 5.34 Comparison of the results of the smooth and the ribbed rods with that of other investigators.

Fig. 5.35 Comparison of the results of the smooth rod with the data of Chamberlain et al.
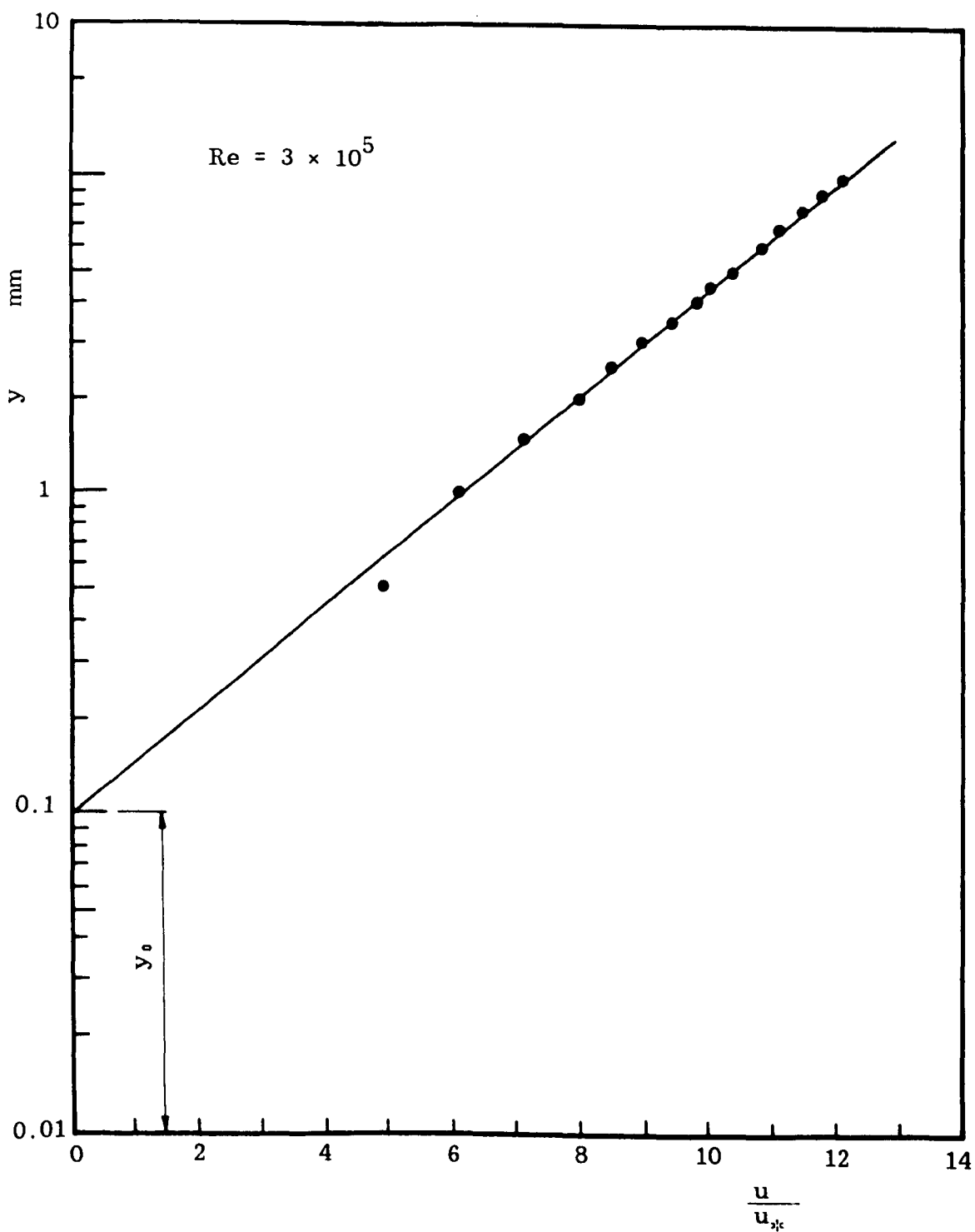
Fig. 5.36 Comparison of the results of the ribbed rod with the data of Chamberlain et al.

Fig. 5.37 Velocity profile over the ribbed rod surface.

Fig. 5.38 Particle deposition velocity versus particle
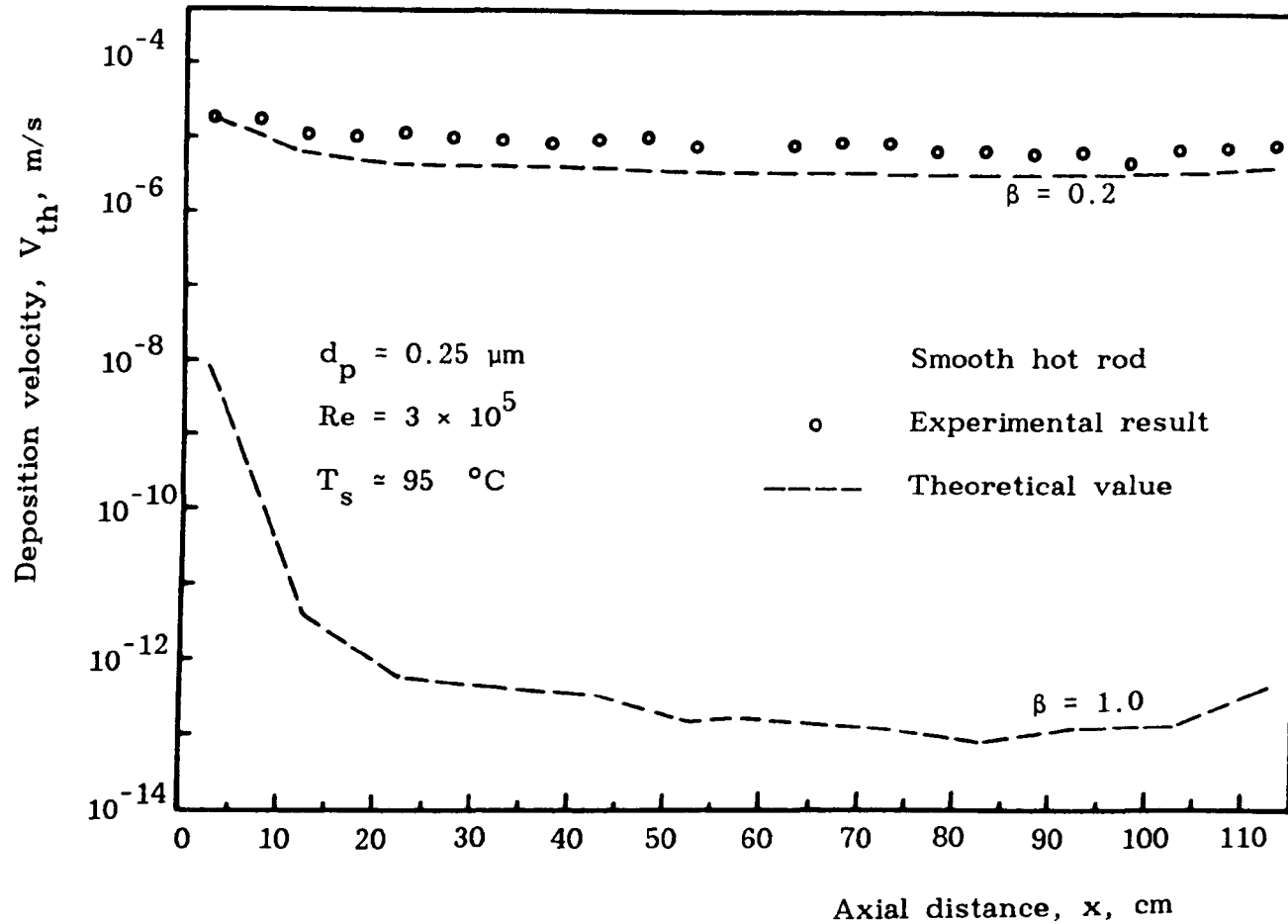
diameter for a rough surface.

Fig. 6.1 Deposition velocity along smooth surface showing the effect of

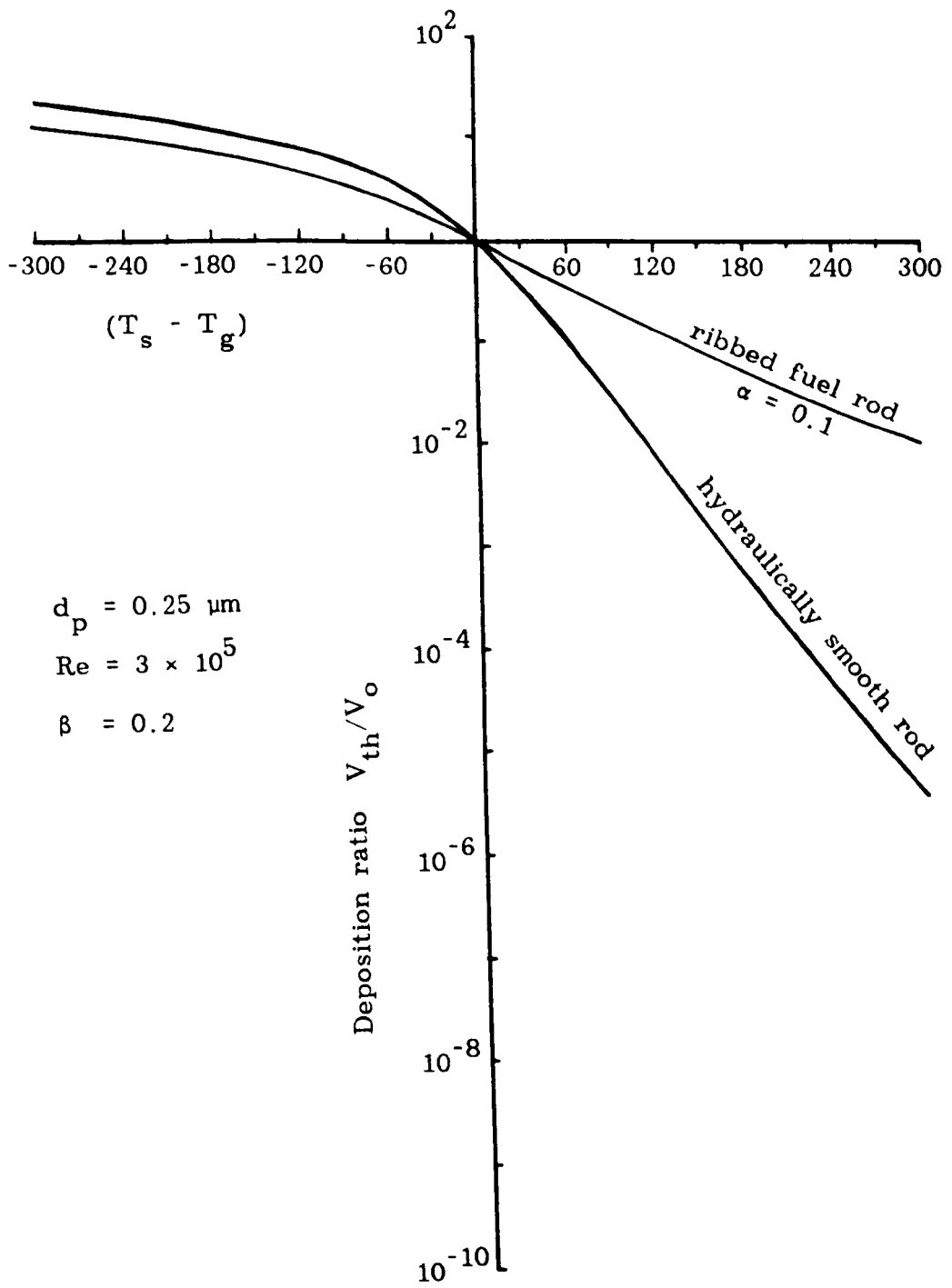thermophoresis and the scaling factor of the temperature gradient.

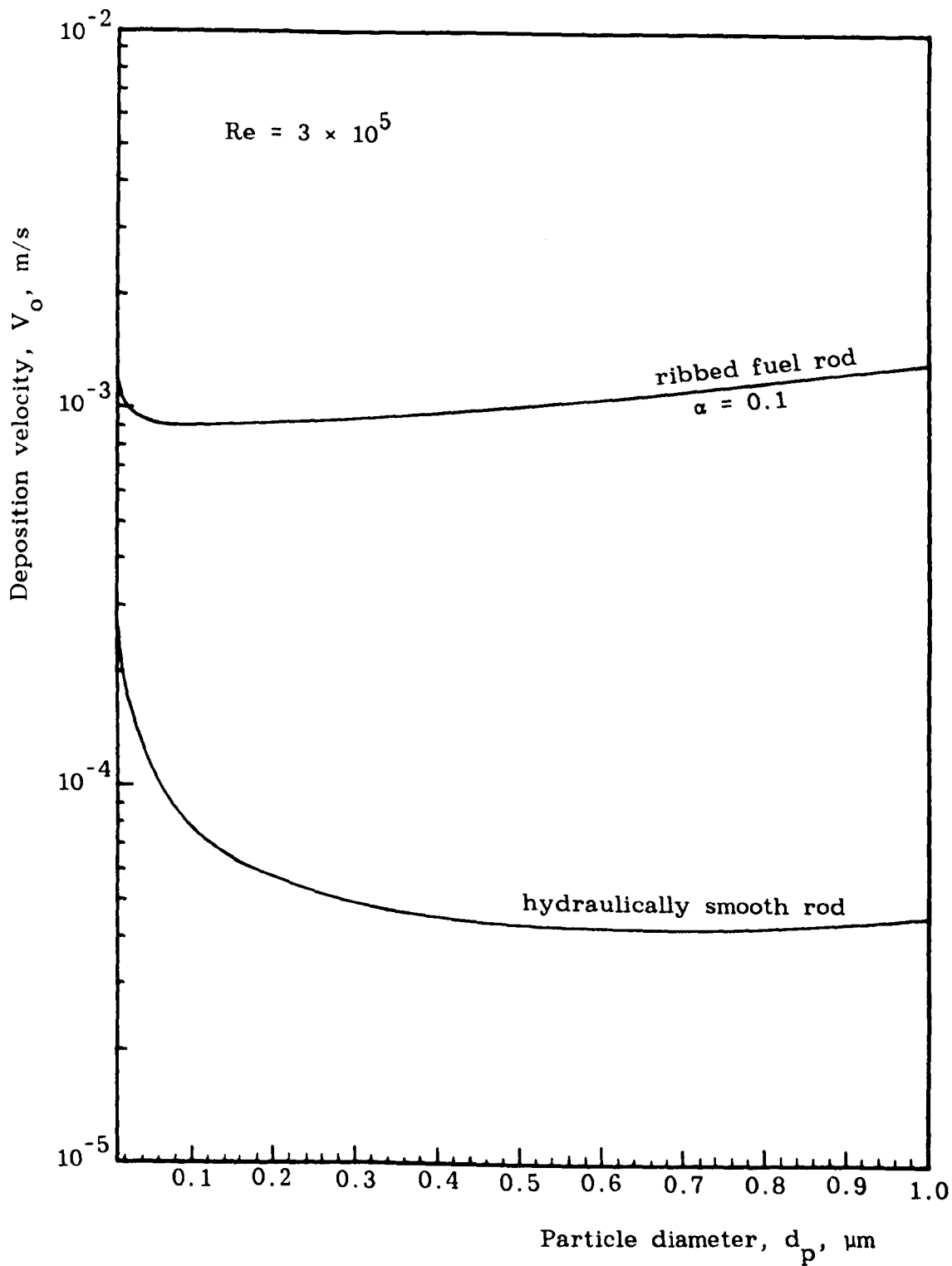Fig. 6.3 Effect of thermophoresis on particle deposition.

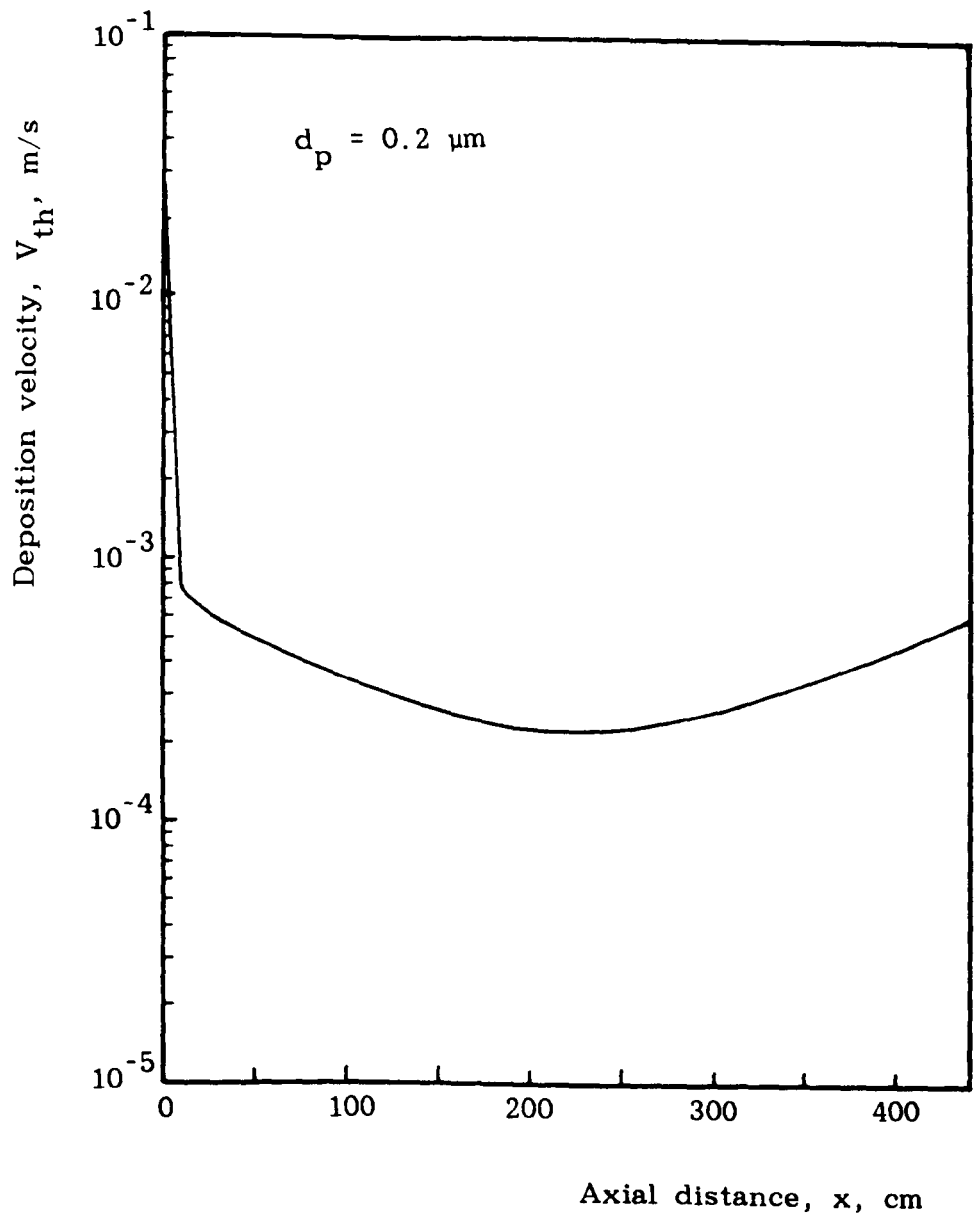Fig. 6.2 Deposition velocity as a function of particle diameter.

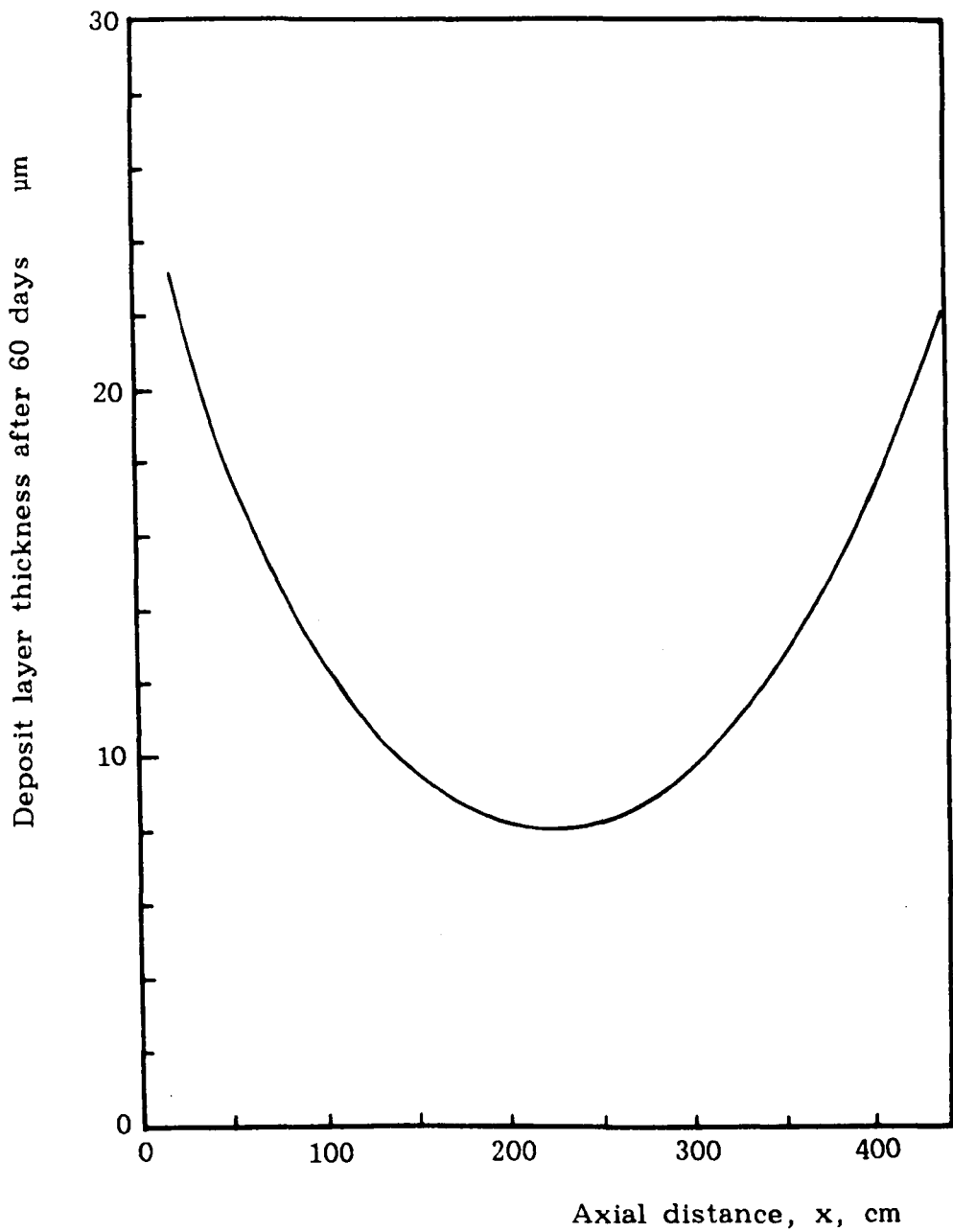Fig. 6.4 Deposition velocity along the axial distance of the reactor channel.

Fig. 6.5 Variation of deposit layer thickness in WAGR.
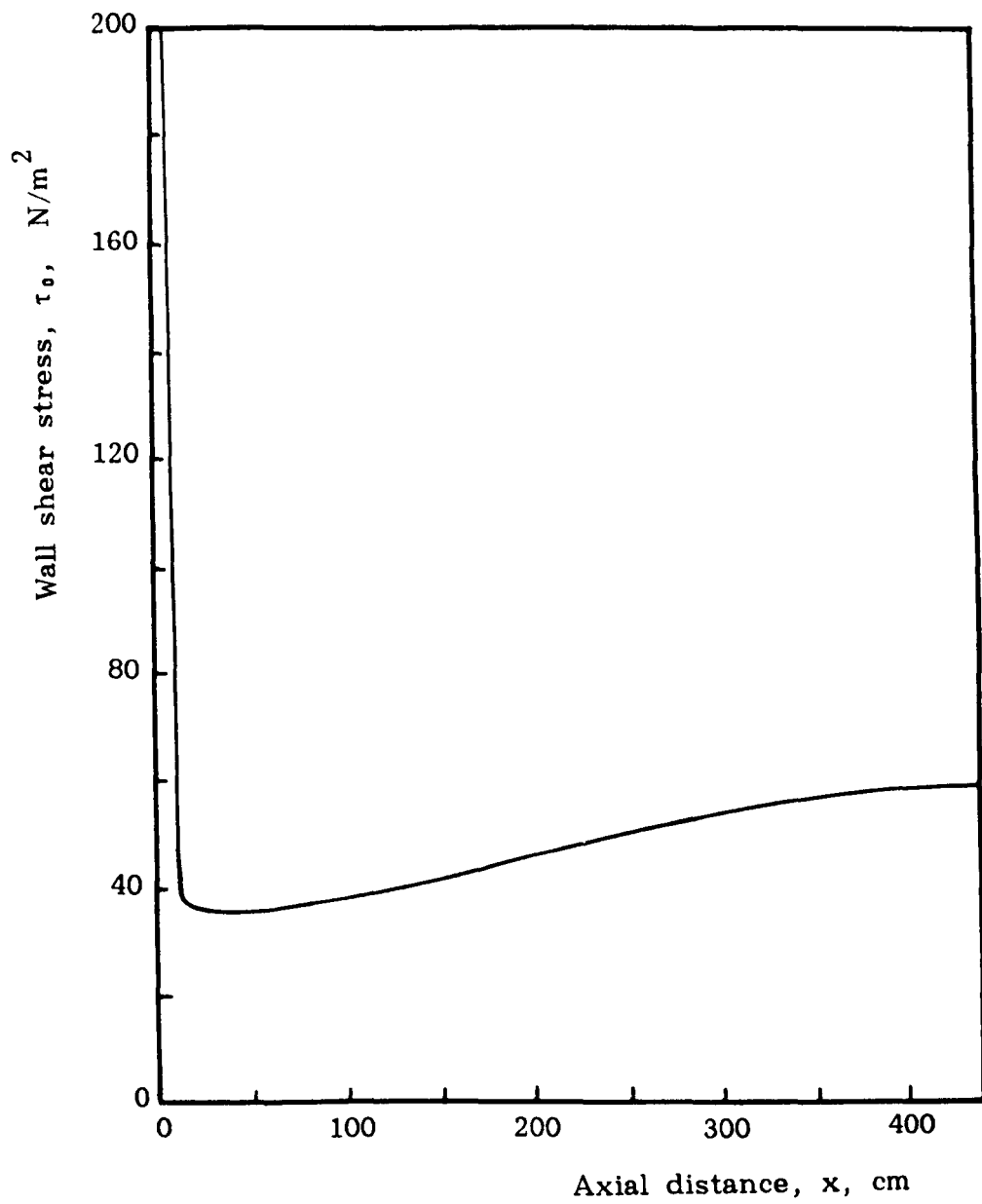
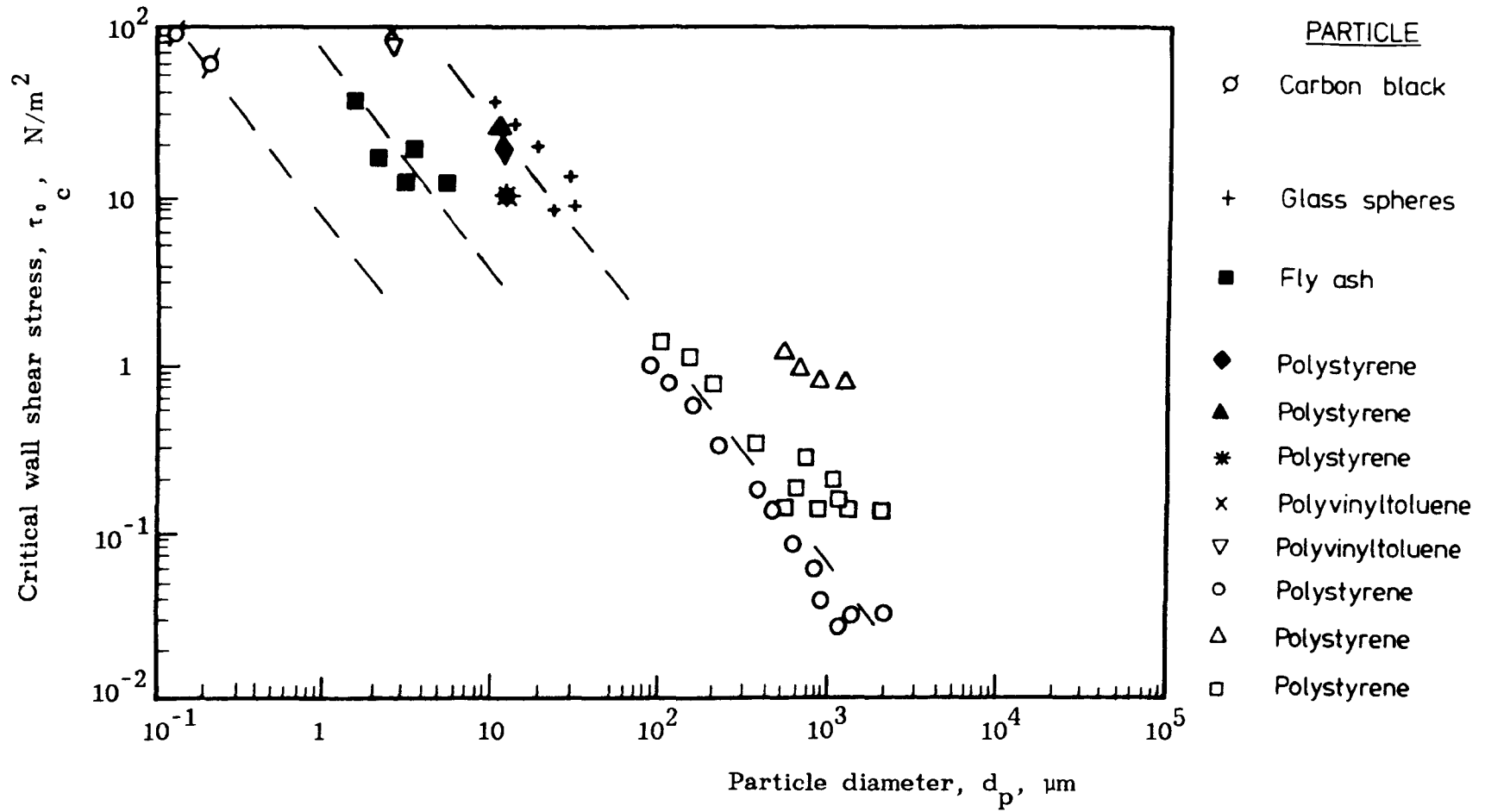Fig. 6.6 Wall shear stress distribution along the fule pins.

Fig. 6.7 Critical wall shear stress at which particles of a given

diameter are removed. (After Cleaver, [119])
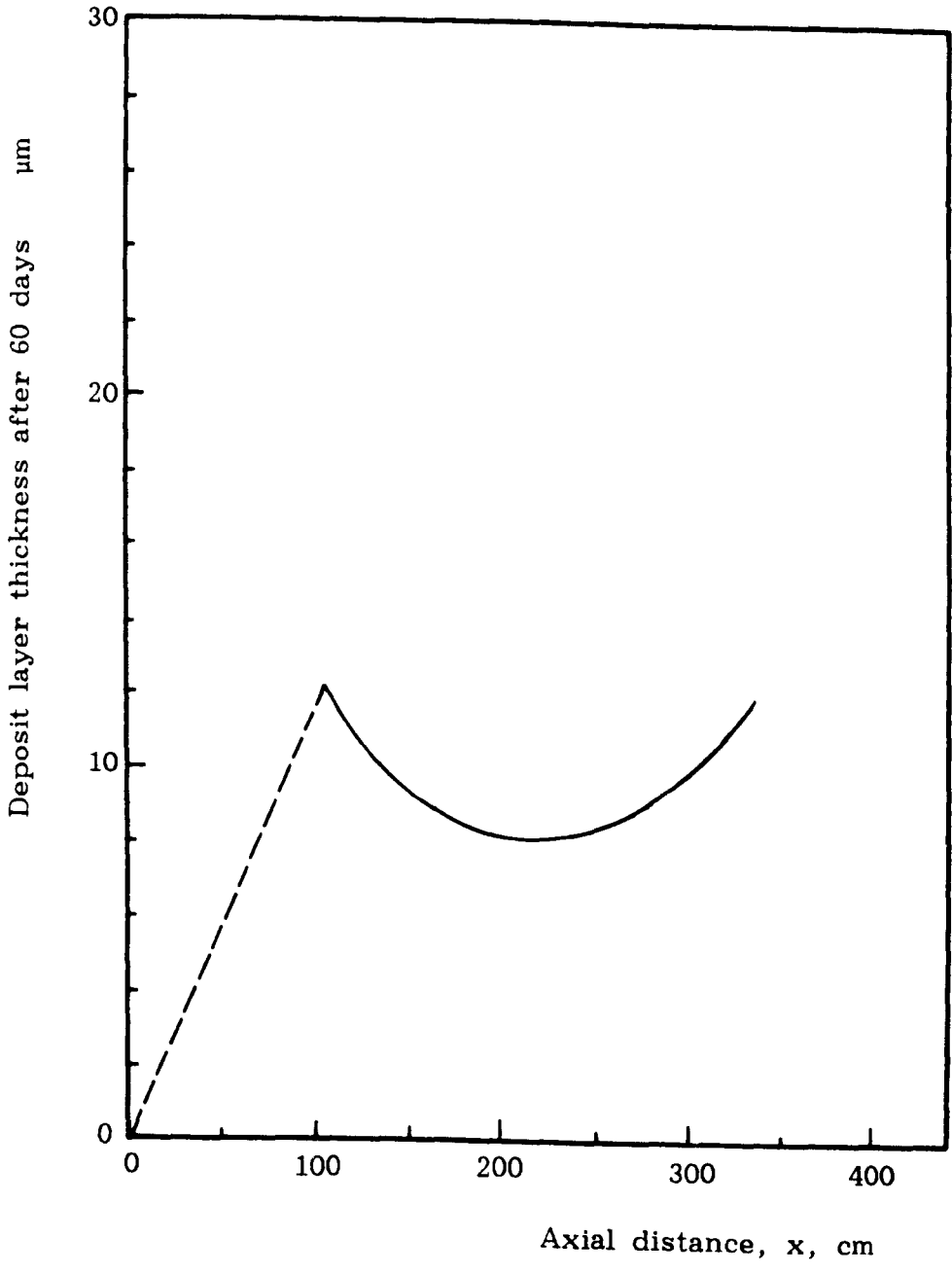
Fig. 6.8 The deposition layer along the ful pins.

APPENDIX A

CALCULATION OF PARTICLE CHARACTERISTICS

A.1 5 $^{\circ}/_{\circ}$ uranin solution

According to the statistical analysis described in section 1.5 and using the data of table 1.1, then

$$\log d_g = \frac{\sum n \log d}{\sum n} \qquad (A.1)$$

$$= \frac{-692.719}{890} = -0.778$$

$$d_g = 0.167 \ \mu m \qquad \underline{\text{geometric mean diameter}}$$

$$\log \sigma_g = \sqrt{\frac{\sum n (\log d - \log dg)^2}{\sum n}} \qquad (A.2)$$

$$= \frac{40.784}{890} = 0.214$$

$$\sigma_g = 1.637 \qquad \underline{\text{geometric standard deviation}}$$

The arithmetic mean diameter and the mass median diameter can be calculated from the Hatch-Choate equation as :

$$\log d_m = \log d_g + 1.51 \log^2 \sigma_g$$

$$= -0.778 + 1.51 (0.214)^2 = -0.709$$

$$d_m = 0.195 \ \mu m$$

$$\log d_{mm}^3 = \log d_g^3 + 10.362 \log^2 \sigma_g$$

$$= -2.335 + 10.362 (0.214)^2 = -1.860$$

$$d_{mm}^3 = 0.014$$

$$d_{mm} = 0.24 \ \mu m$$

Fig. 1.3 shows that the mass-median diameter is 0.25 μm.

A.2 $0.2 \ ^o/_o$ uranin solution

The geometric mean diameter and the geometric standard deviation calculated from data of table 1.3 as follows :

$$\log \ d_g = \frac{-154.877}{108} = -1.434$$

$$d_g = 0.037 \ \mu m$$

and

$$\log \ \sigma_g = \frac{3.018}{108} = 0.167$$

$$\sigma_g = 1.469$$

The arithmetic mean diameter and the mass median diameter can be calculated from the Hatch-Choate equation as :

$$\log \ d_m = -1.434 + 1.51 \ (0.167)^2 = -1.392$$
$$d_m = 0.041 \ \mu m$$

$$\log \ d_{mm}^3 = -4.302 + 10.362 \ (0.167)^2 = -4.013$$
$$d_{mm}^3 = 9.707 \times 10^{-5}$$
$$d_{mm} = 0.046 \ \mu m$$

Fig. 1.4 shows that the mass-median diameter is 0.05 μm.

APPENDIX B

APPROXIMATE DRAG FORCE ON A DEPOSITED PARTICLE

The largest particles used in the deposition tests of the present study have a mass median diameter of 0.25 μm produced from 5 $^o/_o$ uranin solution.

As mentioned earler, the particles produced were quite monodispersed where the largest particle diameter observed was 0.6 μm. The calculation of drag force is based on 1 μm for particles which may possibly be produced. The velocity of the air flow is 25.5 m/s and the corresponding friction velocity is 1.2 m/s.

(a) Thickness of laminar sub-layer, δ_ℓ

This is given by the expression :

$$\delta_\ell^* = \delta_\ell \frac{u_*}{\nu} = 5 \qquad\qquad (B.1)$$

$$\delta_\ell = \frac{5 \times 1.56 \times 10^{-5}}{1.2} = 6.5 \times 10^{-5} \text{ m}$$

$$= 65 \text{ μm}$$

Therefore the particle is submerged with the laminar sub-layer and will subject to the flow conditions inside it.

(b) The velocity at the edge of the laminar sub-layer :

The air velocity at the edge of the laminar sub-layer is described by

$$u^* = y^* = 5$$

Then the velocity at the edge of the laminar sub-layer

u_ℓ = 1.2 × 5 = 6 m/s

It is assumed that the velocity in the laminar sublayer is varying linearly with the distance normal to the surface, therefore the velocity at the centre of the particle will be

$$u = r_p \frac{u_\ell}{\delta_\ell}$$

$$= \frac{0.5 \times 6}{65} = 0.046 \text{ m/s}$$

This value is taken as the average velocity over the particle.

(c) The drag force on the particle :

With the air flow parallel to the surface, the drag force on the deposited particle will be given concervatively by :

$$F_D = \tfrac{1}{2} C_D \rho u^2 A_p \qquad\qquad (B.2)$$

where

C_D Drag coefficient, $f(Re_p)$,

ρ air density = 1.2 kg/m^3, and

A_p cross-sectional area of the particle

In the Stokes' regime the drag coefficient is given by :

$$C_D = \frac{24}{Re_p} \qquad\qquad \text{for } Re_p < 1$$

$$Re_p = 2.95 \times 10^{-3}$$

$$C_D = 8139$$

$$A_p = \frac{\pi}{4} d_p^{\,2} = 7.854 \times 10^{-13} \; m^2$$

$$F_D = 8.116 \times 10^{-12} \; N$$

APPENDIX C

PUBLISHED PAPERS

1- Owen, I., El-Kady, A.A. and Cleaver,J.W. (1985)

"A note comparing the rates of deposition of sub-micron particles with the rates of heat transfer for ribbed surfaces exposed to turbulent gas streams"

J. Aerosol Sci., 17 (2), 145-148.

2- Owen, I., El-Kady,A.A. and Cleaver, J.W. (1987)

"Fine particle fouling of roughened heat transfer surfaces"

Proc. ASME-JSME Thermal Engineering Cof., Hawaii, March, 3, 95-102.

3- Owen, I., El-Kady,A.A. and Cleaver, J.W. (1988)

"Sub-micron particulate fouling of heated AGR fuel rod surfaces"

To be presented at the 2nd. U.K. National Heat Transfer Conerence, Glasgow, Sept.

A NOTE COMPARING THE RATES OF DEPOSITION OF SUB-MICRON PARTICLES WITH THE RATES OF HEAT TRANSFER FOR RIBBED SURFACES EXPOSED TO TURBULENT GAS STREAMS

I. Owen, A. A. El-Kady and J. W. Cleaver

Heat and Mass Transfer Laboratory, Department of Mechanical Engineering,
The University of Liverpool, PO Box 147, Liverpool L69 3BX, U.K.

Abstract—The deposition rates of sub-micron particles on ribbed surfaces as measured by Hahn, Stukel, Leong and Hopke are compared with an empirical formulation for the convective heat transfer over similar surfaces at comparable Reynolds numbers. The comparison is made on the basis of the accepted similarity between the mechanisms of particulate mass transfer and that of convective heat transfer. Although the correlations are shown to be favourable, caution is nevertheless advised when using this technique.

INTRODUCTION

A useful technique which is commonly used to calculate mass transfer rates between a solid boundary and a fluid is to draw an analogy with the rates of convective heat transfer under similar conditions. This technique is often known as the Chilton–Colburn analogy or, more simply, the Heat and Mass Transfer Analogy. The method is an extension of the Reynolds Analogy between momentum and heat transfer and depends on the similarity between transport mechanisms for momentum, heat and matter. The underlying principles of the technique can be found in any standard text on chemical engineering or similar fields of technology. In brief, if the heat transfer process is described in terms of the usual non-dimensional parameters

$$Nu = f(Pr, Re), \tag{1}$$

then a similar function can be assumed for the mass transfer such that

$$Sh = f(Sc, Re). \tag{2}$$

For complete similarity between the two transport processes the diffusivities of each should be of comparable magnitude. In the case of diffusing gases and vapours this is usually achieved. In the case of particles in gas streams, however, the ratio of the Schmidt number to the Prandtl number can be of the order of 10^5. Under circumstances such as these the analogy has to be applied with caution. Care has to be taken, for example, to ensure that the particles are sufficiently small that they carry insignificant inertia and that their deposition will not therefore be enhanced by eddy impaction. Also, because the particle diffusivity will usually be substantially smaller than the thermal diffusivity ($Sc \gg Pr$), where low levels of eddy diffusivity occur they will have a significantly greater effect on the particle transfer than on the heat transfer. This is particularly true for particle diffusion through turbulent boundary layers where the eddies in the viscous sub-layer are damped. If the analogy is applied in this case then predictions for the particle deposition on the basis of the corresponding heat transfer substantially underestimate the measured deposition rates. To re-align the model a particle diffusivity has to be assigned to the sub-layer (Lin et al., 1953). Similarly, laminar boundary layers in turbulent streams can be invaded by mainstream eddies, thereby enhancing the deposition. It is evident, therefore, that this technique cannot be applied universally. For this reason it is useful to be able to offer confirmation that it can be used under specific circumstances. This is particularly so in view of the general lack of reliable

experimental data for the deposition of particles in the sub-micron range on surfaces other than smooth walls in fully developed turbulent pipe flow.

Despite the differences between particle and thermal diffusivities, provided the particles are sufficiently small to follow faithfully the turbulent eddies then their physical transport through the fluid will be the same as that of the thermal transport. On this basis, the case of a gas stream flowing over a ribbed surface is one where the analogy should hold. In a recent paper, Hahn et al. (1985) published experimental data and a formulation for the deposition of sub-micron particles (0.04–0.2 μm) on a surface having regular roughness elements mounted transverse to the flow. The purpose of the present paper is to compare this data with an empirical formula for the heat transfer between a ribbed surface and a turbulent stream under conditions of comparable roughness geometry and Reynolds number.

PARTICLE DEPOSITION AND CONVECTIVE HEAT TRANSFER ON RIBBED SURFACES

An empirical formula for the convective heat transfer over ribbed surfaces has been deduced from published correlations concerning the friction factor and Stanton number change for flow over ribbed fuel elements in an Advanced Gas Cooled Reactor (Rapier, 1977). The geometric configuration upon which this work is based is shown in Fig. 1. The friction factor is given by:

$$f = 0.115 + 1.325 \, K/d + 0.265 \, K/2r, \tag{3}$$

whilst the Stanton is given by:

$$St = (8.26 \times 10^{-4} + 7.6125 \times 10^{-2} \, Re^{-0.32})(2.4 + 20 \, K/d + 8 \, K/2r), \tag{4}$$

where d is the equivalent hydraulic diameter of the fuel element.

These correlations, together with experimental data describing the gas flow conditions (carbon dioxide) through the fuel element (Johnson, 1985), can be combined to show the following relationship:

$$Nu = 0.021 \, Re^{7.8}. \tag{5}$$

Nu and Re are based on the local heat transfer coefficient and the local mean flow velocity respectively; both are calculated using d as the characteristic length.

To provide experimental data describing significant changes in the Prandtl number it is necessary to use a number of different gases; these data are not available. It has been necessary, therefore, to make an assumption regarding the Prandtl number and in this work the usual one that convective heat transfer is a function of $Pr^{1/3}$ has been made. This assumption will be discussed later. Therefore, equation (5) becomes:

$$Nu = 0.023 \, Pr^{1/3} \, Re^{7.8}, \tag{6}$$

and it follows that the convective mass transfer should be described by:

$$Sh = 0.023 \, Sc^{1/3} \, Re^{7.8}. \tag{7}$$

The particle deposition results of Hahn et al. were obtained using the experimental surface configuration shown in Fig. 2. Three roughness parameters P/K of 2, 13 and 25 were tested. A solution of Uranin was atomised to produce monodisperse particles, the presence of which was detected using fluorimetric techniques. Particles with diameters of 0.041, 0.059, 0.087, 0.13 and 0.20 μm were used. The results of these experiments were compared with an analysis
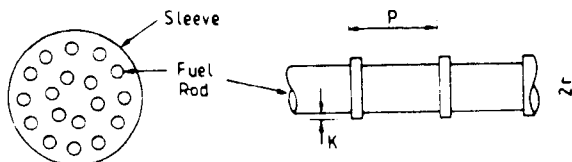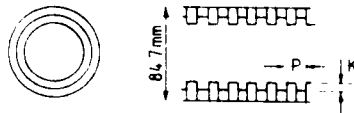

Fig. 1. AGR fuel element.

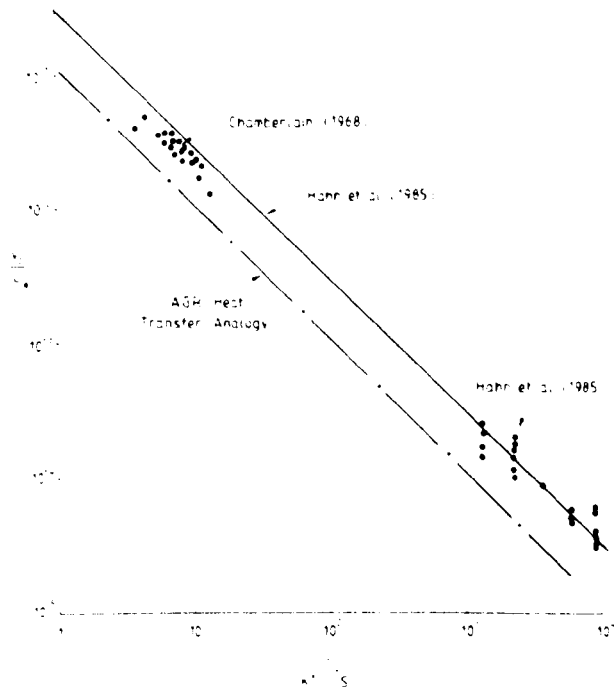Fig. 2. Ribbed geometry used by Hahn *et al.* (1985).

Fig. 3. Deposition on ribbed surfaces.

developed by Kader and Yaglom (1977). Hahn *et al.* went on to suggest that the equation developed by Kader and Yaglom can be further reduced such that the deposition velocity, V_d, is given by:

$$V_d^+ u_* = 1 (3.2 (K^+)^{1.4} Sc^{2.3}),$$ (8)

where K^+, the non-dimensional roughness parameter, is given by (Ku_*/v).

Equation (8), using the shear velocity, u_*, given by equation (3), is shown graphically in Fig. 3 together with the experimental data of Hahn *et al.* Also shown in Fig. 3 are the data obtained by Chamberlain (1968) for the deposition of water vapour and thorium B vapour over rough surfaces. Hahn *et al.* used these data to demonstrate the range over which equation (8) is applicable. From Fig. 3 it can be seen that the deposition predicted by equation (7) agrees well with the results presented by Hahn *et al.* and that the correlation between the heat and mass transfer over a ribbed surface is a valid one.

DISCUSSION AND CONCLUSIONS

There is a lack of reliable data concerning the deposition of sub-micron particles on irregular surfaces and on bodies having two or three dimensional geometries. On the other hand, there is a relative wealth of data for the corresponding processes of heat transfer. By taking advantage of the similarity between the transport mechanisms of the two processes it is sometimes possible to make calculations for the mass transfer based on the formulation for the corresponding heat transfer. Comparing equations (6) and (7) at the same Reynolds

number produces a relationship between the Sherwood and Nusselt numbers,

$$Sh/Nu = (Sc/Pr)^{1/3}. \qquad (9)$$

For diffusing gases and vapours $Sc/Pr \sim 1$ and the conditions of similarity between the two are satisfied. For sub-micron particles, however, $Sc/Pr \sim 10^5$ and the relationship between Sh and Nu becomes very sensitive to the power by which Sc/Pr is raised. In the present work the power of $1/3$ has been assumed and, as shown in Fig. 3, the resulting correlation is a good one. However, in convective heat transfer formulations it is not unusual to see functions containing $Pr^{0.25}$ or even $Pr^{0.75}$, since Pr usually has a value of about 0.7; the heat transfer rates are not particularly sensitive to these differences. When Sc/Pr is of the order of 10^5, however, such differences will result in the heat and mass and transfer correlations changing by a factor of about 300.

In the majority of cases the $Pr^{1/3}$ relationship is a sound one and the analogy can be used with some confidence. This paper has presented a favourable correlation between the convective heat transfer and the deposition of sub-micron particles over ribbed surfaces in order to lend support to the technique whilst at the same time drawing attention to its inherent weaknesses.

REFERENCES

Chamberlain, A. C. (1968) *Q. J. R. Soc.* **94**, 318.
Hahn, L. A., Stukel, J. J., Leong, K. H. and Hopke, P. K. (1985) *J. Aerosol Sci.* **16**, 81.
Johnson, P. A. V. (1985) U.K.A.E.A. private communication.
Kader, B. A. and Yaglom, A. M. (1977) *Int. J. Heat Mass Transfer* **20**, 345.
Lin, C. S., Moulton, R. W. and Putnam, G. L. (1953) *Ind. Chem. Engng* **45**, 636.
Rapier, A. C. (1977) U.K.A.E.A. Report ND-R-63(W).

FINE PARTICLE FOULING OF ROUGHENED HEAT TRANSFER SURFACES

I. OWEN, A.A. EL-KADY AND J.W. CLEAVER

Heat and Mass Transfer Laboratory,
Department of Mechanical Engineering,
The University of Liverpool,
P.O. Box 147, Liverpool, L69 3BX, U.K.

ABSTRACT

Roughened heat transfer surfaces are occasionally used to enhance the rate of forced convection heat transfer by causing an increase in the turbulence of the flow adjacent to those surfaces. If the gas flow is contaminated with aerosols the increased turbulence will also accelerate the rate of particle deposition onto the surface by eddy diffusion. In the event of the spaces between the roughness elements being filled by the deposit, the beneficial effects of roughening are soon lost. There are two reasons for this: firstly, the material forms an insulating layer and secondly, the level of turbulence in the flow is reduced as the surface becomes more smooth.

In this paper the role of ribbed roughness elements are discussed in relation to their use on fuel rod surfaces in gas-cooled nuclear reactors. In addition, the process and rate of deposition of sub-micron particles is described by means of a theoretical model which includes the effects of surface roughness and thermophoresis.

NOMENCLATURE

A,B,C constants
c   particle concentration ($\mu g/m^3$)
c_0 free stream particle concentration ($\mu g/m^3$)
c^+ dimensionless particle concentration = (c/c_0)
C_m momentum exchange coefficient
C_s thermal slip coefficient
C_t thermal jump coefficient
C_p specific heat (J/kg.K)
d   equivalent hydraulic diameter of flow channel (m)
d_p particle diameter (m)
D   particle diffusivity (m^2/s)
e   rib height (m)
f   fanning friction factor
h   heat transfer coefficient ($W/m^2 K$)
k_g gas thermal conductivity (W/m.K)
k_p particle thermal conductivity (W/m.K)
N   particle mass flux ($\mu g/m^2.s$)
r   fuel pin radius (m)

r_p particle radius (m)
Re   Reynolds number = (Ud/ν)
St   Stanton number = ($h/\rho C_p U$)
T   absolute temperature (K)
T_c temperature of fuel rod surface (K)
Tg   temperature of gas coolant (K)
u   fluid velocity (m/s)
u_* friction velocity (m/s)
U   mean velocity of flow (m/s)
V   particle deposition velocity (mass transfer coefficient) (m/s)
V_0 particle deposition velocity with no thermophoresis (m/s)
V_T thermophoretic velocity (m/s)
V_{th} particle deposition velocity with thermophoresis (m/s)
v^+ dimensionless deposition velocity (V/u_*)
V_T^+ dimensionless thermophoretic velocity = (V_T/u_*)
y^+ dimensionless normal distance from surface
       = ($\frac{yu_*}{\nu}$)

ΔP pressure drop (N/m^2)
ϵ eddy diffusivity (m^2/s)
λ mean free path (m)
ν kinematic viscosity (m^2/s)
ρ gas density (kg/m^3)

INTRODUCTION

Convective heat transfer between a surface and a moving fluid is enhanced in the presence of turbulence. Surface roughening is one technique used to generate turbulence immediately adjacent to the surface and thus preventing the formation of a structured boundary layer. Early studies of "surface spoilers" or "turbulence promoters" took the view that the technique was ineffective if the gain in heat transfer was less than the increase in momentum transfer (drag). A closer inspection of the role of surface roughening by Walker and Wilkie (1966) showed that this criterion was inappropriate and that in many cases the roughening of the surface was highly beneficial to the overall heat transfer process. Consequently the fuel rod surfaces

in all U.K. Advanced Gas Cooled Reactors (AGR's) are machined to produce transverse ribs closely spaced along the length of the rod. With reference to fouling, however, if the fluid flowing over the roughened surface is contaminated by very fine particulates, or even molecular material capable of forming a deposit, then the increased heat and momentum transfer will be accompanied by an increase in the mass transfer to the surface, i.e. the fouling rate will increase.

This paper will firstly describe how the heat transfer in an AGR is enhanced by the use of ribs. Secondly, the effect of fouling on such surfaces will be described together with the consequences for heat transfer. Finally the paper will present a mathematical model which has been developed to describe the deposition of sub-micron particles onto roughened surfaces in the presence of thermophoresis.

RIBBED HEAT TRANSFER SURFACES

Convective heat transfer between a solid boundary and a moving fluid is significantly influenced by the presence of turbulence which moves the fluid away from the surface replacing it with fresh fluid, thus helping to maintain a high surface temperature gradient. Even in turbulent boundary layers, however, the viscous sub-layer acts as a resistance to the convective heat transfer. By having roughness elements in the shape of small rectangular ribs on the surface it is possible to destroy the structured boundary layer and produce a turbulent flow close to the surface. The shape, size and spacing of the ribs is very important, this can be demonstrated with reference to Fig. 1. In Fig. 1(a),
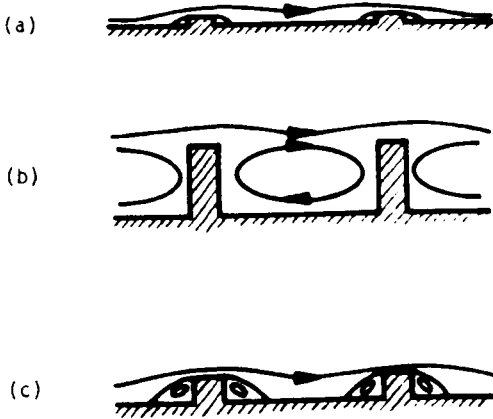

Fig. 1 Effects of ribs height on flow

the rib is too small to be very effective since the flow soon re-attaches after the rib and a viscous layer has time to develop. In 1(b), the other extreme is shown where the flow skims over the top of the ribs and a recirculating region forms between them. Clearly an optimum pitch/height ratio lies somewhere between these two cases. After extensive experimental work (Wilkie, 1966) a ratio of 7.2 has been adopted for AGR fuel rods. Fig. 2 shows a flow channel configuration in which 36 ribbed fuel rods are contained within a graphite sleeve. This is the configuration used in commercial nuclear reactors in the U.K.

An obvious drawback of roughening is that it also causes an increase in the surface friction factor.
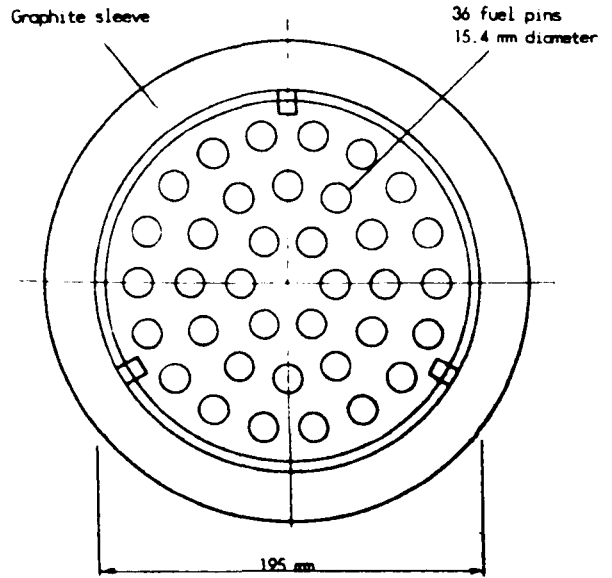

Fig. 2 Cross-section of flow channel in commercial A.G.R.

When the pressure drop across a flow channel whose surface is roughened is expressed as a function of the friction factor and the Stanton number, for a given geometry and for a fixed gas flow rate, the result is:

$$\Delta P \propto \frac{f}{St^3} \qquad (1)$$

Walker and Wilkie (1966) investigated the relation between rib geometry and pressure drop in some detail and came to the firm conclusion that in many circumstances the benefits of increased heat transfer rates significantly outweigh the penalties associated with the increased friction factor - the AGR being an example. The effects of rib height for a fixed pitch/height ratio on heat transfer and friction factor are shown in Figs. 3 and 4 respectively.
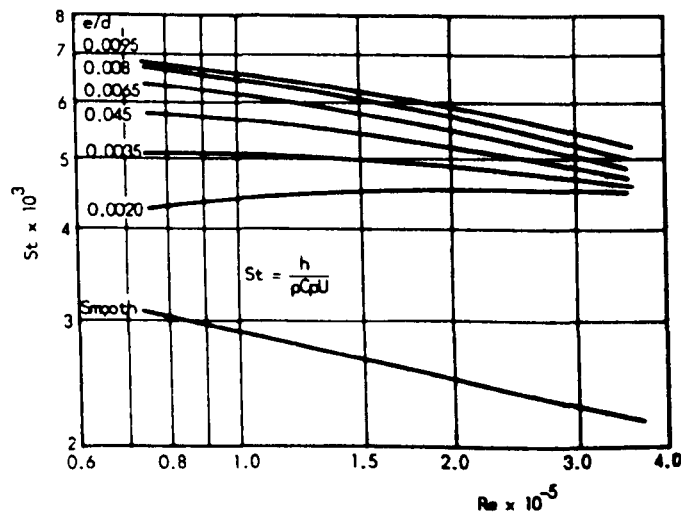

Fig. 3 Stanton number for surfaces with pitch/height ratio 15 (Walker and Wilkie)
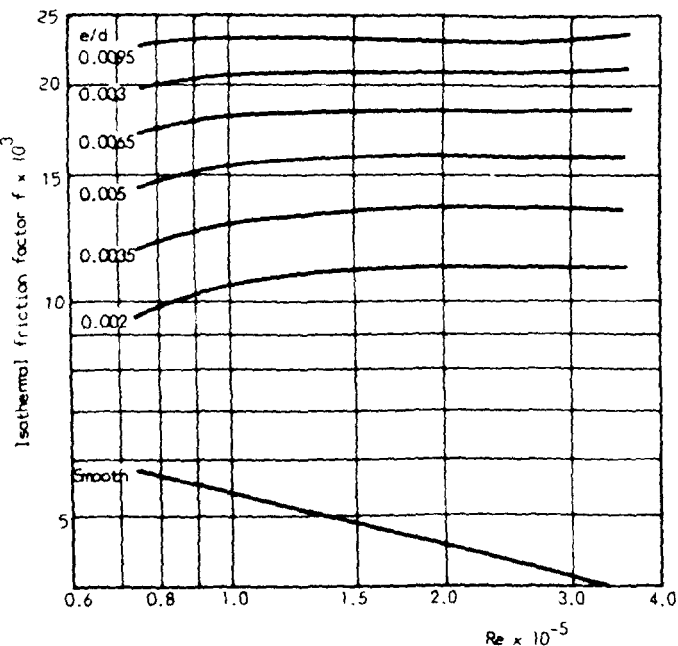
Fig. 4   Friction factor for surfaces with pitch/height
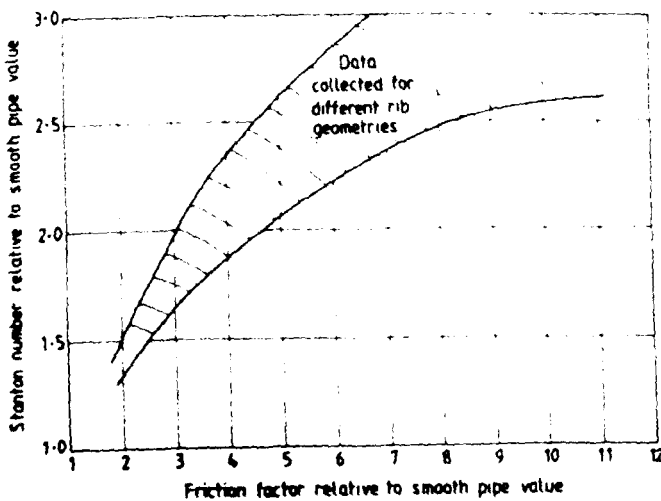ratio of 15 (Walker and Wilkie)

Fig. 5   Effect of ribs on surface friction factor
and heat transfer

Fig. 5 shows the variation of Stanton number with
friction factor for different rib geometries under the
same flow condition.   The data is extracted from
Figs. 3 and 4 and provides the basis of the argument
used by Walker and Wilkie.   Referring to equation (1)
together with Fig. 5, it is seen that in this case ΔP
in fact decreases as a result of using roughened
surfaces.

FOULING OF RIBBED SURFACES

Operating experience with gas cooled nuclear
reactors has shown that, under certain conditions, the
formation of a carbonaceous deposit can occur on the
fuel rods.   By using instrumented fuel stringers
inserted into the core of the Windscale prototype AGR,
it has been possible to measure the effects of the
deposit on the heat transfer.

The advanced gas-cooled reactor is graphite
moderated and uses carbon dioxide gas as a coolant.
The system operates at a pressure of 41.4 bar.   At
typical reactor operating conditions there will be
radiolytic oxidation of the graphite.   To ensure the
reactor has a satisfactory operating life, it is
important that this rate of oxidation is kept to a
minimum.   The reaction produces carbon monoxide which
has the advantageous effect of inhibiting the oxidation
rate; in addition methane is introduced to further
contain the reaction rate.   The methane itself, however,
will also experience radiolysis and thereby initiate a
series of chemical reactions which can produce carbon
or carbonaceous species and ultimately the formation of
deposits on the reactor surfaces (Blanchard et al. 1979,
Campion 1980).   The tendency for deposition to occur in
gas cooled reactors when operating under certain
conditions has long been recognised.   There is still
controversy however over the exact route to the formation
of the carbon species and the mechanisms of deposition
onto the surfaces.   The effect of cooling circuit
design is also known to be important since different
experimental systems produce different fouling
characteristics.   Deposition in commercial reactors is
closely monitored both by instrumented fuel within their
cores and by visual and metallographic scrutiny of
discharged fuel.   However a large body of data was
obtained from the Windscale AGR, now decommissioned,
with additional data coming from other experimental rigs.
The advantage of the Windscale reactor was that it was
a fully operational prototype in which experimental
coolant compositions could readily be tested.

Photographs of typical deposits from the Windscale
reactor are shown in Figs. 6 and 7.   The effects of
the deposit are twofold: firstly it covers the metal
surface of the fuel rod with an insulating layer of
material, and secondly it fills in the space between
the ribs thereby tending to return the rod to a smooth
surface and reducing the convective heat transfer.
These two effects will combine to cause a reduction in
reactor power output or an increase in the surface
temperature of the fuel rod.   The latter will influence
the period of service of the fuel element and will lead
to uneconomic premature withdrawal from the reactor.
Each stringer in the Windscale reactor is made up of
four fuel elements (eight in commercial reactor), the
measured change in Stanton number of the second element
in a particular channel is shown in Fig. 8.   After
130 days the CO content of the coolant was changed and
a corresponding change in Stanton number can be seen.
In practice the methane levels can be monitored and
adjusted and in any case the fuel is withdrawn after a
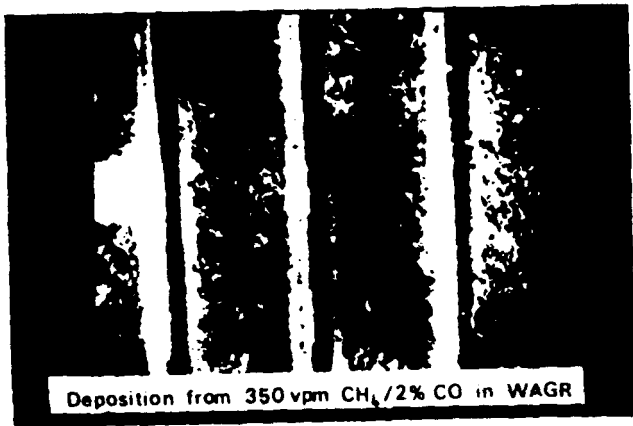
Deposition from 350 vpm CH₄/2% CO in WAGR
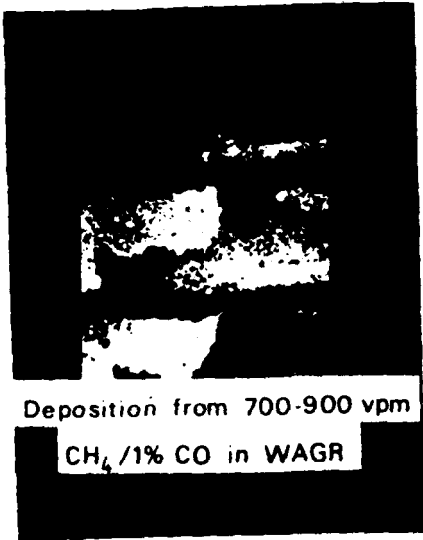
Deposition from 700-900 vpm
CH₄/1% CO in WAGR

Figs. 6 and 7 Deposition on AGR ribbed fuel elements

certain period so that the fouling, whilst undesirable, is not as serious as it might be.

To further complicate the fouling process two distinctly different kinds of deposit have been found; these are associated with different surface temperatures and are therefore known as High and Low Temperature Deposit - HTD and LTD. The high temperature deposit occurs at temperatures above approximately 700°C and is seen to consist of straight tubular filamentary growths which are produced by catalytic decomposition of hydrocarbon at the fuel rod surface. In other words there is molecular mass transfer to the surface and the deposit grows, through chemical reaction, away from the surface. In contrast, the low temperature deposit (500 - 700°C) consists of highly irregular filaments of 0.1 - 0.2 μm diameter. Electron micrographic examination of LTD shows it to be similar in structure to deposits of soot. It has also been observed that LTD is unaffected by the composition of the surface upon which it is found, this would not be expected if it were a chemical growth. These observations suggest that LTD is formed by discrete particles being deposited onto the surface from the gas by eddy-diffusion impaction.
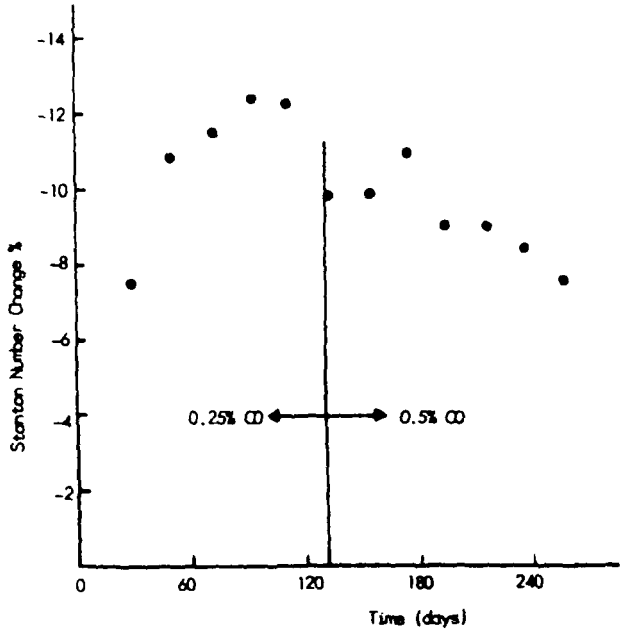

Fig. 8 Change in Stanton number

Further weight is given to this argument by the discovery of iron in the deposit. It is believed that Fe(CO)₅ is generated at metal surfaces in the coolant circuit (hence explaining the circuit dependence which has been observed) and is then destroyed to form minute iron particles. It is further believed that the iron particles act as nucleation sites for the growth of particles of carbon derived from the methane in the gas.

Although the processes described above relate directly to heat transfer in nuclear reactors they can be viewed in a wider perspective. The use of roughness elements in the form of small ribs placed transverse to the flow is seen to be highly beneficial to the heat transfer from a solid surface and could, perhaps, be used more widely. From the viewpoint of fouling, the gas in the reactor would be considered, by many observers, to be both inert and clean - particularly when compared with most process fluids. It is evident therefore that a fluid is not necessarily as clean as it might appear. There is a direct link between turbulence enhanced heat transfer and fouling since the turbulent transport mechanisms of each are fundamentally the same. The turbulent bursts and eddies which scour the surface and efficiently remove the heated (or cooled) fluid are equally as effective in bringing the small particles into contact with the surface where they will almost certainly stick due to strong forces of adhesion. The corners either side of the ribs shelter small recirculation zones which will encourage particle deposition, the deposit can then spread to completely fill the gap between the ribs. The evidence suggests that the depositing particles are typically 0.2 μm diameter (Kelly, 1984). Predicting the motion and deposition of particles of this size can be difficult since they are too large to be considered as gas molecules whose transport could be related to that of a diffusing gas whilst they are too small to possess sufficient inertia for them to be considered as discrete spheres moving in a viscous fluid.

The specific role of the authors in this work is to investigate the mechanism of deposition of submicron

particles onto roughened surfaces and in the presence of steep temperature gradients which introduce the phenomenon of thermophoresis. The following section describes a theoretical model of the deposition which has been developed and which will shortly be tested in the laboratory using experimental aerosol techniques.

THEORETICAL MODEL

The theoretical treatment for this study has been based on a diffusive model in which the particle flux is expressed in terms of particle diffusivities and a concentration gradient, thus:

$$N = (D + \epsilon) \frac{dc}{dy} \qquad (2)$$

The diffusion across perfectly laminar flows is mainly governed by the particle diffusivity D, but in turbulent flows this is quickly overwhelmed by the turbulent diffusivity, ϵ. Expressing equation (2) in dimensionless form gives:

$$v^+ = (\frac{D}{\nu} + \frac{\epsilon}{\nu}) \frac{dc^+}{dy^+} \qquad (3)$$

The deposition process is therefore seen to be influenced by the shear velocity u_*, where:

$$u_* = U \sqrt{\frac{f}{2}} \qquad (4)$$

The friction factor of a fuel element with ribbed surface was experimentally measured by Rapier (1977) and found to be:

$$f = 0.0115 + 1.325 \frac{e}{d} + 0.265 \frac{e}{2r} \qquad (5)$$

The turbulent diffusivity of the particles is assumed to be the same as that for the fluid. This assumption is reasonable for particles less than about 1 μm (Rouhiainen and Stachiewicz, 1970). Davies (1966) derived an empirical expression for the eddy diffusion coefficient at a non-dimensional distance y^+ from the wall, thus:

$$\frac{\epsilon}{\nu} = \frac{0.001 (y^+)^n}{(C/Re)^m} \qquad (6)$$

where $n = 4 - (y^+)^{0.08}$

$m = y^+/(400 + y^+)$

and $C = 2.5 \times 10^7$

Surface irregularities, as well as causing turbulence, also have a direct effect on the capture of particles since the peaks of the irregularities (or ribs in this case) will tend to "catch" them as they drift past. Consequently, the rate of deposition of particles onto rough surfaces is well known to be much greater than that onto smooth surfaces (Wells and Chamberlain 1969, Chamberlain 1967). To allow for this effect Brown (1974) modified Davies' approach by essentially using a shifted origin for the surface. The particle stopping distance, velocity and diffusivity, were then considered from this displaced origin. The analysis of Brown applies to a randomly rough surface and should therefore be considered with some caution in relation to the regular roughness of the fuel rod surfaces. The deposition between the ribs will not be uniform and the analysis presented herein will give average values. A comparison of different studies into

deposition onto surfaces with random roughness (Owen et al. 1986) has shown that in the absence of thermophoresis surfaces with regular and with irregular roughness experience similar average rates of deposition. However, the scale of roughness considered by Brown is comparable in size to the particle radius. This limits the applicability of Brown's work and for the present study the size of the roughness elements (0.28 mm x 0.28 mm on a 2 mm pitch) makes it unsuitable. It is therefore appropriate to use Davies' theory and to allow for the surface roughness through the rough surface shear velocity from equation (5) which influences equation (3) and, later, equation (8).

Thermophoresis

Particles of sub-micron size respond to the motion of the gas molecules around them. In the presence of steep temperature gradients the molecular activity on the hotter side of the particle is greater than that on the cooler side. The result is the phenomenon of thermophoresis whereby particles are driven away from hot surfaces and attracted towards cold surfaces.

The strength of the thermophoretic force and the velocity acquired by the particles has been the subject of a number of investigations, (Epstein 1929, Brock 1962, Derjaguin and Yalamov, 1965). Talbot et al (1980) found that Brock's theory, with an improved value for the thermal slip coefficient, C_s, gave good agreement with experiment over a wide range of Knudsen number (λ/r_p). In the present work, therefore, the expression proposed by Talbot et al has been adopted where the thermophoretic velocity is given by:

$$V_T = \frac{2C_s \nu \; (\frac{k_g}{k_p} + \frac{C_t \lambda}{r_p}) \left[1 + \frac{\lambda}{r_p} (A + B \exp (-C \frac{r_p}{\lambda})) \right]}{(1 + 3C_m \frac{\lambda}{r_p}) (1 + 2 \frac{k_g}{k_p} + 2C_t \frac{\lambda}{r_p})} \frac{1}{T} \frac{dT}{dy} \qquad (7)$$

where $C_s = 1.149$, $C_m = 1.14$, $C_t = 2.18$, $A = 1.2$

$B = 0.41$ and $C = 0.88$

Incorporating the thermophoretic effect into the diffusion equation gives:

$$v^+ = (\frac{D}{\nu} + \frac{\epsilon}{\nu}) \frac{dc^+}{dy^+} + V_T^+ c^+ \qquad (8)$$

The solution for the deposition rate is found by integrating this expression from the surface into the flow. The procedure is essentially the same as that used by Davies (1966) and Brown (1974). It should be emphasised that the model does not take into account any removal by aerodynamic forces, which may occur.

Figure 9 shows the effect of particle size on the predicted deposition velocity for different surface roughnesses in the absence of thermophoresis. Initially, as the particle size increases so the particle diffusivity and hence deposition velocity decreases. As the particle size is increased further so the deposition velocity increases again as the effects of particle inertia begin to be seen. As would be expected, the inertia effects become more important as the surface roughness is increased, such that for e/2r = 0.036 inertia effects are seen to increase deposition for particles greater than 0.5 μm whereas for e/2r = 0.009 the corresponding particle size is 0.7 μm. Also the
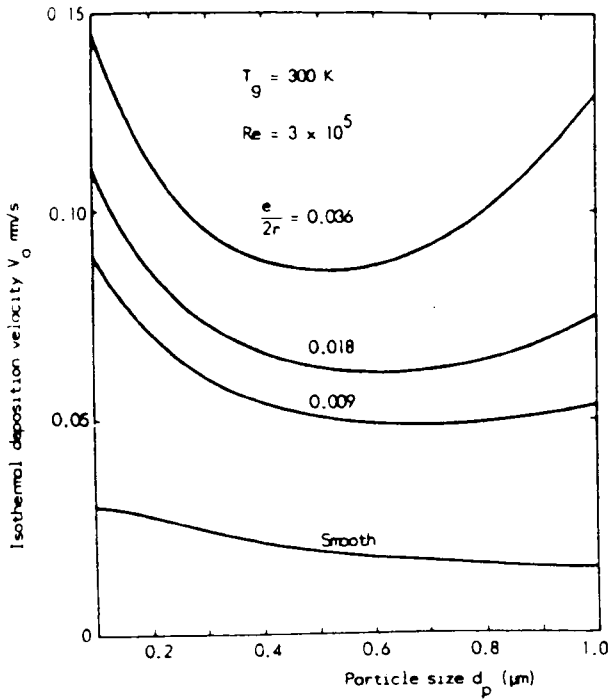
Fig. 9 Effect of particle size and surface roughness
        on deposition velocity (no thermophoresis)
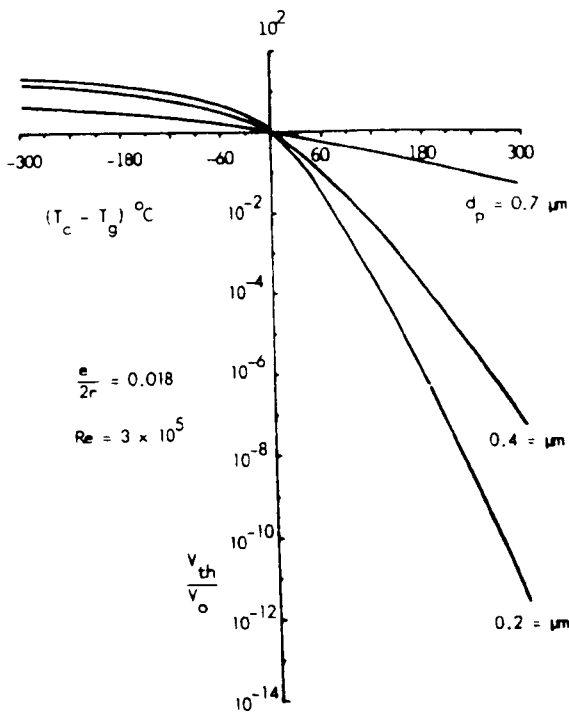

Fig. 10 Effect of thermophoresis on particle
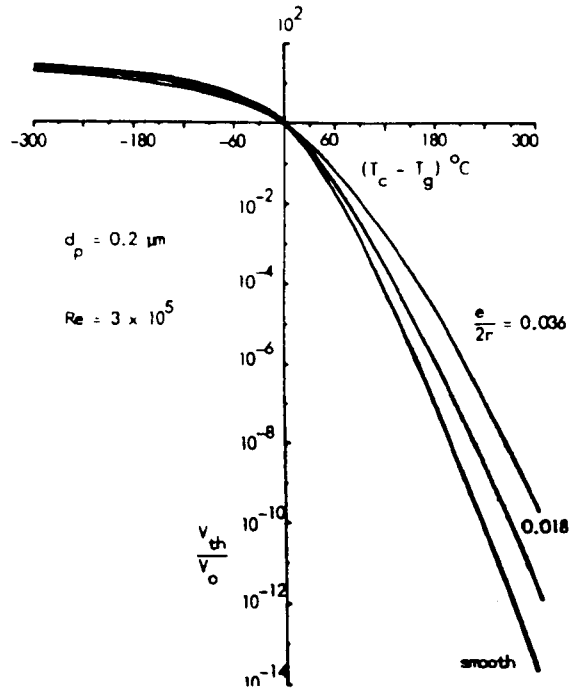   deposition

Fig. 11 Effect of thermophoresis on particle deposition

rate of increase of deposition velocity with particle
size is greater for the rougher surface.

Examples of the predicted effects of thermophoresis
are shown in Figs. 10 and 11. The potential of
thermophoresis in preventing deposition onto surfaces is
considerable. For example, the theory suggests that
for surface to gas temperature differences of 60°C the
deposition velocity for 0.2 μm particles will fall to 1%
of its value without thermophoresis. It can also be
seen in Fig. 10 that thermophoresis has a much greater
effect on 0.2 μm particles than on 0.7 μm particles.
In fact particles of about 0.2 μm are those most
susceptible to thermophoresis - below this size there is
only a small temperature difference across them (hence
reducing the thermal imbalance) and above this size
inertial effects begin to dominate. From Fig. 11 it
can be seen that thermophoretic effects are reduced over
rough surfaces. This is again due to the particle
inertial deposition being influenced by the surface
roughness.

The preceding discussion has implied that the
surface is a perfect sink and that once a particle
reaches the surface it will not be removed. For sub-
micron particles the adhesive forces are believed to be
sufficiently large for such an approximation to be valid.
Under such conditions the deposit will steadily increase
with time. There is however a limited amount of
evidence to suggest that even sub-micron particles can
be removed provided the mean wall shear stress is high
enough, (Cleaver and Yates, 1973). When this occurs the
deposit no longer increased indefinitely with time but
reaches an asymptotic value (Cleaver and Yates, 1976).
As indicated earlier the deposit encountered in AGR's
is not uniformly dispersed and agglomeration of small
sub-micron particles at the surface will occur. These
will be susceptible to aerodynamic removal. This two-
stage mechanism leading to removal of deposits further
complicates the process.

CONCLUDING REMARKS

The purpose of this paper has been to discuss the role of roughened heat transfer surfaces and their sensitivity to fouling, especially by sub-micron particles. The use of roughened surfaces and the consequences of fouling have been described through the specific example of gas cooled nuclear reactors. To investigate more fundamentally the deposition process a theoretical model has been developed which includes the effects of surface roughness and thermophoresis. The thermophoresis in particular is shown to be a very influential component of the deposition process especially with particle sizes between, say, 0.1 and 0.7 μm. The majority of deposits which are found in heat exchangers lie outside this narrow size range and consequently thermophoresis is not generally recognised as an important mechanism. One method through which particles within this size range can be formed is by a nucleation process which will be initiated by either a thermal or chemical disequilibrium. The original formation and subsequent growth of these particles will normally lead to a near monodisperse distribution of particle size. In the event of a foulant being produced in this way the role of thermophoresis should not be overlooked.

REFERENCES

Blanchard, A., Faircloth, R.L. and Wood, C.J., 966, "The radiolytic oxidation rate of nuclear graphites as a function of point coolant composition in moderator blocks", 14th Biennial Conf. on Carbon, Penn. State Univ., June 25-29, p.447.

Brock, J.R., 1962, "On the theory of thermal forces acting on aerosol particles", J. Colloid Sci., Vol. 17, pp. 768-780.

Brown, L.W.B., 1974, "Deposition of particles on rough surfaces during turbulent gas flow in a pipe", Atmo. Envir. 18, pp. 801-816.

Campion, P., 980, "Carbon formation processes relevant to advanced carbon dioxide cooled reactors", Gas Chemistry in Nuclear Reactors and Large Industrial Plant, Edited by A. Dyer, Haden Press, London, pp. 53-66.

Chamberlain, A.C., 1967, "Transport of Lycopodium Spores and other particles to rough surfaces", Proc. Roy. Soc., A296, pp. 45-70.

Cleaver, J.W. and Yates, B., 1973, "Mechanics of detachment of colloidal particles from a flat substrate in turbulent flow", Int. J. Coll. Sci., Vol. 44, pp. 464-473.

Cleaver, J.W. and Yates, B., 1976, "The effect of re-entrainment on particle deposition", Chem. Eng. Sci., Vol. 31, pp. 147-151.

Davies, C.N., 1966, "Deposition of aerosols from turbulent flow through pipes", Proc. R. Soc., A289, pp. 235-247.

Derjaguin, B.V. and Yalamov, Yu, 1965, "Theory of thermophoresis of large aerosol particles", J. Colloid Sci., Vol. 20, pp. 555-570.

Epstein, P.S., 1929, "Zur theorie des radiometers", Z. Phys., Vol. 54, pp. 537-563.

Kelly, B.T., 1984, "A particulate model for low temperature deposition in Advanced Gas-Cooled Reactors", UKAEA Report ND-M-2537(S).

Owen, I., El-Kady, A.A. and Cleaver, J.W., "A note comparing the rates of deposition of sub-micron particles with the rates of heat transfer for ribbed surfaces exposed to turbulent gas streams", J. Aerosol Sci., Vol. 17, pp. 145-148.

Rapier, A.C., 1977, "A correlation of flow and heat transfer data for surfaces roughened with transverse square ribs of pitch to height ratio of 7.2", UKAEA Report ND-R-63.

Rouhiainen, P.O. and Stachiewicz, J.W., 1970, "On the deposition of small particles from turbulent streams", J. Heat Trans., Trans. ASME, Vol. 92, pp. 169-177.

Talbot, L., Cheng, R.K., Schefer, R.W. and Willis, D.R., 1980, "Thermophoresis of particles in a heated boundary layer", J. Fluid Mech., Vol. 101, 4, pp. 737-758.

Walker, V. and Wilkie, D., 1966, "The wide application of roughened heat transfer surfaces as developed for advanced gas-cooled reactors", Proc. I.Mech.E., Vol. 181, 31, Paper 26, pp. 190-197.

Wells, A.C. and Chamberlain, A.C., 1969, "Transport of small particles to vertical surface", Brit. J. Appl. Phys., Vol. 18, pp. 1793-9.

Wilkie, D., 1966, "Forced convection heat transfer from surfaces roughened by transverse ribs", Paper No. 1, 3rd Int. Heat Transfer Confer., Chigago, August.

I. Owen, A.A. El-Kady and J.W. Cleaver
Heat and Mass Transfer Laboratory, Department of Mechanical Engineering,
University of Liverpool, P.O. Box 147, Liverpool, L69 3BX, U.K.

SUB-MICRON PARTICULATE FOULING OF HEATED A.G.R. FUEL ROD SURFACES

This paper describes an experimental study of particulate deposition onto ribbed AGR fuel rod surfaces. The deposition rates of 0.25 and 0.05 μm diameter particles onto unheated and heated, smooth and ribbed surfaces have been measured using a fluorimetric technique. On the unheated surfaces the effect of the ribs is to increase the surface deposition about twenty-fold compared with the deposition onto the hydraulically smooth surface. By heating the surface to 95°C, compared with the gas flow temperature of 25°C, the deposition rates of the 0.25 μm particles are reduced by about 90% on the smooth surface and by about 80% on the rough surface. The corresponding values for the 0.05 μm particles, are about 60% for both the smooth and the ribbed surfaces. Comparison of the experimental results with a theoretical model for turbulent diffusion with thermophoresis, emphasises that this aspect of particulate deposition is not at all properly understood.

Nomenclature

$c(c^+)$ particle concentration (dimensionless c/c_o)
c_o free stream particle concentration
d_p particle diameter
D particle diffusivity
e rib height
Kn Knudsen number
p rib pitch
t^+_p dimensionless particle relaxation time
T absolute temperature
u_* friction velocity
$V(V^+)$ deposition velocity (dimensionless V/u_*)
V_o isothermal deposition velocity
V_T thermophoretic velocity
V_{th} net deposition velocity with thermophoresis
$y(y^+)$ distance from wall (dimensionless)
α equivalent rib height scaling factor
β temperature gradient scaling factor
ε eddy diffusivity
λ_g, λ_p gas and particle thermal conductivities

1. INTRODUCTION

The fouling of heat exchanger surfaces can lead to significant problems in terms of reduced plant performance and increased energy costs. A particular example of this which has recently received much attention, although it is not a new problem, is the fouling of the fuel rod surfaces in advanced gas-cooled nuclear reactors (AGR's).

The AGR is graphite moderated and uses carbon dioxide gas as a coolant. The system operates at a pressure of 41.4 bar. At typical reactor operating conditions there can be radiolytic oxidation of the graphite. To ensure that the reactor has a satisfactory operating life, it is important that this oxidation is suppressed. The reaction produces carbon monoxide which has the advantageous effect of inhibiting the graphite oxidation rate; in addition methane is introduced to further contain the reaction. The methane itself, however, will also experience radiolysis and thereby initiate a series of chemical reactions which can produce carbon or carbonaceous species and ultimately the formation of deposits on the reactor surfaces (Blanchard et al, 1979; Campion, 1980). The tendency for deposition to occur in AGR's when operating under certain conditions has long been recognised. There is still controversy however over the exact route to the formation of the carbon species and the mechanisms of deposition onto the surface. Deposition in commercial reactors is closely monitored both by instrumental fuel rods within their cores and by visual and metallographic scrutiny of the discharged fuel. Furthermore, a large body of data was obtained from the Windscale AGR, now decommissioned, with additional data coming from other experimental rigs. In the commercial reactors the level of deposition can be controlled to a certain degree by monitoring and adjusting the methane content of the coolant gas.

In conventional tube heat exchangers the gas flow is across the tube and the heat transfer is assisted by the chaotic turbulent flow that results. In a nuclear reactor, however, the coolant flows along the tube and, if allowed to form, the developed boundary layer will reduce the level of heat transfer. Consequently the fuel rod surfaces in all AGR's are machined to produce circumferential ribs closely spaced along the length of the rod transverse to the direction of the gas flow. The purpose of these is to enhance the convective heat transfer by promoting turbulence at the surface. With reference to fouling, however, if the fluid flowing over the surface is contaminated by very fine particles or molecular material capable of forming a deposit, then the increased heat and momentum transfer will be accompanied by an increase in mass transfer to the surface, i.e. the fouling rate will increase. When fouling does occur, the effects of the deposit are twofold: firstly it covers the metal surface of the fuel rod with an insulating layer of material, and secondly it fills in the space between the ribs thereby returning the rod to a smooth surface and reducing the convective heat transfer. Johnson (1985) indicated that reductions in Stanton number of 12% or more have been measured using instrumented fuel rods.

Micrographic evidence has shown that two distinctly different types of deposit are formed on the fuel rod surface; these are associated with different surface temperatures and are therefore known as High and Low Temperature Deposit - HTD and LTD. The high temperature deposit occurs at

temperatures above approximately 700°C and is seen to consist of straight tubular filamentary growths which are produced by catalytic decomposition of hydrocarbon at the fuel rod surface (Johnson, 1985). In other words, there is molecular mass transfer to the surface and the deposit grows, through chemical reaction, away from the surface. In contrast, the low temperature deposit (500 - 700°C) consists of highly irregular filaments of 0.1 - 0.2 μm diameter and is similar in structure to deposits of soot.

Whilst the chemistry of the gases within the nuclear reactor was able to explain the presence of the high temperature deposit, the low tempera-ture deposit could not be explained with any satisfaction. It was not clear whether the LTD was formed by gas phase or particulate mass transfer to the surface. Although the chemistry was unable to explain growth of LTD on the surface it was able to show that sub-micron carbon particles could form in the gas flow due to the radiolytic decomposition of the methane. The suggestion was, therefore, that the sub-micron carbon parti-cles formed in the gas and were then deposited by eddy-diffusion onto the fuel rod surfaces (Kelly, 1986). Against this argument, however, was the fact that the large temperature differences (about 200°C) between the gas flow and the hot fuel rod would generate large thermophoretic forces which would prevent any particles from depositing onto the surface. However, the processes which influence the deposition of small particles onto surfaces where the effects of both roughness and thermophoresis are acting are not at all well understood.

The purpose of the work reported in the following sections of this paper was to measure experimentally the deposition of sub-micron particles onto smooth and ribbed surfaces, with and without thermophoresis. The physical aspects of particulate turbulent diffusion onto roughened, and in particular heated, surfaces do not lend themselves easily to analysis. The associated conventional theoretical model is not presented in full in this paper, but the theoretical results will be compared with the experimental data and duly commented upon.

2. EXPERIMENTAL APPARATUS AND PROCEDURE

The generation of the sub-micron particles and the subsequent measurement of their deposition was carried out using a fluorimetric technique. A schematic of the experimental deposition rig is shown in Fig. 1. The figure shows the general layout of the aerosol generator and the pipe flow rig with its working section. Also shown is the method by which the fuel rod was assembled in the working section.

The experimental technique uses fluorescein particles. A fluorescein powder (Uranin) is dissolved in clean, deionised water to produce a rela-tively strong solution. The solution is then atomised in a bank of Collison atomisers, Fig. 1. The resulting spray is passed through an impactor where the larger drops are removed. The remaining fine mist passes through a sonic jet where it is exposed to a cloud of bi-polar ions to neutralise any acquired electrical charge. The mist is then held in a chamber with a relatively long residence time; here the fine mist will evaporate so that each droplet will leave a single spherical particle. The

size of the particles are controlled by varying the strength of the origi-
nal solution. In the present work two particle sizes were used, viz. 0.25
and 0.05 µm diameter. The size distributions of the particles were found
to be relatively mono-dispersed and were measured by an electron micro-
scope.

The particles are then injected into the filtered air stream of the
deposition rig which in this case consisted of a 200 mm diameter pipe
about 10 m long. The air flow passes through the working section which
contains the surface to be deposited upon before being exhausted from the
laboratory to the atmosphere, via filters. The experiments were carried
out using a single fuel rod placed in the pipe axis. Dummy fuel rods ran
the length of the pipe before the working section to ensure the flow was
fully developed.

To measure the spatial distribution of the deposit, the fuel rod,
which is approximately 1 m long, was cut into a number of small sections,
each 50 mm long. These were then reassembled using ferrules and a central
tie rod, Fig. 1. The diameter of the fuel rod was 15.4 mm and the ribs
were 0.28 mm square, spaced on a 2 mm pitch.

The particle-laden air stream was passed through the deposition rig
for up to 3 hours. After that time the fuel rod was removed and carefully
disassembled. Each section was placed into a test tube and flooded with a
measured amount of clean de-ionised water so that the deposited particles
were dissolved off the surface to make a very weak fluorescent solution.
The solution was then placed into a fluorimeter where it was exposed to a
filtered light source and its fluorescence measured by a photo-multiplier.
The strength of the solution, and hence the amount of deposit, was com-
pared to solutions of known concentration. The free stream concentration
was measured by drawing a number of isokinetic samples from the airflow
through a millipore filter, the filter paper was immersed in de-ionised
water and the resulting solution analysed in the fluorimeter. Knowing the
free stream concentration and the mass deposited, the deposition velocity
was calculated.

2.1 Isothermal surfaces

The initial experiments were carried out using smooth and ribbed unheated
surfaces, The smooth surface was constructed from a 15 mm diameter stain-
less steel tube which was cut into 50 mm long sections, as was the fuel
rod, and reassembled over a tie rod. To ensure perfect alignment of adja-
cent sections the end of each was machined to form a spigot which fitted
neatly into the mating piece.

The turbulent diffusion onto surfaces through a concentration gradi-
ent is given by:

$$V^+ = \left(\frac{D}{\nu} + \frac{\varepsilon}{\nu}\right) \frac{dc^+}{dy^+} \tag{1}$$

The first term in the bracket describes the Brownian diffusion whilst the second term is associated with the turbulent diffusion. In turbulent flows the second term dominates the process. The rate of deposition over rough surfaces is known to be much greater than that onto smooth surfaces, (Wells and Chamberlain, 1969; Chamberlain, 1967; Chamberlain et al, 1984). To allow for this effect Browne (1974) modified the solution of equation (1) by using a shifted origin for the surface. The particle stopping distance, velocity and eddy diffusivity were then considered from this displaced origin. The roughness also increases the shear velocity and hence the eddy diffusivity at the surface. The analysis of Browne applies to a randomly rough surface and it therefore needs to be considered with some caution in relation to the regular roughness of the fuel rod surfaces. The method adopted for dealing with this was to take an average roughness whereby the additional area of cross section produced by the rib was assumed to be spread between the ribs, (e.g. for a square rib of height e on a pitch p, the equivalent height would be e^2/p). To evaluate the role of roughness on the smooth rod, its surface topography was measured using a Talysurf. The average roughness, including the join between sections was found to be 1.5 μm. The effects of different Reynolds numbers were observed by changing the flow velocities. The Reynolds numbers were 5×10^3, 6×10^4 and 3×10^5.

2.2 Heated surfaces

To assess the effect of thermophoresis over the rough and smooth surfaces they were both heated. The technique used was that of electrical resistance heating, although it was not possible to directly heat the segmented rod because of the joins between the individual sections. Instead, the tie rod which was used to assemble the section was heated and was therefore electrically insulated from the test rod.

The thermophoretic effect can be incorporated into equation (1) to give:

$$V^+ = \left(\frac{D}{\nu} + \frac{\epsilon}{\nu}\right) \frac{dc^+}{dy^+} + V_T^+ \, c^+ \tag{2}$$

where V_T^+, the dimensionless thermophoretic velocity is given by Talbot et al (1980), as:

$$V_T^+ = \frac{V_T}{u_*} = \frac{1}{T} \frac{dT}{dy} \frac{2 \, C_s \, \nu \left(\frac{\lambda_g}{\lambda_p} + C_t \, Kn\right)\left[1 + Kn \, (A + B \exp (- C/Kn)\right]}{u_* \, (1 + 3 \, Cm \, Kn)(1 + 2 \, \lambda_g/\lambda_p + 2 \, C_t \, Kn)} \tag{3}$$

where $C_s = 1.149$, $C_m = 1.14$, $C_t = 2.18$

   $A = 1.2$, $B = 0.41$ and $C = 0.88$

and $\frac{dT}{dy}$ is the temperature gradient normal to the surface.

To evaluate the thermophoretic velocity from equation (3) it is necessary to insert a value for the surface temperature gradient dT/dy; this was estimated from knowing the heating power through the surface.

As with the isothermal surface, deposition tests were carried out for different Reynolds numbers, the two particles sizes and, in addition, different surface temperatures.

3. RESULTS

In the study of aerosol deposition, obtaining reliable results for a range of operating conditions is extremely time consuming and rather tedious. The results presented in this section are a representative sample of the many that were taken. The experimental spread that is shown is typical of that found in such tests. When the tests are repeated many times, the mean and the 95% confidence limits are seen to be very consistent, (El-Kady, 1988).

3.1 Isothermal surfaces

Figure 2 shows the deposition velocity measured along the unheated smooth surface. Each band represents the spread in the results of three different three hour experiments. The data shows that the deposition along the surface is essentially constant, which is to be expected since the flow is fully developed. Also shown is the theoretical prediction for a perfectly smooth surface which is (and was always seen to be) less than the measured value. However, when the measured surface roughness (1.5 μm) is used in equation (1) to produce a 'real' smooth surface the agreement is seen to be much better, especially at the higher Reynolds number. This raises the question of what constitutes a smooth surface relative to a sub-micron particle. Davies (1983) showed that the micro-surface roughness inherent in most experiments plays an important role in deposition. Using a theory based on the streamwise inertial impaction of particles onto roughness elements, it was clearly demonstrated that experimental differences in deposition velocities to nominally smooth surfaces can be explained if the actual surface roughness is allowed for. When purely diffusional mechanisms are present, for very small values of the dimensionless particle relaxation time t_p^+, Davies reasoned that increases in deposition are due to greater perpendicular eddying associated with the roughness elements. The deposition velocities measured for the (real) smooth surface in the present work are consistent with the data used by Davies.

The deposition velocity measured along the ribbed fuel rod surface is shown in Fig. 3. It can be seen that the effect of the ribs is to increase the deposition rate twenty-fold. When the equivalent roughness, as described in section 2.1, was calculated it was seen that it was greater than the thickness of the concentration layer. Since the relationship between the roughness associated with the ribs and the random roughness model used in the theory is not clear, it was decided that proposed equivalent roughness should be factored such that the experimental and theoretical data, for the different particle sizes and Reynolds numbers,

showed the best agreement. In Fig. 3 the resulting theoretical prediction is shown together with the experimental data. The rate of deposition is again seen to be relatively constant along the fuel rod. The factor (α) required to scale the equivalent roughness to align the data was 0.1. This value was subsequently used in all the analyses.

In Fig. 4 the ribbed surface deposition velocities measured in the present work are shown as a function of t_p^+ and compared with the data of Chamberlain (1967). When reviewing this data Davies (1983) considered that for t_p^+ less than 0.22, the deposition process is that of diffusion whilst for relaxation times greater than this value, the deposition process becomes influenced by impaction. On this basis it can be seen from Fig. 4 that the dominant mechanism of deposition in the present work is that of diffusion.

In Fig. 5 the deposition velocity on the rod surface is shown as a function of Reynolds number. The experimental values are shown superimposed upon the theoretical curves for the ideal and the real smooth surfaces, and for the ribbed surfaces using the procedure outlined above. It can also be seen from Fig. 5 that the deposition velocity increases with Reynolds number, this is a reflection of the higher friction velocity and the more vigorous transport processes. Furthermore, the increased roughness has less effect at the lower Reynolds number whereas at the higher values the effect of the additional surface-generated turbulence is clearly seen.

3.2 Heated surfaces

Notwithstanding the adjustment that had to be made to the rib height to accommodate its particular geometry, the agreement between Browne's model and experimentally measured deposition onto randomly rough surfaces is generally good. The same cannot be said, however, of the agreement between experiment and theory in relation to the heated surface. In Fig. 6 the experimentally measured deposition velocity for the 0.25 μm particles are shown for the smooth surfaces when heated and unheated. The effect of heating the smooth surface to 95°C (ambient air temperature 25°C) is to reduce the deposition rate to about 10% of that measured on the unheated surface. The theoretical prediction using equations (2) and (3) is given by the lower curve in Fig. 5 where it can be seen that the theory underestimates the deposition velocity by many orders of magnitude. The effect of thermophoresis, whilst still significant in practice, is substantially exaggerated in theory. Similar predictions for the effects of thermophoresis were made by Gokoglu and Rosner (1986) using a rather different, and more sophisticated, mathematical approach.

The expression for the thermophoretic velocity given by equation (3) was derived, and supported experimentally, for quiescent conditions where flow and turbulence were not a factor. The aspect of this expression which has to be questioned in the present context is that of the surface temperature gradient, dT/dy. Considering the hectic situation at the surface, there will be turbulent eddies, even in the laminar sublayer, which will be substantially larger than the particles. The particles will be trapped in discrete bursts of fluid, (Cleaver and Yates, (1975)). The particles contained in the eddies will not be exposed to the mean surface

temperature gradient and will be transported to the surface oblivious of the thermophoretic potential that exists. In view of this it is understandable that the theories that are conventionally put forward are found wanting.

If it is accepted that the temperature gradient is the principal source of error, then one way of aligning the experimentally measured results and the theoretically derived values is to scale the temperature gradient. This was done using all of the many experimental results that were obtained for the deposition at smooth heated surfaces, with different surface temperatures, the two particle sizes and different Reynolds numbers. The resulting scaling factor (β) was found to be 0.2 and the effect of installing this into equation (3) is shown on Fig. 6 where the theoretically derived deposition velocities are now much closer to the measured values.

The effect of thermophoresis on the different particle size is shown in Fig. 7, where the ratio of the deposition velocity with thermophoresis to that without is shown, (hot surface temperature of about 95°C, air temperature 25°C). For the 0.25 µm particles the effect of thermophoresis is to reduce the deposition rate to just 10% of that onto the unheated surface whilst the corresponding value for the 0.05 µm particle is about 40%. Also shown in this figure is the theoretically derived value and although the agreement is not perfect it should be pointed out that the vertical scale in Fig. 7 is linear and that in terms of aerosol deposition such agreement is very satisfactory. The reason for the smaller particles being influenced less by thermophoresis is that for a small particle the temperature differential across it is less and so, therefore, is the imbalance in the molecular bombardment. Particles larger than about 0.25 µm will also show less response to thermophoresis due to their increased inertia. Although it is dependent on the state of the carrier gas, it is generally found that particles of about 0.25 µm are most susceptible to thermophoretic forces. The reason that the thermophoretic effect is less at the beginning of the rod in Fig. 7 is due to the fact that the rod heating was not uniform in that area.

The effect of thermophoresis over the ribbed surface is shown in Fig. 8. Here it can be seen that the deposition velocity over the 95°C surface compared with the unheated ribbed surface is about 40 and 20% for the 0.05 and 0.25 µm particles respectively. Also shown are the theoretical values, which show good agreement. These were calculated by including the factor for both the rib height and the temperature gradient. Thus for the heated ribbed surface the roughness increases the deposition rate whilst the thermophoresis decreases it.

4. CONCLUDING REMARKS

The published data relating to the deposition of sub-micron particles onto real surfaces is extremely sparse and one of the principal aims of this paper has been to help rectify this.

Deposits on surfaces fouled by sub-micron particles can take a long time to build up, possible a few months in the case of an AGR. The deposition is, nevertheless, relentless and to such small particles the surface represents a perfect sink. If there is a wide range of particle sizes in the gas stream then the sub-micron particles may act as a surface conditioner making the surface more 'sticky' to the larger particles. Knowledge of the behaviour of sub-micron particle depositing onto real surface is therefore important.

Many studies have been made for the deposition of small particles onto ideal, smooth surfaces and under these conditions the theoretical models have proved useful. From the results presented in this paper, that usefulness does not extend to the deposition onto more 'difficult' surfaces. For the deposition onto the ribbed surface, the equivalent roughness concept did not fit easily into the mathematical model, and a correction had to be made to the roughness height. This approach can be defended since calculations of deposition rates through concentration gradients can only be carried out using average values and the geometry of the ribbed surface, specifically the size and spacing of the ribs in relation to the size of the particles, makes averaging difficult.

In the case of the surface temperature gradient, it is clear that the model doesnot represent the physical mechanisms that are occurring at the surface and the use of a scaling factor in this context is not satisfactory. The use of these corrections, and the magnitude of the scaling factor used, are intended to demonstrate the inadequacies of present theories, the danger in using them, and the need for more reliable experimental data.

REFERENCES

Blanchard, A., Faircloth, R.L. and Wood, C.J., (1972), "The radiolytic oxidation rate of nuclear graphites as a function of point coolant composition in moderator blocks", 14th Biennial Conf. on Carbon, Penn. State Univ., June 25-29, 447.

Browne, L.W.B., (1974), "Deposition of particles on rough surfaces during turbulent gas flow in a pipe", Atmos. Environ., 18, 801-816.

Campion, P., (1980), "Carbon formation processes relevant to advanced carbon dioxide cooled reactors", Gas Chemistry in Nuclear Reactors and Large Industrial Plant. Edited by A. Dyer, Haden Press, London, 53-66.

Chamberlain, A.C., (1967), "Transport of lycopodium spores and other small particles to rough surfaces", Proc. Roy. Soc., A296, 45-70.

Chamberlain, A.C., Garland, J.A. and Wells, A.C., (1984), "Transport of gases and particles to surfaces with widely spaced roughness elements", Boundary Layer Meteorology, 29, 343-360.

Cleaver, J.W. and Yates, B., (1975), "A sub-layer model for the deposition of particles from a turbulent flow", Chem. Eng. Sci., 30, 983-992.

Davies, J.T., (1983), "A new theory of aerosol deposition from turbulent fluids", Chem. Eng. Sci., 38, 135-139.

El-Kady, A.A., (1988), "Deposition of particles onto AGR fuel elements", Ph.D. Thesis, Dept. Mech. Eng., Univ. of Liverpool.

Gokoglu, S.A. and Rosner, D.E., (1986), "Prediction and rational correlation of thermophoretically reduced particle mass transfer to hot surfaces across laminar or turbulent forced convection gas boundary layers", Chem. Eng. Commun., 44, 107-119.

Johnson, P.A.V., (1985), "A channel chemistry model for high temperature carbon deposition in AGR's", Nucl. Energy, 24, 6, 381-395.

Kelly, B.T., (1986), "A theory of low temperature carbon deposition in advanced gas-cooled reactors", Nucl. Energy, 25, 4, 225-233.

Talbot, L., Cheng, R.K., Schefer, R.W. and Willis, D.R., (1980), "Thermophoresis of particles in a heated boundary layer", J. Fluid Mech., 101, 4, 737-758.

Wells, A.C. and Chamberlain, A.C., (1969), "Transport of small particles to vertical surfaces", Brit. J. Appl. Phys., 18, 1793-1799.
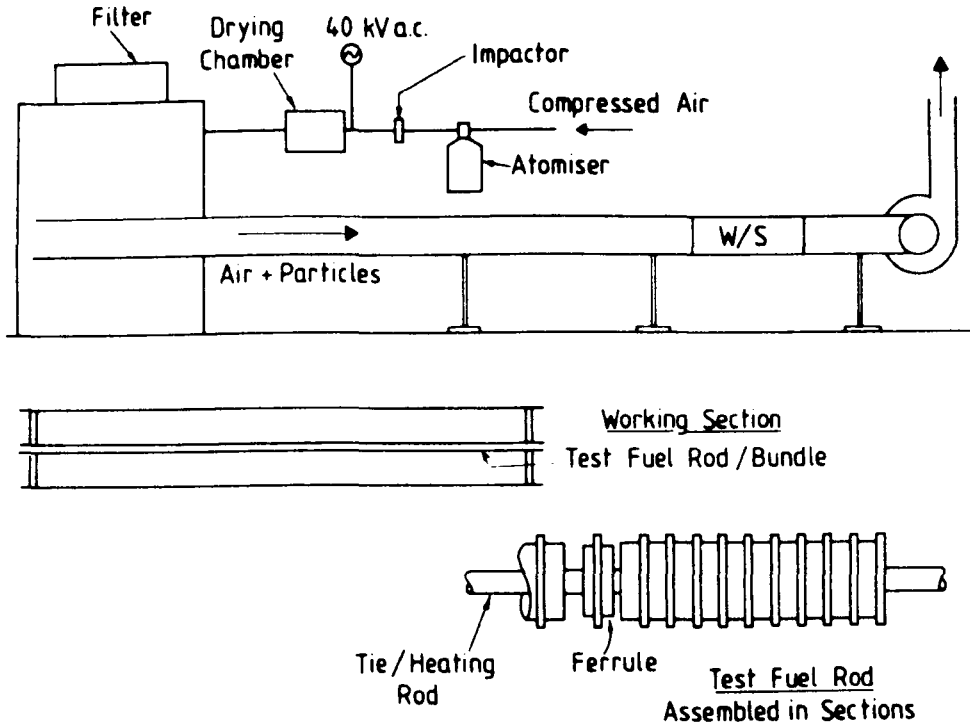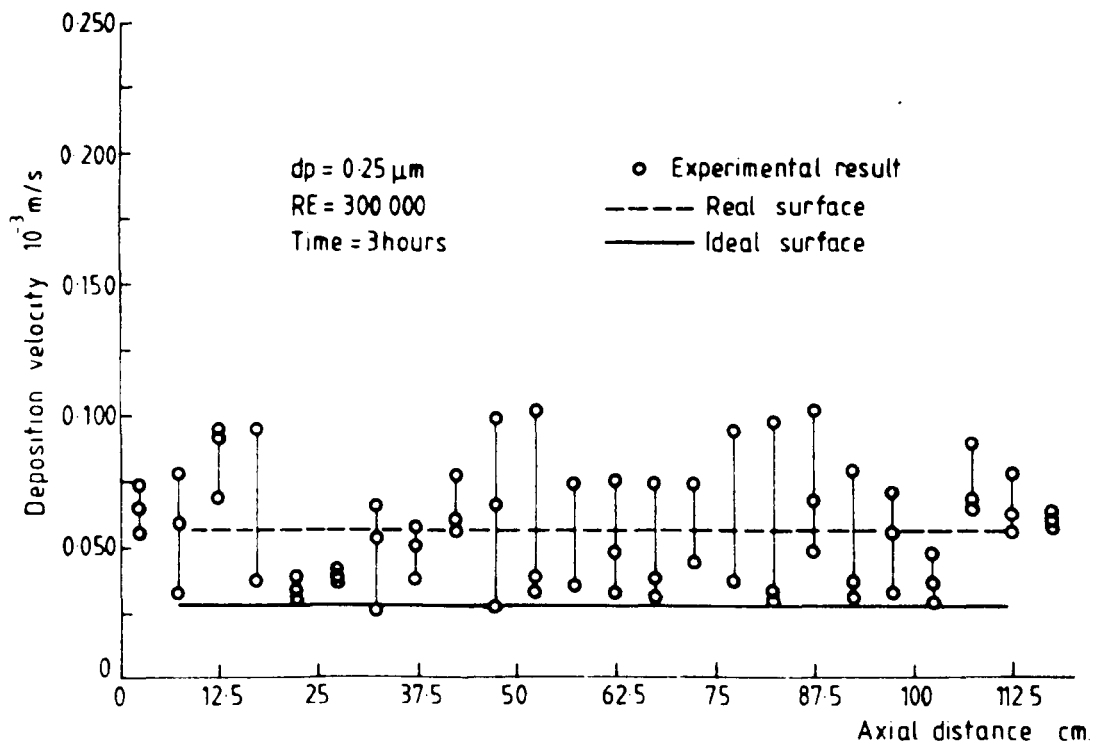
Fig. 1   Schematic of Deposition Rig

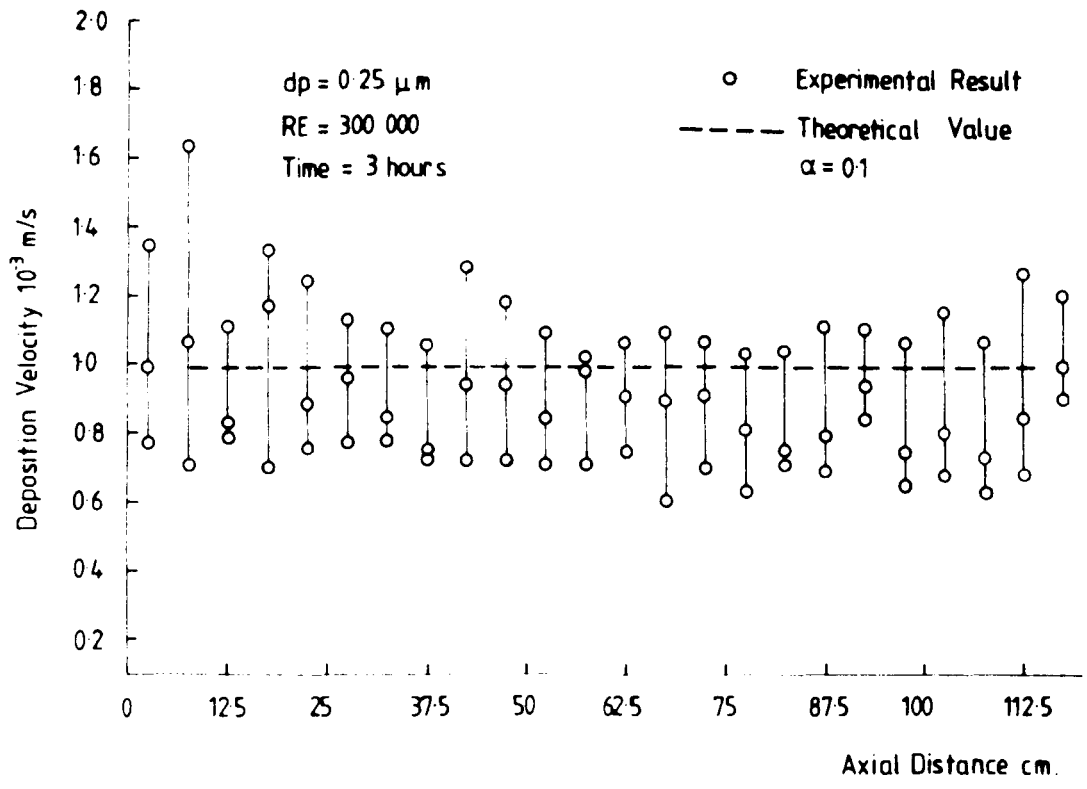**Fig. 2   Deposition Velocity along the Smooth Isothermal Surface**

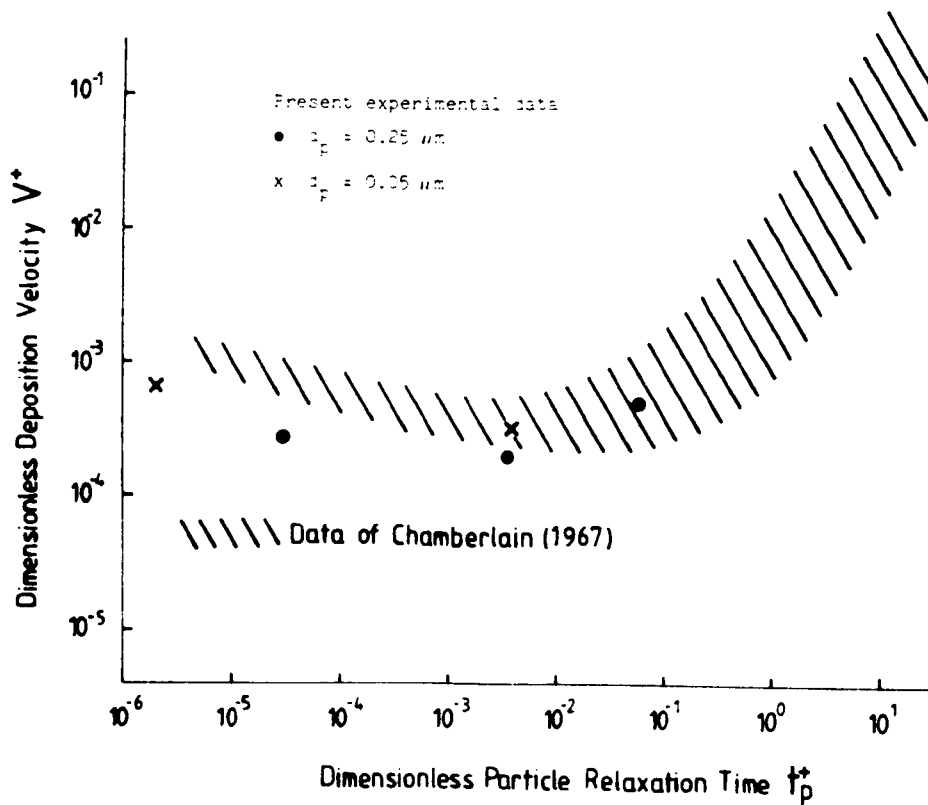**Fig. 3   Deposition Velocity along the Ribbed Isothermal Surface**

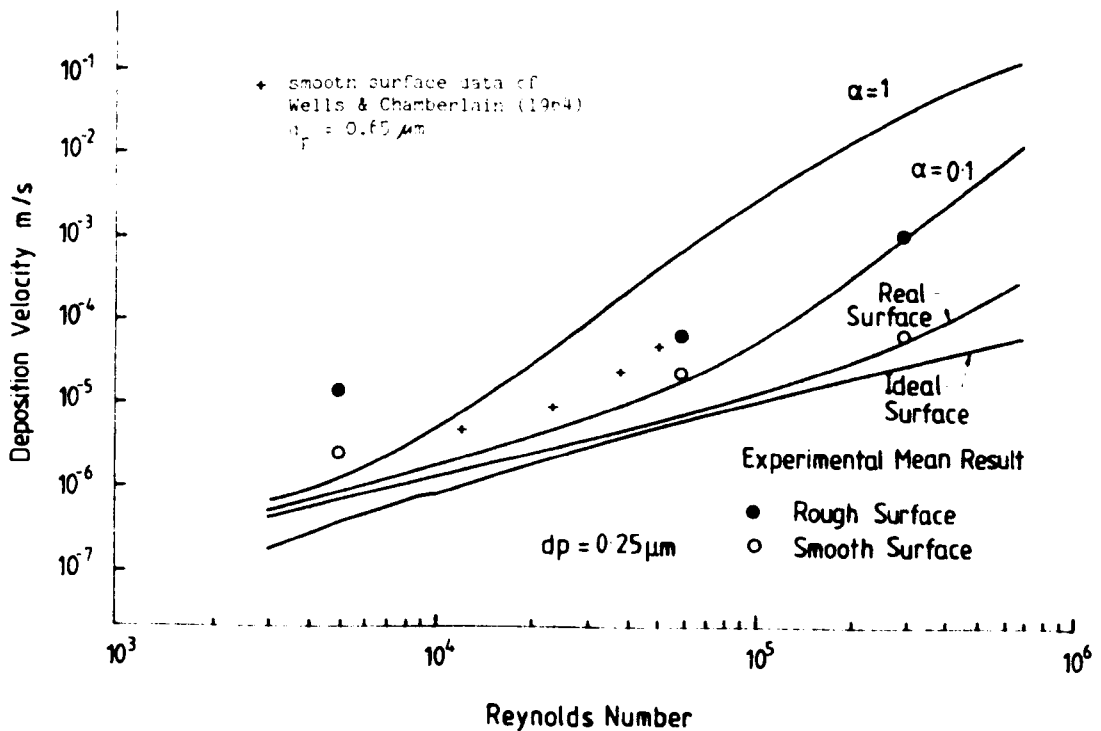**Fig. 4   Deposition onto Rough Isothermal Surfaces**

Fig. 5   Calculated and Measured Deposition Velocities for Isothermal Surfaces Showing the Effect of Scaling the Equivalent Rib Height
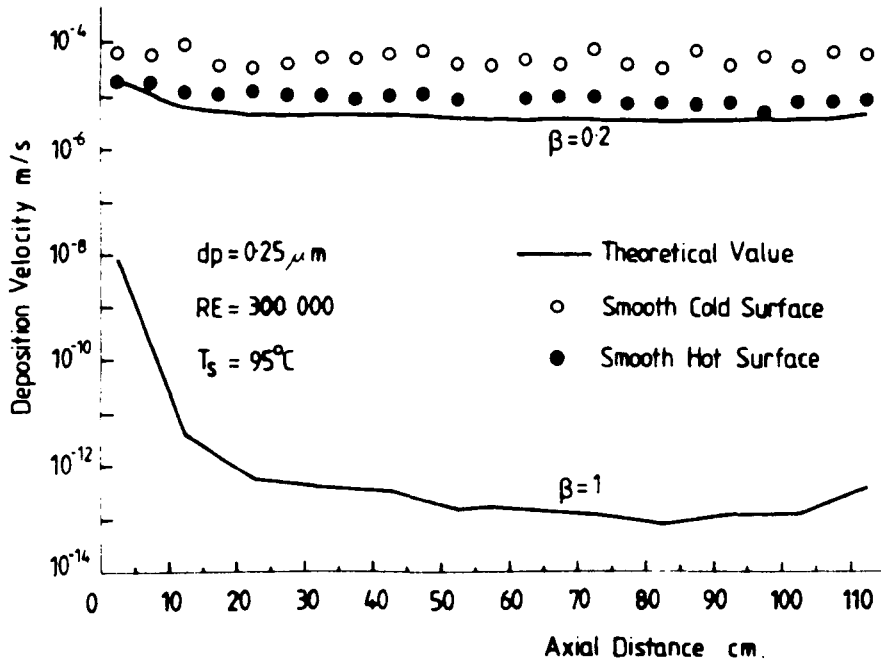
Fig. 6 Deposition Velocity along Smooth Surface Showing the Effect of Thermophoresis and the Temperature Gradient Scaling Factor
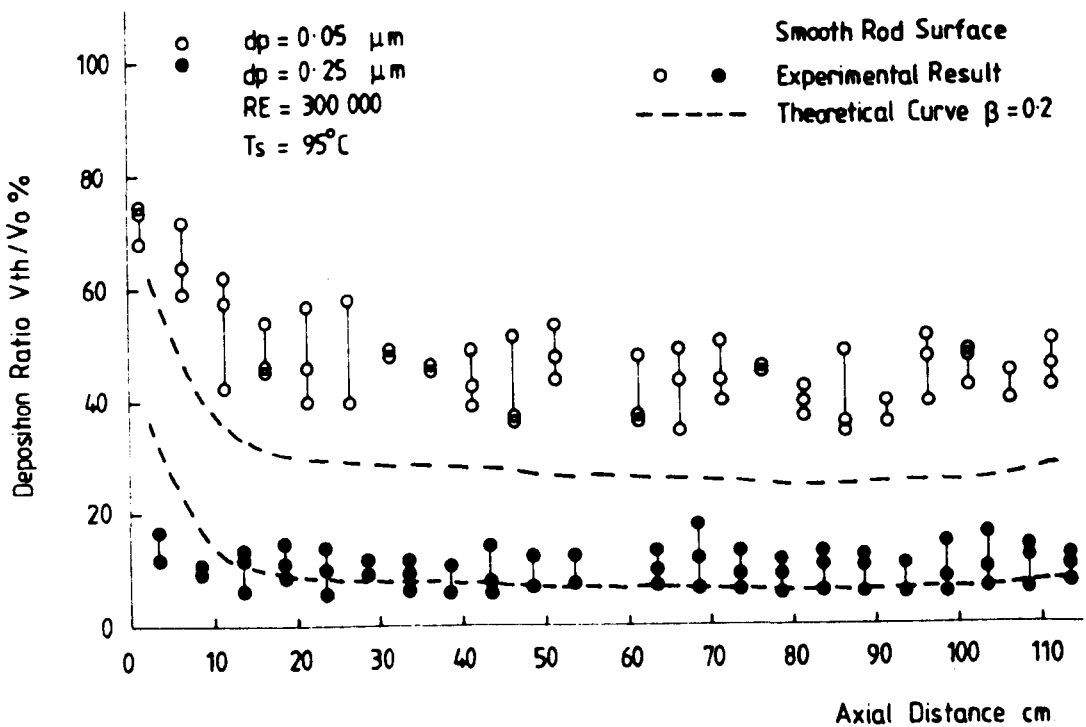

Fig. 7 Effect of Thermophoresis along the Heated Smooth Surface for Different Particle Sizes
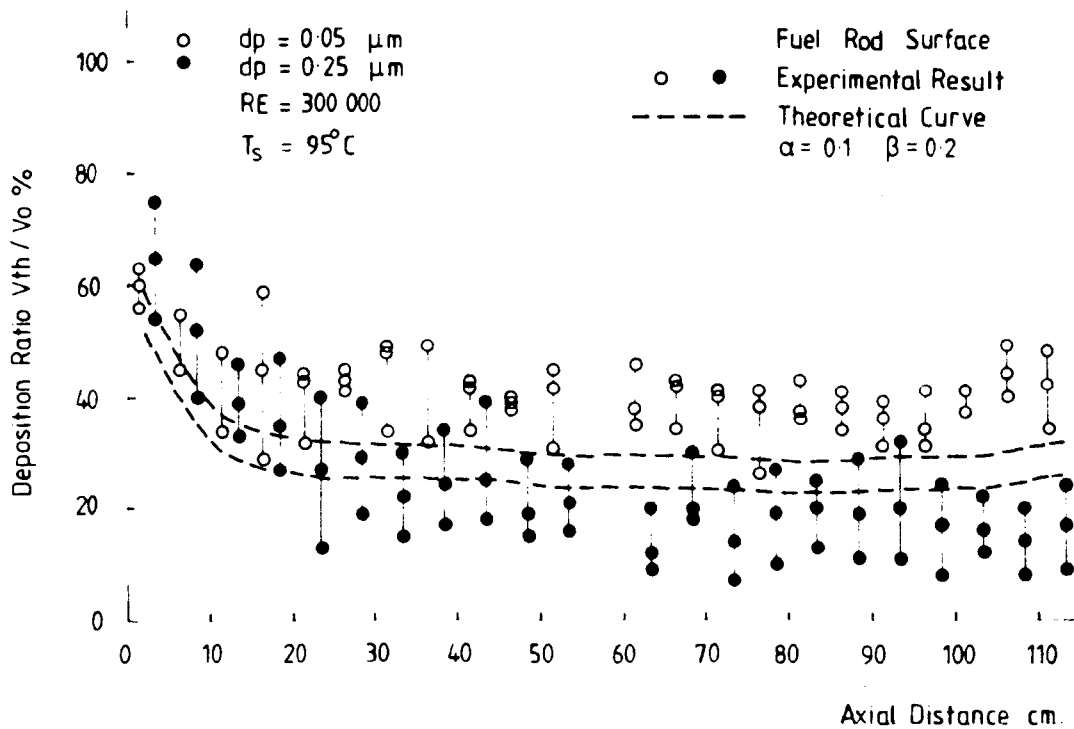
Fig. 8   Effect of Thermophoresis along the Heated Ribbed Surface for Different Particle Sizes